Shear Behaviour of Reinforced Concrete Deep Beams

A thesis submitted for the degree of
Doctor of Philosophy
in the Faculty of Engineering of
The University of Sheffield

By

Kamaran Sulaiman Ismail

ABSTRACT

RC deep beams are key safety critical structural systems carrying heavy loads over short span, such as transfer girders in tall buildings and bridges. Current design provisions in codes of practice fail to predict accurately and reliably the shear capacity of RC deep beams and in some cases they are unsafe. This work aims to develop a better understanding of the behaviour of RC deep beams and governing parameters, and to improve existing design methods to more accurately predict the shear capacity of such members.

An extensive experimental programme examining 24 RC deep beams is carried out. The investigated parameters include concrete strength, shear span to depth ratio, shear reinforcement and member depth. To develop a better insight on the distribution and magnitude of developed stresses in the shear span, finite element analysis is also performed. The microplane model M4 is implemented as a VUMAT code in ABAQUS to represent the behaviour of concrete in a more reliable manner and validated against experimental tests on RC deep beams. This model is utilised in a parametric study to further investigate the effect of concrete strength, shear span to depth ratio and shear reinforcement.

The experimental and numerical results show that concrete strength and shear span to depth ratio are the two most important parameters in controlling the behaviour of RC deep beams, and that shear strength is size dependent. The analysis also shows that minimum amount of shear reinforcement can increase the shear capacity of RC deep beams by around 20% but more shear reinforcement does not provide significant additional capacity.

A lateral tensile strain based effectiveness factor is proposed to estimate the strength of the inclined strut to be used in strut-and-tie model. Additionally, node factors to estimate the developed strength in different type of nodes are proposed. The proposed model is evaluated against a large experimental database and the results show that it yields more accurate and reliable results than any of the existing models. The model is characterized by the lowest standard deviations of 0.26 for both RC deep beams with and without shear reinforcement and accounts more accurately for all influencing parameters.

ACKNOWLEDGMENTS

DISCLAIMER

The Experiments shown in Appendix B were performed as part of author's work on his MSc dissertation. They are added in the appendix to this dissertation because they are used in the discussion (or referenced in the text), but the MSc dissertation is not widely available and these results have not been reported elsewhere.

TABLE OF CONTENTS

LIST OF FIGURES

x

LIST OF TABLES

LIST OF NOTATION

a	Shear span
a/d	Shear span to depth ratio
b	Section width
d	Section effective depth
d_a	Aggregate diameter
ε	Strain
E_c	Modulus of elasticity of concrete
ε_1	Principal tensile strain
ε_2	Principal compressive strain
ε_s	Longitudinal tensile strain
f_c	Concrete compressive strength (cylinder)
f_{cd}	Design concrete compressive strength
f_{ce}	Effective concrete compressive strength
f_{ck}	characteristic concrete compressive strength (cylinder)
f_t	Concrete tensile strength
f_u	Ultimate strength of steel reinforcement
f_y	Yield strength of steel reinforcement
f_{yk}	Characteristic yield strength of steel reinforcement
G_f	Fracture energy of concrete
h	Overall section depth
h_B, h_{CS}	Depth of the compression zone in strut-and-tie model
h_T, h_{Tie}	Depth of the bottom node in strut-and-tie model
L	Member length
l_B, l_{PB}	Length of the bottom plate
l_T, l_{PT}	Length of the top plate
n	Modular ratio of concrete
θ	Angle of the inclined strut
ρ	Main reinforcement ratio
ρ_h	Horizontal shear reinforcement ratio
ρ_v	Vertical shear reinforcement ratio
σ_c	Concrete compressive stress
s	Spacing
V	Shear strength
v'	Effectiveness factor
W_{SB}	Width of the inclined strut at bottom node
W_{ST}	Width of the inclined strut at top node

CHAPTER 1.   INTRODUCTION

1.1. INTRODUCTION

The shear resistance of RC beams, especially shear critical elements such as RC deep beams, is a challenging issue that is still the subject of academic debate. This is because shear behaviour of RC beams is influenced by many parameters [1, 2], the interdependency of which is very complex to model. Additionally, shear forces always act in combination with other types of load such as flexure, axial load and sometimes torsion, further complicating the problem. Accurate shear capacity prediction is paramount since shear failure is catastrophic (Figure 1-1) and could occur without warning.

Deleted due to copyright
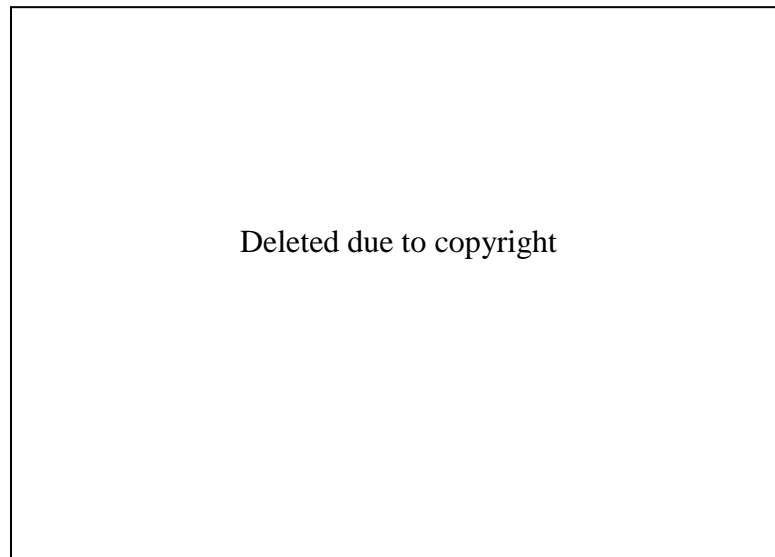
Figure 1-1-Collapse of Laval overpass due to shear failure [2]

RC deep beams are structural members characterized by having relatively deep section comparing to their span for which a substantial proportion of the load is transferred directly to the support through a single strut. In structural applications, deep beams are commonly used as transfer girders in buildings, bridges and offshore structures. According to Eurocode 2 (EC2) [3] beams can be classified as deep beams when the ratio of span to depth is smaller than three. On the other hand, ACI 318-14 [4] classifies

beams as deep beams which satisfy (a) Clear span does not exceed four times the overall member depth h; or (b) Shear span does not exceed two times the overall member depth. The strength of deep beams is usually controlled by shear rather than flexure [1], and since most of the applied load is directly transferred to the support by strut and tie action, strut-and-tie model is the most reliable method for design purposes.

Since the problem is dominated by material properties, most studies related to shear are experimental. However, experimental work is expensive and usually limited by the size of the facilities, the type of member or design parameters investigated in a particular set of experiment. Results from shear tests are notoriously variable and often contradictory; furthermore, most published data do not provide sufficient detail for the in-depth investigation of the shear mechanism. Despite this, all current shear design procedures, such as Eurocode (EC2) [3] and ACI 318-14 [4] code, are based on statistical best fits of experimental data. The inadequacy of these empirical shear design procedures is more pronounce in non-flexural and shear critical members such as deep beams. Numerous theoretical approaches have been proposed to explain the shear mechanism such as the truss analogy theory [5, 6], the variable angle truss model [7], the theory of shear resistance of RC beams by Kupfer et al. [8] the modified compression field theory [9] and strut-and-tie model [10, 11]. The shear strength predicted according to these theories is in general more reliable than that of empirical procedures but there are still parameters that need to be further investigated such as effectiveness factor of concrete used in strut-and tie model.

The strut-and-tie model, which was pioneered by Ritter [5] and Morsch [6], is a rational method for analysing and designing reinforced concrete beams especially deep beams. It is based on the lower bound theorem of the theory of plasticity and assumes that the disturbed regions, which are these along which plane sections do not remain plane before and after bending, can be analysed and designed using hypothetical pin-jointed trusses consisting of struts and ties interconnected at nodes. This model has been incorporated into the design procedures of many codes of practice [3, 4, 12]. The accuracy of shear resistance prediction by a strut-and-tie model are dependent on

various assumptions that need to be made regarding the geometry of the nodes, the width of the struts and the effectiveness factor of concrete strength for the inclined strut. However, the codes of practice provide very little guidance on the use of STM in design [13] which makes the model becomes an approximated method with undetermined level of accuracy. Although, such approaches are generally extremely conservative [14-17], they can also lead to unsafe design solutions [17-19]. Therefore, the current codes provisions need to be reviewed and improved to account for parameters affecting shear behaviour and capacity of RC deep beams. Furthermore, more reliable and detailed experimental data are needed to investigate the effect of key parameters such as shear span to depth ratio, concrete compressive strength, shear reinforcement and member depth.

Despite the fact that nominal shear strength of reinforced concrete beams decreases when increasing the size of the member, most of the existing shear models do not take this into account. The size effect in RC slender beams is well investigated and documented [20-25]; however, for RC deep beams, size effect is still the subject of discussion among researchers [26-32]. Hence, the size effect should be investigated further and the existing shear models should be evaluated to assess their safety.

Due to the rapid advances in the field of computational mechanics, finite element modelling (FEM) has become one of the most powerful tools in simulating structural elements in a variety of fields. The successful simulation of specific elements relies upon the realistic representation of the material properties in FEM. However, due to the complexity of the constitutive material properties of concrete, modelling the behaviour of reinforced concrete in particular shear has been, and still is, a challenging issue.

In the past few decades, analysing reinforced concrete elements by finite element method have witnessed remarkable advancements. Many researchers have made valuable contributions in simulating RC behaviour using plasticity and continuum damage mechanics [33-37]; however, these material models are not capable of realistically simulating the very complex stress-strain behaviour of RC elements [38]. The more detailed microplane model [39, 40] has been shown to simulate the

microscopic behaviour of concrete in a more reliable manner and it has been successfully implemented in some finite element analysis packages to capture the non-linear and shear behaviour of RC elements [40-43]. The main characteristic of microplane constitutive model is written in terms of vectors on microplanes rather than tensors at the macro level [39]. Therefore, inelastic physical phenomena such as slip and friction can be characterized directly in terms of stress and strain on the microplanes.

1.2. RESEARCH AIM AND OBJECTIVES

The main aim of the present study is to develop a numerical and analytical model to predict shear behaviour and capacity of RC deep beams more accurately than the available models, and this is achieved through the following objectives:

- Gain understanding of the effect of key parameters such as shear span to depth ratio, concrete compressive strength, shear reinforcement, and size effect on the behaviour of RC deep beams.
- Develop a suitable finite element procedure that can be used as a platform to predict shear behaviour and capacity of RC deep beams.
- Analytically evaluate the accuracy and applicability of strut-and-tie model in predicting the shear resistance of RC deep beams.
- Propose a reliable effectiveness factor for the strength of concrete cracked in tension and node strength factors that can be easily implemented in existing design codes.

The above objectives can be fulfilled through the following methodologies:

- Review the current state-of-the art on the behaviour of RC beams subjected to shear forces.
- Compile a comprehensive database of tests published in peer reviewed and reliable journal publications and use it to evaluate existing shear models.

- Experimental investigation on the effect shear span to depth ratio, concrete compressive strength, shear reinforcement, and size effect on the behaviour of RC deep beams.

- Implement microplane material M4 model as a VUMAT in ABAQUS and numerically investigate the effect of shear span to depth ratio, concrete compressive strength, and shear reinforcement on the behaviour of RC deep beams using ABAQUS.

- Analytical investigation of strut-and-tie model.

1.3. THESIS LAYOUT

This thesis is divided into six chapters and presented in a non-conventional manner. The thesis combines two types of chapters: chapters written following the traditional thesis format (chapters 2 and 6), and chapters consisting of stand-alone journal papers (chapters 3 to 5). The following is a brief description of each chapter.

Chapter 2 presents a brief background of the research problem and a review the current understanding of the important aspects regarding shear behaviour of RC beams. A database compiling 60 years of research on shear of RC beams is established and used to assess the effect of different design parameters such as shear span to depth ratio, concrete compressive strength, shear reinforcement and member size on the shear capacity of RC beams. In addition, this chapter presents critical and extensive evaluation of existing shear design models in predicting experimental results.

Chapter 3 is based on Ismail K. S., Guadagnini M. and Pilakoutas K., (2016a) Shear Behaviour and Size Effect of RC Deep Beams (submitted to ACI Structural Journal) and investigates the behaviour and size effect of RC deep beams. A total of 24 RC deep beams were tested in two phases. Phase I comprises 21 RC deep beams tested at the Structural Engineering Laboratory of the University of Salahaddin\Hawler in Iraq to investigate the effect of concrete compressive strength, shear span to depth ratio and

shear reinforcement. Phase II comprised three geometrically similar RC deep beams with different sizes to examine size effect and was carried out at the Heavy Structures Laboratory of the University of Sheffield in the UK. Based on the results, the effect of above design parameters on shear behaviour and capacity of RC deep beams is presented and discussed in detail. The provisions of EC2, ACI 318-14 and Model Code 2010 are then assessed and recommendations are drawn for further improvements in design procedures.

Chapter 4 is based on Ismail K. S., Guadagnini M. and Pilakoutas K., (2016b) Numerical Investigation on the Shear strength of RC Deep Beams Using the Microplane Model (accepted for publication in Journal of Structural Engineering) and presents a numerical investigation on RC deep beams. The general finite element program ABAQUS is utilised as a platform and the concrete material models available in ABAQUS are first examined and compared to the experimental results. Then, to better simulate the behaviour of RC deep beams, the microplane material model M4 is implemented. The validity of the model in capturing the structural response of RC deep beams is assessed against an experimental database of 20 specimens with different characteristics. The developed model is then used to perform a parametric study aimed at investigating the effect of concrete compressive strength and shear span to depth ratio in RC deep beams with and without shear reinforcement. The results of the analysis are compared to the provisions of EC2 and ACI 318-14 codes and recommendations are drawn.

Chapter 5 is based on Ismail K. S., Guadagnini M. and Pilakoutas K., (2016c) Strut-and-Tie Modelling of RC Deep Beams (submitted to Journal of Structural Engineering) and it presents the development of strut-and-tie model for RC deep beams. The development of the model includes the selection of an appropriate strut-and-tie layout and an accurate size for each element in the model. In addition, the paper proposes a lateral tensile strain based effectiveness factor which can be used to estimate the strength of the inclined strut in the model. Finally, it presents and discusses the accuracy of the model and other models found in the literature against the experimental database.

Chapter 6 summarises the research work, presents the concluding remarks and gives recommendations for future work.

CHAPTER 2.   REVIEW AND EVALUATION OF AVAILABLE SHEAR PROCEDURES

2.1. OVERVIEW

Despite numerous research studies on shear behaviour of RC members, there is still discord regarding the transfer mechanisms and influencing parameters. This is because shear always acts in combination with other actions such as bending, torsion and axial load and is influenced by many parameters such as concrete compressive strength, shear span to depth ratio, element size, flexural reinforcement, shear reinforcement (if provided) and aggregate size.

This chapter reviews the current understanding on the shear behaviour of RC members in terms of a) shear transfer mechanisms and b) effect of different parameters on the shear capacity of RC members. Code shear provisions are also presented and evaluated. For the code evaluations, all safety factors are excluded.

2.2. MECHANISMS AND THEORIES OF SHEAR TRANSFER

2.2.1. FUNDAMENTAL MECHANISMS

The free-body diagrams shown in Figure 2-1, illustrate the fundamental mechanisms of shear transfer in RC beams [44]. In beams without shear reinforcement, the applied shear (V) is transferred through a combination of shear in the compression zone (V_{cz}), dowel action (V_d) and the vertical component of aggregate interlock stresses (v_a) over the surface of the inclined crack. These three components represent the concrete contribution to shear resistance mechanism. The proportions transferred by each of these components have been the subject of research for decades and remain a matter of

discussion. This proportion of shear transfer by each component is affected by the compression zone depth, shear span to depth ratio, crack width roughness, concrete strength and other parameters. In addition to these three shear resisting mechanisms, some shear is transferred by residual tension across the crack; however, this component is relatively small, especially in the case of wide cracks. In the case of beams with shear reinforcement, there is an additional vertical force (V_s) due to the presence of stirrups; this is considered to be the steel contribution to shear resistance.
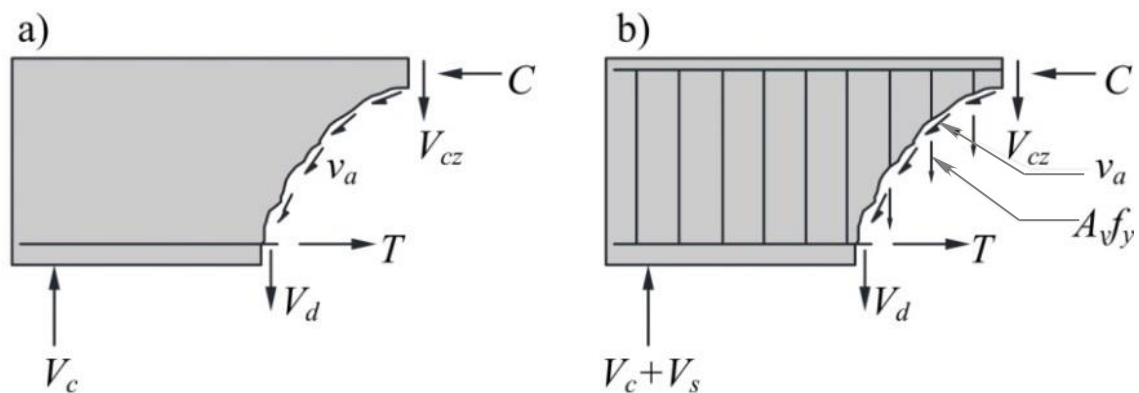
Figure 2-1-Shear transfer mechanisms in RC beams [44] a) beams without shear reinforcement b) beams with shear reinforcement

2.2.2. STRUT-AND-TIE MECHANISM

When the applied shear is close to the support, such as in deep beams and corbels, the proportions transferred by the aforementioned mechanisms change and the majority of the applied shear can be considered to be transferred by a strut-and-tie mechanism as shown in Figure 2-2. In this case, the tensile forces are carried by the flexural reinforcement, whilst the concrete is supposed to transfer shear only in compression. When the member is subjected to distributed load, the arch action is developed (Figure 2-2-b) rather than just the strut-and-tie mechanism.
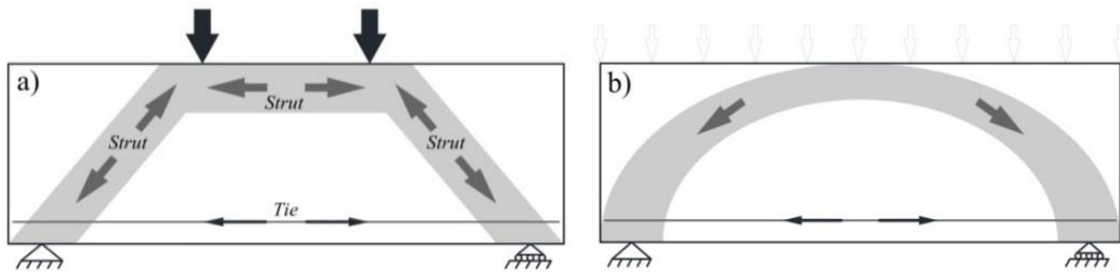
Figure 2-2- a) Strut and Tie mechanism and b) Arch action

2.2.3. TRUSS MECHANISM

When the applied load is far away from the support, such as slender flexural element, a truss action [5, 6] (Figure 2-3) is activated. This has a longitudinal compression chord on top through the concrete and a tension chord at the bottom formed by the longitudinal tension reinforcement. The shear forces are transferred up and down the beam depth by inclined compressive forces which can be carried by the concrete and vertical ties which are formed by the shear reinforcement.
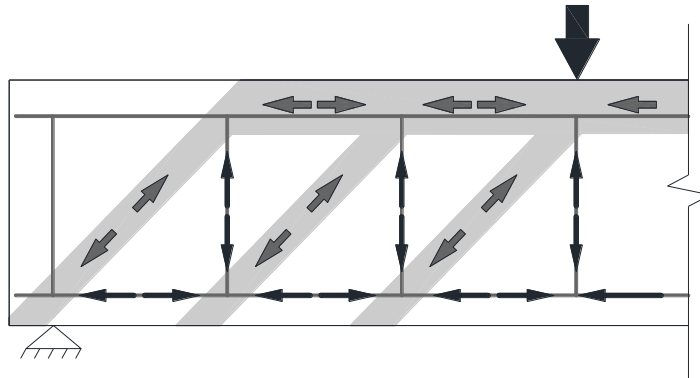
Figure 2-3-Truss mechanism

2.2.4. MODIFIED COMPRESSION FIELD THEORY (MCFT)

In 1986, Vecchio and Collins [9] conducted an experimental programme on thirty RC-panels and developed the Modified Compression Field Theory (MCFT) to predict the load-deformation response of RC elements subjected to in-plane shear and normal stresses. MCFT is an improvement on the Compression Field Theory (CFT) that was developed in the seventies by Mitchell and Collins [45] as a theory to describe the

behaviour of RC elements under pure torsion. The main difference between CFT and MCFT is the utilization of the tensile strength of the concrete in MCFT. Depending on the measured stress and strain of the tested elements, Vecchio and Collins noticed that cracked concrete is capable of carrying a substantial amount of stress in the principal tensile direction. Therefore, the tensile strength of the cracked concrete, which was previously ignored, was added to the constitutive material models.

MCFT was derived based on the simplified assumption that the average direction of principal compressive stress in the cracked concrete is related to the average direction of principal tensile strain and that the inclination of the critical cracks is parallel to the direction of the principal compressive stress. Additionally, the theory assumes that for any state of stress there is only one corresponding state of strain, and concrete and reinforcement are perfectly bonded together. The equilibrium equations, compatibility equations and stress-strain relationship of the MCFT are summarised in Figure 2-4.

As MCFT was derived mainly on the basis of test results on concrete panels subjected to pure shear forces and with well distributed reinforcement, it cannot be used directly to predict the load-deformation of RC beams and columns subjected to a complex combination of bending, shear and axial loads. To predict the load-deformation of beam and column members, Vecchio and Collins [46] presented an analytical model called layered model based on an implementation of the MCFT. The model assumes that the beam can be represented as an assemblage of finite layers of concrete and longitudinal steel reinforcement. Each layer is analysed individually with the compatibility requirement of plane sections before bending remain plane after bending.

Based on the layered model, Response-2000, a computer software that implements basic engineering beam theory, was developed at the University of Toronto by Bentz [47]. The program is capable to predict the load-deformation response of reinforced and prestressed concrete beams and columns. As mentioned in the program manual, Response-2000 is based on the principle of section analysis and assumes that plane sections before bending remain plane after bending.

Equilibrium:

Average Stresses:

1. $f_x = \rho_x f_{sx} + f_1 - v \cot\theta$
2. $f_y = \rho_y f_{sy} + f_1 - v \tan\theta$
3. $v = (f_1 + f_2)/(\tan\theta + \cot\theta)$

Stresses at cracks:

4. $f_{sxcr} = (f_x + v\cot\theta + v_{ci}\cot\theta)/\rho_x$
5. $f_{sycr} = (f_y + v\tan\theta - v_{ci}\tan\theta)/\rho_y$

Geometric Conditions:

Average Strains:

6. $\tan^2\theta = \dfrac{\varepsilon_x + \varepsilon_2}{\varepsilon_y + \varepsilon_2}$
7. $\varepsilon_1 = \varepsilon_x + \varepsilon_y + \varepsilon_2$
8. $\gamma_{xy} = 2(\varepsilon_x + \varepsilon_2)\cot\theta$

Crack Width:

9. $w = s_\theta \varepsilon_1$
10. $s_\theta = 1/\left(\dfrac{\sin\theta}{s_x} + \dfrac{\cos\theta}{s_y}\right)$

Stress-Strain Relationships:

Reinforcement:

11. $f_{sx} = E_s \varepsilon_x \le f_{ys}$
12. $f_{sy} = E_s \varepsilon_y \le f_{yy}$

Concrete:

13. $f_2 = \dfrac{f_c'}{0.8 + 170\varepsilon_1}\left[2\dfrac{\varepsilon_2}{\varepsilon_c'} - \left(\dfrac{\varepsilon_2}{\varepsilon_c'}\right)^2\right]$
14. $f_1 = 0.33\sqrt{f_c'}\,/\left(1 + \sqrt{500\varepsilon_1}\right)$

Shear Stress on Crack:

15. $v_{ci} \le \dfrac{0.18\sqrt{f_c'}}{0.31 + \dfrac{24w}{a_g + 16}}$
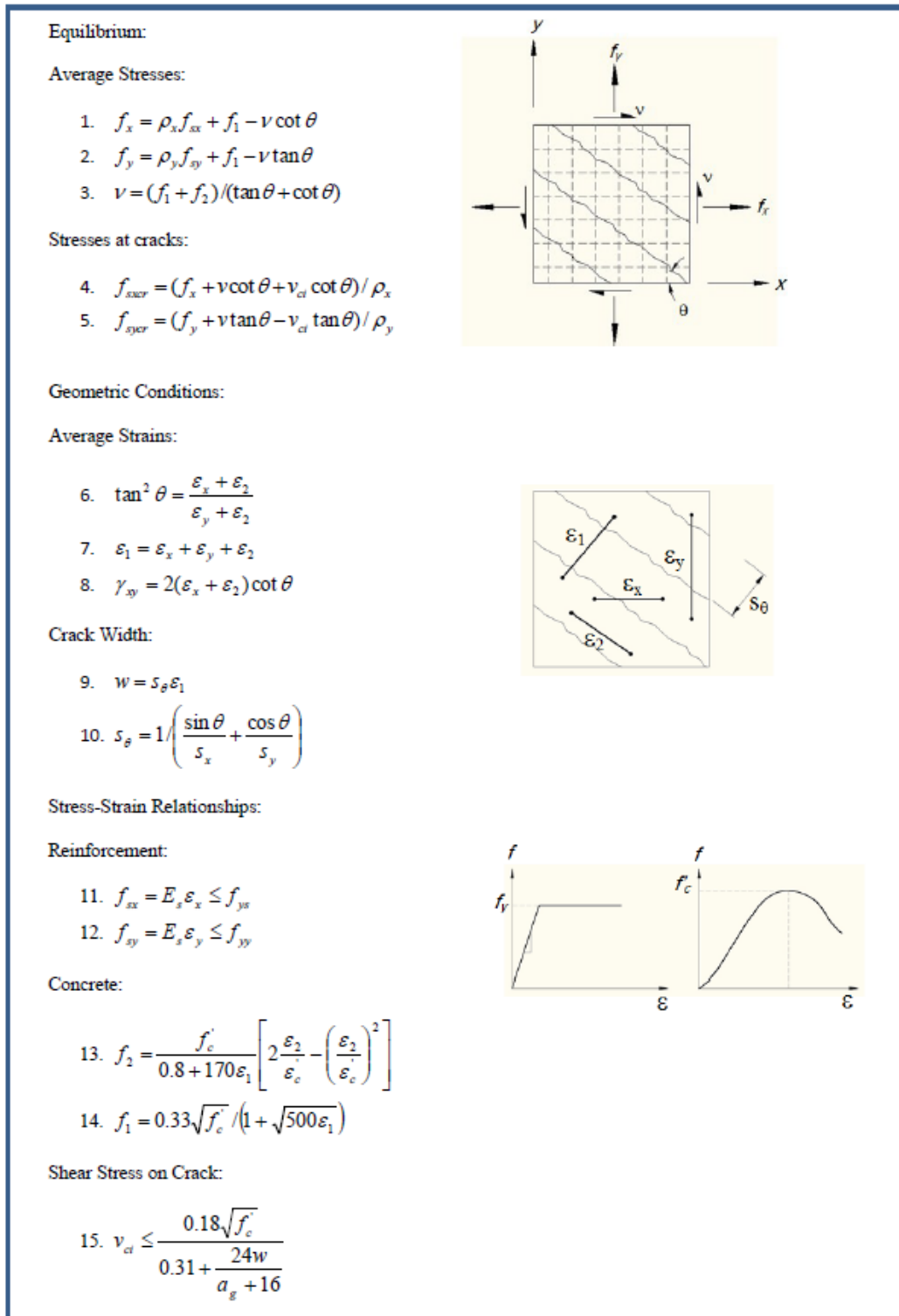
Figure 2-4-Equations of Modified Compression Field Theory [9]

Additionally, the program assumes that there are no transverse clamping stresses near point loads and supports. These assumptions might be correct for slender beams, which most likely fail in regions that are not near point loads or supports. However, in the case of disturbed regions, such as deep beams, these assumptions are far from correct and their implementation would lead most likely to inaccurate predictions.

Based on the results obtained from tests on concrete panels, Vecchio and Collins [9] develop a shear strength-axial strength interaction diagram (Figure 2-5) for reinforced concrete that can be used to predict the type of failure in beams with different mechanisms. In the case of strut-and-tie or arch action mechanism, when the applied force is transferred to the support by the strut or arch, the concrete in the shear span is subjected to high compressive stresses and failure is expected to be by concrete crushing. In this case the compressive strength of concrete plays a significant role in carrying the shear. In the case of the truss mechanism, due to high tensile stresses in the shear span (resisted by concrete in tension and vertical shear reinforcement), the expected failure is due to yielding of the shear reinforcement rather than crushing of the concrete. In such case, the tensile strength of concrete has more influence on the shear capacity than the compressive strength.
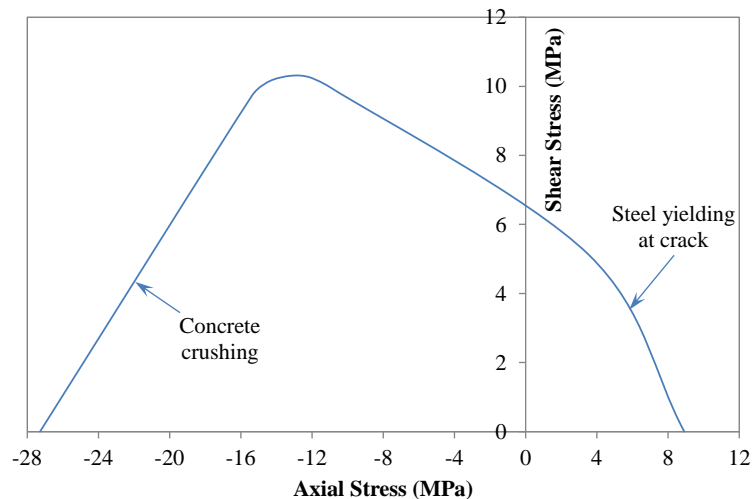
Figure 2-5-Shear strength-axial strength interaction diagram for reinforced concrete [9]

13

2.3. EFFECT OF DIFFERENT DESIGN PARAMETERS ON THE SHEAR CAPACITY OF RC BEAMS

To assess the effect of different design parameters on the shear capacity of RC beams, a database was compiled from the experimental data obtained from research studies found in the literature spanning 60 years. A total of 1629 RC beams are included, all of which were reported to have failed in shear. The specimens are divided into two groups. The first group comprises beams without shear reinforcement and includes 1252 specimens. The concrete compressive strength of the tested beams in the first group ranges from 6 to 128MPa, while overall beam depth ranges from 25 to 2200mm, shear span to depth ratio from 0.25 to 9.4, and the main steel reinforcement ratio from 0.09 to 7.94%. The second group comprises beams with shear reinforcement (vertical or horizontal shear reinforcement) and contains 377 RC beams. The concrete compressive strength of these beams ranges from 14 to 125MPa, overall beam depth from 160 to 2000mm, shear span to depth ratio from 0.27 to 4.01, main steel reinforcement ratio from 0.16 to 6.7%, vertical shear reinforcement ratio from 0 to 2.45% and horizontal shear reinforcement ratio from 0 to 3.17%. Full details are given in Appendix A.

2.3.1. CONCRETE COMPRESSIVE STRENGTH

The compressive strength of concrete has been reported to be the most important parameter influencing shear behaviour of members without shear reinforcement [48]. Figure 2-6 shows the effect of concrete compressive strength on the normalized shear capacity of RC beams. Its effect is more pronounced in short span beams [49, 50] as shown in Figure 2-7, in which the mechanism of shear load transfer is primarily strut-and-tie or arch action, while in slender beams the truss action reduces the effect of concrete compressive strength and the capacity is mostly controlled by tensile strength as mentioned in the previous section (Figure 2-5).
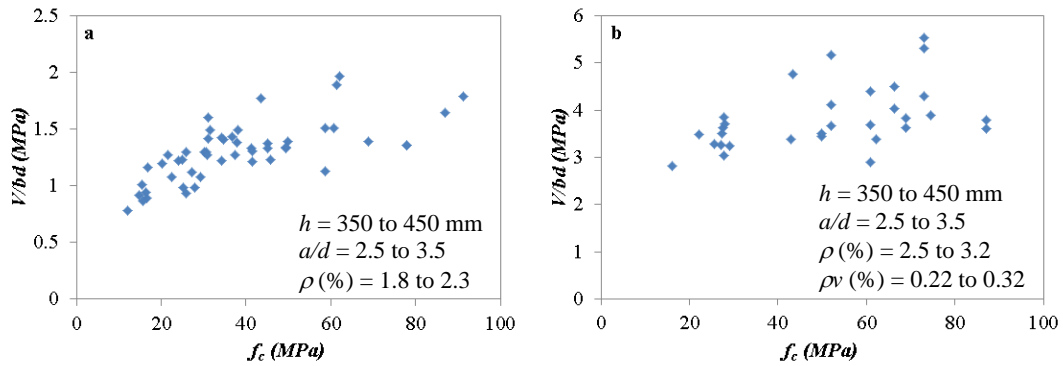
Figure 2-6-Effect of concrete compressive strength on the shear strength of a) RC beams without shear reinforcement and b) with shear reinforcement
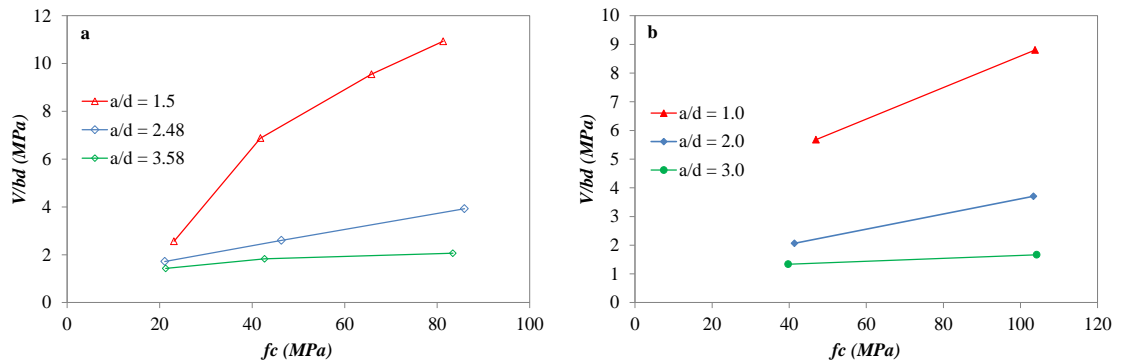
Figure 2-7-Effect of concrete compressive strength on the shear strength of a) RC beams without shear reinforcement [49] b) RC beams with shear reinforcement [50] with different shear span to depth ratio

2.3.2. SHEAR SPAN TO DEPTH RATIO

Another critical parameter that affects the behaviour of RC beams in shear is the shear span to depth ratio (a/d). In 1967 Kani [20] found out that there is a strong relation between the shear behaviour of RC members and their shear span to depth ratio. He also concluded that when shear failure occurs, in some cases, the beam is not developing its full flexural capacity, and this is controlled by shear span to depth ratio as shown in Figure 2-8. This was confirmed by other researchers such as Tan et al. [51] and Oh and Shin [52]. Figure 2-9 shows the effect of shear span to depth ratio on the shear capacity of RC beams.

15
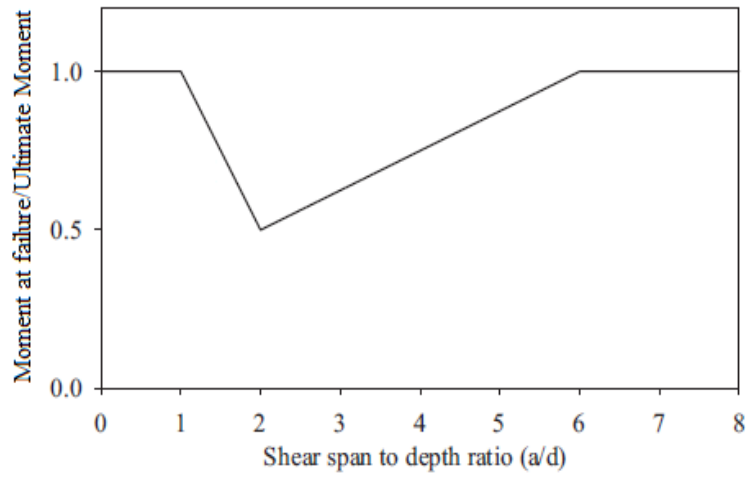
Figure 2-8-Kani's Shear Valley
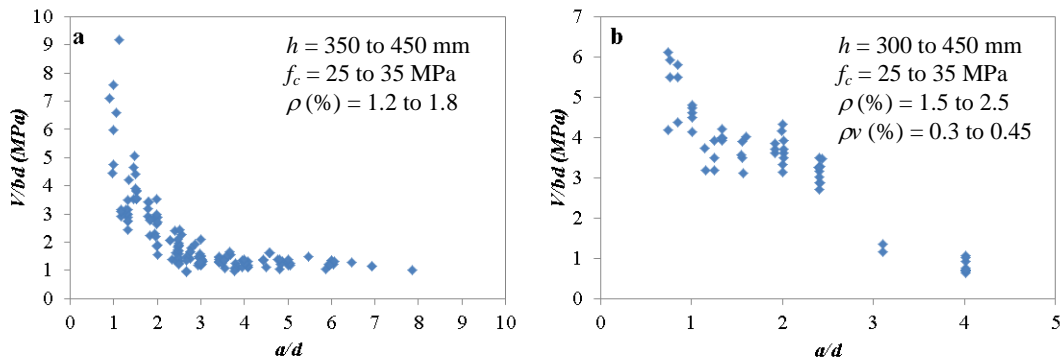
Figure 2-9-Effect of shear span to depth ratio on the shear strength of a) RC beams without shear reinforcement and b) with shear reinforcement

According to the experimental results of Leonhardt & Walther [53], Kani [20] and Kim & Park [54], the effect of shear span to depth ratio is negligible on the shear strength of RC beams when the shear span to depth ratio is greater than three (Figure 2-10), but has great influence on the shear capacity for values less than three as shown in Figure 2-10.

16
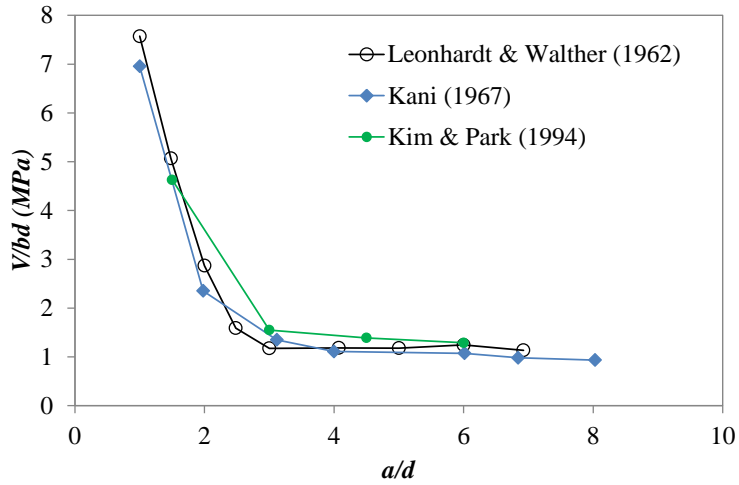
Figure 2-10-Effect of shear span to depth ratio on the shear strength of RC beams

2.3.3. VERTICAL SHEAR REINFORCEMENT

Prior to diagonal cracking, concrete resists predominantly the applied shear stress and shear reinforcement carries almost zero stress [44]. After the formation of diagonal cracks, a portion of the applied shear force is transferred by the shear reinforcement through truss action. Figure 2-11 shows the effect of shear reinforcement ratio on the shear capacity of RC beams. This action is more effective in slender beams as there is more room in the shear span to develop a proper truss and experimental results show that by increasing vertical shear reinforcement ratio (ρ_v) the shear capacity of the specimen increases [55] as shown in Figure 2-12.
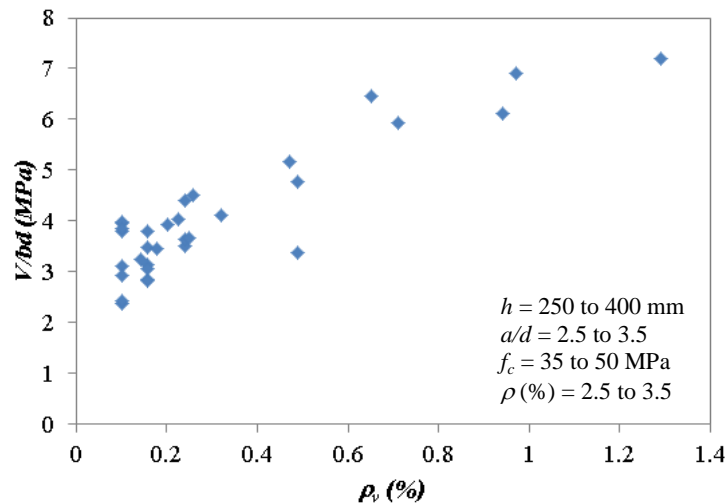
Figure 2-11-Effect of shear reinforcement ratio on the shear strength of RC beams

17
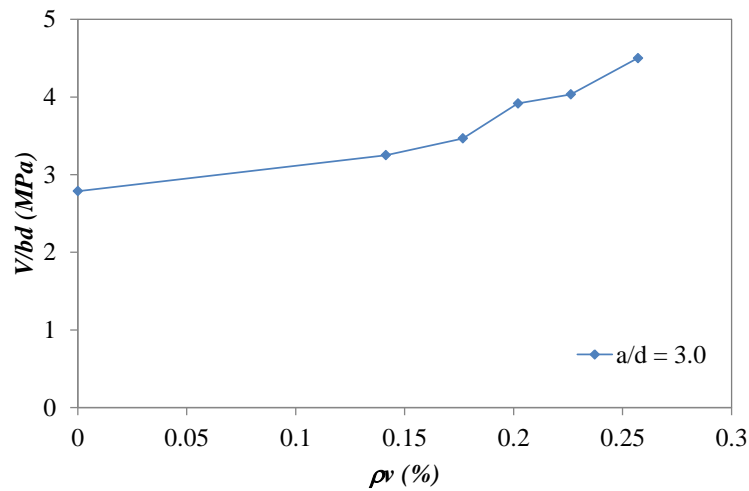
Figure 2-12-Effect of shear reinforcement on the shear strength of RC slender beams [55]

In the case of deep beams, shear reinforcement helps provide confinement to the concrete, control crack propagation and transfers shear force by truss action. However, the truss action is less effective compared to slender beams, because in deep beams most of the applied shear force is transferred by the strut-and-tie action. According to experimental results by Smith and Vantsiotis [1], providing sufficient shear reinforcement can increase shear capacity, but further increase in shear reinforcement does not enhance the shear capacity (see Figure 2-13) as failure is dominated by crushing of the concrete.
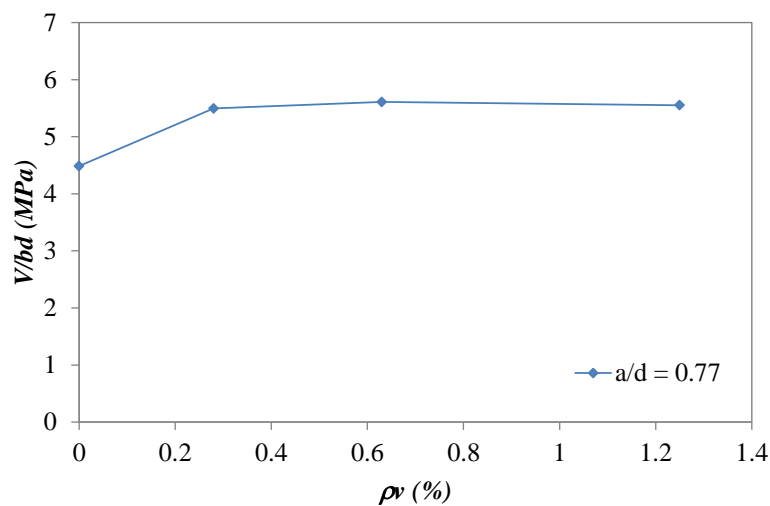
Figure 2-13-Effect of shear reinforcement on the shear strength of RC deep beams [1]

2.3.4. SIZE EFFECT

Since Kani's [20] early work in 1967 on reinforced concrete beams with different sizes, much research has been undertaken to investigate the influence of size on the behaviour and shear strength of reinforced concrete beams. Size effect is a phenomenon of a decrease in average shear strength due to increasing depth of the member. It has been confirmed that by increasing the depth of beams, the shear strength decreases and this is also reflected in Figure 2-14. Figure 2-15 shows the experimental results of the beams tested by Taylor [21], Bazant and Kazemi [24] and Kawano and Wantanabe [56], and it can be seen that by increasing the member depth the shear strength reduces. These experimental results led to Bazant's crack band theory [22, 24, 26, 27]. A number of other experimental investigations [26, 57] focused on the size effect in beams with shear reinforcement and they found that size effect is still present (Figure 2-16). In 2007, Bazant et al. [58] explained that though shear reinforcement can reduce the size effect in RC beams, it cannot eliminate size effect completely.
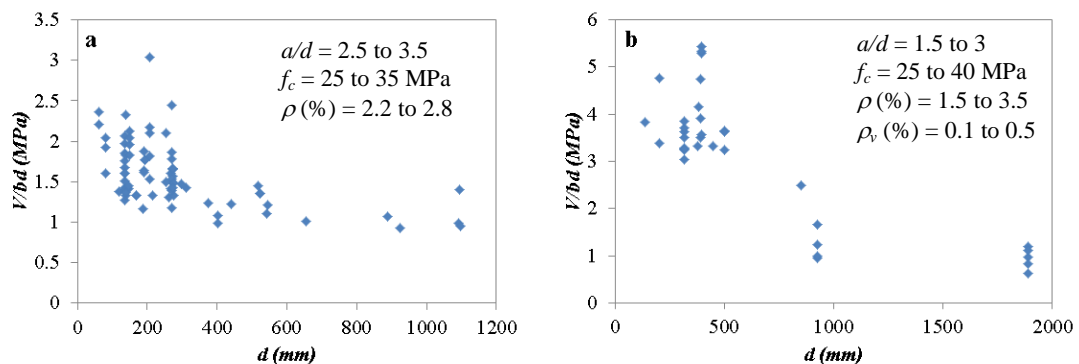
Figure 2-14-Effect of member depth on the shear strength of a) RC beams without shear reinforcement and b) with shear reinforcement.

19
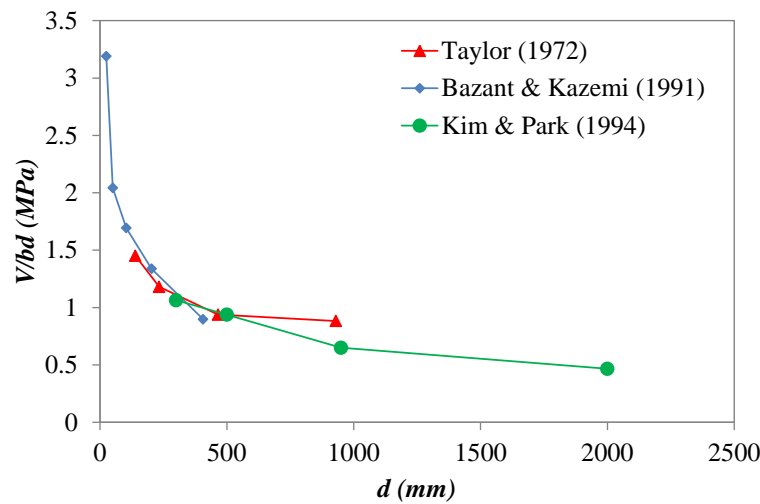
Figure 2-15-Effect of size of the beam on the shear strength
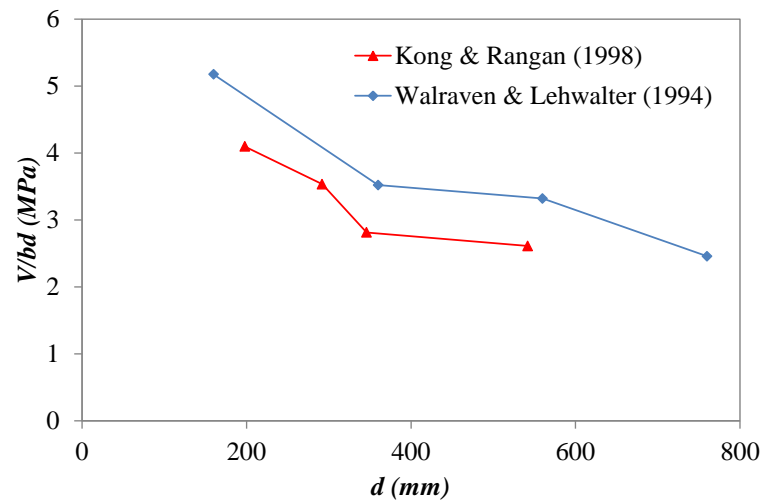
Figure 2-16-Size effect in beams with shear reinforcement

2.3.5. FLEXURAL REINFORCEMENT

Flexural reinforcement can influence shear capacity of RC beams by means of a) dowel action through a combination of the tensile resistance of the concrete across the splitting plane and the bending capacity of the reinforcement bar, and b) controlling the neutral axis depth which affects the portion of the shear stresses transferred through the compression zone. According to Wight and MacGregor [44] flexural reinforcement also

affects friction and aggregate interlock mechanisms as flexural cracks extend higher and open wider in beams with smaller flexural reinforcement ratios. Figure 2-17 shows the effect of flexural reinforcement on the shear capacity of RC beams.
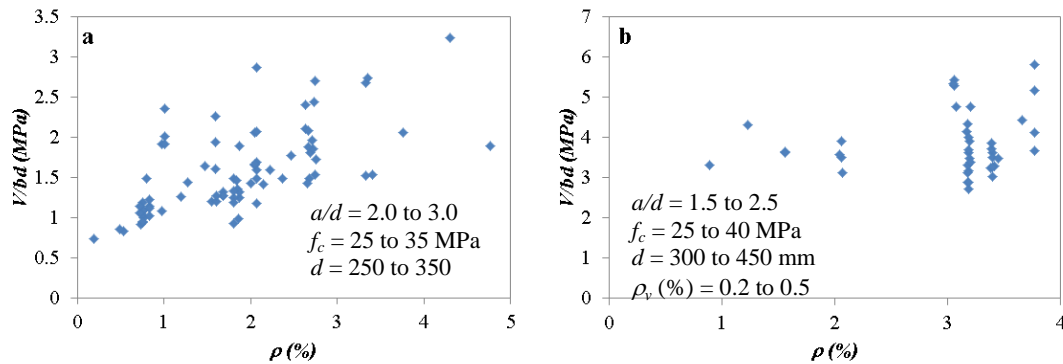
Figure 2-17-Effect of flexural reinforcement on the shear strength of a) RC beams without shear reinforcement and b) with shear reinforcement.

2.3.6. AGGREGATE SIZE

Friction and aggregate interlock provide one of the major shear transfer mechanisms in RC beams without shear reinforcement. In 1970, Taylor [59] concluded that the relative magnitude of the shear force transferred by aggregate interlock can be estimated to be between 33 % and 50% of uncracked concrete for beams without shear reinforcement. However, in beams with shear reinforcement as crack sliding is restrained by the presence of shear links, this mechanism is likely to be less effective. This mechanism is controlled by the roughness of crack surfaces which changes with aggregate size. However, Walraven [60] concluded that the crack surface roughness is a function of concrete strength and type of aggregate rather than aggregate size. Figure 2-18 shows the effect of aggregate size on the shear capacity of RC beams. There is no conducive trend as the larger aggregate were also likely to have been used in larger beams.
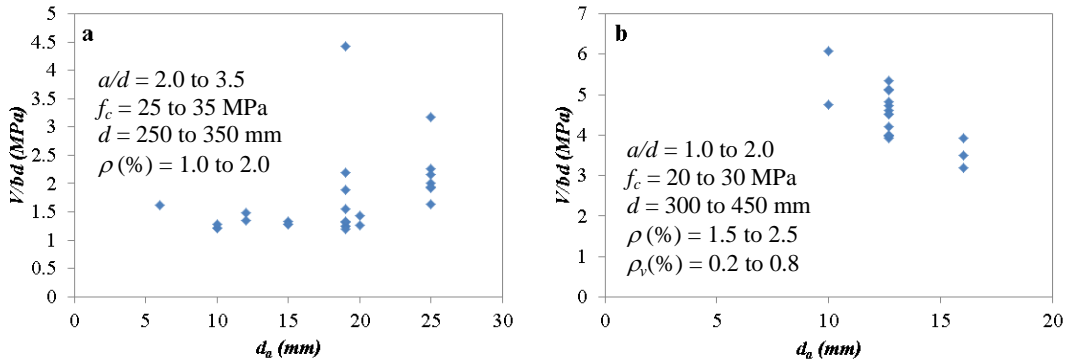
Figure 2-18-Effect of aggregate size on the shear strength of a) RC beams without shear reinforcement and b) with shear reinforcement.

2.4. EVALUATION OF AVAILABLE SHEAR MODELS

There are numerous models in the literature proposed to predict the shear capacity of RC beams, too many to cover in this thesis. What is common at the end of the day they all rely on calibration against empirical data. The most used shear design procedures for RC members with and without shear reinforcement (Eurocode 2 (EC2) [3], ACI 318-14 [4], Model code 2010 [12] and Modified Compression Field Theory [9]) are evaluated against experimental data in the database to assess their effectiveness and identify their weaknesses.

2.4.1. EUROCODE SHEAR PROVISION

2.4.1.1. Beams without Shear Reinforcement

Eurocode 2 [3] provides an empirical equation (Eq.2.1) to predict the ultimate shear strength of RC beams without shear reinforcement. This equation accounts for the effect of concrete compressive strength, flexural reinforcement and size effect.

$$V = \left[C_{Rd,c} (100\rho_1 f_{ck})^{1/3} (1 + \sqrt{\frac{200}{d}}) \right] b_w d \qquad (2.1)$$

where ρ_1 is the percentage of longitudinal reinforcement, f_{ck} is the characteristic concrete compressive strength, d is the effective depth of the member, and b_w is the width of the member. For members loaded within a distance 2d from the support, the capacity is increased by the ratio *2d/a*, where *a* is shear span of the member, to account for the increase in shear strength due to arch action.

The accuracy of EC2 in predicting the shear strength of RC beams without shear reinforcement was assessed against the compiled database. As shown in Figure 2-19, this analysis indicates that while the EC2 equation can predict relatively well the shear strength of slender beams, a large scatter is observed in predicting the shear strength of short shear span members.

To assess the effect of each of the parameters included in the EC2 equation, smaller data samples were extracted from the database so that only the examined parameter varied within each group while all of the other parameters were constant.
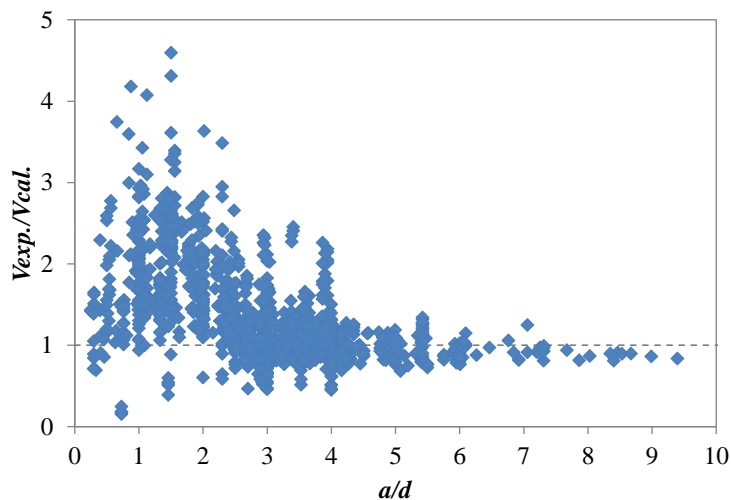
Figure 2-19-Predicting shear strength of beams without stirrups by EC2 procedure.

Concrete compressive strength

The effect of concrete compressive strength was examined based on a group of 211 RC beams without shear reinforcement as shown in Figure 2-20. The value of concrete compressive strength in this group ranged from 14.6 to 127.5 MPa. Although the range of applicability of compressive strength of concrete in EC2 is 90 MPa, in this analysis the equation is used for the entire range. Test results indicate that the effect of concrete compressive strength on the member shear strength is mainly controlled by shear span to depth ratio as shown in Figure 2-21. EC2 equation for shear strength underestimates the influence of concrete compressive strength for members with shear span to depth ratio less than two; however, predictions for beams with shear span to depth ratio greater than two are in better agreement with the tests results.
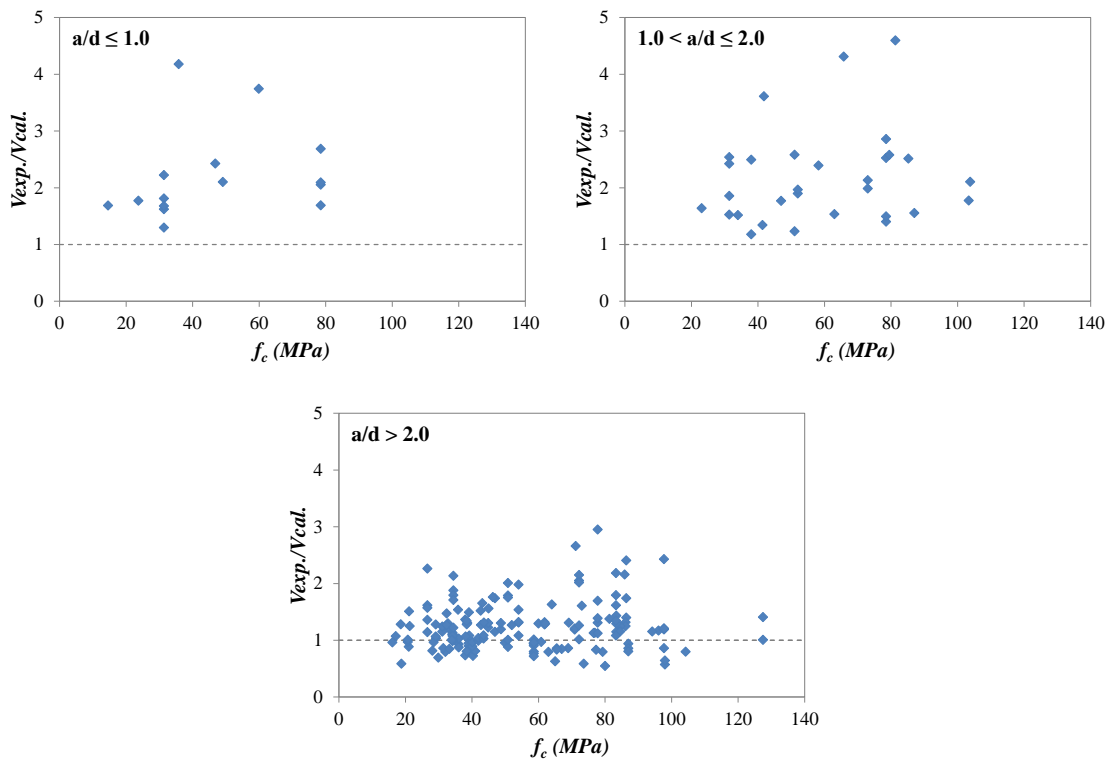
Figure 2-20-Effect of concrete compressive strength on predicting of shear strength for beams without stirrups by EC2 procedure
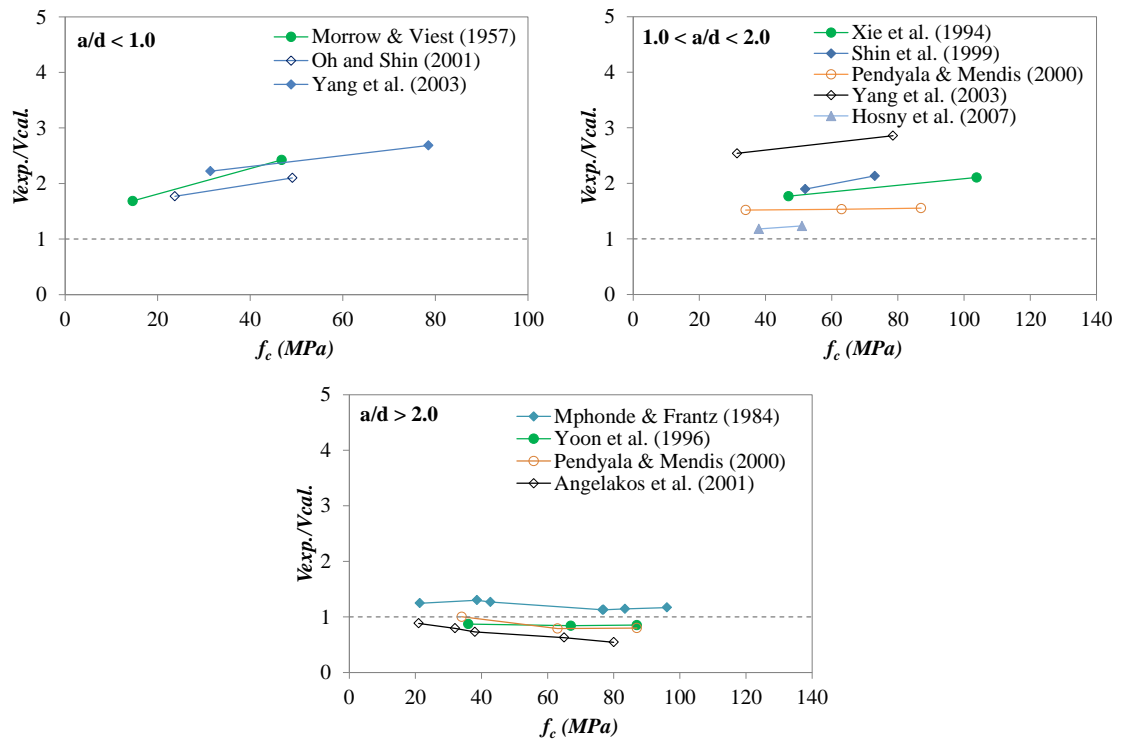
Figure 2-21-Effect of concrete compressive strength for different shear span to depth ratio on predicting of shear strength for beams without stirrups by EC2 procedure

Flexural reinforcement ratio

The effect of the main flexural reinforcement ratio is examined in the following. Experimental results of Collins et al. [2] showed that shear strength of RC beams without shear reinforcement is related to the percentage of and strain developed in longitudinal reinforcement. It was reported that shear strength of beams decreased when the strain in longitudinal reinforcement increased. This is because with increasing strain in the flexural reinforcement cracks widen and the contribution of shear stress transfer by both compression and aggregate interlock reduce as explained earlier. The EC2 prediction seems to have a good correlation with the experimental results for slender beams. However, more conservative results are obtained for RC deep beams, as shown in Figure 2-22.
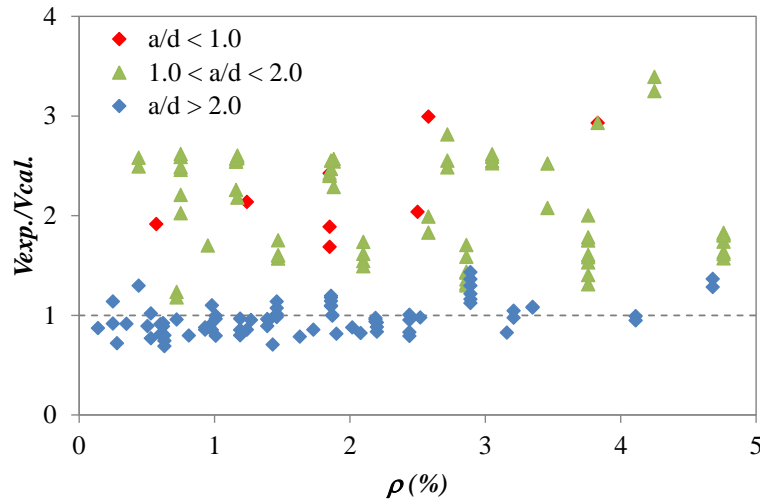
Figure 2-22-Effect of main longitudinal reinforcement ratio on predicting of shear strength for beams without shear reinforcement by EC2 procedure.

Shear span to depth ratio

EC2 predictions are also overall accurate for slender beams; however, these predictions become very conservative with a great scatter for deep beams, as shown in Figure 2-23. This can be attributed to the fact that the 'enhancement factor' used in EC2 to account for the increase in shear resistance cannot accurately capture the development of the different shear resisting mechanisms (e.g. arch action) in members with shear span to depth ratio less than two.
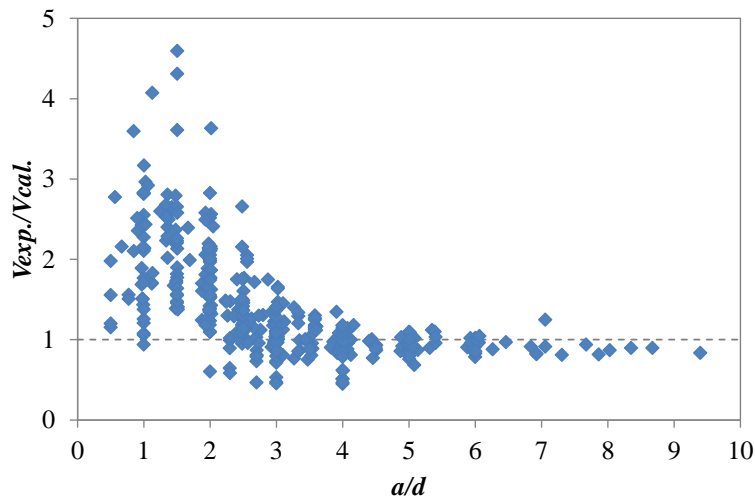
Figure 2-23-Predicting of shear strength for beams without shear reinforcement by EC2 procedure (Effect of a/d).

Size effect

EC2 equation accounts well for the influence of size effect for RC beams without shear reinforcement; however predictions are affected by a significant scatter and can be unsafe for beams with effective depth larger than 1000mm as shown in Figure 2-24.
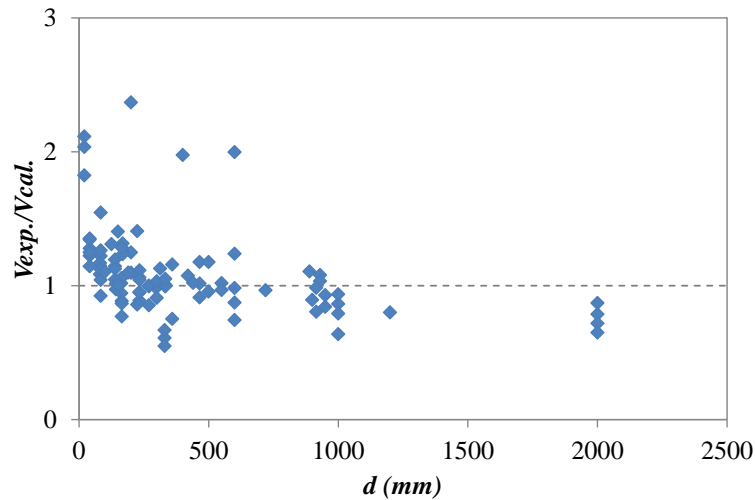
Figure 2-24-Predicting of shear strength for beams without shear reinforcement by EC2 procedure (Effect of depth).

2.4.1.2. Beams with Shear Reinforcement

The EC2 shear design procedure for the members with shear reinforcement (Eq. 2.2) is based on the plasticity theory and the truss model. This model accounts for the effect of transverse steel reinforcement and strut inclination with respect to the member's neutral axis in the range of $21.8°$ to $45°$. The result of this equation should be multiplied by an amount equal to *2d/a* as an enhancement factor to account for the increase in shear capacity due to arch action in members with shear span to depth ratio less than or equal to two.

$$V_{Rd,s} = \frac{A_{sw}}{s} z f_{ywd} (\cot \theta + \cot \alpha) \sin \alpha \qquad (2.2)$$

where A_{sw} is the cross-sectional area of shear reinforcement, *s* is the spacing of shear reinforcement, *z* is lever arm (can be considered as *0.9d*), f_{ywd} is the yield strength of the

27

shear reinforcement, θ is the angle of the inclined struts, and α is the angle of the stirrups with respect to the axis of the member.

To evaluate the accuracy of this equation in predicting the shear strength of RC members with vertical links, 382 RC beams available in the literature were utilised. The comparison indicates that analytical predictions are affected by a large scatter, as shown in Figure 2-25.
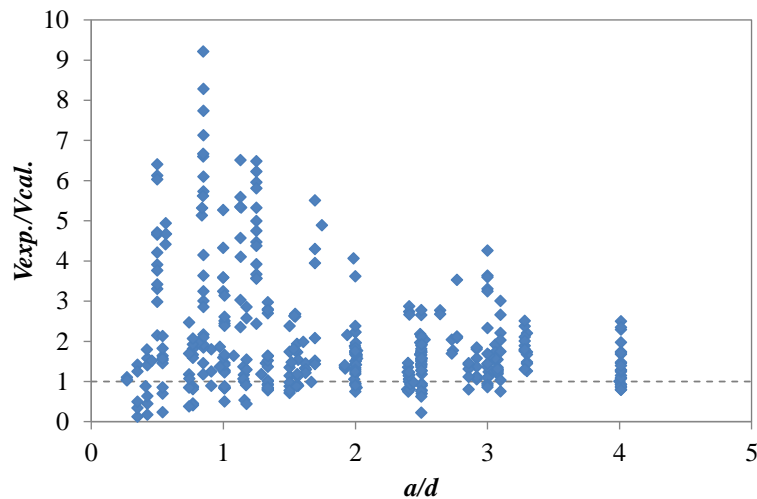
Figure 2-25-Comparison of experimental and predicted shear strength by EC2 for beams with stirrups

The model tends to be overall very conservative for members with shear reinforcement ratio less than 0.25% (Figure 2-26) and can become unsafe for members with shear reinforcement ratio higher than 0.5%. This inadequacy can be partly attributed to the fact that the EC2 shear model depends only on the truss action and neglects the contribution of concrete in transferring shear stresses. For members loaded within a distance smaller than two times the effective member depth, EC2 suggests that the result of the Eq. 2.2 is multiplied by an enhancement factor (*2d/a*) to increase shear strength due to arch action. This enhancement increases the degree of scatter and the prediction becomes very conservative in this region.
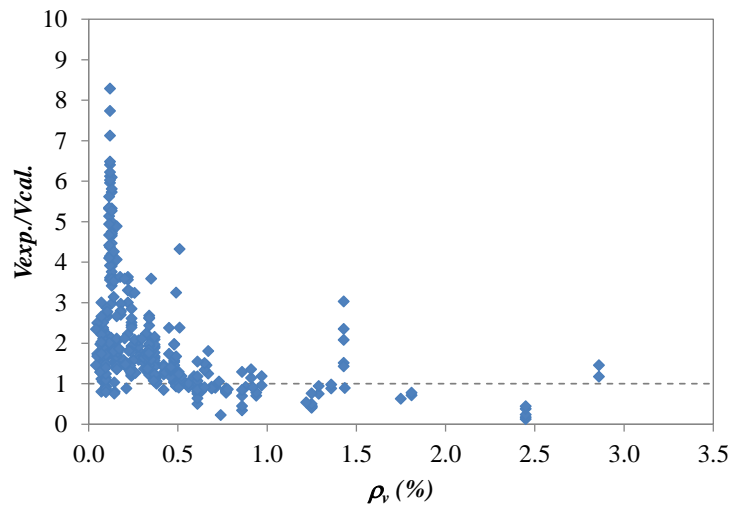
Figure 2-26-Effect of shear reinforcement ratio on predicting of shear strength by EC2 procedure.

Concrete compressive strength

The analysis of experimental results of Yoon et al. [61] on RC beams with varying concrete strength (Figure 2-27) indicates that the influence of shear links on the ultimate shear strength decreases as concrete strength increases. Also concrete compressive strength has greater role in carrying shear strength than shear reinforcement for short shear span members. Thus, neglecting the contribution of concrete in transferring shear stresses by EC2 shear model leads to conservative results for beams that are lightly reinforced in shear (shear reinforcement ratio less than 0.25%) and becomes unsafe with the increasing shear reinforcement ratio (Figure 2-26).
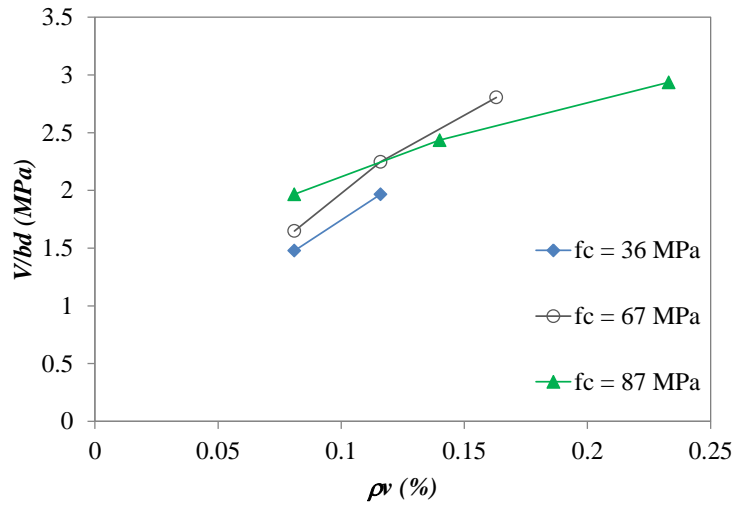
Figure 2-27-Effect of concrete compressive strength on the efficiency of vertical shear reinforcement.

Shear span to depth ratio

Experimental results by Smith and Vantsiotis [1] indicate that vertical shear reinforcement has minor influence on the ultimate shear strength of members with shear span to depth ratio less than two and its impact seems to decrease considerably for beams loaded within a distance equal to the effective member depth from the support. Figure 2-28 shows the influence of shear reinforcement on beams with different shear span to depth ratio.
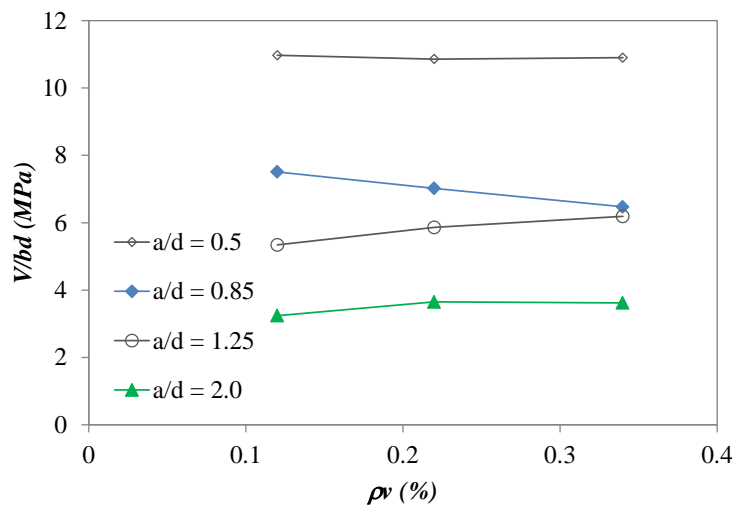
Figure 2-28-Effect of shear span to depth ratio on the efficiency of vertical shear reinforcement [52].

Size effect

In calculating the shear strength of RC beams the size effect should always be taken in consideration for members with or without shear reinforcement. Research shows that the presence of shear reinforcement can reduce the influence of size effect on the shear strength of RC members, but size effect is always present [58]. Nevertheless, as the concrete contribution is neglected in the EC2 design procedure for beams with transverse reinforcement, size effect cannot be taken in consideration. This results in very conservative predictions for small size members, whilst the degree of conservatism decreases with increasing member depth. Figure 2-29 shows a comparison between experimental and predicted results according to the EC2 shear model.
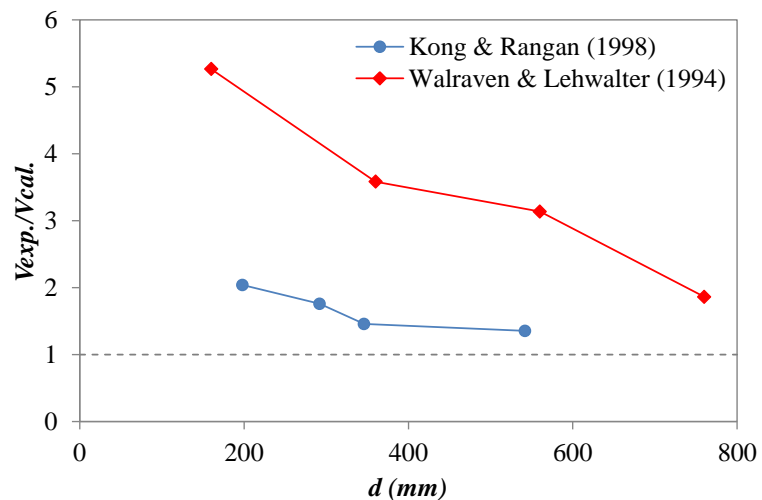
Figure 2-29-Experimental shear strength and EC2 shear strength prediction for beams with shear reinforcement (Size effect).

2.4.2. EVALUATION OF SHEAR PROVISIONS OF ACI 318-14 CODE

Based on the concept of average shear stress acting on the full effective cross section, ACI 318-14 [4] provides simple equations to calculate the strength at first diagonal crack of RC beams. In a member without shear reinforcement, the shear strength is carried by the concrete web of the member and can be calculated using Eq.2.3. This

equation accounts for the influence of concrete compressive strength, main flexural reinforcement ratio and shear span to depth ratio. For the sake of simplicity, ACI 318-14 [4] allows the replacement of the second term of Eq.3 with $0.01\sqrt{f'_c}$ leading to simplified Eq. 2.4, which only accounts for the effect of concrete compressive strength. In a member with shear reinforcement a part of the applied shear force is carried by the concrete web and the remaining is carried by the shear reinforcement. Eq. 2.5, which is based on the truss analogy, is used to calculate the contribution of shear reinforcement to the overall shear capacity of the RC members.

$$V_c = (0.16\sqrt{f'_c} + 0.17\rho_w \frac{V_u d}{M_u})b_w d \tag{2.3}$$

$$V_c = 0.17\sqrt{f'_c}b_w d \tag{2.4}$$

$$V_s = \frac{A_v f_{yt}(\sin\alpha + \cos\alpha)d}{s} \tag{2.5}$$

where f'_c is the concrete compressive strength, ρ_w is the main flexural reinforcement ratio; V_u/M_u is the ratio of shear force and bending moment at the section being considered; b_w, d are the width of the web and effective depth of the member, respectively, A_v is the area of transverse reinforcement, f_{yt} yield strength of transverse reinforcement, α is the angle between inclined stirrups and longitudinal axis of the member, and s is the spacing of the transverse reinforcement measured in the direction of the longitudinal reinforcement. The value of $\sqrt{f'_c}$ should not exceed 8.3 MPa and the ratio $V_u d/M_u$ in Eq. 3 can be considered as d/a, where a is the shear span of the member.

Concrete compressive strength

The accuracy of the aforementioned equations in predicting shear strength was examined against the experimental database. The result of this comparison indicates that the ACI 318-14 [4] equations underestimate the influence of concrete compressive strength on the ultimate shear strength of RC beams without shear reinforcement

(Figure 2-30) and this underestimation increases for members with shear span to depth ratio less than two. This can be attributed to the fact that ACI 318-14 shear equations are based on the cracking shear force rather than the ultimate shear force. However, the ultimate shear capacity of RC beams is not limited to the load causing initiation of diagonal cracking. Once the first diagonal crack develops, the stiffness of the member decreases significantly but shear force can still be transferred through different shear transfer mechanisms such as friction, aggregate interlock, dowel action, as well as significant arch action in members with shear span to depth ratio less than two.

For members with concrete compressive strength more than 70MPa, ACI318-14 becomes more conservative as summarized in Table 2-1.
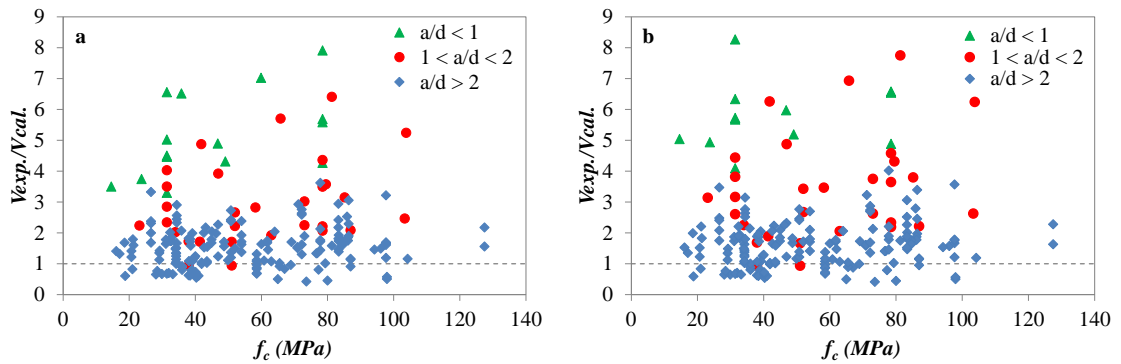
Figure 2-30-Shear strength prediction of RC beams without shear reinforcement by ACI 318-14 a) more detailed equation (Eq. 2.3) and b) simplified equation (Eq. 2.4).

Table 2-1: ACI 318-14 shear strength prediction (Effect of concrete compressive strength)

	$f_c < 70$MPa		$f_c \geq 70$MPa	
	Simplified method (Eq. 2.4)	Detailed method (Eq. 2.3)	Simplified method	Detailed method
Mean	2.12	1.83	2.47	2.26
STD	2.01	1.24	1.68	1.40
COV	0.95	0.67	0.68	0.62

Flexural reinforcement ratio

The second parameter that is considered in ACI 318-14 detailed shear equation (Eq. 2.3) is the main flexural reinforcement ratio. From an analysis of Figure 2-31 it is clear that predictions are unsafe for members with main flexural reinforcement ratio less than 0.01, whilst these become conservative with a great degree of scatter for members that are heavily reinforced in flexure.
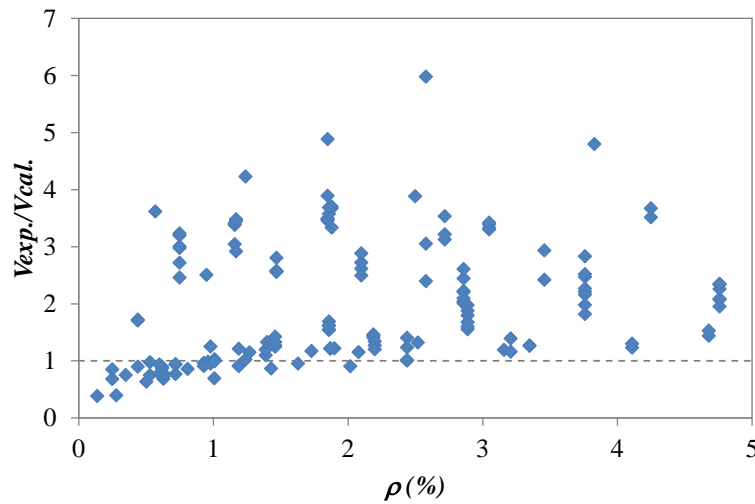
Figure 2-31-ACI 318-14 shear strength prediction of RC beams without shear reinforcement (Effect of main flexural reinforcement ratio).

Shear span to depth ratio

Despite the fact that shear span to depth ratio has been shown to affect greatly shear behaviour, ACI 318-14 [4] considers this ratio as a minor parameter when determining the strength of both deep and slender beams. As a result, predictions become very conservative with a high degree of scatter for deep beams and tend to approximate better the experimental results for higher shear span to depth ratios. Figure 2-32 shows shear strength predictions for members without shear links against shear span to depth ratio.
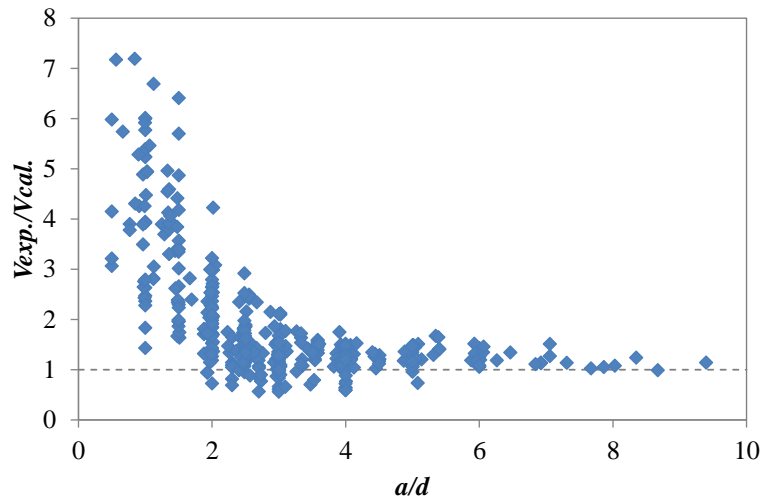
Figure 2-32-ACI 318-14 shear strength prediction of RC beams without shear reinforcement (Effect of shear-span-to-depth ratio).

Shear reinforcement

For members with shear reinforcement, ACI 318-14 [4] implements the classic equation based on the truss analogy theory (Eq. 2.5) to determine the contribution of shear reinforcement in transferring shear forces, while the portion of shear stress carried by the concrete web (Eq. 2.3 or 2.4) is assumed to be unaffected by the presence of shear reinforcement and their effects can be added together to estimate the total shear resistance. However, shear reinforcement also provides a confinement to the concrete in the web which enhances the concrete contribution and transfer of shear forces by the truss mechanisms. As a result, neglecting this interaction leads to very conservative results with a high degree of scatter as shown in Figure 2-33.
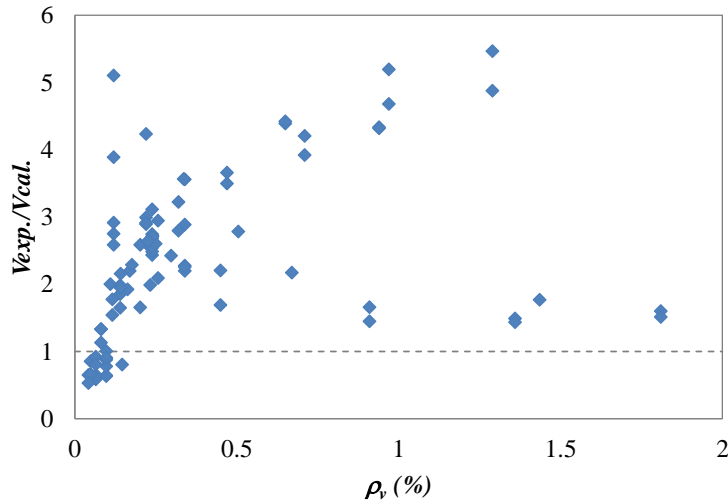
Figure 2-33-ACI 318-14 shear strength prediction of RC beams with shear reinforcement.

Size effect

The current ACI 318-14 shear design procedures can yield very unconservative predictions for large RC beams without shear reinforcement, as size effect is not taken into account. This is clearly shown in Figure 2-34 for beams with effective depth more than 1000mm. On the other hand, ACI 318-14 [4] requires that a minimum area of shear reinforcement be provided if the design factored shear force exceeds *0.5ϕVc*. The presence of shear reinforcement has been shown to mitigate size effect and this can moderate the unconservative nature of the ACI expression for *Vc* (see Figure 2-34). However, this aspect deserves more investigation, especially in the case of very deep members with shear reinforcement.
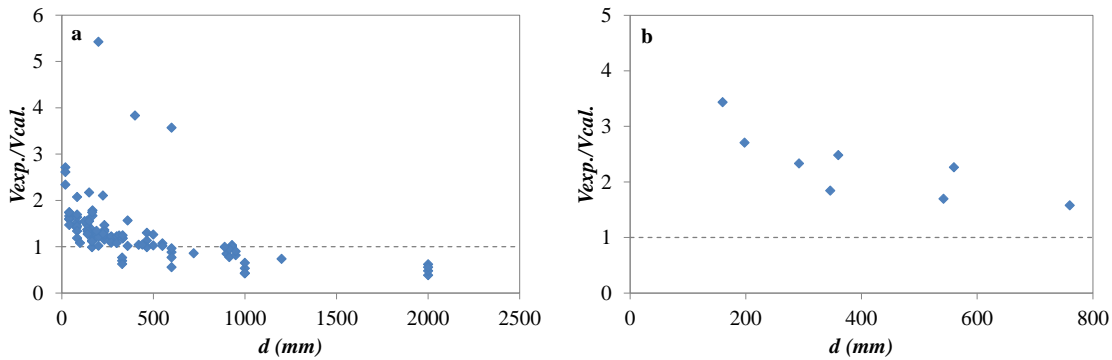
Figure 2-34-ACI 318-14 shear strength prediction of RC beams against size effect for members a) without shear reinforcement b) with shear reinforcement

36

Overall, for shear span to depth ratio greater than four, predictions obtained by implementing the ACI 318-14 shear design procedure are in good agreement with experimental results for beams without shear reinforcement, however, they are conservative for beams with shear reinforcement. With decreasing shear span to depth ratio, the degree of conservatism increases and predictions are affected by a high degree of scatter. This trend becomes more obvious when using the simplified equation (Eq. 2.4). Figure 2-35 and Figure 2-36 show the performance of ACI 318-14 against the experimental results included in the database described in section 2.3.
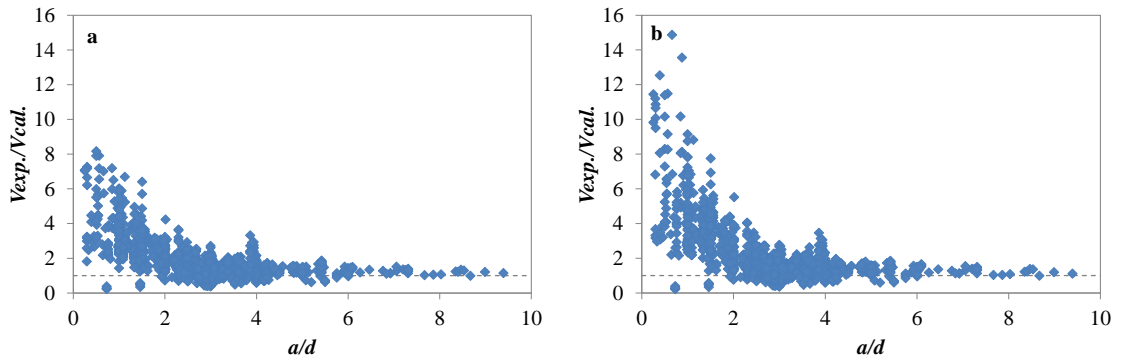
Figure 2-35-Shear strength prediction of RC beams without shear reinforcement by ACI 318-14 a) more detailed equation (Eq. 2.3) and b) simplified equation (Eq. 2.4)
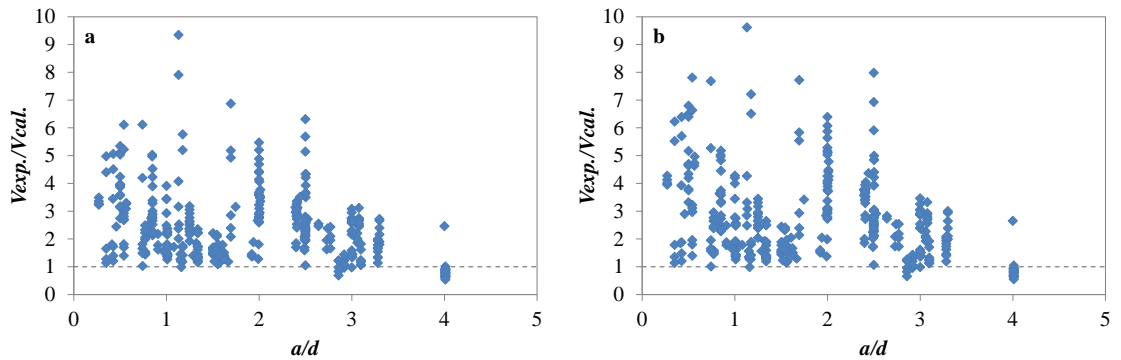
Figure 2-36-Shear strength prediction of RC beams with shear reinforcement by ACI 318-14 a) more detailed equation (Eq. 2.3) and b) simplified equation (Eq. 2.4).

2.4.3. EVALUATION OF SHEAR PROVISION OF MODEL CODE 2010

The shear design provisions included in the 2010 edition of Model Code [12] assume that the shear strength (V_{Rd}) of RC member is the summation of a concrete contribution ($V_{Rd,c}$) and shear resistance provided by shear reinforcement ($V_{Rd,s}$).

$$V_{Rd} = V_{Rd,c} + V_{Rd,s} \tag{2.6}$$

With a limiting value of:

$$V_{Rd\,max} = k_c \frac{f_{ck}}{\gamma_c} b_w z \frac{\cot\theta + \cot\alpha}{1 + \cot^2\theta} \tag{2.7}$$

The design shear resistance attributed to the concrete in Eq.2.6 can be determined as:

$$V_{Rd,c} = k_v \frac{\sqrt{f_{ck}}}{\gamma_c} z b_w \tag{2.8}$$

In members with a percentage of shear reinforcement exceeding $0.08\sqrt{f_{ck}} / f_{yk}$, the design shear resistance provided by stirrups can be determined as:

$$V_{Rd,s} = \frac{A_{sw}}{s_w} z f_{ywd} (\cot\theta + \cot\alpha) \sin\alpha \tag{2.9}$$

where b_w is the minimum concrete web width within the effective shear depth z, which can be taken as *0.9d*, θ is the inclination of compression stresses, α is the inclination of stirrups with respect to the beam axis. In Eq. 2.8, a maximum limiting value of $\sqrt{f_{ck}}$ equal to 8MPa is recommended. The value of k_c and k_v can be determined on the basis of different levels of approximation depending on the desired accuracy and complexity of the required analysis and design procedures.

Level I approximation can be used at the conceptual design stage and for members without a significant axial load. This level of approximation cannot be used for members with $f_{ck} > 64\text{MPa}$, $f_{yk} > 500\text{MPa}$, and maximum aggregate size smaller than 10mm. The angle θ is taken as 36. The values of k_c and k_v in Eq. 2.7 and Eq. 2.8 can be calculated as:

$$k_c = 0.5\left(\frac{30}{f_{ck}}\right)^{1/3} \leq 0.5 \tag{2.10}$$

$$k_v = \begin{cases} \dfrac{200}{(1000 + 1.3z)} \leq 0.15 & \text{if } \rho_w = 0 \\ 0.15 & \text{if } \rho_w \geq 0.08\sqrt{f_{ck}} \, / \, f_{yk} \end{cases} \tag{2.11}$$

The shear equations used for a Level II approximation are based on the variable truss field approach and are appropriate for members with shear reinforcement ratio not less than $0.12\sqrt{f_{ck}} \, / \, f_{yk}$. This level of approximation neglects the concrete shear resistance. For calculating shear resistance of shear reinforcement, the angle of inclination of the compression stresses must be within the range specified in Eq. 2.12. In this equation, ε_x is the mid-depth longitudinal strain and can be taken as 0.001 for a preliminary design. Model Code 2010 [12] allows designers to calculate ε_x based on section analysis and the principle of plane sections but ε_x shall not be taken smaller than -0.0002. The value of k_c can be determined according to Eq. 2.13.

$$20° + 10000\varepsilon_x \leq \theta \leq 45° \tag{2.12}$$

$$k_c = 0.55\left(\frac{30}{f_{ck}}\right)^{1/3} \leq 0.55 \tag{2.13}$$

Level III approximation is a general form of sectional shear model that is applicable to beams and slabs. The equations were derived based on the Modified Compression Field Theory (MCFT) [9] with the assumption that the member contains well-detailed reinforcement, especially in the longitudinal direction. According to this level of

approximation the shear stress is equally distributed throughout the effective member depth and the angle of compression stresses can be determined based on the longitudinal strain at mid-depth of the member (Eq. 2.14).

$$\theta = 29° + 7000\varepsilon_x \qquad (2.14)$$

$$\varepsilon_x = \frac{M_{Ed}/z + V_{Ed}}{2E_s A_s} \qquad (2.15)$$

where M_{Ed} and V_{Ed} are design moment and shear force at the section being analysed; and E_s and A_s are Young's modulus and cross-sectional area of the main longitudinal reinforcement. Calculating mid-depth longitudinal strain by Eq. 2.15 is quite simple for real design and analysis, however, in the case of prediction for research purposes, it is not easy to calculate this strain as the design moment and design shear force are not known; however, it can be calculated by performing sectional analysis and the principle of plane section [2, 62].

The values of k_c and k_v can be calculated as follows:

$$k_c = 0.5\left(\frac{30}{f_{ck}}\right)^{1/3} \leq 0.55 \qquad (2.16)$$

$$k_v = \begin{cases} \dfrac{0.4}{(1+1500\varepsilon_x)}\dfrac{1300}{(1000+0.7k_{dg}z)} \leq 0.15 & if \ \rho_w = 0 \\ \dfrac{0.4}{(1+1500\varepsilon_x)} & if \ \rho_w \geq 0.08\sqrt{f_{ck}}/f_{yk} \end{cases} \qquad (2.17)$$

where

$$k_{dg} = \frac{48}{16+d_g} \geq 1.15 \qquad (2.18)$$

in which d_g is aggregate diameter.

The performance of the shear provisions included in Model Code 2010 [12] was examined against the experimental shear strength of the beams available in the database. For beams without shear links, the prediction using Level I approximation is in good agreement with the experimental results for slender beams while prediction according to Level III are slightly unsafe for beams with shear span to depth ratio in the range of two to six but improve for higher slenderness ratios. In case of beams with shear span to depth ratio less than two (i.e. deep beams) the prediction according to both levels of approximation is very conservative but the predictions resulting from Level I approximation are affected by a higher degree of scatter. The performance of the predictive models implemented in both levels of approximation is shown in Figure 2-37.
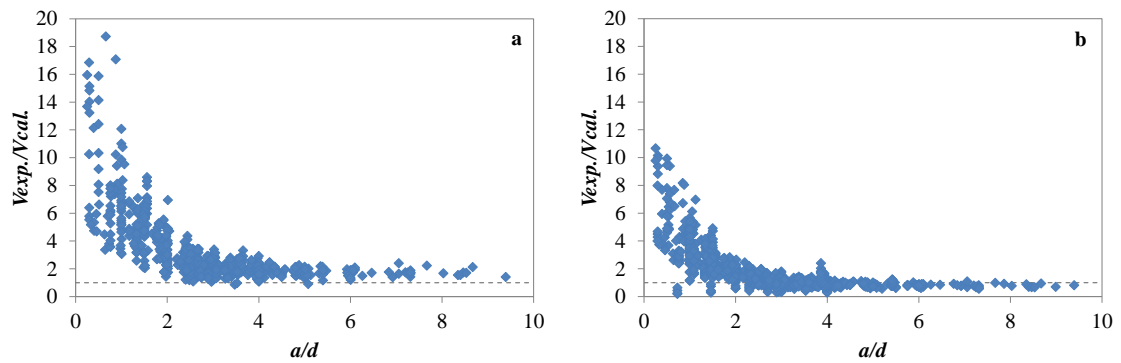
Figure 2-37-Predicting of shear strength for beams without shear reinforcement by Model Code 2010 a) Level I Approximation procedure and b) Level III Approximation procedure.

For slender beams with shear reinforcement, the predictions according to Level I and II approximation are in good agreement with the experimental results while level III approximation is slightly unsafe. For deep beams with shear links, the prediction of all levels of approximation is overly conservative with a high degree of scatter. The shear strength predictions for beams with shear reinforcement according to all levels of approximation against the experimental results are shown in Figure 2-38.
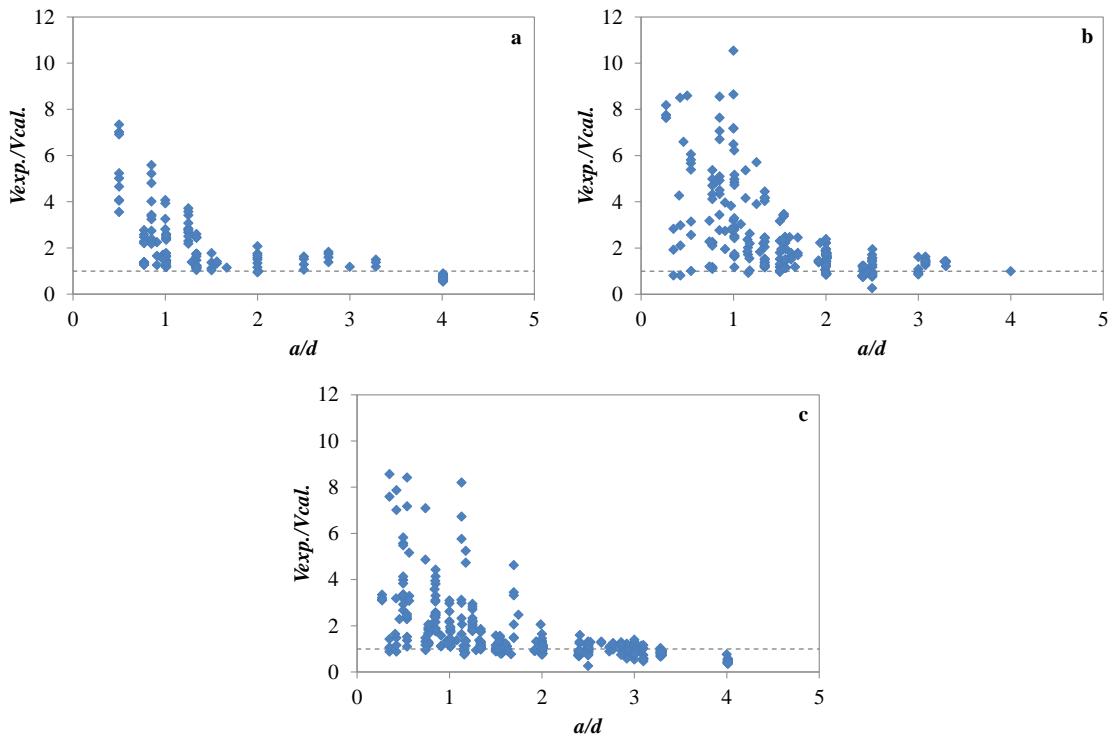
Figure 2-38-Predicting of shear strength for beams with shear reinforcement by Model Code 2010 a) Level I Approximation procedure, b) Level II Approximation procedure and c) Level III Approximation procedure.

For beams without shear reinforcement, level I and III approximation can be applied to determine ultimate shear strength. Level I accounts for concrete compressive strength and size effect but neglects the effect of shear span to depth ratio and dowel action. Generally, shear span to depth ratio controls the shear behaviour of RC beams with shear span to depth ratio less than two and affects other parameters such as concrete compressive strength; however its effect seems to diminish for beams with shear span to depth ratio more than three. As the influence of concrete compressive strength becomes more important in beams with smaller shear span to depth ratios, level I approximation is more conservative for beams with shear span to depth ratio less two, while its performance improves in the case of slender beams (see Figure 2-39-a). As Model Code 2010 level I approximation does not account for the effect of the main flexural reinforcement, which provides dowel action and affects the position of the neutral axis, the predictions are affected by a high degree of scatter as shown in Figure 2-39-b. In

general, as shown in Figure 2-37 and Figure 2-38, the procedure of shear strength determination according to level I approximation gives acceptable results for beams with shear span to depth ratio more than two but for deep beams it gives highly scattered and very conservative results.
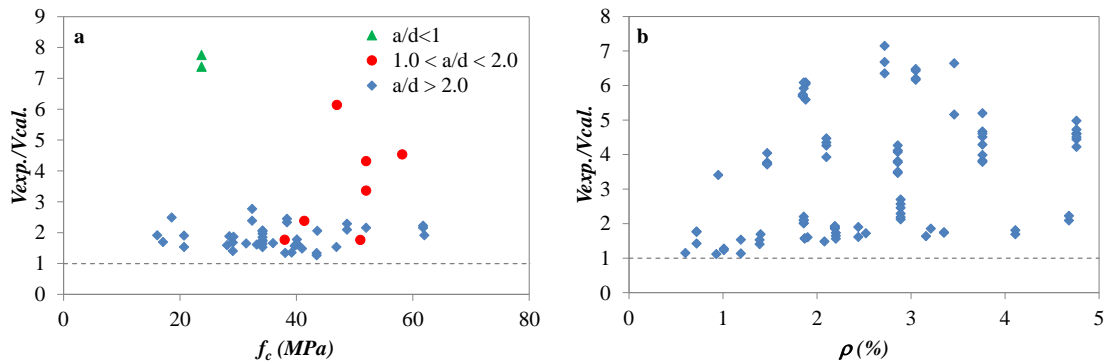
Figure 2-39-Predicting of shear strength for beams without shear reinforcement by Model Code 2010 Level I Approximation procedure a) Effect of concrete compressive strength in different shear span to depth ratio beams and b) Effect of main flexural reinforcement

Level III approximation can also be used to predict the ultimate shear capacity of RC members without shear reinforcement. This level of approximation assumes that the main flexural reinforcement reaches its yield strain, which is not always true in members for which the ultimate failure is dominated by shear. The conservative prediction in the case of deep beams and unsafe results in the case of slender beams are a result of neglecting the effect of shear span to depth ratio as well as assuming that the main flexural reinforcement always reaches its yield strain.

Both level I and III approximation can account for size effect, however the prediction of level I approximation is more conservative than level III approximation (Figure 2-40). Figure 2-40-b indicates that the shear strength prediction by level III approximation procedure is slightly unsafe for members with effective depth more than 1000mm.
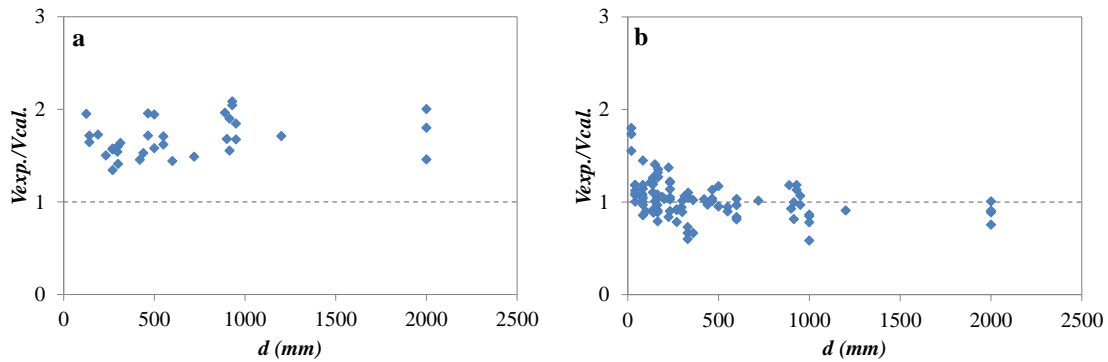
Figure 2-40-Effect of effective member depth on predicting of shear strength for beams without shear reinforcement by Model Code 2010 a) Level I and b) Level III Approximation procedure

In the case of beams with shear reinforcement, all approximation level can be used to determine ultimate shear capacity. The observations made earlier for beams without shear reinforcement, also hold true for beams with shear reinforced and analysed according to approximation level I and III. It should be noted that, as for the design procedure implemented in EC2, level II approximation is characterized by the fact that the concrete contribution is neglected, thus it ignores the influence of concrete compressive strength and dowel action. Predicting shear strength according to any of the recommended levels of approximations yields results that are not accurate for slightly RC beams while performance improves with increasing shear reinforcement ratio (see Figure 2-41).
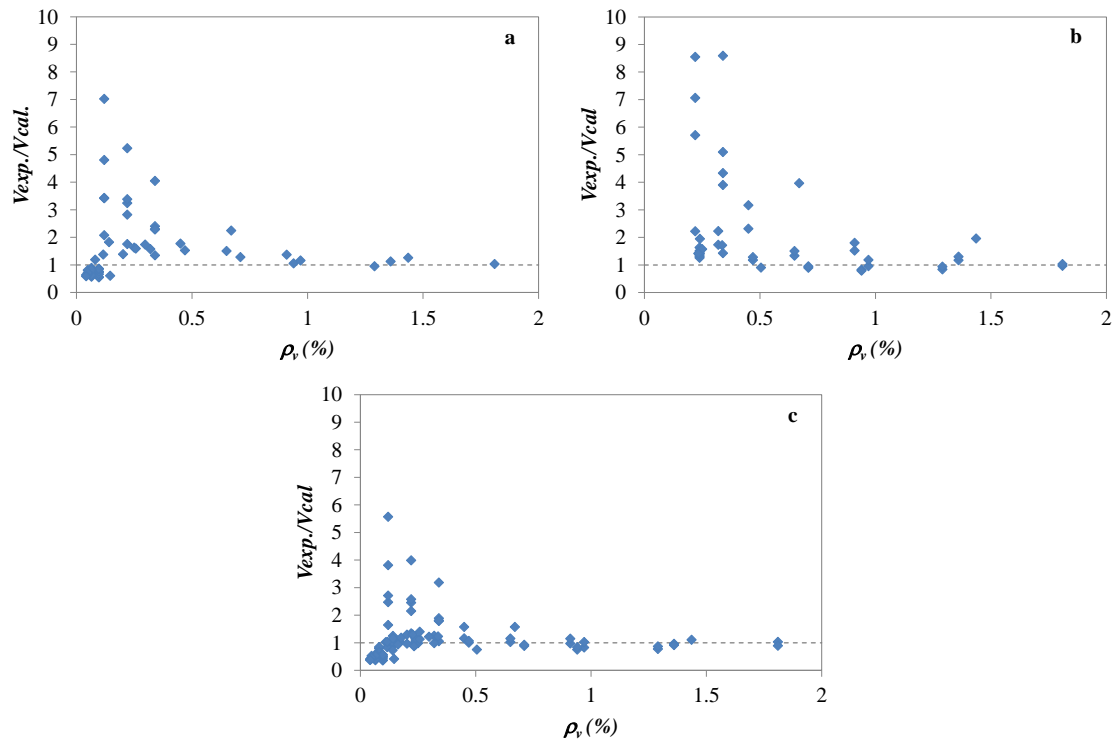
Figure 2-41-Effect of shear reinforcement ratio on predicting of shear strength for beams with shear reinforcement by Model Code 2010 a) Level I, b) Level II and c) Level III procedure

Model Code 2010 shear procedure neglects size effect in members with shear reinforcement. This, probably, leads to the unsafe shear strength prediction for large size members. Figure 2-42 shows that the ratio of experimental shear strength to the predicted shear strength by Model Code 2010 [12] procedure reduces by increasing the effective depth of the member, however, this aspect deserves more experimental investigation in the case of very deep members.
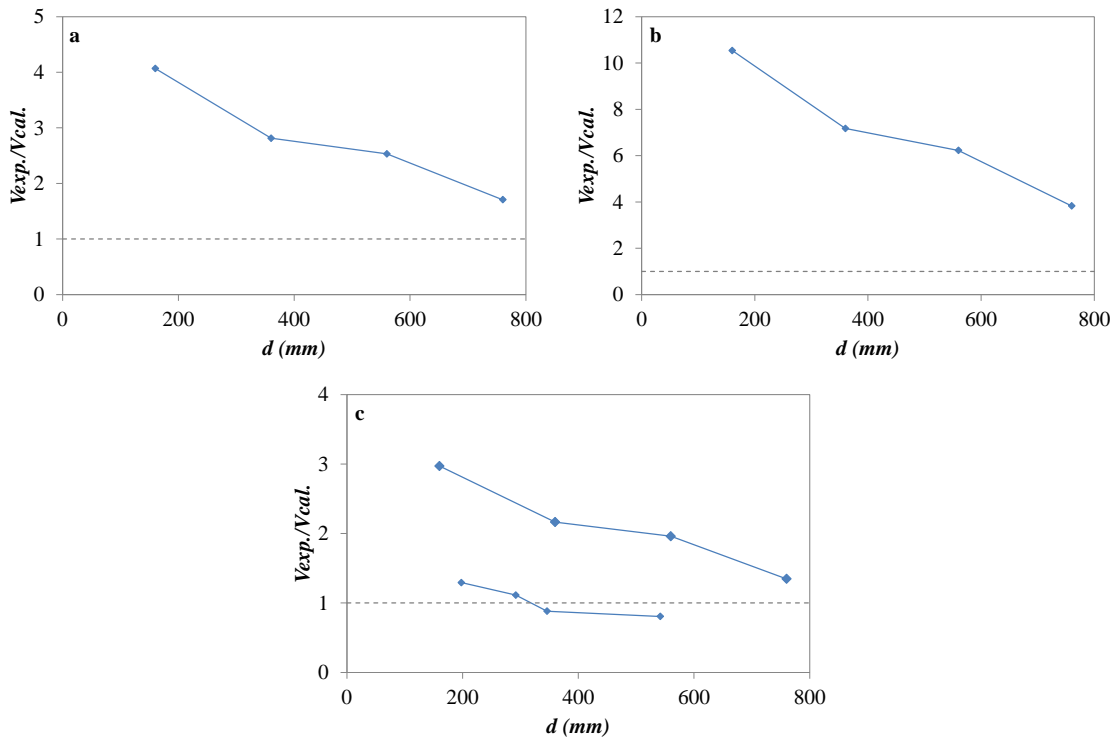
Figure 2-42-Effect of effective member depth on predicting of shear strength for beams with shear reinforcement by Model Code 2010 a) Level I b) Level II and c) Level II Approximation procedure.

2.4.4. STRUT-AND-TIE MODEL

The strut-and tie model is a rational yet simple method based on the lower bound theorem of plasticity theory and can be used to design discontinuous regions (D-regions) of RC members. This is an alternative method to predict shear strength of RC beams. Most current codes of practice recommend using this model to design RC deep beams, for which shear is the critical mode of failure. Current codes of practice, such as EC2 [3], ACI 318-14 [4] and Model Code 2010 [12], however, provide very little guidance in using strut-and-tie models [13], and the information provided is mainly limited to defining the design concrete strength for concrete struts and nodes. Figure 2-43 shows a typical strut-and-tie layout for beams under three and four point bending.
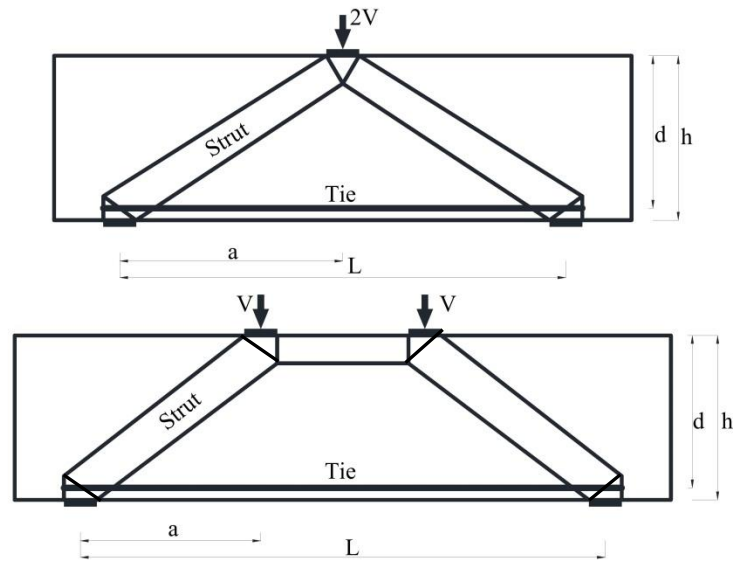
Figure 2-43-Strut-and-tie model arrangement

The design concrete compressive strength for strut-and-tie elements according to EC2 are summarized in Table 2-2. The value of *v'* can be calculated using the following equation:

$$v' = 1 - \frac{f_{ck}}{250} \tag{2.18}$$

Table 2-2-EC2 design concrete compressive strength for nodes and struts of STM

Element	Effective concrete strength		
	C-C-C Nodes	C-C-T Nodes	C-T-T Nodes
Node	$v'f_{cd}$	$0.85v'f_{cd}$	$0.75v'f_{cd}$
	Without transverse tension	With transverse tension	
Strut	f_{cd}	$0.6v'f_{cd}$	

Table 2-3 summarises the provisions of ACI 318-14 to determine the effective concrete compressive strength at nodes and struts. ACI 318-14 also recommends to provide a

shear reinforcement ratio that satisfies Eq. 2.16 along the element shear spans. The main role of this shear reinforcement is to resist the transverse tensile force resulting from the compression force spreading in the strut, thus controlling crack width and enhancing the performance of the compressive strut.

$$\sum \frac{A_{si}}{b_s s_i} \sin \alpha_i \geq 0.003 \tag{2.19}$$

where A_{si} is the area of the reinforcement at spacing s_i in the *i-th* layer of reinforcement crossing the strut at an angle α_i to the axis of the strut.

Table 2-3 ACI 318-14 effective concrete compressive stress for nodes and struts of STM

Element	Effective concrete strength		
	C-C-C Nodes	C-C-T Nodes	C-T-T Nodes
Node			
	0.85f'$_c$	*0.85x0.8f'$_c$*	*0.85x0.6f'$_c$*
	Without transverse tension	With transverse tension and satisfying Eq16	With transverse tension and not satisfying Eq16
Strut			
	0.85f'$_c$	*0.85x0.75f'$_c$*	*0.85x0.6f'$_c$*

The reduced concrete compressive strength for nodes and struts according to Model code 2010 is summarised in Table 2-4.

Table 2-4-Model code 2010 reduced concrete compressive strength for nodes and struts of STM

Element	Effective concrete strength	
	C-C-C Nodes	C-C-T and C-T-T Nodes
Node	$(30/f_{ck})^{1/3}$	$(30/f_{ck})^{1/3}0.75$
	Without transverse tension	With tension normal to the direction of compression / With tension oblique to the direction of compression
Strut	$(30/f_{ck})^{1/3}$	$(30/f_{ck})^{1/3}0.75$ $\quad$ $(30/f_{ck})^{1/3}0.55$

The strut-and-tie model was used with the provisions of all three codes of practice to predict the shear capacity of all deep beams included in the database (295 without shear reinforcement and 224 with shear reinforcement. The result of the analysis (Figure 2-44, Figure 2-45 and Figure 2-46) showed that using the strut-and-tie model leads to better results compare to the convensional shear equations decribed in the previous sections. However, the estimated theorethical values are still affected by a large scatter and the method can still yield unsafe results, especially for deep beams without shear reinforcment (Figure 2-44, Figure 2-45 and Figure 2-46).
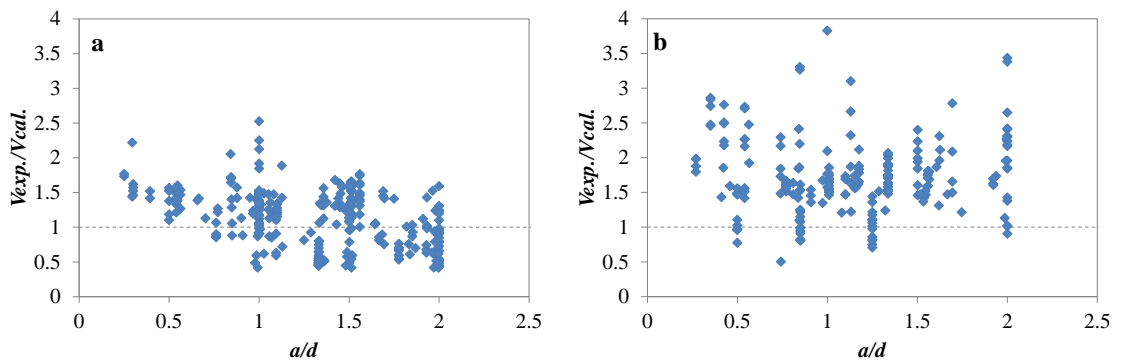
Figure 2-44-Shear strength prediction by STM with EC2 provisions for beams a) without shear reinforcement b) with shear reinforcement.

49
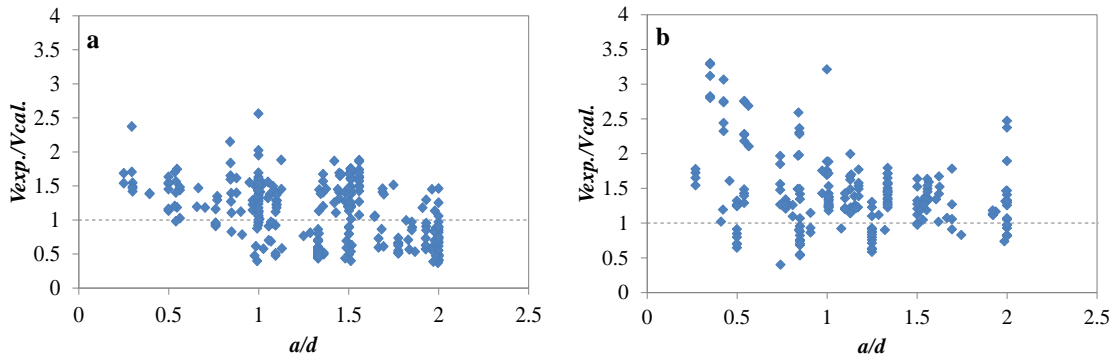
Figure 2-45-Shear strength prediction by STM with ACI 318-14provisions without a) shear reinforcement and b) with shear reinforcement
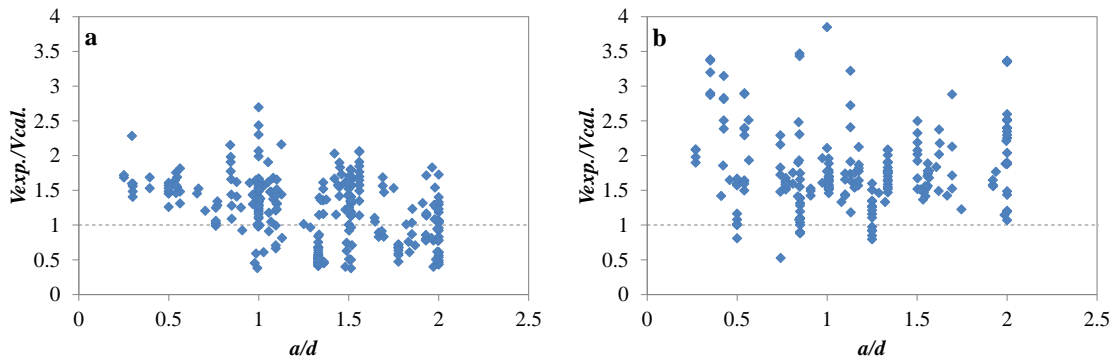
Figure 2-46-Shear strength prediction by STM with Model code 2010 provisions a) without shear reinforcement and b) with shear reinforcement

2.4.5. MODIFIED COMPRESSION FIELD THEORY

The performance of Response-2000 was also examined based on experimental data of 23 deep beams with and without shear reinforcement, in addition to 13 slender beams with and without shear reinforcement.

The result of the comparison confirms that Response 2000 is not an efficient program for predicting the behaviour of RC deep beams. As shown in Figure 2-47, the shear strength prediction for deep beams with shear reinforcement is unsafe. This can be attributed to the fact that the program is based on sectional analysis and linear strain distribution which is not correct for RC deep beams [63] and no enhancement of stress is defined for regions with complex stress distribution such as disturbed regions near supports and point loads.
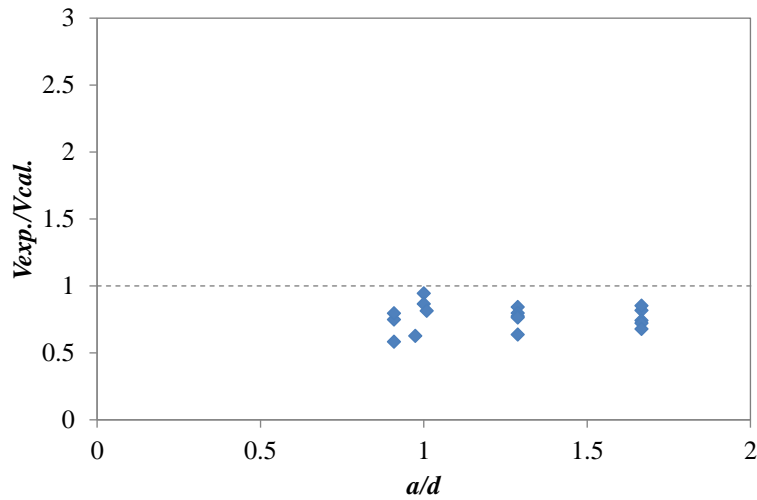
Figure 2-47-Shear strength prediction by Response-2000 against experimental shear strength for deep beams with shear reinforcement

For deep beams without shear reinforcement the prediction obtained from Response 200 is conservative, as shown in Figure 2-48. This can be attributed to the fact that the underlying MCFT material model was derived for elements with well distributed reinforcement in both horizontal and vertical direction and cannot model in a suitable manner the behavior of unreinforced or lightly reinforced concrete. Additionally the material model cannot account for aggregate interlock in a correct fashion [64], although this load carrying mechanism can be consider to contribute to the total shear resistance of beep beams only to a small extent.
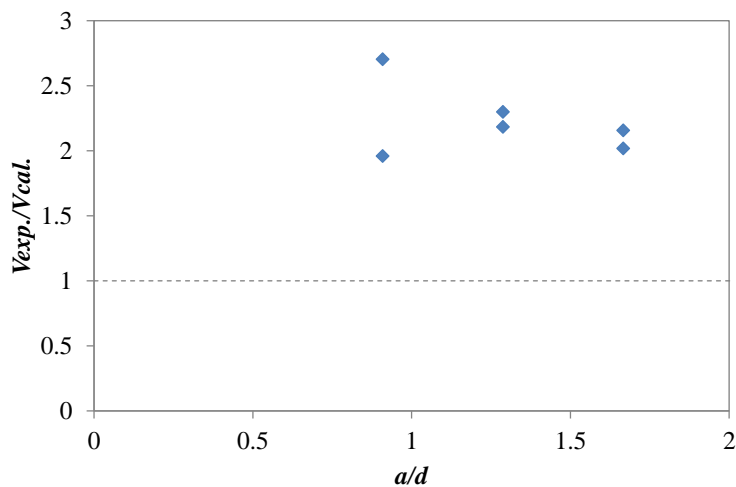
Figure 2-48-Shear strength prediction by Response-2000 against experimental shear strength for deep beams without shear reinforcement

In the case of slender beams, the prediction is in good agreement with the experimental results (Figure 2-49). This can be related to the fact that failure in slender beams occurs in a region that are not adjacent to the loading point or support, within which the assumption of plane section remains plane can be considered to be appropriate.
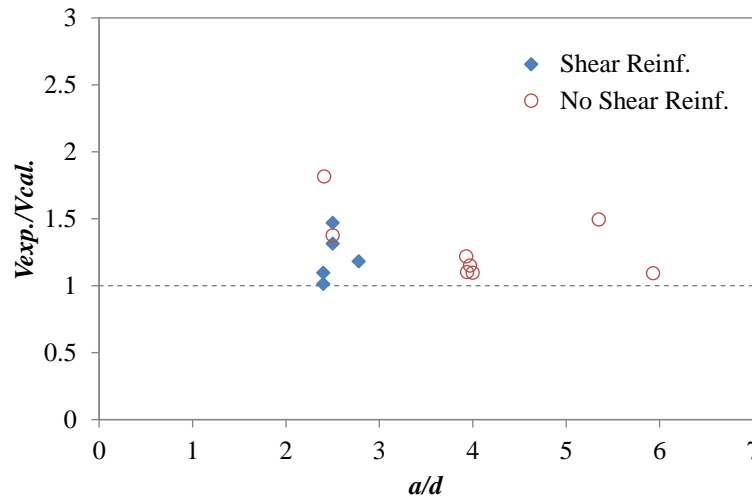
Figure 2-49-Shear strength prediction by Response-2000 against experimental shear strength for RC slender beams.

Response-2000 cannot account for size effect in either deep beams or slender beams because size effect is not implicitly accounted for by the material models that form the basis of MCFT. Models based on stress and strain tensors and their invariants, such as used in MCFT, are not capable of accounting for size effect and thus the ultimate failure of members is predicted as independent of the member size when geometrically similar members are considered [38, 65]. Figure 2-50 shows experimental results and MCFT predictions against the effective depth of the member for both slender beams and deep beams. As can be seen in both figures, although there is a decrease in the estimated shear strength according to the implementation of the MCFT; this is mainly due to the fact that the beams are not geometrically similar in all aspects. For exact geometrically similar beams with different size, Response 2000 predicts the same shear strength regardless of the member size.
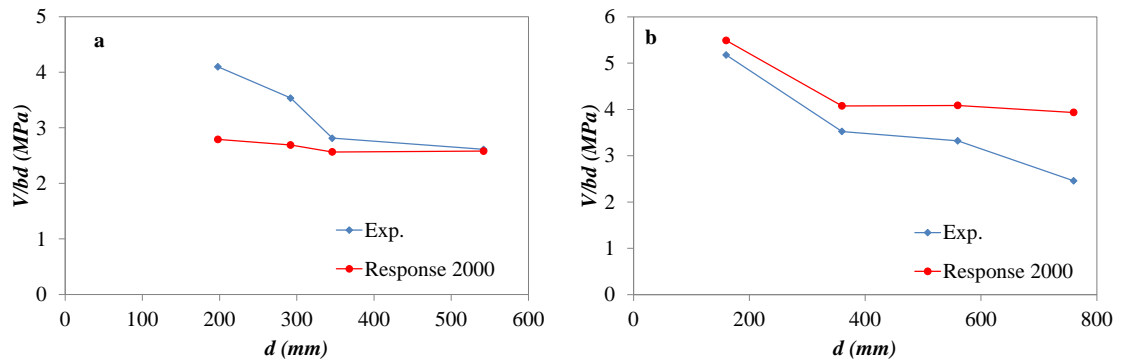
Figure 2-50-Experimental and predicted shear strength of a) slender beams and b) deep beams by Response-2000 (Size effect).

2.5. SUMMARY

This chapter presented an outline of the current understanding of shear behaviour of RC beams and available models that can be used in design. In Particular, it has focused on evaluating these models against an extensive experimental database to identify their weakness and limitations.

The results show that the shear equations provided by EC2, ACI 318-14 and Model Code 2010 can predict the shear capacity of slender beams (beams with shear span to depth ratio greater than two) with a reasonable degree of accuracy. Nonetheless, in the case of RC deep beams (beams with shear span to depth ratio less than two), the prediction by these equations give highly scattered and mostly over-conservative results, but can also yield very unsafe results. Therefore, such equations cannot be used to predict the shear behaviour of RC deep beams with an appropriate margin of safety.

Another rational model for the shear design in RC members is the strut-and-tie model. This model is recommended for the design of shear in discontinuous regions such as RC deep beams. This model is implemented in the current codes of practice and it is recommended for the design of RC deep beams. However, codes of practice do not provide detailed guidance on how to select an appropriate model and define the size of

its elements. Additionally, the reliability of the equations provided by the codes of practice to predict the effective concrete strength in the inclined strut is poor.

The implementation of the MCFT into layer analysis software appears to be a rational way for predicting shear behaviour of RC elements. This model can yield acceptable results in the case of RC slender beams, but fails to capture appropriately the more complex behaviour of RC deep beams.

In conclusion, the available shear design procedures can reasonably predict the behaviour and capacity of RC slender beams. However, there is still need for more research to deepen the understanding of RC deep beam behaviour and examine the effect of different design parameters, such as shear span to depth ratio, concrete compressive strength, shear reinforcement and member depth (i.e. size effect).

CHAPTER 3.   SHEAR BEHAVIOUR AND SIZE EFFECT OF RC DEEP BEAMS

This chapter consists of the "stand alone" journal paper: Ismail K. S., Guadagnini M. and Pilakoutas K., (2016a) Shear Behaviour and Size Effect of RC Deep Beams, Submitted to ACI Structural Journal. All of the test results are reported in detail in Appendix B.

This paper presents an experimental investigation into the structural behaviour of 24 RC deep beams examining parameters affecting shear capacity such as shear span to depth ratio; concrete compressive strength; web reinforcement ratio and effective beam depth. The results reveal that concrete compressive strength and shear span to depth ratio have the most significant influence on the behaviour and capacity of RC deep beams and the shear strength at failure is size dependent. The test results are compared with code predictions and it is shown that the ACI 318-14 predictions are conservative for normal strength concrete, but unconservative for high strength concrete beams. The EC2 and Model Code 2010 predictions are shown to be overall conservative but the degree of conservatism decreases with increasing concrete strength. It is concluded that for improved prediction efficiency, current strength reduction factors used in design guidelines for inclined concrete struts need to include all three main parameters, concrete strength, shear span to depth ratio and shear reinforcement.

3.1. INTRODUCTION

RC deep beams are structural members for which the load is applied at a distance from the support so that a substantial proportion of the load is transferred directly to the support by arching action. Common structural applications of deep beams include transfer girders in buildings, bridges and offshore structures. According to ACI 318-14 [4] "Deep beams are members that are loaded on one face and supported on the opposite face such that strut-like compression elements can develop between the loads and

supports and that satisfy (a) or (b): (a) Clear span does not exceed four times the overall member depth h; (b) Concentrated loads exist within a distance $2h$ from the face of the support". On the other hand, Eurocode 2 (EC2) [3] defines deep beams as all beams with span to depth ratio smaller than three.

The strength of deep beams is usually controlled by shear rather than flexure [1]. As the shear behaviour of RC members is still not well understood and it is influenced by many parameters, existing design models rely on empirical equations [1, 2]. Although, such approaches are generally extremely conservative [14-17], they can also lead to unsafe design solutions [17-19]. Therefore, the provisions of current codes of practice need to be reviewed and improved to account for parameters affecting shear behaviour and capacity of RC deep beams.

It is well accepted that in shear critical members, size effect plays a significant role and different approaches can be found in the literature to address this issue. Weibull statistical size effect theory [66] shows that the shear strength is expected to vary with $d^{-1/6}$. Based on experimental work, Kani [20] and Shioya et al. [23] found that the shear strength is proportional to $d^{-1/4}$. Using the energy release size effect theory, Bazant and Kim [22] predicted that the shear strength is proportional to $d^{-1/2}$. These approaches are aimed at slender beams. The mechanisms of shear stress transfer in slender beams and deep beams, however, are different; hence the accuracy of these approaches in capturing size effect in RC deep beams needs to be investigated further.

In the past decades, several experimental research programmes have examined the shear behaviour of RC beams. However, only a few focused on deep beams [1, 20, 27, 31, 67-71] or issues such as the development of a strut-and-tie mechanism and size effect. With the exception of the work of Walraven & Lehwalter [26], Tan & Lu [27], Zhang and Tan [31] and Birrcher et al. [72], most of the experimental work on size effect available in the literature focused on slender beams [20, 21, 23, 24, 26, 27, 31, 57, 73]. Additionally, researchers have different observations about size effect in deep beams. Based on their experimental results on RC deep beams with and without shear

reinforcement, Walraven & Lehwalter [26], Tan & Lu [27] concluded that the shear strength at failure is size dependent. However, Zhang and Tan [31] and Birrcher et al. [72], concluded that size has no effect on the average shear strength, while there is decreasing in average shear strength of their beams by increasing the depth. Hence, there is a need for additional comprehensive experimental studies that account for all influencing parameters.

To develop a better understanding of the shear behaviour of RC deep beams and the aforementioned issues, 24 RC specimens were tested and the effects of concrete compressive strength, shear span to depth ratio, amount of vertical and horizontal shear reinforcement, and effective depth were examined in detail. This paper presents the adopted experimental methodology and discusses the main results. This is followed by a comparison of test results with code provisions and recommendations on how existing models can be improved.

3.2. RESEARCH SIGNIFICANCE

This work aims to provide experimental evidence on the behaviour of RC deep beams to enable a better understanding of the effects of shear span to depth ratio and size effect, and lead to improved design procedures. The results will also allow an evaluation of the current code provisions and help identify their limitations.

3.3. THE STRUT-AND-TIE MODEL IN DESIGN

The strut-and-tie model is a simple equilibrium model based on the lower bound solution of the plasticity theory and can be used to design D-regions, such as deep beams. Design based on the strut-and-tie model (STM) is allowed in all three major international codes, ACI 318-14, EC2 and Model Code 2010 [12]. The first step in designing with strut and tie model is to choose an appropriate strut-and-tie layout and define the size of each element (Figure 3-1). All three codes allow designers to choose

the size of the elements that transfer the imposed loads to the supports. The height of the bottom node (h_B) (see Figure 3-1) can be assumed as twice the distance between the centre of force of the main longitudinal reinforcement and the tension face. According to Yang and Ashour [74] the height of the top node (h_T) can be determined from the equilibrium between the limit of resultant compressive force at the top node (C-C-C), and the limit of resultant tensile force of the bottom node (C-C-T). According to this hypothesis, the height of the top node (h_T) is equal to 80%, 85% and 75% of the height of the tie according to ACI 318-14, EC2 and Model Code 2010, respectively, while the strut angle (θ) can be calculated from geometry using Eq. 3.1. The top and bottom width of the inclined strut (W_{ST} and W_{SB}) can be calculated using Eqs 3.2 and 3.3 [4], respectively.

$$\theta = \tan^{-1}\left(\frac{d - h_T/2}{a}\right) \tag{3.1}$$

$$W_{ST} = l_T \sin\theta + h_T \cos\theta \tag{3.2}$$

$$W_{SB} = l_B \sin\theta + h_B \cos\theta \tag{3.3}$$
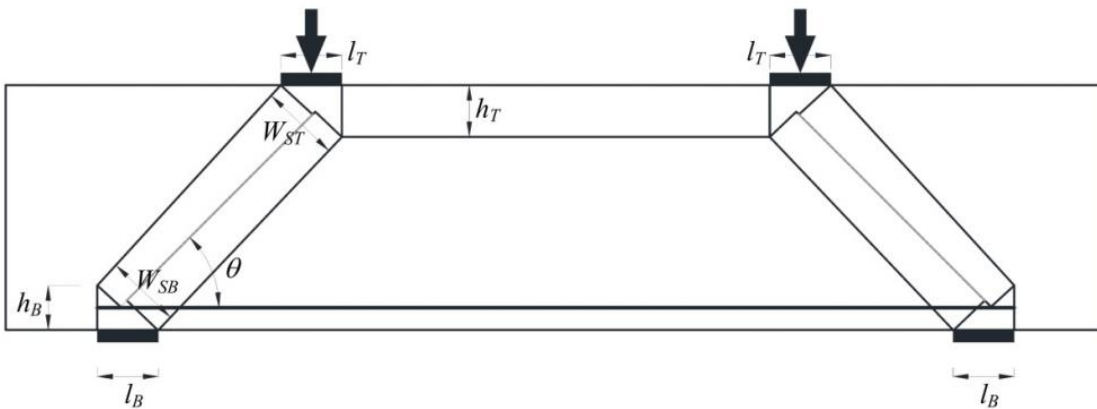
Figure 3-1-Typical strut-and-tie model used to predict the load capacity of the tested beams

58

Cracked reinforced concrete is an orthotropic material, for which its principal stresses can be assumed to have the same directions of the principal tensile and compressive strains. The presence of lateral tensile strain in the concrete strut, however, can reduce its compressive strength. This is accounted for by using an effectiveness factor to calculate an effective concrete compressive strength. According to ACI 318-14, the effective concrete strength (f_{ce}) can be calculated using Eq. 3.4 while EC2 and Model Code 2010 use Eq. 3.5 and Eq. 3.6, respectively.

$$f_{ce} = 0.85\beta_s f'_c \tag{3.4}$$

where β_s is 0.75 for strut with shear reinforcement satisfying Eq. 3.4a, else β_s taken as 0.6.

$$\sum \frac{A_{si}}{b_s s_i} \sin\alpha_i \geq 0.003 \tag{3.4a}$$

where A_{si} is the area of the reinforcement at spacing s_i in the i-th layer of reinforcement crossing a strut at an angle α_i to the axis of the strut.

$$f_{ce} = 0.6\nu' f_{cd} \tag{3.5}$$

where ν' can be calculated according to Eq. 3.5a and f_{cd} is the design concrete compressive strength.

$$\nu' = 1 - \frac{f_{ck}}{250} \tag{3.5a}$$

$$f_{ce} = k_c f_{cd} \tag{3.6}$$

$$k_c = 0.55 \left(\frac{30}{f_{ck}} \right)^{1/3} \leq 0.55 \tag{3.6a}$$

The strut-and-tie model shown in Figure 3-1 with the above element size definitions will be used for the analysis of the experimental results obtained from the programme presented in this paper.

3.4. EXPERIMENTAL INVESTIGATION

A total of 24 RC deep beams were tested in two phases. Phase I comprised 21 RC deep beams and was carried out at the Structural Engineering Laboratory of the University of Salahaddin\Hawler in Iraq [75]. Phase II comprised three geometrically similar RC deep beams with different sizes and was carried out at the Heavy Structures Laboratory of the University of Sheffield in the UK.

3.4.1. TEST SPECIMEN AND DESIGN PARAMETERS

3.4.1.1. Phase I

All RC beam specimens tested in Phase I [75] had identical dimensions and main flexural reinforcement ratio. The geometry of the specimens and the arrangement of both flexural and shear reinforcement are shown in Figure 3-2. Table 3-1 shows the shear span to depth ratio and percentage of vertical and horizontal shear reinforcement for each beam. Three parameters were examined in this phase: a) shear span to depth ratio (1.67, 1.29 and 0.91); b) concrete compressive strength (30 to 85MPa); and c) amount of horizontal (0 to 0.215%) and vertical shear reinforcement (0 to 1.26%) crossing the primary strut.

The beams were 1800mm long, had a clear span of 1400mm and a section of 400mm deep by 100mm wide. The specimens were flexurally reinforced with six 16mm bars distributed in three layers, two bars in each layer. At both ends of the beams, the longitudinal reinforcement was extended beyond the supports and terminated with 90 degree hooks to ensure proper anchorage and prevent bond failure. Two 12mm deformed bars were used as compression reinforcement. Where provided, vertical

reinforcement comprised 8mm deformed bars, while 6mm deformed bars were used as horizontal shear reinforcement.
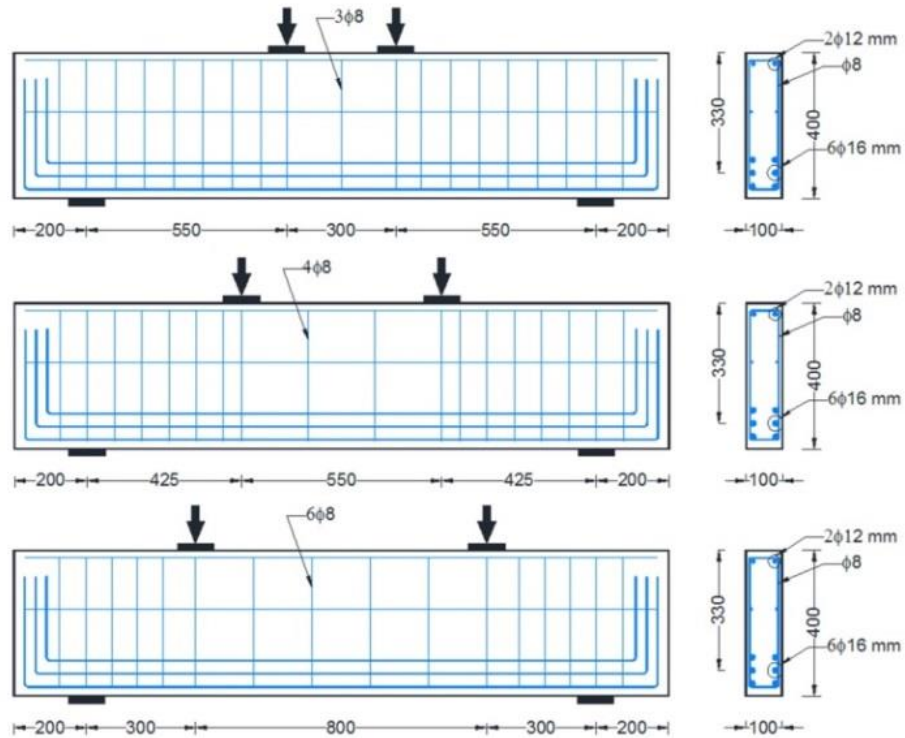
Figure 3-2-Dimensions and reinforcement details of the specimens tested in Phase I

3.4.1.2. Phase II

Phase II aimed to investigate the size effect of deep beams without shear reinforcement. Figure 3-3 shows the reinforcement details and the dimensions of the three tested beams. The beams were geometrically similar with overall depths of 250mm (H3), 375mm (H2) and 500mm (H1), resulting in a constant shear span to depth ratio of 1.67. A constant width of 150mm was adopted, as width is not expected to influence the size effect [24, 31]. A flexural reinforcement ratio of 1.4% was used in all three specimens to ensure adequate flexural capacity and ensure shear failure.

Table 3-1- Details and Properties of Tested Beams

No	Phase	Spec.	a/d	f_c MPa	f_t MPa	V.Shear Reinf ratio, %	H.Shear Reinf ratio, %	First flexural cracking load, kN	First diagonal cracking load, kN	Total failure load, kN	Mid-span Deflection at failure, mm	Mode of failure
1		A1	1.67	85.2	6.5	0	0	79	118	353	4.6	Shear-compression
2		A2	1.67	85.7	6.4	0.56	0.215	79	157	422	7.0	Compression
3		A3	1.67	85.1	6.8	1.26	0.215	79	177	466	7.4	Compression
4		B1	1.29	86.9	6.8	0	0	59	137	491	7.4	Compression
5		B2	1.29	86.6	6.6	0.59	0.215	59	137	564	8.8	Compression
6		B3	1.29	88.1	6.7	1.34	0.215	79	157	567	8.7	Compression
7		C1	0.91	85.7	6.6	0	0	98	157	741	8.4	Compression
8		C2	0.91	85.8	6.8	0.67	0.215	98	235	>920*	4.8	Not failed
9		C3	0.91	86.0	6.7	1.44	0.215	98	216	>920*	4.9	Not failed
10		D1	1.67	58.8	4.8	0	0	79	137	296	4.1	Shear-compression
11	I	D2	1.67	59.7	4.9	0.56	0.215	79	137	373	7.9	Compression
12		D3	1.67	58.1	5.7	1.26	0.215	79	137	369	8.8	Compression
13		E1	1.29	58.2	5.8	0	0	79	118	415	4.7	Shear-compression
14		E2	1.29	59.1	6.0	0.59	0.215	79	137	513	8.1	Compression
15		E3	1.29	59.2	5.8	1.34	0.215	79	118	506	8.3	Compression
16		F1	0.91	60.5	6.0	0	0	98	157	545	7.5	Strut crushing
17		F2	0.91	60.6	5.9	0.67	0.215	79	157	706	7.6	Strut crushing
18		F3	0.91	59.5	5.8	1.44	0.215	79	157	748	5.9	Strut crushing
19		G1	1.67	30.9	3.4	0.56	0.215	39	79	292	4.8	Diagonal splitting
20		G2	1.29	30.5	3.1	0.59	0.215	59	118	372	3.7	Shear-compression
21		G3	0.91	31.3	3.3	0.67	0.215	98	137	489	4.5	Strut crushing
22		H1	1.67	35.8	3.1	0	0	80	150	375	7.5	Diagonal splitting
23	II	H2	1.65	35.8	3.1	0	0	60	120	316	7.5	Shear-compression
24		H3	1.64	35.8	3.1	0	0	45	90	254	7.3	Shear-compression

* The ultimate capacity of the testing machine was reached before failure of the specimen.
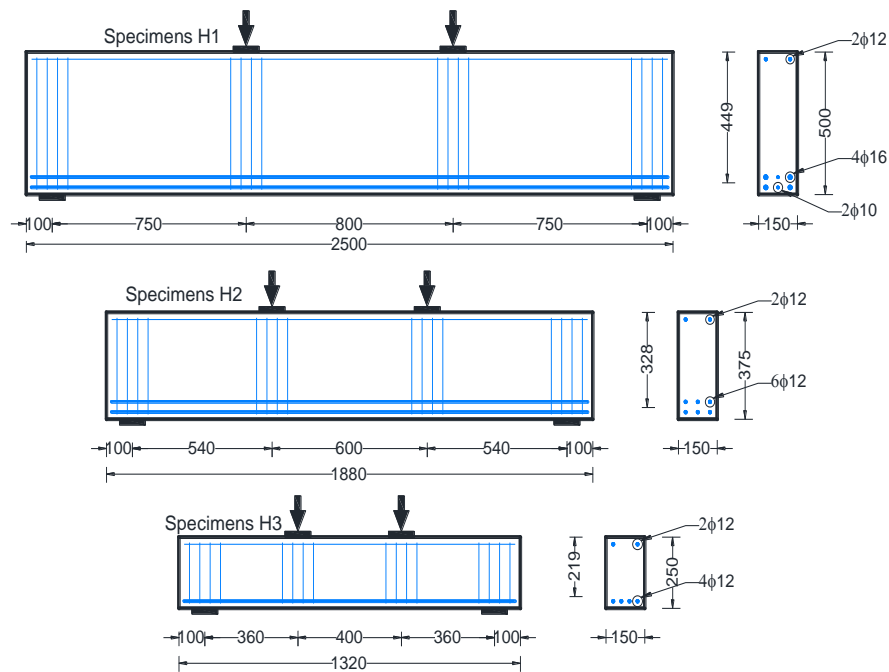
Figure 3-3-Dimensions and reinforcement details of the specimens tested in Phase II

3.4.1.3. Materials

The specimens tested in Phase I were manufactured using three different concrete mixes to obtain the desired compressive strengths of 30, 60 and 85MPa. Ordinary Portland cement was used for all mixes and the maximum aggregate size was 12.5mm. Standard cubes (150 x 150 mm) were tested to determine the compressive strength of the concrete according to BS EN 12390-3 [76]. The compressive strength (f'_c) reported is calculated as 85% of the average cube strength. The concrete tensile strength was evaluated from splitting tests on standard cylinders (150 x 300 mm) according to BS EN 12390-3 [76].

The three specimens tested in phase II were manufactured using ready-mix concrete with a maximum aggregate size of 10mm and a target compressive strength of 35MPa. All specimens were cast and cured under the same laboratory conditions. Compression and splitting tests were performed to determine the mechanical properties of the concrete and the results are summarised in Table 3-1

Standard ribbed reinforcing bars were used in both phases. The yield stress and ultimate strength for bars used in Phase I were determined according to ASTM-A370 [77] and are reported in Table 3-2. For Phase II, the steel bars had nominal characteristic yield strength of 500MPa.

Table 3-2-Details and mechanical properties of reinforcing bars

Phase	Size mm	Area mm^2	Yield strength f_y ,MPa	Ultimate strength f_u, MPa
I	6	28	577	660
	8	50	448	693
	12	113	404	635
	16	199	364	550

3.4.1.4. Test Setup and Instrumentation

The specimens were simply supported and tested in four point-bending, as shown in Figure 3-4. A testing machine with capacity of 1000 kN was used to test the specimens in phase I while a machine with a capacity of 2000kN was used in phase II. Displacement transducers, electrical strain gauges, inclinometers, and demec points were used to monitor deflections, strains in the longitudinal and transverse steel reinforcement, end rotations and strain in the concrete, respectively.

The load was applied in increments of 20 kN until failure. At each increment, cracks were marked and the width of critical cracks was measured using a micrometre with an accuracy of 0.02mm. In addition, all beam specimens tested in phase II were subjected to an initial load cycle that induced a level of strain in the main flexural reinforcement corresponding to the serviceability limit state recommended in EC2 [3].
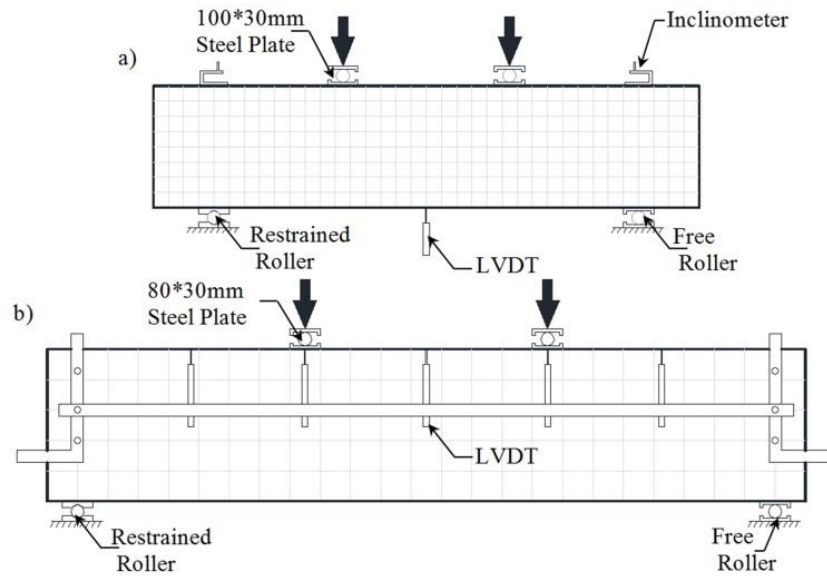
Figure 3-4-The load configuration and instrumentation a) Phase I and b) Phase II

3.5. EXPERIMENTAL RESULTS AND DISCUSSION

3.5.1. LOAD-DEFLECTION RESPONSE

The applied load versus mid-span deflection curves for all 24 beams are shown in Figure 3-5 in groups according to their target compressive strength. As expected, the initial stiffness and overall response of the specimens differ depending on the shear span to depth ratio. For beams with shear span to depth ratio greater than 1.0, the load-deflection response shows that the beam stiffness reduces considerably after developing the first diagonal crack. This stiffness degradation decreases with decreasing shear span to depth ratio. No significant stiffness reduction was observed after the formation of diagonal cracks for beams with shear span to depth ratio less than 1.0. As expected, specimens of the same shear span to depth ratio but higher span to depth ratio (L/d), show a higher drop in stiffness after the formation of the first diagonal crack (Figure 3-6). An additional predictable change in stiffness is observed after yielding of the main flexural reinforcement.
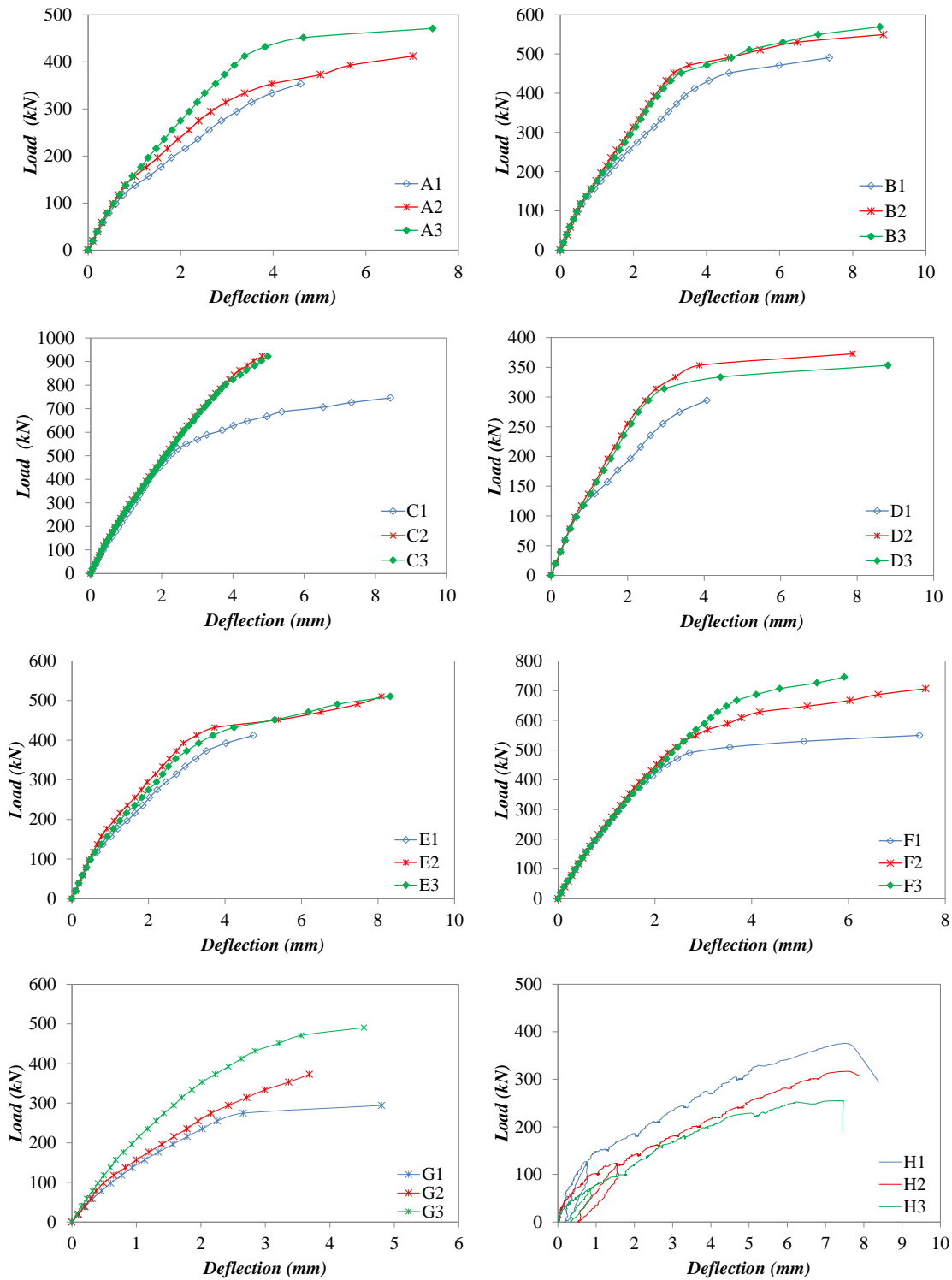
Figure 3-5-Load-Deflection response for specimens
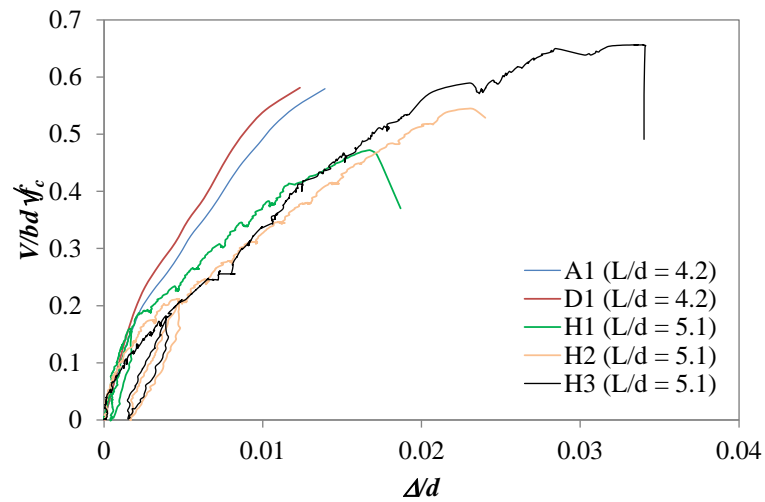
Figure 3-6-Effect of span to depth ratio on the stiffness of the RC deep beams

3.5.2. CRACK PATTERNS AND FAILURE MODES

In all cases, flexural cracks developed first in the constant bending moment region outside the shear span, and then spread into the shear span. With further increase in the applied load, a) diagonal cracks formed suddenly at mid-depth in the middle of the shear span and their orientation was mainly governed by the shear span to depth ratio; b) the flexural cracks propagated further towards the compression side of the beam until they reached about two thirds of the total depth of the beam and c) the diagonal cracks propagated initially towards the load and subsequently backwards towards the support. In most cases, a second major inclined crack developed parallel to the initial crack and together they induced failure.

The modes of failure for all specimens are listed in Table 3-1, while typical failure modes are shown in Figure 3-7. Four different modes of failure were observed:

   a. Diagonal Splitting failure occurred when the diagonal cracks propagated initially towards the load and then towards the support. This type of failure was less brittle compared to the shear failure modes of other specimens.

   b. Shear-Compression failure occurred after diagonal cracks propagated in the shear span causing high stresses to be developed in the compression zone above the tip of the cracks, which lead to an explosive failure.

67

c. Strut compression failure occurred abruptly due to crushing of the concrete between inclined cracks in the shear span. This mode of failure was observed for beams with shear span to depth ratio less than one.

d. Flexural Compression failure occurred after yielding of the main flexural steel reinforcement, due to crushing of the concrete in the constant moment region.
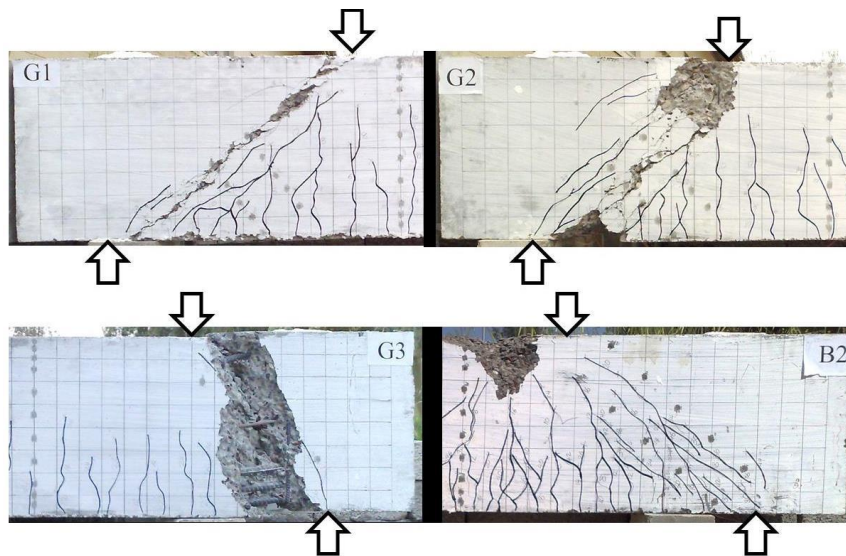
Figure 3-7-Modes of failure, G1-Diagonal Splitting failure, G2-Shear-Compression failure, G3-Strut Compression failure and B2-Flexural compression failure.

3.5.3. EFFECT OF SHEAR SPAN TO DEPTH RATIO

The experimental results confirm that the behaviour of RC deep beams is dominated by the shear span to depth ratio and the shear capacity increases with decreasing shear span to depth ratio (Figure 3-8). This is mainly due to direct transfer of the load to the supports primarily through a single strut. Based on resolution of strains in the vertical and horizontal shear reinforcement, it can be seen (see Figure 3-9) that the tensile strain developed perpendicular to the inclined strut increases with decreasing shear span to depth ratio. With increased transverse tensile strain, the compressive capacity of the inclined strut is expected to reduce and the ultimate capacity of the member is affected. Crack patterns and modes of failure are also affected by the shear span to depth ratio, as can be seen in Table 3-1 and Figure 3-7. The flexural cracks in beam G1 (a/d =1.67) extended to about 80% of the total height of the beam while for beam G3 (a/d = 0.91)

the flexural crack propagated to about 50% of the beam height. The failure mode changed from diagonal splitting failure in beam G1, to strut crushing in beam G3.
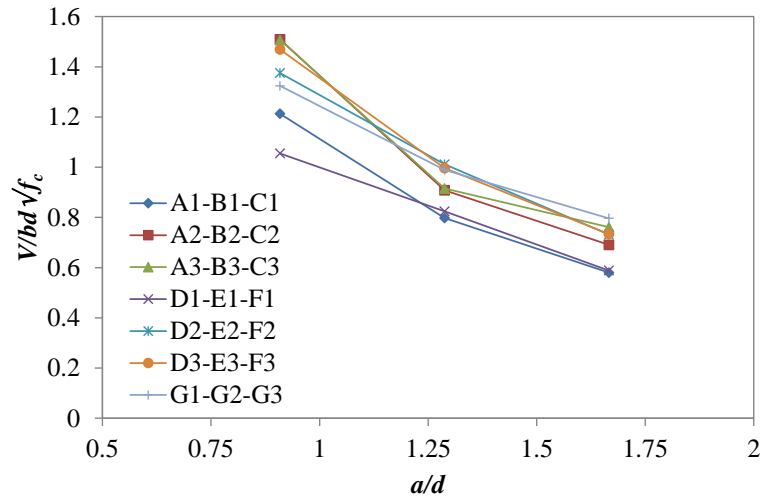
Figure 3-8-Effect of shear span to depth ratio on the ultimate failure load of the specimens

Figure 3-10 shows the performance of the three codes of practice in predicting the shear capacity of specimens with different shear span to depth ratio and the prediction values are given in Table 3-3. The results show that ACI 318-14 is generally unconservative, while EC2 and Model Code 2010 yield conservative results, though slightly unconservative for beams without shear reinforcement (D1-E1-F1 in Figure 3-10). With increasing shear span to depth ratio, predictions according to all codes become less conservative. This is because these codes only account for the effect of shear span to depth ratio through a change in the angle of the inclined strut, which in turn changes the width of the strut. However, the codes do not account for any strength reduction in the strut concrete strength.
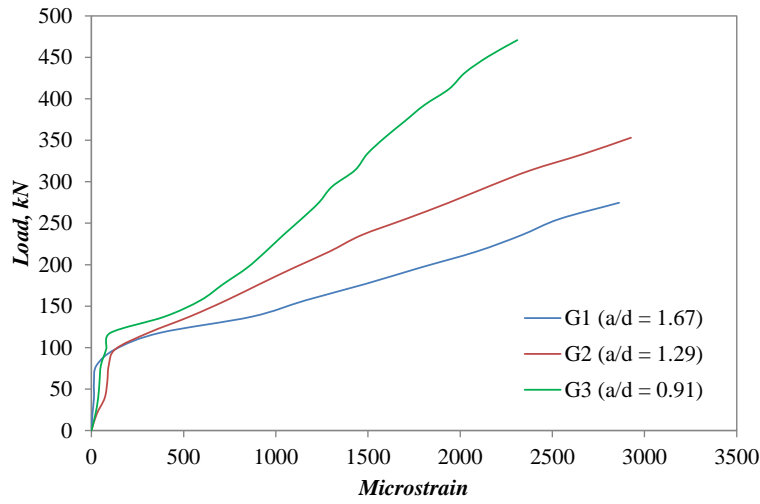
Figure 3-9-Developed strain in the direction perpendicular to the inclined strut for beams with different shear span to depth ratio.
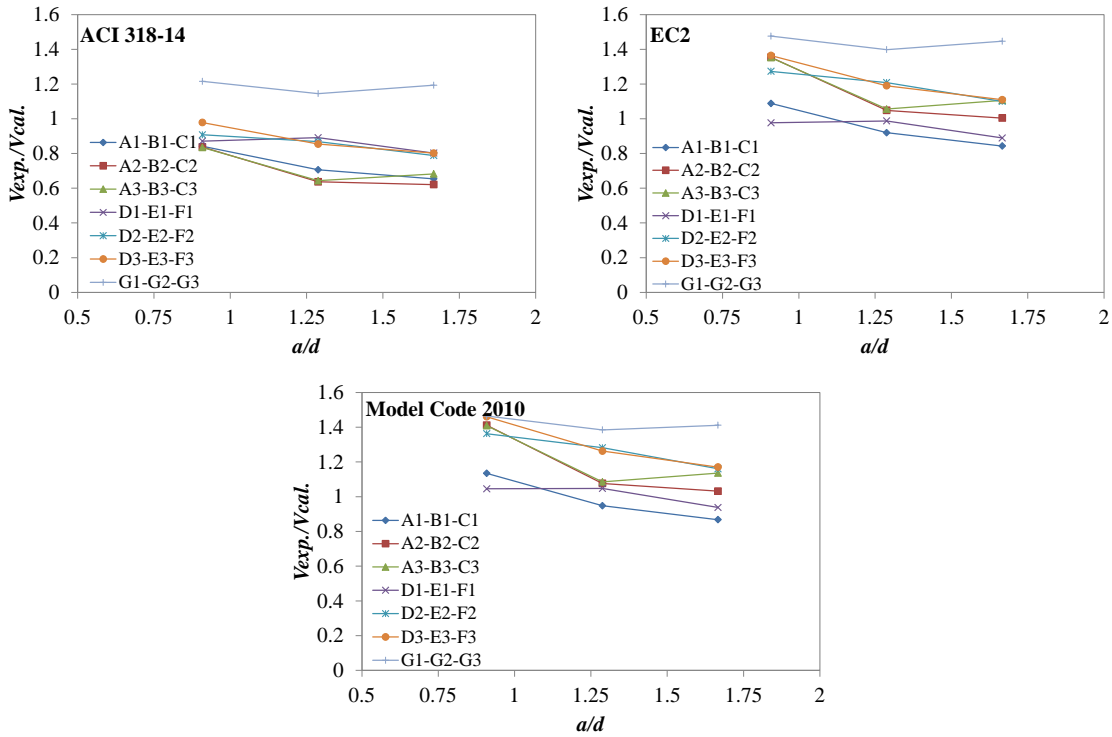
Figure 3-10-Comparison of code predictions to test results (effect of a/d)

Table 3-3-ACI318-14 and EC2 shear strength predictions against experimental data

Speci men	Vexp. (kN)	ACI 318-14		EC2		Model Code 2010	
		Without Shear Reinf.	With Shear Reinf.	Without Shear Reinf.	With Shear Reinf.	Without Shear Reinf.	With Shear Reinf.
		Vtest/Vcal.	Vtest/Vcal.	Vtest/Vcal.	Vtest/Vcal.	Vtest/Vcal.	Vtest/Vcal.
A1	176.60	0.65		0.84		0.87	
A2	210.90		0.62		1.00		1.03
A3	233.00		0.68		1.11		1.14
B1	245.25	0.71		0.92		0.95	
B2	282.05		0.64		1.05		1.08
B3	283.50		0.64		1.06		1.09
C1	370.35	0.84		1.09		1.13	
D1	148.15	0.80		0.89		0.94	
D2	186.40		0.79		1.10		1.16
D3	184.50		0.80		1.11		1.17
E1	207.50	0.89		0.99		1.05	
E2	256.50		0.87		1.21		1.28
E3	253.10		0.85		1.19		1.26
F1	270.75	0.87		0.98		1.05	
F2	353.15		0.91		1.27		1.36
F3	373.75		0.98		1.36		1.46
G1	146.15		1.19		1.45		1.41
G2	186.00		1.14		1.40		1.38
G3	244.25		1.22		1.48		1.46
H1	187.50	1.31		1.30		1.31	
H2	158.00	1.15		1.14		1.15	
H3	127.00	1.05		1.04		1.03	
Average		0.92	0.87	1.02	1.21	1.05	1.25
STD		0.20	0.20	0.13	0.16	0.13	0.15

3.5.4. EFFECT OF CONCRETE COMPRESSIVE STRENGTH

Due to arching action, concrete compressive strength is a dominant parameter influencing the shear capacity of RC deep beams. As shown in Figure 3-11, the results show that shear capacity of deep beams increases with increasing concrete compressive strength and this enhancement is more pronounced for beams with smaller shear span to depth ratios.

71
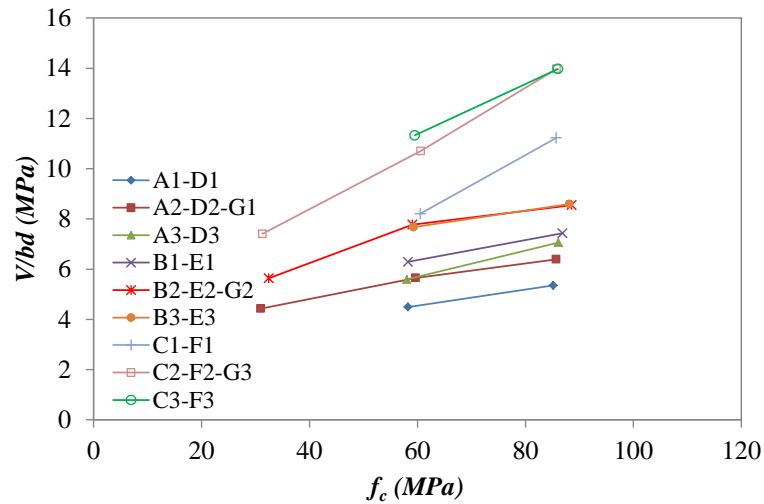
Figure 3-11-Effect of concrete compressive strength on the ultimate failure load of the specimens

Comparisons between the experimental and predicted shear strengths according to the three codes are shown in Figure 3-12 as a function of concrete compressive strength. The predictions of ACI 318-14 are conservative for the beams with concrete strength of around 30MPa; however, with increasing concrete compressive strength they become unconservative. This is because the provisions neglect the effect of concrete compressive strength on the effectiveness factor of the inclined strut. On the other hand, the EC2 and Model code 2010 provisions account for this effect and, as a result, yield more accurate and generally conservative predictions.
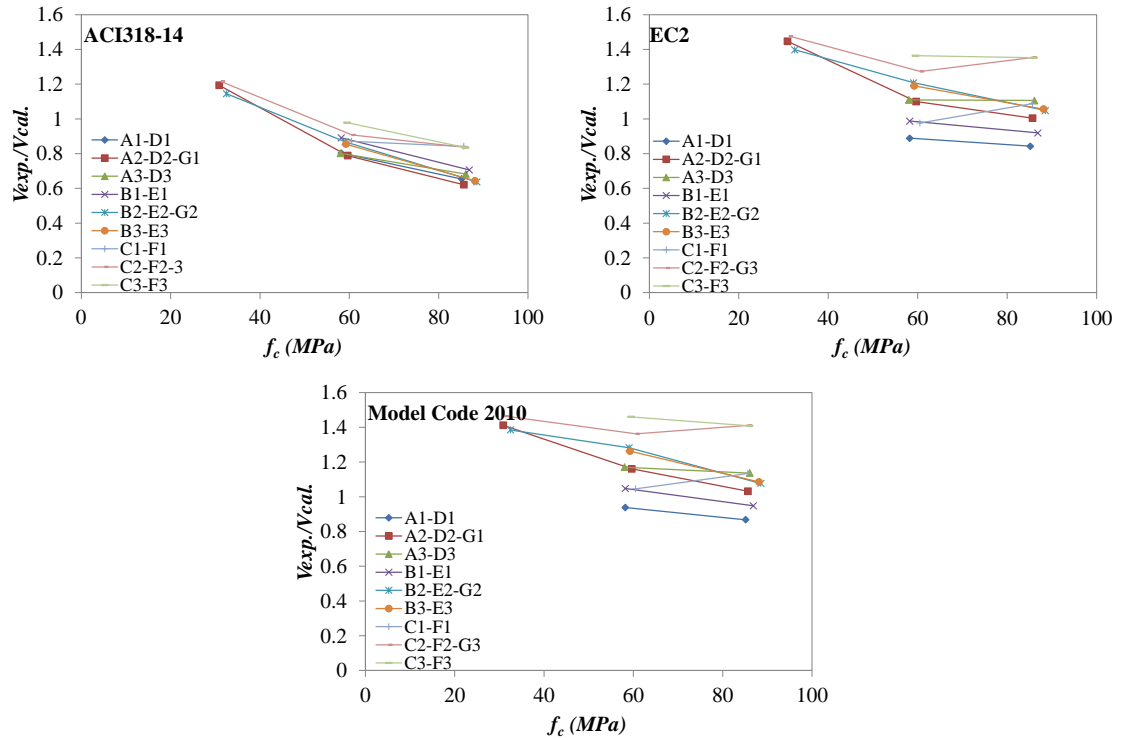
Figure 3-12-Comparison of code predictions to test results (effect of f_c)

3.5.5. EFFECT OF VERTICAL AND HORIZONTAL SHEAR REINFORCEMENT

Increasing the vertical shear reinforcement ratio from 0.0 to around 0.6%, and the horizontal shear reinforcement (placed at mid-depth of the section) ratio from 0.0 to 0.215%, led to roughly 20% increase in load capacity. Further increases in shear reinforcement had no significant influence on load capacity (Figure 3-13), as failure was dominated by crushing of the concrete.

Strain measurements (see Figure 3-14) show that the horizontal shear reinforcement is more effective than vertical shear reinforcement only in beams with shear span to depth ratio less than 1.0. For higher ratios, conventional vertical web reinforcement becomes more effective. These results are in good agreement with the findings of Smith and Vantsiotis [1]. By examining the state of stress developed in the shear span of beams G1 and G3 in Figure 3-15, it can be seen that in G1 the vertical component of the transverse tensile stress is larger than the horizontal component, thus more stress is expected to be

carried by the vertical shear reinforcement. As the strut angle becomes steeper in beam G3, the horizontal component of the transverse tensile stress is larger than the vertical thus the demand on the horizontal reinforcement increases.
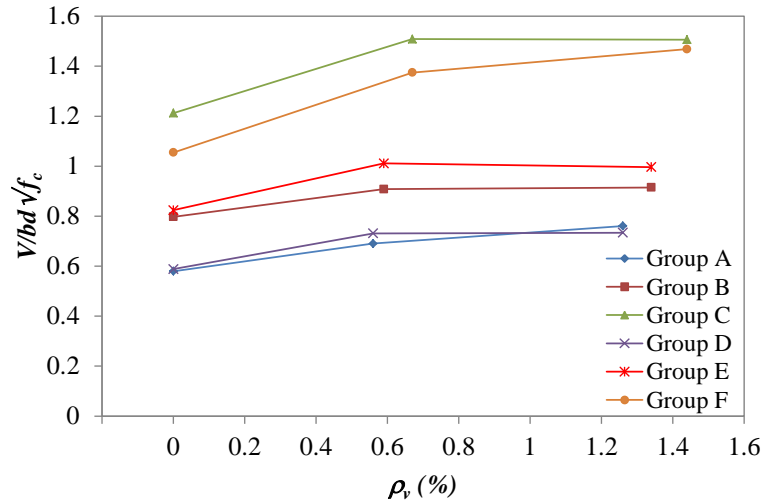
Figure 3-13-Effect of shear reinforcement on the ultimate failure load of the specimens
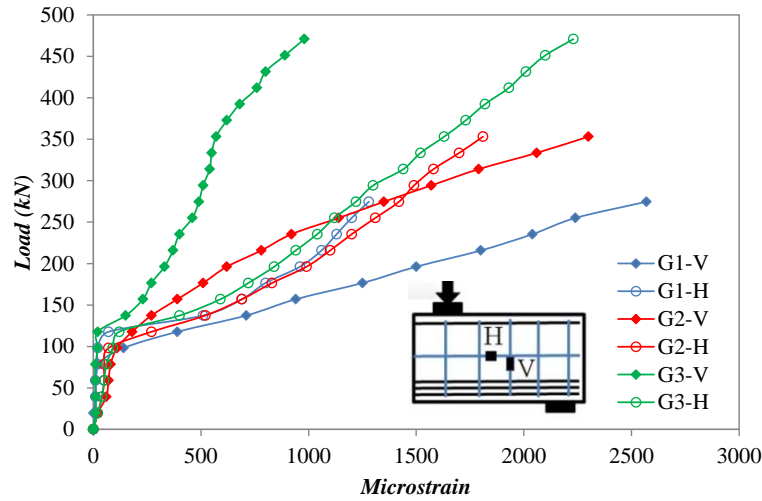
Figure 3-14-Effectiveness of vertical and horizontal shear reinforcement in beams with different shear span to depth ratio
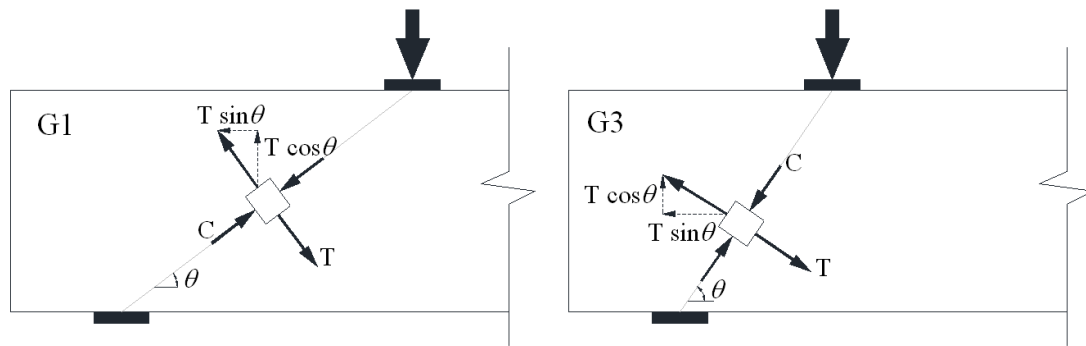
Figure 3-15-Compression and tension stresses orientation

Prior to the formation of inclined cracks, the shear reinforcement was found to play no significant influence on the overall behaviour. Both the vertical and horizontal shear reinforcements were mobilised after the development of the inclined cracks and had an impact on crack patterns and modes of failure. Typically, one major crack developed in the shear span of the beams without shear reinforcement, indicating that the applied load was transferred to the support by one major strut (e.g. beam D1 Figure 3-16). When shear reinforcement was provided, a group of inclined cracks developed in the specimens, indicating that the applied load was transferred to the support by more than one strut (beam D3 in Figure 3-16). The propagation of diagonal cracks was controlled by the shear reinforcement and in some cases the mode of failure changed from brittle shear failure to compression failure, such as in beams of group A, D and E (Table 3-1).
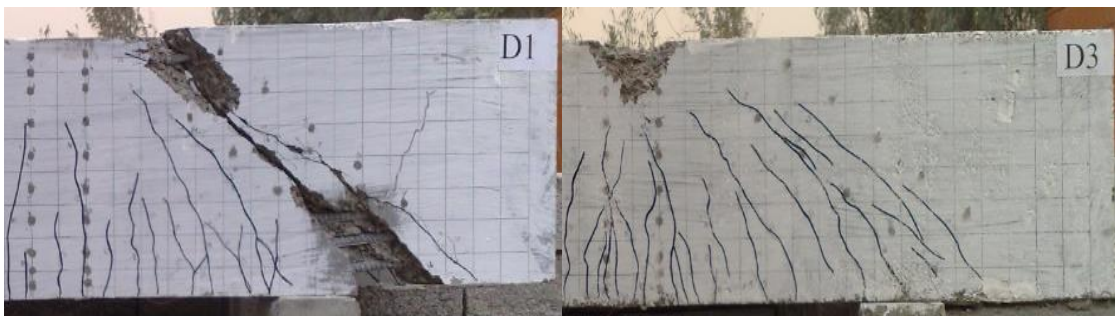
Figure 3-16-Crack patterns and failure modes of beams D1 and D3

From the analysis of Figure 3-17, which shows that the level of safety of ACI 318-14 remains almost constant when varying the vertical shear reinforcement ratio, it can be deduced that the effect of the shear reinforcement on overall shear strength is modelled

adequately. The unconservative nature of the predictions can be mainly attributed to the fact that the model does not take into account the effect of shear span to depth ratio and concrete compressive strength. The EC2 and Model code 2010 predictions are overall conservative for deep beams with shear reinforcement, while they are slightly unconservative for deep beams without shear reinforcement (Figure 3-17). This is because the provisions of these two codes neglect the effect of shear reinforcement on the effectiveness factor this leading to an overestimation of this factor for beams without shear reinforcement.
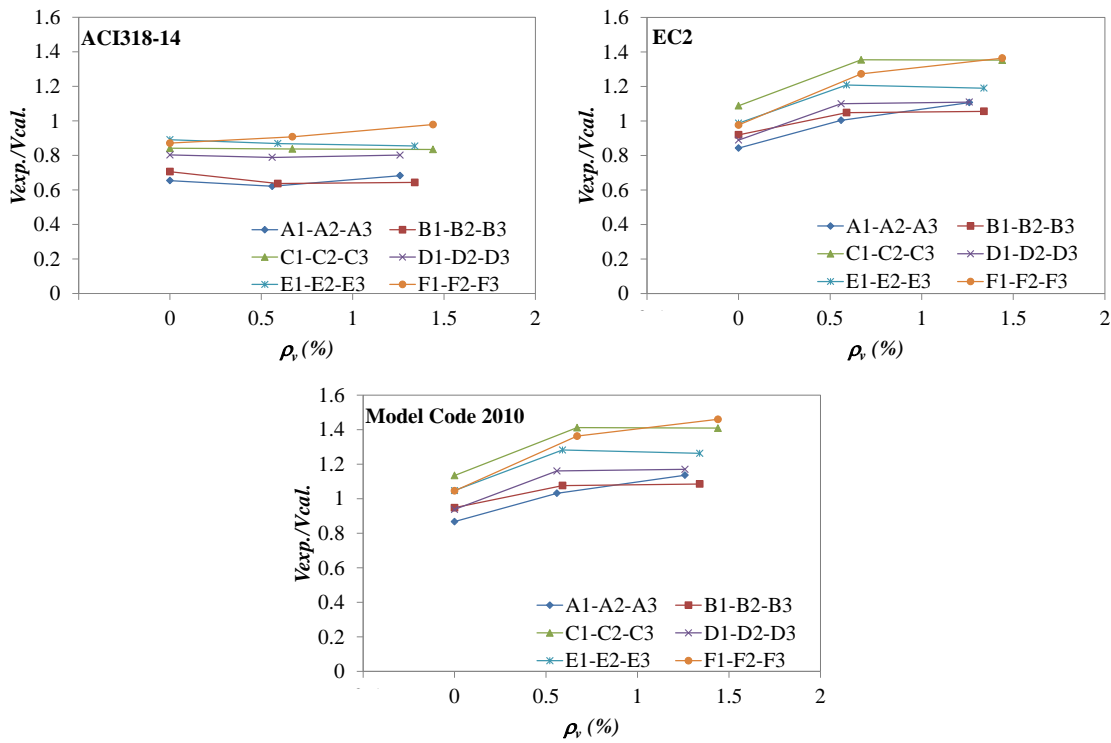
Figure 3-17-Comparison of code predictions to test results (effect of ρ_v)

3.5.6. EFFECT OF EFFECTIVE DEPTH (SIZE EFFECT)

Figure 3-18 shows the average shear stresses (*V/bd*) at first diagonal cracking and at failure for the three beams in group H. It can be seen that, although the shear stresses developed at diagonal cracking do not vary considerably for all three specimens; the ultimate average shear strength shows strong size dependence.
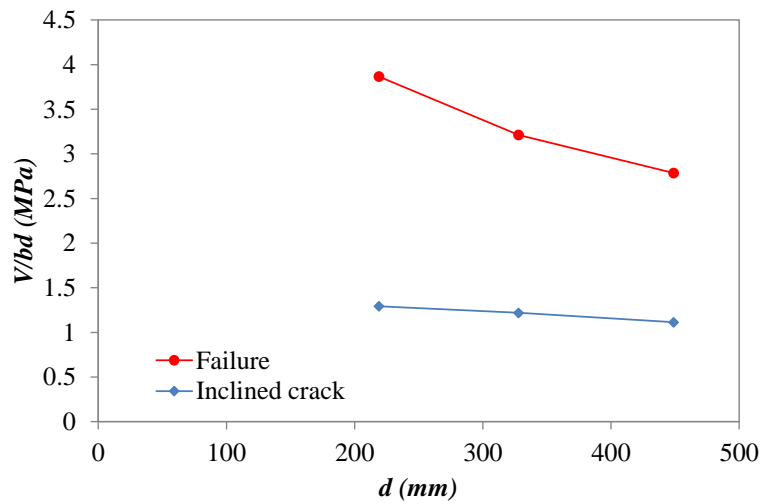
Figure 3-18-Shear stresses at inclined cracking and failure for beams in group H

Figure 3-19 shows experimental and predicted shear strength by the STM with the provisions of the three codes of practice against the effective depth of the beams. It can be seen that with increasing beam size, both experimental and calculated average shear strength (*V/bd*) decreased. Although size effect is not explicitly included in the STM procedure of the three codes of practice, the implementation of STM can predict the experimental capacity of deep beams with a good degree of accuracy. However, the decrease in the shear strength prediction by the STM can be attributed to the fact that the widths of loading and support plate were kept constant during the tests. Therefore, the cross-sectional area of the strut was not increased proportionally with member size. To test this hypothesis, the STM with the provision of the three codes is used to calculate the shear capacity of the same beams, but with the width of the loading and supporting plate increasing proportionally with the member size. The results (Figure 3-20) confirm that the code provisions do not account for size effect.
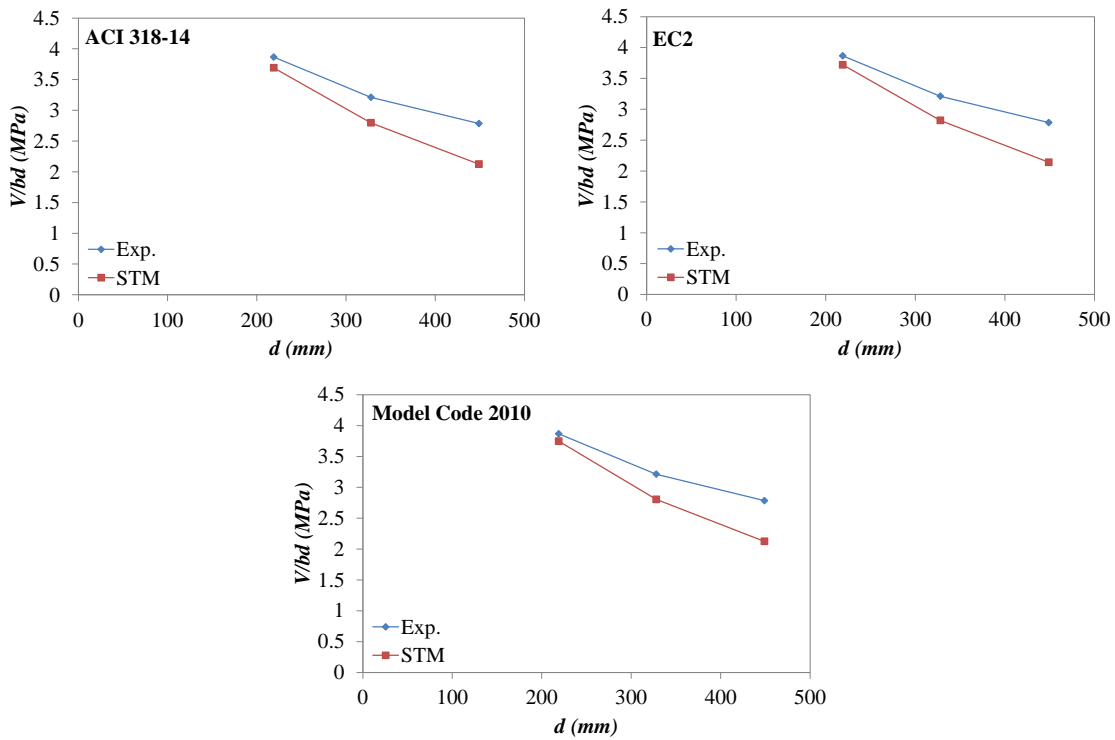
Figure 3-19-Comparison of code predictions to test results (effect of *d*)
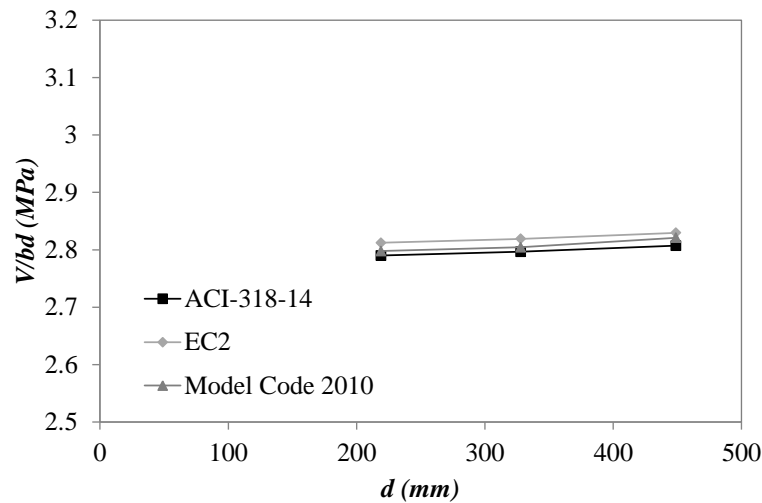
Figure 3-20-Size effect in STM provisions of the Codes

3.5.7. EFFECTIVENESS FACTOR

The equivalent experimental effectiveness factor for the tested beams was calculated by implementing an inverse analysis of a given STM. The effects of different parameters on

the determined effectiveness factor are shown in Figure 3-21. Although, both shear span to depth ratio and shear reinforcement seem to affect effectiveness factor (v'), a stronger dependency is associated with concrete compressive strength.
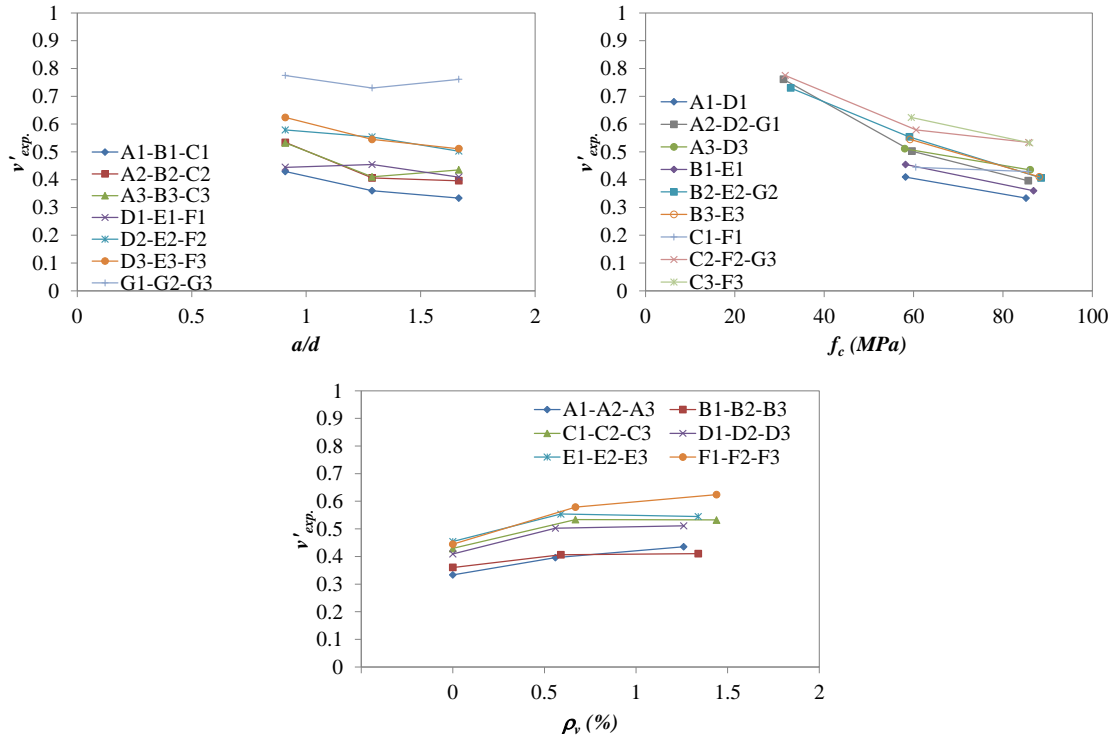
Figure 3-21-Effect of different design parameters on the effectiveness factor

The determined effectiveness factor decreases by increasing the concrete compressive strength (Figure 3-21). The ACI 318-14 effectiveness factor (Figure 3-22), which is constant for beams with and without shear reinforcement, is conservative for normal-strength concrete but becomes unconservative for higher strength. The EC2 and Model code 2010 provisions account for the effect of concrete compressive strength, and their predictions are overall conservative, being more conservative for lower strength concrete (Figure 3-22).
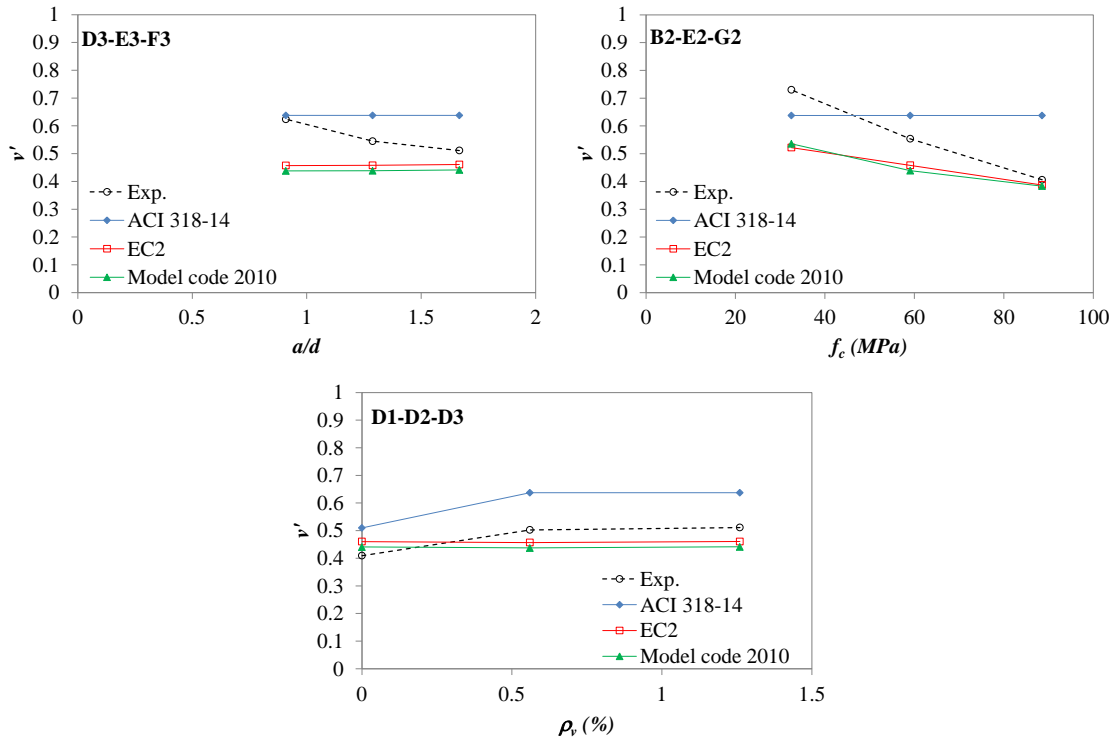
Figure 3-22-Comparison of code predictions to the experimental effectiveness factor

With changing shear span to depth ratio the width of the inclined strut changes also affecting the intensity of the lateral tensile strain developed perpendicular to the strut direction. The former can be accounted for through the angle of the inclined strut (already included in the code provisions). However, the latter has an effect on concrete compressive strength and should be accounted for through the effectiveness factor. Nonetheless, the effect of shear span to depth ratio is neglected in calculating the effectiveness factor in all aforementioned codes of practice as confirmed by their predictions shown Figure 3-22.

The effectiveness factor for concrete elements reinforced in shear increases by about 15% to 20% (Figure 3-21). This can be attributed to the fact that the transverse reinforcement enables more efficient transfer of tensile stresses upon diagonal cracking, thus reducing damage within the concrete struts and increasing their capacity. However, increasing shear reinforcement does not affect considerably the value of the effectiveness factor. ACI 318-14 takes this into account through the use of β_s, which is

0.75 and 0.6 for deep beams with and without shear reinforcement, respectively. On the other hand, EC2 and Model code 2010 do not include any factor to account explicitly for the effect of shear reinforcement on the effectiveness factor (Figure 3-22) this could explain the slightly unconservative predictions obtained for deep beams without shear reinforcement (Figure 3-17).

3.6. CONCLUSION

On the basis of the experimental results presented above and the assessment of different design approaches, the following conclusions can be drawn:

1. Shear span to depth ratio is the most important parameter that controls behaviour and shear capacity of RC deep beams.

2. Concrete compressive strength has more influence on the shear strength of deep beams than shear reinforcement. However, the presence of shear reinforcement is crucial in controlling crack propagation and providing ductility to deep beams.

3. There is a pronounced size effect on the average shear strength (V/bd) of deep beams; however, the first diagonal cracking strength is hardly size dependent.

4. The effectiveness factor is dominated by concrete compressive strength but it is also influenced by the shear span to depth ratio. ACI 318-14 provisions neglect the effect of these two parameters in estimating the effective concrete strength of the inclined strut and as a result lead to unconservative predictions.

5. There is a difference of about 15% to 20% on the experimental effectiveness factor of deep beams with and without shear reinforcement. Amongst the models examined in this paper, ACI 318-14 is currently the only code of practice that accounts for the effect of shear reinforcement on the effectiveness factor. The EC2 and Model code 2010 could be modified to account for the effect of shear reinforcement on controlling crack growth and enabling a more efficient transfer of shear forces.

6. Shear strength predictions by the STM with the provisions of both EC2 and Model Code 2010 are generally conservative; however, their conservatism

reduces with increasing shear span to depth ratio because these two codes neglect the effect of shear span to depth ratio on the concrete effectiveness factor.

CHAPTER 4.   NUMERICAL INVESTIGATION ON THE SHEAR STRENGTH OF RC DEEP BEAMS USING THE MICROPLANE MODEL

This chapter consists of a "stand alone" journal paper: Ismail K. S., Guadagnini M. and Pilakoutas K., (2016b) Numerical Investigation on the Shear strength of RC Deep Beams Using the Microplane Model, Submitted to Journal of Structural Engineering. Full analysis details are presented in Appendix C.

Although much work has been done on the shear behaviour of RC elements, current design provisions are still based on empirical data and their predictions, especially for deep beams, are not always reliable and can lead to unconservative results. This paper presents an extensive numerical investigation on the role of key parameters on the shear performance of RC deep beams using the microplane M4 material model. The model is validated against experimental results of 20 RC deep beams. A parametric study is then carried out to investigate the effect of shear span to depth ratio and concrete compressive strength for RC deep beams with and without shear reinforcement. Although a single strut mechanism is generally mobilised in deep beams, the presence of shear reinforcement can enable a more uniform distribution of shear stresses within the shear span and enhance the effectiveness of concrete cracked in tension. The study confirms that both shear span to depth ratio and concrete strength are the key parameters that affect the shear capacity of RC deep beams and should be taken into account in code equations.

4.1. INTRODUCTION

Deep beams are structural members characterized by shear span to depth ratio smaller than two [3, 4], and their analysis and design cannot be carried out according to conventional bending theory [78, 79]. Generally such members appear as transfer girders in tall building, bridges, and offshore structures. Shear action is critical in these members and, if underestimated, could lead to catastrophic failure without warning. Thus, reliable method to determine their structural performance is needed.

Codes of practice, such as Eurocode 2 (EC2) [3] and ACI 318-14 [4], provide design procedures, such as the strut-and-tie model (STM), to predict the ultimate capacity of RC deep beams. The performance of STM relies on a) selecting appropriate strut-and-tie layout and sizes of each element and b) estimating the maximum allowable stress in each element. The strength of the inclined strut is lower than the uniaxial concrete compressive strength due to the existence of lateral tensile strain. Therefore, a reduction factor, known as the effectiveness factor, is used in the design process to account for this effect. EC2 recommends the use of an effectiveness factor that can only account for the effect of concrete compressive strength, while ACI 318-14 only accounts for the effect of shear reinforcement. Although the STM concept as a lower bound plasticity approach should yield conservative results [14-17], there is evidence that its current implementation in the codes can lead to unsafe predictions [17-19]. Therefore, the code provisions need to be re-assessed and improved to more accurately account for the effect of all relevant parameters.

Experiments can provide key information on the behaviour of RC deep beams, but such tests can be expensive, time consuming and sometimes impractical due to the limiting capabilities of structural laboratories, especially when dealing with large elements. Finite element analysis can provide a valid alternative to laboratory testing, but its accuracy depends on the accuracy of the constitutive models implemented. Generally, the available material models can be classified into two categories: 1) macroscopic models, according to which the material behaviour is simplified from a complex

microstructural stress transfer mechanism to a relationship between average stress and strain at the continuum level; 2) microscopic models, which describe the material behaviour as a stress-strain relationship at the micro level. Although, the latter is considered to be more accurate and can capture the microscopic material behaviour, such as cohesion, aggregate interlock, and friction [38], this approach has two main drawbacks: a) cracks are forced to follow a predefined path along element edges; b) it needs remeshing throughout the solution process due to change in nodal connectivity because of the crack development. From a practical point of view, the implementation of microscopic models is computationally extremely expensive; hence, macroscopic models are more widely used.

In numerical analysis, modeling of concrete and other quasi-brittle materials has always been a challenging issue because of the complexity of their behaviour, and different approaches have been proposed based on the plasticity theory, the plastic-fracturing theory, continuum damage mechanics, or their combinations [39]. In these models, the constitutive relationships are written in terms of tensors on one or two loading surfaces; however, in reality many simultaneous loading surfaces intersect at every point [39]. Hence, these models have limited success in predicting realistically the behaviour of concrete [38]. The more sophisticated microplane model [39, 40] has been shown to capture the microscopic behaviour of concrete in a more reliable manner and it has been successfully implemented in finite element analysis to simulate the non-linear behaviour of concrete and capture shear behaviour of RC elements [40-43]. The main difference between microplane and other material models is that the constitutive law is written in terms of vectors on microplanes rather than tensors at the macro level [39]. Therefore, inelastic physical phenomena such as slip and friction can be characterized directly in terms of stress and strain on the microplanes. The model utilises a frictional yield surface that can account for the effect of shear cracking [39]. The microplane model M4 [39, 40] is adopted in this paper and implemented in a commercially available finite element package, ABAQUS 6.9-2 [80], to simulate and analyze the behaviour of RC deep beams. The concrete material models of ABAQUS, including the smeared crack

model (SCM) and the damage plasticity model (DPM), are also examined and their performance is assessed against experimental results.

On the basis of a series of finite element analyses and a larger numerical parametric study, the effect of shear span to depth ratio, concrete compressive strength and shear reinforcement on the shear strength of RC deep beams is investigated. Particular attention is paid to the development and distribution of principal stresses within the shear span of the modeled beams to gain deeper insight into the development and capacity of shear carrying mechanism. The results of this study are compared to the provisions of EC2 and ACI 318-14 and recommendations are given to improve existing design models.

4.2. NUMERICAL ANALYSIS

4.2.1. MODEL DESCRIPTION

A total of 20 RC deep beams (4 specimens tested as part of this research programme and 16 from literature [68, 81]) are analyzed. The beam details and their failure load are summarized in Table 4-1 and the geometry of the beams is shown in Figure 4-1. Taking advantage of symmetry in geometry and loading conditions, only half specimen are modeled (see Figure 4-1) to reduce overall computational time. The loading is applied through prescribed displacement at the loading points to capture the failure load and post-peak response. The concrete is modeled using 4-noded plane stress elements (CPS4R). The thickness of the plane stress elements is taken as the width of the tested specimens.

The steel reinforcement is modeled using 2-noded linear 2-D truss elements (T2D2). The reinforcement is embedded in the concrete and perfect bond between concrete and reinforcement is assumed. In the present study, the elastic-perfect plastic stress-strain relationship is used to simulate the behaviour of reinforcing steel in both tension and compression. For the simulation of the studied beams, the yield strength of 365MPa, 448MPa and 577MPa for main longitudinal reinforcement, vertical stirrups and

horizontal shear reinforcement, respectively, are used for beams E1, G1, G2 and G3 as determined from tensile tests.

Table 4-1-Summary of the beams used for model validation

	Researcher	Specimen	L, mm	h, mm	b, mm	a, mm	f_{ck} MPa	A_s mm^2	$\rho_{v\,\%}$	$\rho_{h\,\%}$	Failure Load kN
1		E1	1800	400	100	425	58	1206	0	0	415
2	Current work	G1	1800	400	100	550	31	1206	0.56	0.22	292
3		G2	1800	400	100	425	33	1206	0.59	0.22	372
4		G3	1800	400	100	300	31	1206	0.67	0.22	489
5		B2.0-1	1900	700	125	825	83	1880	0.6	0.33	1590
6		B2.0-2	1900	700	125	825	120	1880	0.6	0.33	1650
7		B2.0-3	1900	700	125	825	78	1880	0.6	0.33	1400
8		B2.0A-4	1900	700	125	675	86	1880	0.6	0.33	1900
9		B2.0B-5	1900	700	125	825	89	1880	0	0	1170
10	Foster & Gilbert [68]	B2.0C-6	1900	700	125	825	93	1880	0.9	0	1460
11		B2.0D-7	1900	700	125	825	104	1880	0.6	0	1440
12		B3.0-1	2600	700	125	1175	80	1880	0.6	0.33	1020
13		B3.0-2	2600	700	125	1175	120	1880	0.6	0.33	1050
14		B3.0-3	2600	700	125	1175	77	1880	0.6	0.33	1050
15		B3.0A-4	2600	700	125	925	88	1880	0.6	0.33	1550
16		B3.0B-5	2600	700	125	1175	89	1880	0	0	870
17		ACI-I	4470	915	305	915	33	2940	0.31	0.46	2713
18	Aguilar et al. [81]	STM-I	4470	915	305	915	33	2940	0.31	0.15	2268
19		STM-H	4470	915	305	915	28	2940	0.31	0.15	2571
20		STM-M	4470	915	305	915	28	2940	0.15	0	2553

Since explicit analysis is more robust, ABAQUS/EXPLICIT is adopted; however, ABAQUS/STANDARD is used when comparisons are made with the smeared crack model, as this cannot be used with explicit procedure. Although ABAQUS/EXPLICIT is a true dynamic platform, it can also be used for quasi-static analysis; however, special consideration is required to change the procedure from dynamic to quasi-static. The quasi-static analysis is achieved in ABAQUS by using mass scaling or by changing the loading rate [80] or a combination thereof. The simulation is carried out in displacement control with the smooth amplitude option. The kinetic and internal energy is monitored

to ensure the kinetic energy does not exceed 5% to 10% of its internal energy throughout most of the analysis process [80]. When this is not achieved through the implementation of the loading rate, mass scaling is also used along with loading rate to keep the kinetic energy within the required limits.
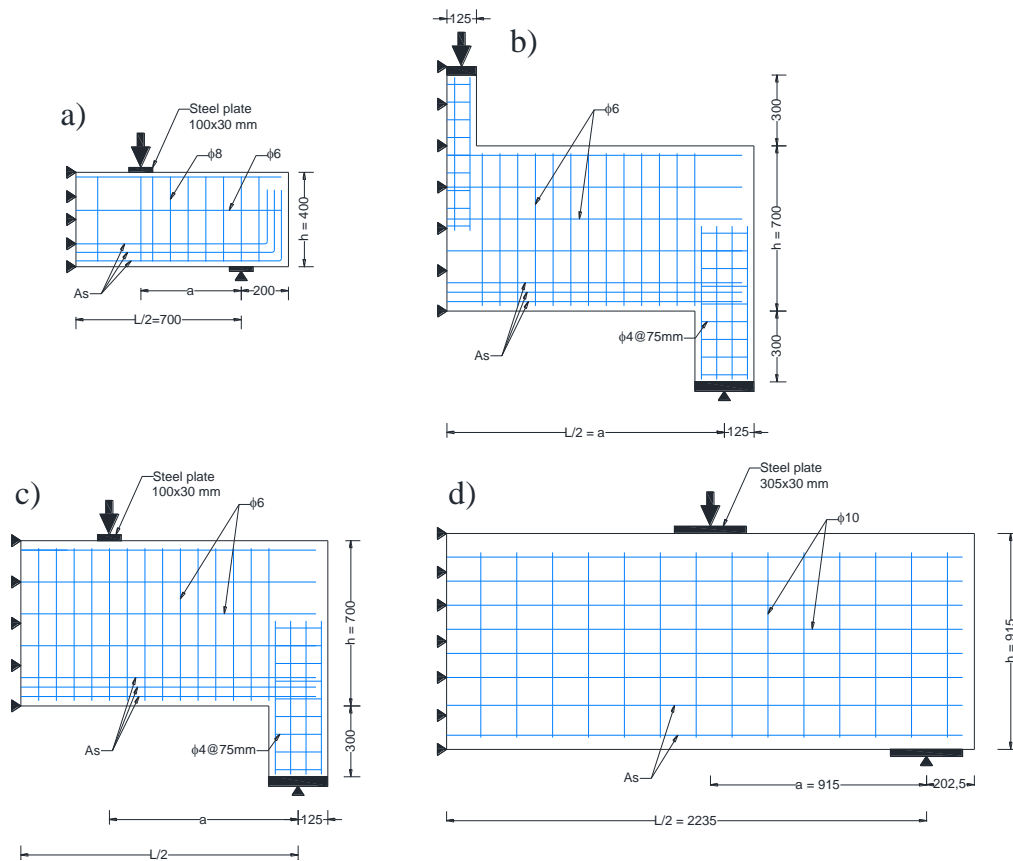
Figure 4-1-Detail of the analysed beams, a) current research, b) beams tested by Foster & Gilbert [68](except for B2.0A-4 and B3.0A-4 beams), c) B2.0A-4 and B3.0A-4 beams [68] and d) beams tested by Aguilar et al. [81]

The element size is chosen on the basis of a systematic mesh sensitivity analysis, as explained later and to maintain the balance between kinetic energy and internal energy. The element size is 4 times the maximum aggregate size for beams with overall depth less than 500mm, while an approximate global element size of 100mm is used for beams with overall depth greater than 500mm. It is worth mentioning that these element sizes are 10 to 15% of the total height of the beams. The relevant element sizes were used to

calibrate the performance of the microplane model before conducting any subsequent analysis.

4.2.2. EVALUATION OF CONCRETE MATERIAL MODELS AVAILABLE IN ABAQUS

The concrete constitutive models implemented in ABAQUS include the smeared crack model (SCM) and the damage plasticity model (DPM). The smeared crack model is based on the smeared cracking approach first developed by Rashid [33]. Cracks in concrete can be detected at any location when the concrete stresses reach one of the failure surfaces (crack detection surfaces) in the biaxial tension region or combined tension-compression region. The smeared crack model does not track each macrocrack, but it performs independent constitutive calculations at each integration point of the finite element model by using degraded stiffness. This model accounts for the effect of shear through a shear retention factor, which can specify the amount of shear stresses that can be transferred after cracking. The damage plasticity model (DPM) is a continuum damage plasticity-based model proposed by Lubliner et al. [37]. This model represents the inelastic behaviour of concrete by using the concepts of isotropic damaged elasticity in combination with isotropic tensile and compressive plasticity. The model describes the irreversible damage in concrete due to the fracturing process by a combination of non-associated multi-hardening plasticity and scalar damaged elasticity. Tensile cracking and compressive crushing are assumed to be the two main failure mechanisms of concrete. The evolution of the failure surface is controlled by two hardening variables describing the failure mechanisms under tension and compression.

These two models are examined first to assess their accuracy in capturing the shear behaviour of RC deep beams. The models had been earlier optimized using mesh sensitivity and the chosen mesh size which is 4 times the maximum aggregate size was found to best approximate overall structural response of the examined beams. Figure 4-2 and Figure 4-3 show the load-deflection response and strain in both horizontal and vertical shear reinforcement for one of the beams that were tested by the authors. It can

be seen that the numerical responses are much stiffer than the experimental responses after cracking. This can be attributed mainly to the inability of the implemented concrete models to realistically predict the behaviour of the concrete subjected to shear stress and lateral tensile stresses. In reality, high shear stresses and lateral tensile stresses develop in the shear span of RC deep beams and this makes the concrete softer than under uniaxial conditions. This softening reduces the overall stiffness of the member and eventually leads to shear failure in the shear span. However, this softening behaviour accompanied by increasing shear deformation, cannot be realistically estimated by either approaches. From the analysis of the experimental results shown in Figure 4-3, it can be seen that shear cracking occurred at earlier loading stages compared to the numerical predictions and strain in shear reinforcement is vastly underestimated after cracking at similar load levels. This means that, for the same applied load concrete is more damaged in the experiments and this is the main reason why the numerical response is stiffer than the experimental and the failure load is overestimated.
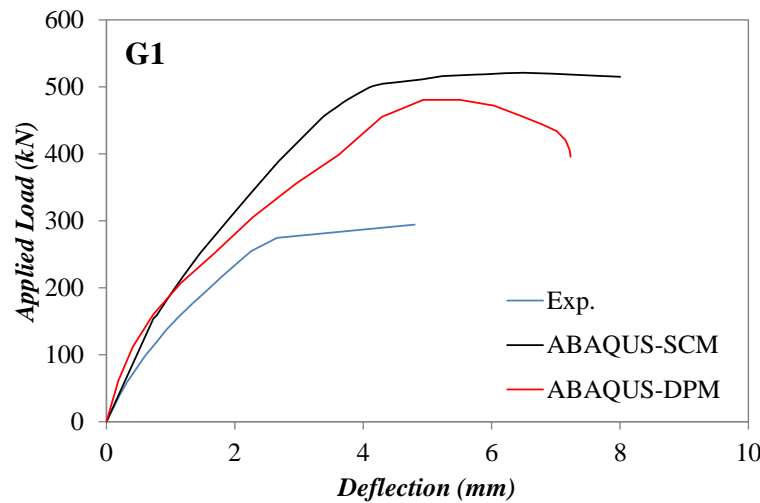
Figure 4-2-Experimental and predicted load–deflection curves (specimen G1)
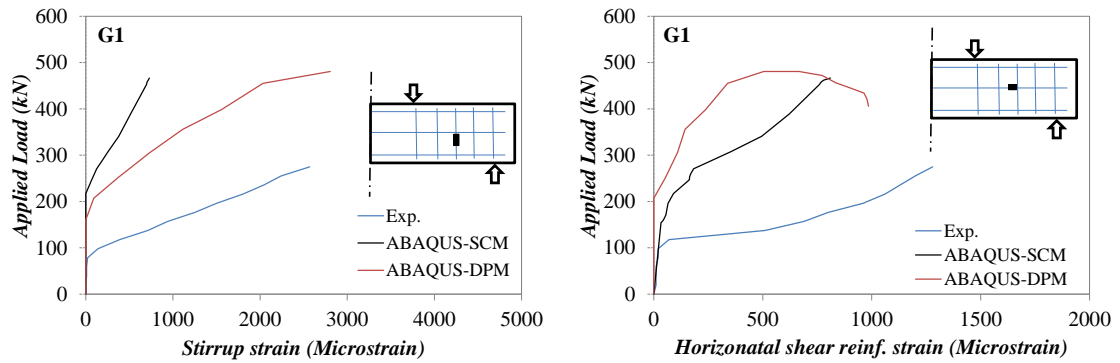
Figure 4-3-Experimental and predicted shear reinforcement strain (specimen G1)

Another reason for this discrepancy between experimental and numerical results is the adoption of average stress and strain. However, this is not necessarily a major issue, because an accurate constitutive law that can capture the behaviour of concrete material in a more realistic way can compensate for this assumption to a reasonable degree, as will be discussed later in this paper.

The inclusion of a shear retention factor in the smeared crack model of ABAQUS[80], can theoretically account for the effect of shear cracking. However, previous studies [82] have shown that even the use of a wide range of shear retention values could not affect significantly the global behaviour and the calculated shear strength did not vary significantly for the analysed beams. Hence, more accurate constitutive models are required to simulate the behaviour of RC deep beams, such as the microplane model.

4.2.3. MICROPLANE MATERIAL MODEL M4 FOR CONCRETE

The microplane material model is a macroscopic material model that defines the relation between the stress and strain vectors on planes of various orientations (microplanes). These microplanes can be assumed as cracked planes or weak planes, such as the contact faces between aggregate particles in concrete. The basic idea of the microplane model can be traced back to the pioneering idea of Tayler [83] which was later developed by Batdorf and Budianski [84] for polycrystalline metals and became known as the slip theory of plasticity. This model was later extended by Bazant and co-workers [39, 40, 43, 85-90] who added extra features to better represent the behaviour of quasi

91

brittle materials, including concrete. These features can be briefly summarized as follows:

The static micro-macro constraint should be replaced by kinematic micro-macro constraint to stabilize the postpeak strain softening; that is, the strain vectors on microplanes are the projection of the strain tensors.

Elastic strain is included at the microplane level instead of adding it at the macro level due to the replacement of the static micro-macro constraint with the kinematic.

The principle of virtual work is used instead of simple superposition of the microplane stresses to relate the stresses on the microplane, which can have any possible orientation to the stress at macro level.

Since the kinematic constraint is used, the microplane strain vector ε_{Ni} is determined as the projection of the strain tensor ε_{ij}. The normal strain ε_N and both shear strains ε_M, ε_L on the microplane can then be found according to the following equations:

$$\varepsilon_N = N_{ij}\varepsilon_{ij}, \quad \varepsilon_M = M_{ij}\varepsilon_{ij}, \quad \varepsilon_L = L_{ij}\varepsilon_{ij} \tag{4.1}$$

where $N_{ij}=n_in_j$, $M_{ij}=(m_in_j+m_jn_i)/2$ and $L_{ij}=(l_in_j+l_jn_i)/2$ and n,m and l are direction cosines, the values of which can be found elsewhere [91].

Bazant et al. [39] calculated the stress at the continuum level from the microplane stresses applying the principle of virtual work, which can be approximated by optimal Gaussian integration for a spherical surface.

The constitutive law of microplane M4 is characterized by an elastic stress-strain relationship up to a defined set of limits, which is called stress-strain boundaries, followed by a strain softening behaviour. The stresses are never allowed to exceed the boundaries, however, traveling along the boundaries is allowed if the strain increment and the total stress have the same sign, otherwise, unloading occurs.

Bazant and co-workers [39, 40] split the normal stress and strain components into volumetric and deviatoric parts ($\sigma_N = \sigma_V + \sigma_D$ and $\varepsilon_N = \varepsilon_V + \varepsilon_D$) to realistically model the compression failure and to control the value of Poisson's ratio.

The microplane elastic moduli can be used in the case of loading as well as reloading. Additionally, they can be used for unloading if the sign of $\sigma\Delta\varepsilon$ is positive, otherwise stiffness degradation occurs and the value of the tangential stiffness modulus is used for unloading.

The microplane model M4 was implemented in general finite element package ABAQUS using a VUMAT subroutine. This allowed the development of a more robust numerical platform that could be used to obtain an invaluable insight on the behaviour of RC elements. This also allowed a more systematic and reliable analysis of the effect of different parameters on the structural behaviour of the examined specimens. The number of microplanes adopted in each integration points is 21, which is the minimum number of microplanes needed to yield acceptable results [92]. With the exception of the adjustable material parameter (k_1), which controls the concrete uniaxial tensile and compressive peak strength, the values of the other adjustable material parameters k_2, k_3 and k_4 were optimized to best represent the biaxial compressive and tensile stress-strain relationships and a systematic parametric study was carried out to choose these values that best represent the experimental results and had values of 200, 15 and 100, respectively. A value of 0.0003 was used for the adjustable material parameter k_1 for beams with shear span to depth ratio greater than 1.0, while a value of 0.0004 was used for beams with shear span to depth ratio less than 1.0. In all cases for which the experimental modulus of elasticity was not available the modulus of elasticity was determined according to EC2.

4.3. MODEL VALIDATION

4.3.1. EFFECT OF ELEMENT SIZE

Concrete and other quasi-brittle materials exhibit strain softening in the post-peak response in tension and compression. Due to this strain softening, finite element modeling results are sensitive to mesh size. When the model mesh is refined, the fracture energy dissipated during brittle failure in the critical regions of strain-softening damage can decrease considerably, thus affecting overall failure load. Mesh sensitivity techniques such as crack band [42, 93] can be implemented in the model to control crack propagation and compressive post peak behaviour. However, these are not easy to apply to complex material model such as Microplane model M4 in its current form, because in this model it is not easy to identify which material parameters should be adjusted according to the element size to ensure correct energy dissipation in the softening regime. Therefore, in the current study, mesh sensitivity analysis is performed and best mesh sizes are chosen based on this analysis

To examine the effect of element size on global behaviour, four element sizes were considered. Figure 4-4 shows the effect of element size on the load deflection response and failure load for beams G1 and B2-0-1. It can be seen that for beam G1, with an overall depth of 400mm, the 50x50mm element size, which is equal to four times the maximum aggregate size, is in better agreement with the experimental results. However, for beam B2-0-1, with an overall depth of 700mm, the use of larger elements yields slightly better correlation with the experimental results. The result from all 20 RC deep beams showed that for beams with overall depth less than 500mm, using an element size equivalent to four times the maximum aggregate size is in good agreement with the experimental results. The use of elements with a size of 100x100mm seem to better approximate experimental results of deep beams with an overall depth greater than 500mm regardless of their maximum aggregate size. These mesh sizes are within 10 to 15% of the height of the specimens.
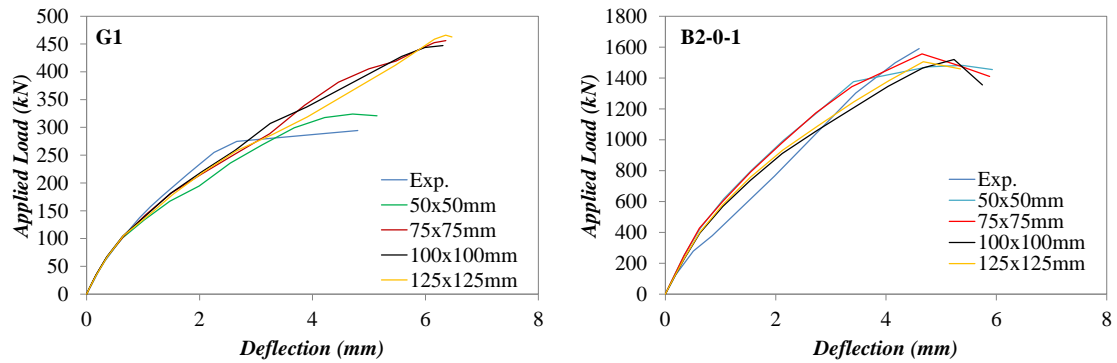
Figure 4-4-Effect of element size on the predicted load-deflection response

4.3.2. LOAD-DEFLECTION RESPONSE

The load deflection curves obtained from the numerical analyses of eight of the examined beams are presented in Figure 4-5 along with the experimentally measured load deflection responses. As can be seen, the results show an overall good agreement with the experimental data, although, in some beams the FE results still exhibit a slightly stiffer response, as also seen from the strain results (see section 4.3.3). Figure 4-6 and Figure 4-7 show the ratio of experimental to predicted failure load and deflection at failure, respectively, for all 20 analyzed beams. Figure 4-8-a, shows the ratio of experimental to FE failure load as a function of shear span to depth ratio. From the analysis of the load deflection response of beams G1, G2 and G3, with shear span to depth ratio of 1.67, 1.29 and 0.91 respectively (Figure 4-5), it can be seen that the numerical prediction for beams with smaller shear span to depth ratio is in better agreement with the experimental results. This can again be attributed to the inability of a smeared crack approach to capture realistically the behaviour of the member in terms of cracking and local strain distribution. For beams with shear span to depth ratio less than 1.0, the applied load is directly transferred to the support through a strut and the shear span has less discrete cracks. This can be better represented by the smeared crack approach than for shear span to depth ratios greater than one, which are typically characterized by multiple discrete cracks.

95
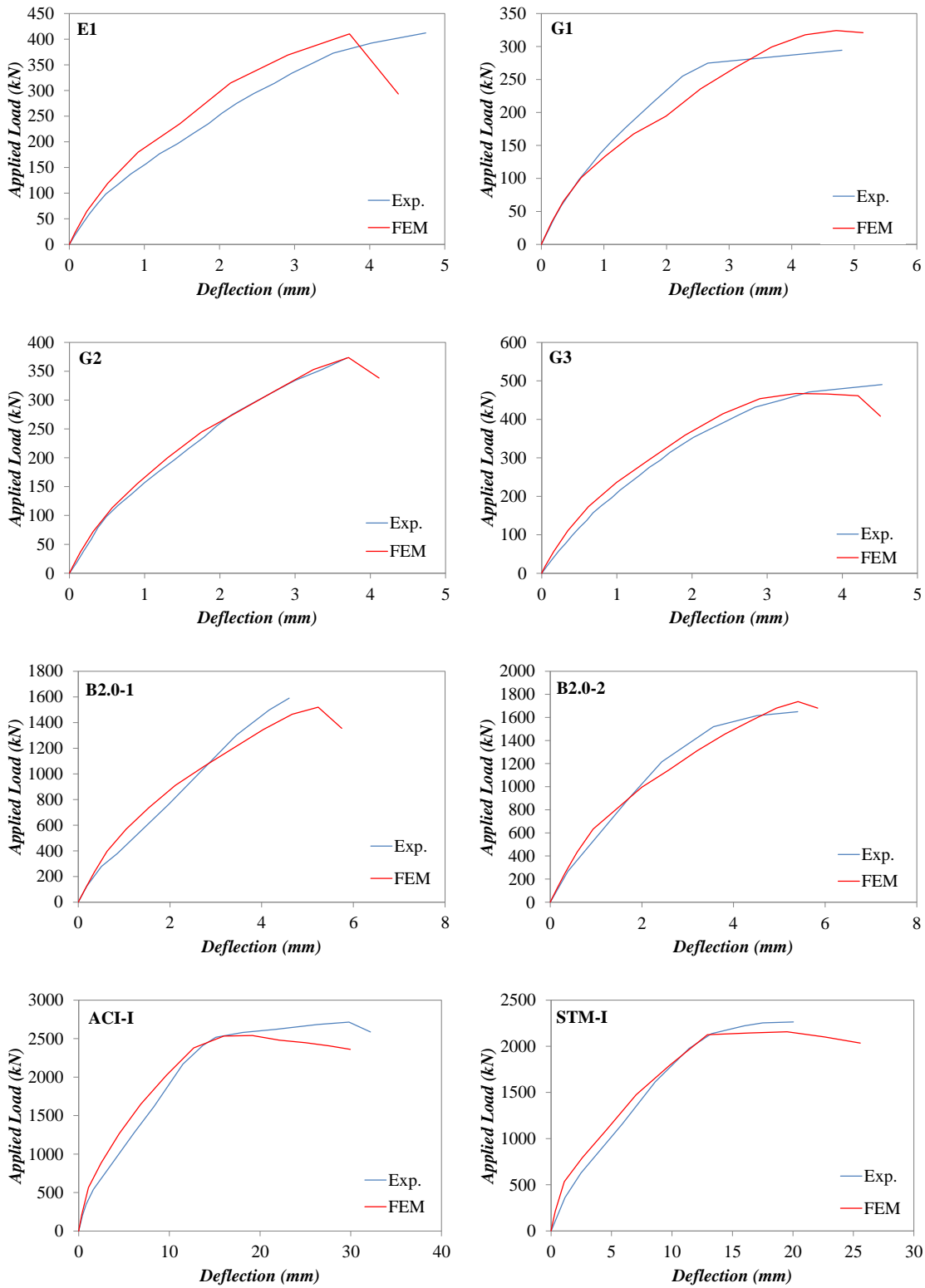
Figure 4-5-Experimental and predicted load–deflection curves
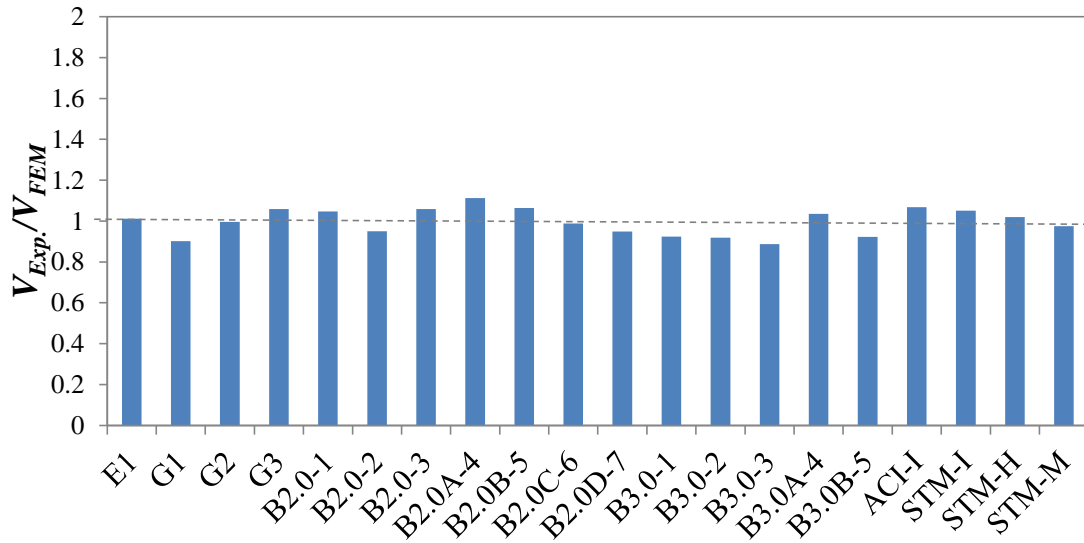
Figure 4-6-Ratio of experimental to predicted failure load for the analysed beams
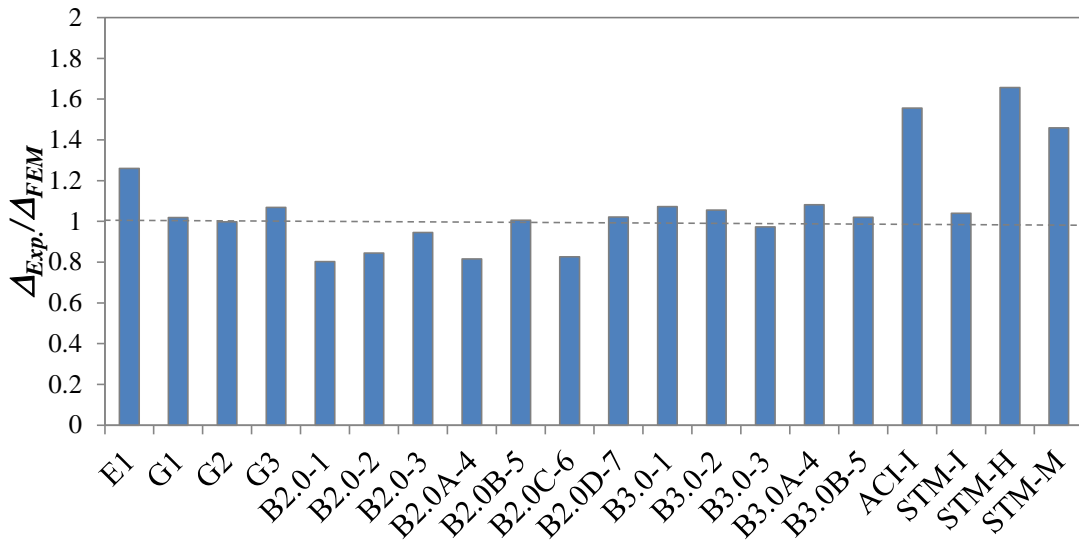
Figure 4-7-Ratio of experimental to predicted deflection at failure for the analysed beams

Figure 4-8-b shows the ratio of experimental and predicted failure load as a function of the shear reinforcement ratio. The results show that the model can provide reasonable predictions for both beams with shear reinforcement and without shear reinforcement. Figure 4-9 shows the comparison between the experimental crack pattern at failure and predicted failure by finite element analysis for two of the analysed beams.

97
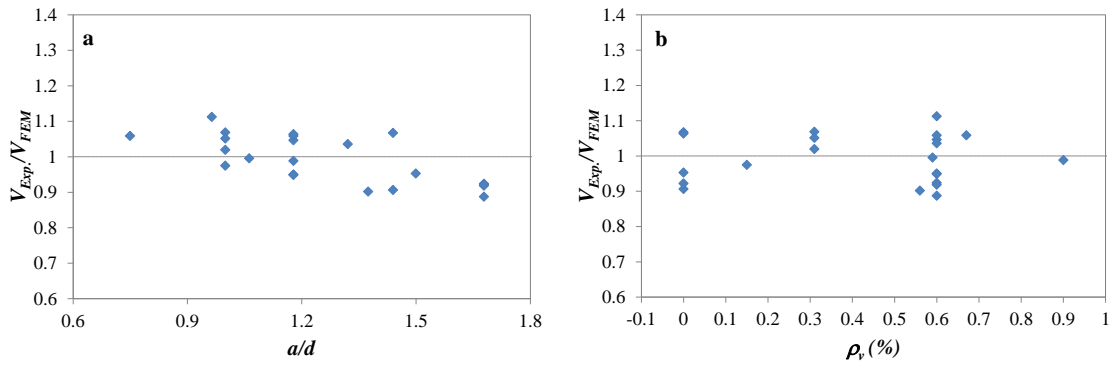
Figure 4-8-Effect of a) shear span to depth ratio and b) shear reinforcement ratio on the predicted capacity of the analysed beams
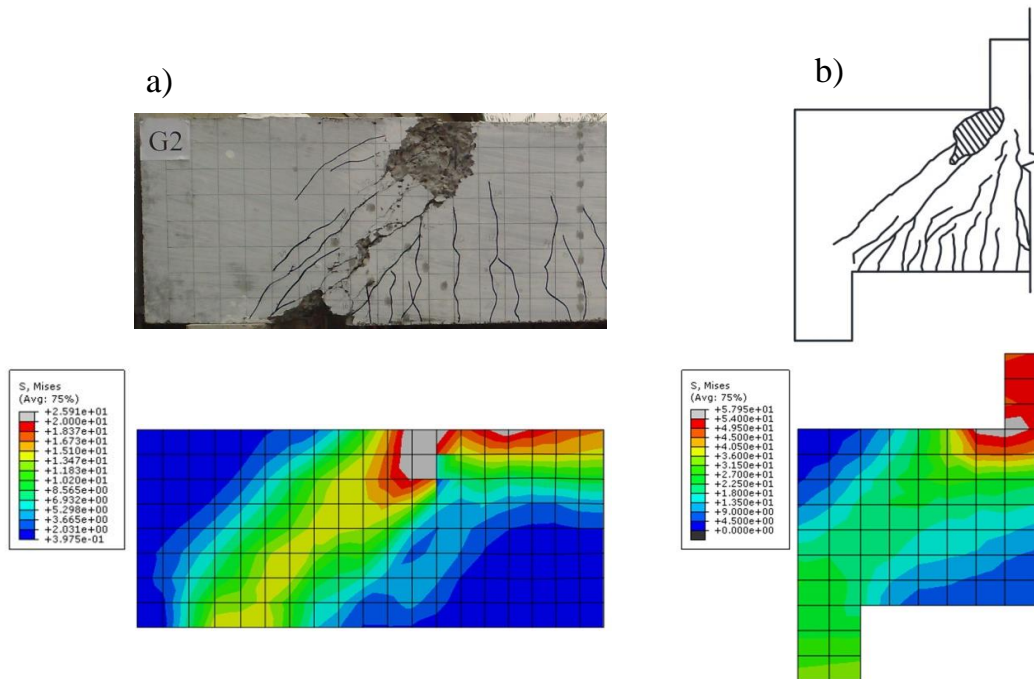
Figure 4-9-Experimental and numerical failure a) beam G1 b) beam B2.0-2 [68]

4.3.3. STRAIN IN LONGITUDINAL AND SHEAR REINFORCEMENT

The load-strain plots for the main flexural, vertical and horizontal shear reinforcement at specified locations are shown in Figure 4-10, Figure 4-11 and Figure 4-12, respectively.

For the elastic stage, up to the formation of cracking, the results from the finite element analysis show a good agreement with the experimental data. After the formation of flexural cracks, the experimental response in terms of strain in the main flexural reinforcement is generally softer than the finite element results; however, the trends are generally comparable.
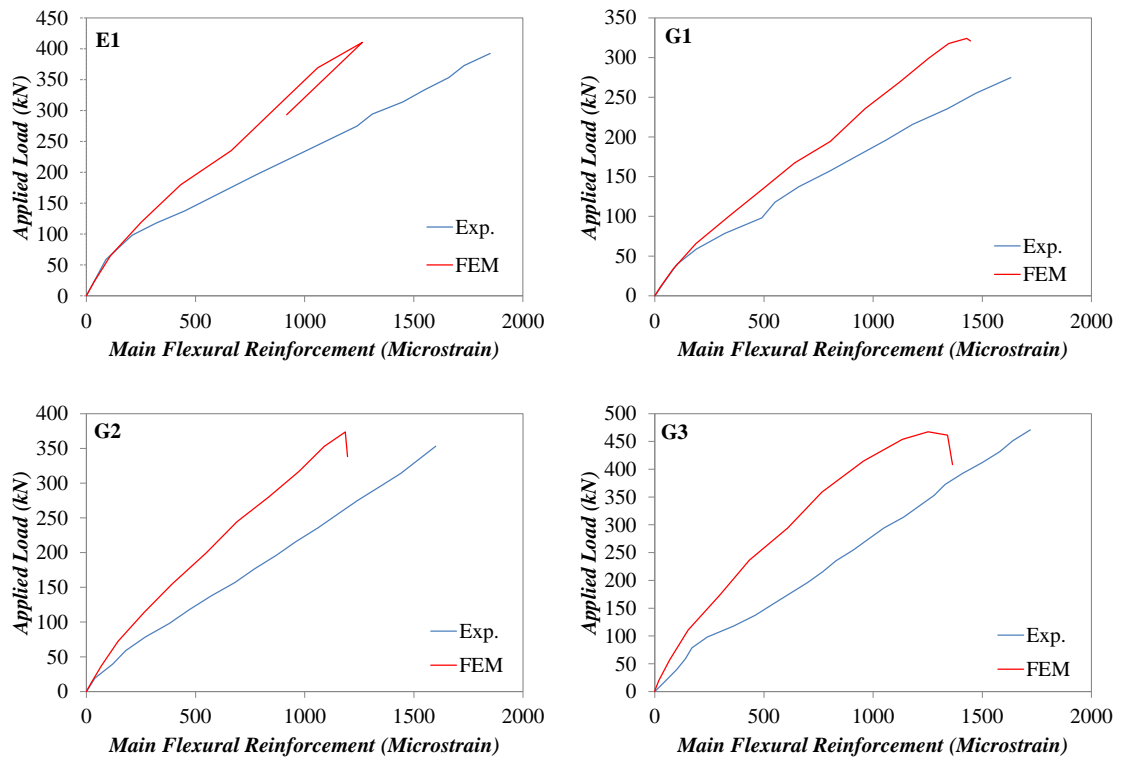
Figure 4-10-Experimental and predicted main flexural reinforcement strain

This discrepancy in the load-strain response after crack formation can be attributed to the following:

- Concrete tensile strains are highly localized at crack locations and the intact area of concrete between cracks can still contribute to the load resisting mechanism by means of tension stiffening; however, in numerical analysis, due to the use of average stress and strain, such tension stiffening and strain localization cannot be properly modeled. This can result in the inaccurate prediction of the stiffness of

cracked concrete and strain distribution within the member, which in turn directly affects overall stiffness.

- Perfect bond between concrete and reinforcing bars is used in the simulations and thus the numerical model is unable to capture the stiffness degradation due to debonding and local slip of the reinforcement at the location of the cracks.

- To prevent local concrete crushing at the location of application of point loads and supports, steel spreader plates are used in both experimental and numerical analysis. In numerical analysis the spreader plates are rigidly connected to the concrete to prevent them from moving. This means that at the location of the tie, concrete and the steel plates share the same nodes; as a result, the stiffness of the element in the surrounding area is increased by the high stiffness of the steel plates.
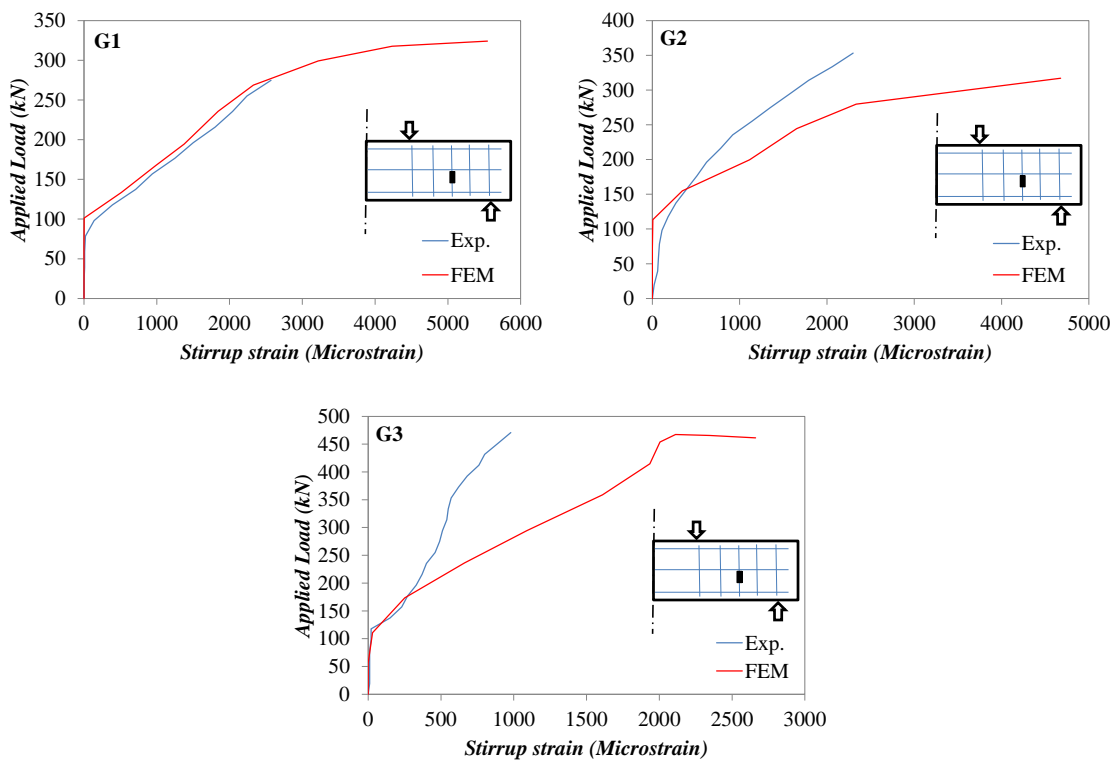
Figure 4-11-Experimental and predicted vertical shear reinforcement strain for beams G1, G2 and G3
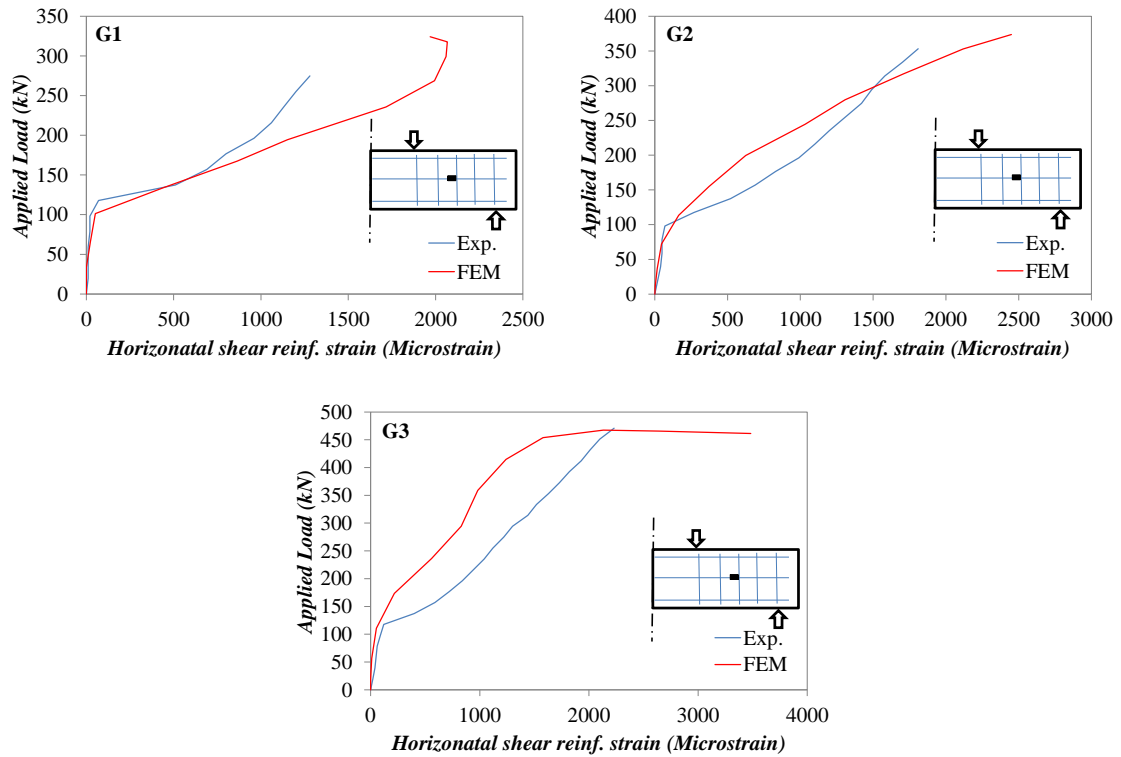
Figure 4-12-Experimental and predicted horizontal shear reinforcement strain for beams G1, G2 and G3

Despite some inherent modelling deficiencies, overall the implementation of the microplane model gives very good predictions of the behaviour of RC deep beams and can be a useful tool in understanding the accuracy of design equations used in codes of practice.

4.4. PARAMETRIC STUDY

On the basis of the numerical model described above, a parametric study was carried out to investigate the effect of different design parameters on the shear capacity of RC deep beams. The details of the beams used in this parametric study are given in Table 4-2. The design parameters are: shear span to depth ratio (0.75, 1.3 and 2.0) and concrete compressive strength (30, 55 and 80MPa). As shear in RC deep beams is primarily resisted through the development of a single strut, the overall behaviour is not greatly

affected by an increasing amount of shear reinforcement. Thus, only beams without shear reinforcement and with the minimum amount of shear reinforcement (according to ACI 318-14 and EC2) were considered in this study. The width of support and loading plates are 150mm.

Table 4-2 Details of the beams used in parametric study

	Specimen	L, mm	h, mm	d, mm	b, mm	a, mm	a/d	f_c, MPa	ρ, %	ρ_v & ρ_h, %
1	BN-S-30	2965	750	710	200	532.5	0.75	30	1.3	0
2	B-S-30	2965	750	710	200	532.5	0.75	30	1.3	0.25
3	BN-S-55	2965	750	710	200	532.5	0.75	55	1.3	0
4	B-S-55	2965	750	710	200	532.5	0.75	55	1.3	0.25
5	BN-S-80	2965	750	710	200	532.5	0.75	80	1.3	0
6	B-S-80	2965	750	710	200	532.5	0.75	80	1.3	0.25
7	BN-M-30	3746	750	710	200	923	1.3	30	1.3	0
8	B-M-30	3746	750	710	200	923	1.3	30	1.3	0.25
9	BN-M-55	3746	750	710	200	923	1.3	55	1.3	0
10	B-M-55	3746	750	710	200	923	1.3	55	1.3	0.25
11	BN-M-80	3746	750	710	200	923	1.3	80	1.3	0
12	B-M-80	3746	750	710	200	923	1.3	80	1.3	0.25
13	BN-B-30	4740	750	710	200	1420	2	30	1.3	0
14	B-B-30	4740	750	710	200	1420	2	30	1.3	0.25
15	BN-B-55	4740	750	710	200	1420	2	55	1.3	0
16	B-B-55	4740	750	710	200	1420	2	55	1.3	0.25
17	BN-B-80	4740	750	710	200	1420	2	80	1.3	0
18	B-B-80	4740	750	710	200	1420	2	80	1.3	0.25

4.4.1. RESULTS AND DISCUSSION

Figure 4-13 shows the effect of shear span to depth ratio and concrete compressive strength on the capacity of RC deep beams. The results of the analysis on beams without shear reinforcement (specimens NSR) are shown along those of their counterparts with shear reinforcement (specimens SR). It can be seen that with increasing shear span to depth ratio the shear strength decreases. This can be attributed to the fact that in beams with low shear span to depth ratios, the applied load is directly transferred through one strut, which means that the concrete is more directly loaded in compression, whilst with

increasing shear span to depth ratio the angle of the strut becomes shallower
(Figure 4-14-b) which leads to larger lateral tensile strains that weaken the compressive
strut.
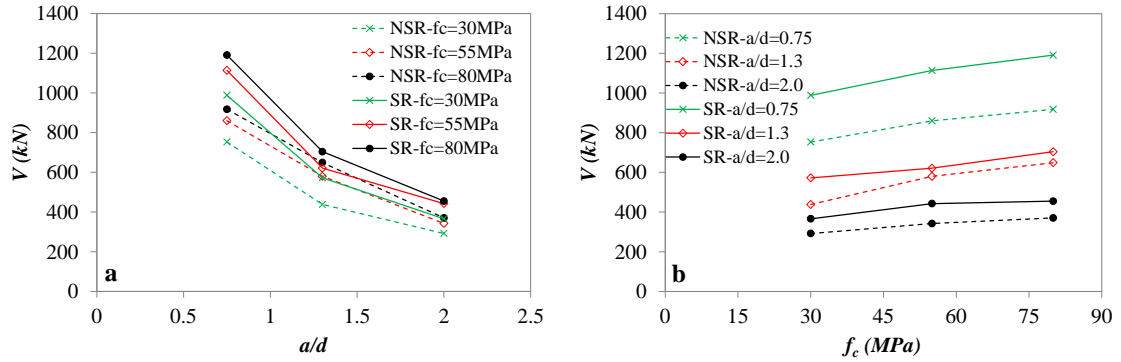
**Figure 4-13-Effect of a) shear span to depth ratio and b) concrete compressive strength on
shear strength of RC deep beams**
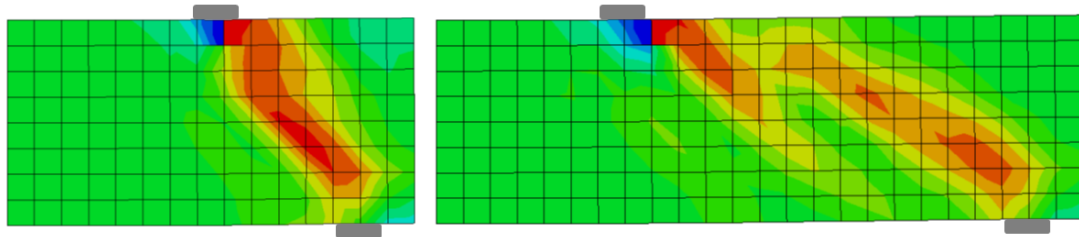
Figure 4-14-Shear stress transfer in beams with different shear span to depth ratio

With increasing concrete compressive strength, as expected, the shear capacity of the
RC deep beams increases. Since the applied load is transferred directly by a single
inclined strut, increasing concrete strength leads to an increase in resistance capacity of
this strut as shown in Figure 4-15-a. However, the compressive stress at failure in the
strut of the beam with concrete strength of 80MPa was only 30% higher than that
developed in the same beam with concrete strength of 30MPa. The maximum principal
compressive stress in the beam with concrete strength of 30MPa was about 75% of its
concrete strength, whilst values of less than 40% were observed in the beams with
concrete strength of 80MPa. This is probably due to the fact that: 1) the tensile strength
of concrete increases at a lower rate than its compressive strength and 2) with increasing

strength and load capacity, the lateral tensile stress in the strut also increases, which reduces further the effective compressive strength.
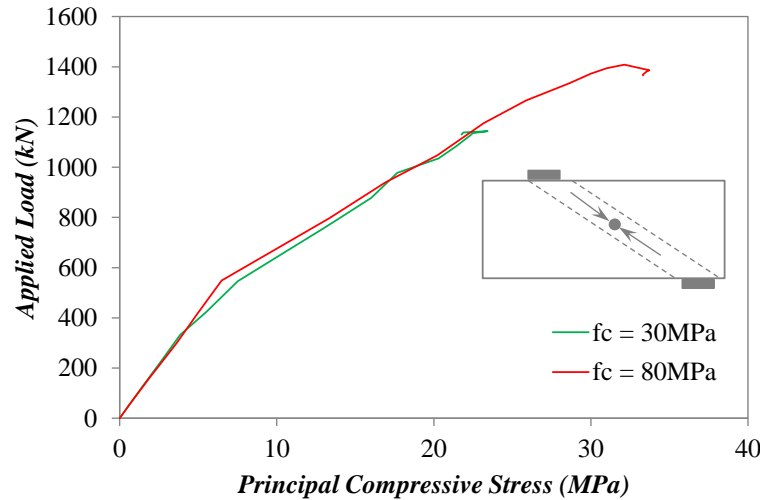
Figure 4-15-Effect of concrete strength on principal compressive strength in the shear span

Since strut and tie action is the primary mechanism of shear stress transfer in RC deep beams, shear reinforcement is not expected to have a significant effect on the shear capacity. The presence of shear reinforcement, however, is important as it increases ductility and limits the propagation of inclined cracks, thus changing the shear stress distribution in the shear span as shown in Figure 4-16. A difference of about 15% to 20% between the shear capacity of beams with and without shear reinforcement was found in the parametric study. Figure 4-17 shows the effect of shear reinforcement on the principal tensile strain in the shear span. For beams with shear reinforcement, the strain developed at a given applied load is lower due to the contribution of shear reinforcement in resisting and controlling the development of cracks. Thus, by reducing the principal tensile strain, the presence of shear reinforcement can enable the development of higher concrete compressive stresses and increase the effectiveness of the concrete strut.
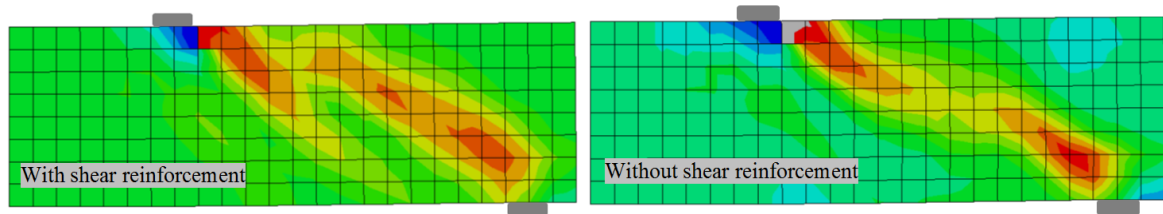
Figure 4-16-Effect of shear reinforcement on shear stress distribution in shear span
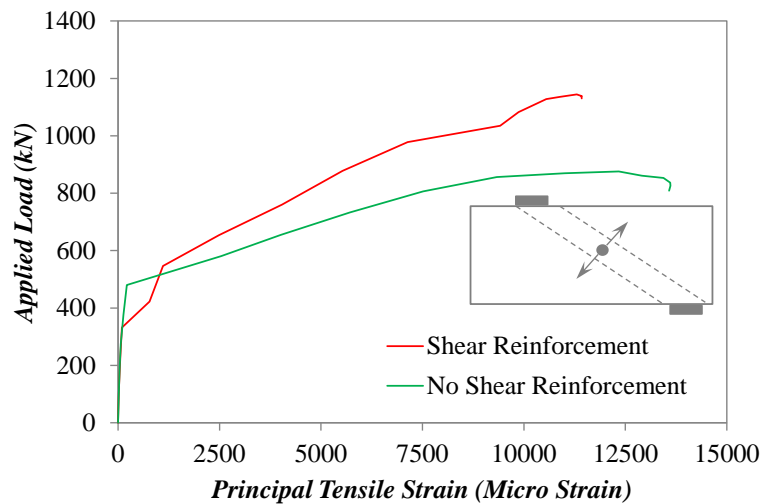
Figure 4-17-Effect of shear reinforcement on principal tensile strain in shear span

4.4.2. EFFECTIVENESS FACTOR

A key parameter in the strut and tie model as used in design is the definition of the effectiveness factor (v), which is used to calculate the strut strength. This factor which accounts for the reduced compressive strength of concrete when subjected to lateral tensile strains, as in the web of deep beams, and can be expressed as a ratio of the maximum principal compressive stress to the uniaxial compressive strength. The main variables that affect the effectiveness factor are shear span to depth ratio, compressive strength of concrete and shear reinforcement ratio [94]. The effect of these variables are investigated numerically using the microplane M4 model and are compared to the provisions of EC2 [3] and ACI 318-14 [4].

Figure 4-18 shows that increasing either shear span to depth ratio or concrete compressive strength can reduce the effectiveness factor. The presence of a minimum

amount of shear reinforcement (shown with dotted line in the figure) can lead to an increase in the effectiveness factor by about 15%. Nonetheless, the provisions of EC2 only account for the effect of concrete compressive strength, whilst ACI 318-14 only accounts for the effect of shear reinforcement.

Figure 4-19 shows the ratio of the calculated effectiveness factor to that obtained according to the provisions of EC2 and ACI 318-14 as a function of concrete compressive strength and shear span to depth ratio. It can be seen that the EC2, even though it accounts for concrete strength, it still slightly overestimates the effectiveness factor for beams with higher strength concrete. This is because on the one hand it does not account accurately for strength and on the other because it neglects the effect of shear span to depth ratio on the effectiveness factor. ACI 318-14 ignores both variables and yields conservative results only for concrete strengths of around 30MPa, becoming unsafe for higher concrete strength as well as higher shear span to depth ratios.
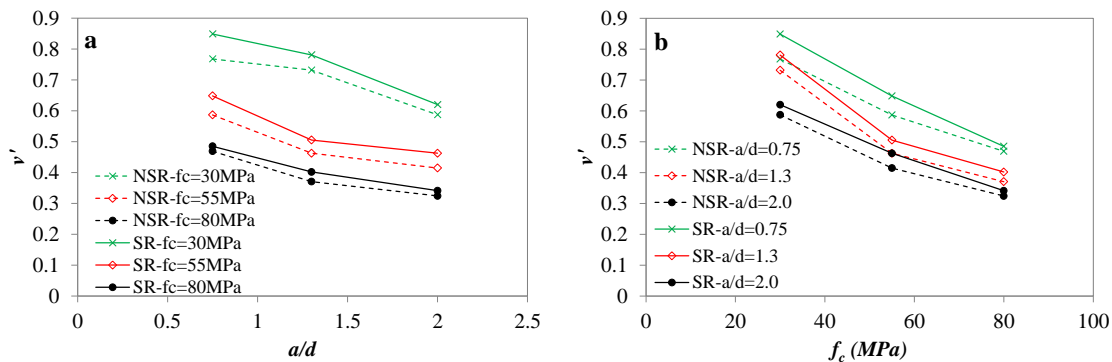
Figure 4-18-Effect of a) shear span to depth ratio and b) concrete compressive strength on the effectiveness of concrete
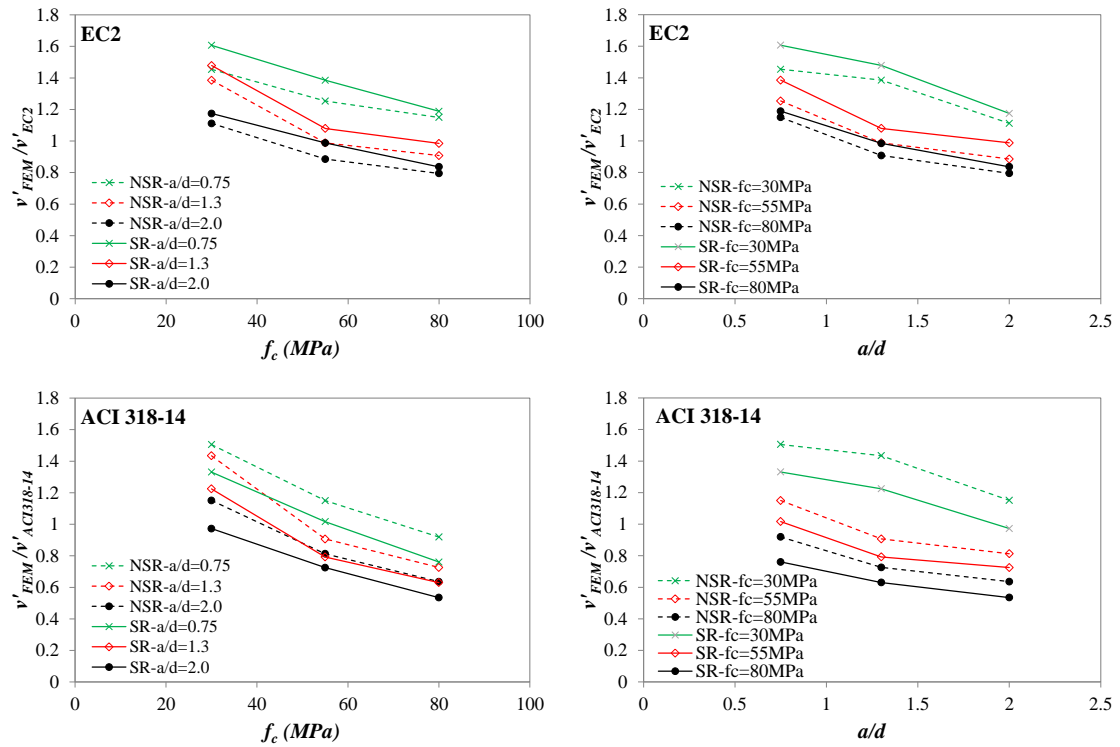
Figure 4-19-Comparison of code predictions with the numerically obtained effectiveness factors

Figure 4-20 shows the performance of the strut-and-tie model in predicting the shear capacity of specimens used in the parametric study by using the effectiveness factors from EC2 and ACI318-14 codes along with the effectiveness factor obtained from the numerical analysis. It can be seen that the calculated effectiveness factor leads to more accurate predictions with lower standard deviations. The poorer performance of EC2 and ACI 318-14 can be attributed to the fact that key parameters in estimating the effectiveness factor are neglected
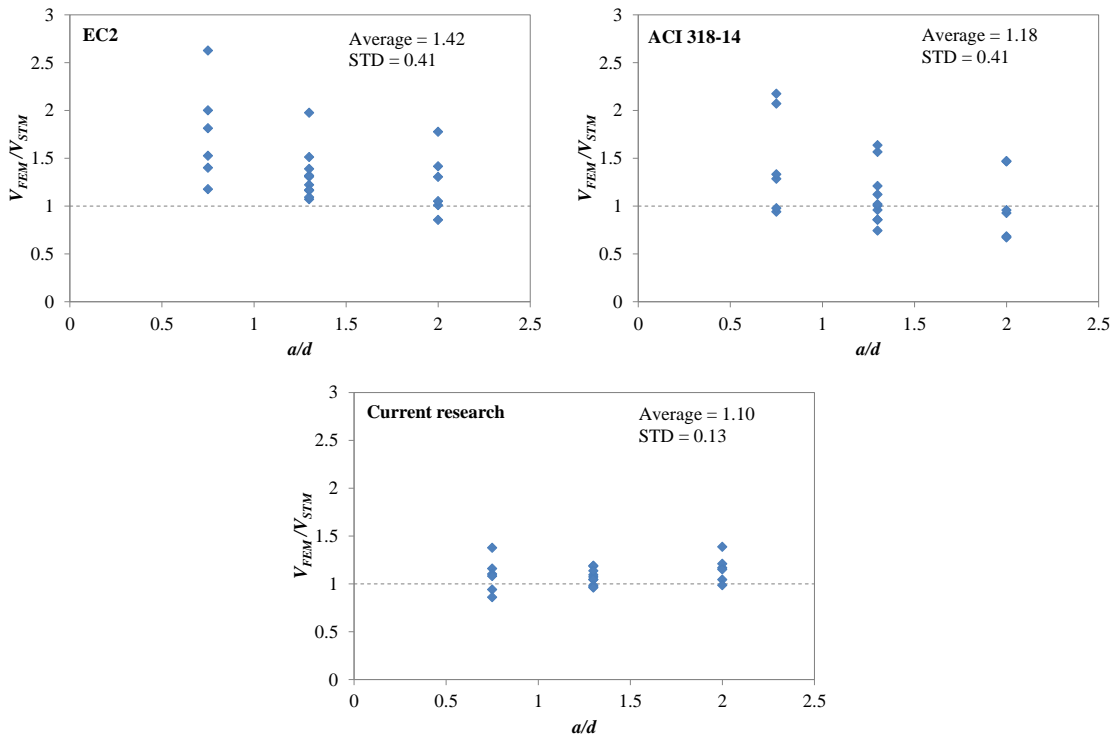
Figure 4-20-Effect of different effectiveness factor on the shear capacity prediction by strut-and-tie model

4.5. CONCLUSION

Based on the results of the numerical investigation and parametric study discussed above, the following conclusions can be drawn:

- Smeared crack and damage plasticity models are unable to realistically simulate the shear behaviour of RC deep beams. This is because these models cannot predict realistically shear deformation in discontinuity regions.
- The implementation of the microplane material model M4 in ABAQUS led to reasonably accurate predictions of the overall behaviour of the RC deep beams analyzed; however, local strain values were generally underestimated because a smeared approach is unable to realistically simulate the tension stiffening of the concrete.

- Concrete compressive strength and shear span to depth ratio are the key parameter affecting the concrete effectiveness factor in the shear span of deep beams.

- Minimum shear reinforcement can enable a better distribution of stresses within the shear span, control tensile strain and increase the effectiveness of the concrete by up to 15%.

- An accurate model to estimate the effectiveness factor should include the effect of concrete strength, shear span to depth ratio and shear reinforcement.

CHAPTER 5.   STRUT-AND-TIE MODELLING OF RC DEEP BEAMS

This chapter consists of a "stand alone" journal paper: Ismail K. S., Guadagnini M. and Pilakoutas K., (2015c) Strut-and-Tie Modelling of RC Deep Beams. To be submitted

5.1. ABSTRACT

Strut-and-tie models are often used for the design of shear critical deep members since they can rationalise the shear transfer within discontinuous or disturbed regions in RC structural elements. Most current codes of practice adopt the strut-and-tie method but provide very little guidance on how to select appropriate strut-and-tie layout and dimensions. Furthermore, the effectiveness factors used to account for the biaxial state of stresses in struts of deep beams are not reliable. This paper reviews the application of strut-and-tie models for the design of RC deep beams and evaluates current formulations of the effectiveness factor. Experimental and numerical studies are used to assess how the effectiveness factor is influenced by different parameters including concrete compressive strength, shear span to depth ratio and shear reinforcement ratio and to arrive at a more reliable strain based effectiveness factor. Various effectiveness factors are examined against an extensive database of experimental results on RC deep beams with and without shear reinforcement. The results show that the proposed effectiveness factor yields the most reliable and accurate predictions and can lead to more economic and safe design guidelines.

5.2. INTRODUCTION

RC deep beams where behaviour is predominantly controlled by shear are used in a wide range of structures, such as transfer girders in tall buildings and bridges. It is crucial to predict their capacity accurately as the safety of the entire structure relies on

their performance. However, the shear behaviour of RC members is a complex phenomenon, which is influenced by a large number of parameters [2, 27]. This complexity is more pronounced in deep beams as the applied load is transferred mainly through the formation of arching action which causes a highly nonlinear strain distribution in the cross section.

Most codes of practice rely on empirical or semi-empirical equations for design; however, these equations are limited by the extent of the experimental results used for their calibration. Although designing RC deep beams based on these empirical approaches is generally very conservative, they can also lead to very unsafe results [18]. Collins et al. [2] examined the accuracy of the shear approaches available in codes of practice such as EC2 and ACI, against and extensive database of RC beams, it was found that shear strength prediction of vast number of the beams are unconservative. There are also unsafe results even after application of the safety factors [2]. Approaches based on finite element analysis can account for the nonlinearities that describe the behaviour of this type of members, and can lead to good results if an accurate concrete material model is used; however, their implementation is not always practical for design purposes. Thus, design approaches based on the implementation of strut-and-tie mechanistic models have been adopted by modern design codes such as EC2 [3], ACI 318-14 [4] and Model Code [12] since they appear more rational and relatively simple to apply.

The use of strut-and-tie models (STM) dates back to the pioneering work of Wilhelm Ritter [5] who tried to explain the contribution of shear reinforcement to the shear strength of beams. Ritter's truss mechanism was later modified by Morsch [6] to better represent the shear behaviour of RC beams. The design of RC members by STM relies on the lower bound theory of plasticity and assumes that both concrete and steel are perfectly plastic materials. As this is not true, there is a need to implement modification factors to adjust both dimension and strength of the strut elements. However, existing guidelines do not provide sufficient information on the effect of all important parameters or the size and strength of the strut elements [95]. This paper aims to develop a unified

procedure for using the STM for the design of RC deep beams and predict accurately the size and strength of each element.

5.3. STRUT-AND-TIE MODEL

Strut-and-tie models attempt to represent the stress field that develops in the D-regions of concrete elements by approximating the flow of internal compression and tension stresses by means of struts and ties, respectively. The selection of an adequate strut-and-tie model is necessary to capture the strength of RC deep beams with acceptable accuracy. It is commonly accepted that the strut-and-tie mechanism is the basic load transfer mechanism in RC deep beams [96]; however, in some cases the truss action mechanism is also thought to contributes to the transfer of the applied load [97, 98]. The type of load transfer mechanism that develops in RC deep beams is mainly controlled by the shear span to depth ratio (a/d) and amount of shear reinforcement. For beams with a/d less than 1.0, the applied load is transferred to the support through the formation of one concrete strut regardless of the amount of shear reinforcement. The adoption of the STM (Figure 5-1-a) is therefore suitable for the design and analysis of such elements. Beams with a/d between 1.0 and 2.0 and with shear reinforcement, can develop a combination of both tied-arch and truss action mechanism [97]. However, estimating the percentage of load transferred by each of these mechanisms is quite challenging as this varies based on a/d and amount and spacing of shear reinforcement [97]. For the sake of simplicity, the adoption of a model based on the development of either a single strut-and-tie (Figure 5-1-a) or a truss (Figure 5-1-b) is generally adopted. The ability of these models to capture the real structural behaviour of RC deep beams is assessed in this paper with the aim of developing enhanced design equations.

The current codes of practice do not provide adequate guidance on selecting the size of the elements in the STM. ACI 318-14 provides Eq. 5.1 and 5.2 for estimating the width of the inclined strut at the top (W_{ST}) and bottom nodes (W_{SB}) (Figure 5-1-a), respectively. However, there is no guidance on how to estimate the independent parameters (h_{CS}, h_{Tie} and θ) in these equations. Therefore designers are free to choose the size of the elements

in the model; however, this could lead to unsafe or over conservative design solutions [17-19].
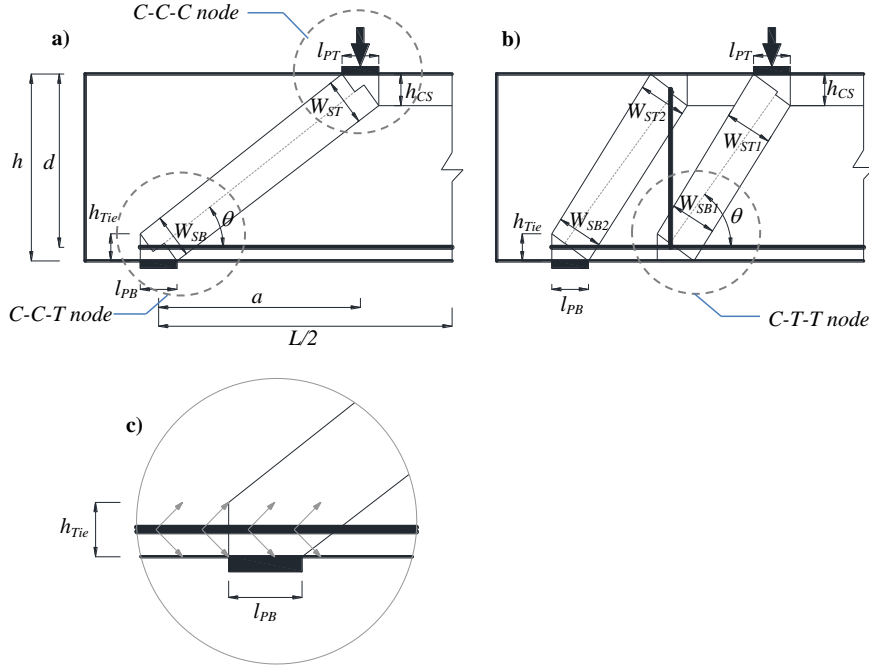
Figure 5-1-Load transfer mechanism in RC deep beams, a) strut-and-tie model b) truss model and c) height of the bottom node

$$W_{ST} = l_{PT} \sin\theta + h_{CS} \cos\theta \tag{5.1}$$

$$W_{SB} = l_{PB} \sin\theta + h_{Tie} \cos\theta \tag{5.2}$$

In the current research programme the width of the strut in the top compression zone (h_{cs}) is assumed to be equal to the depth of neutral axis as determined by section analysis (Eq. 3).

$$h_{CS} = \left(\sqrt{(n\rho)^2 + n\rho} - n\rho \right) d \tag{5.3}$$

where l_{PT} and l_{PB} are the width of the loading and support plates, and θ is the angle of the strut with respect to the horizontal axis of the beam (Eq. 5.4).

$$\theta = \tan^{-1} \frac{d - h_{CS}/2}{a} \tag{5.4}$$

where d is the effective depth and a is the shear span of the beam.

The height of the bottom node (h_{Tie}) is taken as twice the distance from the centre of the main longitudinal reinforcement to the outer tensile face of the beam as shown in (Figure 5-1-c). The width of the strut at the top (W_{ST}) and bottom (W_{SB}) nodes can be determined by the ACI 318-14 Eq.s 5.1 and 5.2 respectively.

In the case of the truss model shown in Figure 5-1-b, the width of the strut in compression (h_{cs}) and the height of the bottom node (h_{Tie}) remain the same for both diagonals. The intersections of strut, ties and applied loads or support reactions are termed nodes and their capacity is critical when assessing a given STM.

5.4. CONCRETE EFFECTIVENESS FACTOR

5.4.1. NODE STRENGTH FACTOR

Nodes are generally named according to the type of interconnected members, i.e. C-C-C (Compression-Compression-Compression), C-C-T (Compression-Compression-Tension) and C-T-T (Compression- Tension -Tension), and their strength is a function of the state of stress they are subjected to. C-C-C nodes are located in well confined regions and their strength can generally exceed the uniaxial strength of concrete, but the latter can be conservatively used for design. In this paper, with the exception of EC2, ACI 318-14 and Model Code 2010, which they provide strength factors for the C-C-C nodes, to assess other strut effectiveness factors available in the literature the uniaxial concrete strength is adopted.

Owing to the existence of tension forces in C-C-T and C-T-T nodes the maximum stress that can be developed in such nodes is generally lower that the uniaxial concrete strength and reduction factors are used to take this into account. Based on the test results of isolated C-C-T and C-T-T nodes, Jirsa et al. [99] concluded that by using 80% of the

uniaxial concrete compressive strength, the prediction of the nodal zone strength is conservative. Unless it is provided, a reduction factor of 0.8 is used to determine the strength of all C-C-T and C-T-T nodes in the assessment of STM with different strut effectiveness factor.

5.4.2. EFFECTIVENESS FACTOR FOR INCLINED STRUT

The presence of a transverse tensile field within the shear span weakens the resistance of the concrete struts. This is taken into account through the use of a concrete effectiveness factor (v). In 1985, Marti [10] proposed the use of a simple reduction coefficient ($v=0.6$) as effectiveness factor, whilst Collins and Mitchell [62] proposed Eq. 5.5 for their modified compression field theory [9].

$$v = \frac{1}{0.8 + 170\varepsilon_1} \tag{5.5}$$

$$\varepsilon_1 = \varepsilon_s + (\varepsilon_s + 0.002)/\tan^2\theta \tag{5.5a}$$

where ε_1 is the principal tensile strain, ε_s is the longitudinal tensile strain at mid-depth of the beam, which can be estimated assuming that plane sections remains plane [2].

In 1993, Vecchio and Collins [100] proposed a refined equation for the concrete effectiveness factor as shown in Eq. 5.6.

$$v = \frac{1}{1.0 + K_c K_f} \tag{5.6}$$

$$K_c = 0.35\left(\frac{-\varepsilon_1}{\varepsilon_2} - 0.28\right)^{0.8} \geq 1.0 \tag{5.6a}$$

$$K_f = 0.1825\sqrt{f_c} \geq 1.0 \tag{5.6b}$$

where ε_1 and ε_2 are the principal tensile and compressive strain, respectively, and f_c is the concrete compressive strength.

Foster and Gilbert [101] argued that concrete compressive strength and shear span to depth ratio (a/d) influence the effectiveness of concrete cracked in tension and modified Collins and Mitchell's equation (Eq. 5.5) to integrate the effect of these two parameters. This modified equation (Eq. 5.7) was calibrated against a database of beams with concrete compressive strength ranging from 20 to 100MPa.

$$v = \frac{1}{1.14 + (0.64 + f_c/470)(a/d)^2}$$
(5.7)

Based on a series of nonlinear finite element analyses, Warwick and Foster [102] proposed the following concrete effectiveness factor (Eq. 5.8) for concrete compressive strength ranging from 20 to 100MPa

$$v = 1.25 - \frac{f_c}{500} - 0.72\left(\frac{a}{d}\right) + 0.18\left(\frac{a}{d}\right)^2 \le 1.0$$
(5.8)

EC2 provides Eq. 5.9 to calculate the effective concrete strength of the inclined concrete strut

$$f_{ce} = 0.6v' f_{cd}$$
(5.9)

where v' can be calculated according to Eq. 5.9a and f_{cd} is the design concrete compressive strength.

$$v' = 1 - \frac{f_{ck}}{250}$$
(5.9a)

According to ACI 318-14, the effective concrete strength (f_{ce}) can be calculated using Eq. 5.10

$$f_{ce} = 0.85\beta_s f'_c$$
(5.10)

where β_s is 0.75 for strut with shear reinforcement satisfying Eq. 5.10a, else β_s is taken as 0.6.

$$\sum \frac{A_{si}}{b_s s_i} \sin \alpha_i \geq 0.003 \tag{5.10a}$$

where A_{si} is the area of the reinforcement at spacing s_i in the i-th layer of reinforcement crossing a strut at an angle α_i to the axis of the strut.

Model Code 2010 use Eq. 5.11.

$$f_{ce} = k_c f_{cd} \tag{5.11}$$

$$k_c = 0.55 \left(\frac{30}{f_{ck}} \right)^{1/3} \leq 0.55 \tag{5.11a}$$

The above effectiveness factor models are assessed in this paper through a parametric investigation to gain additional insight on the role of each of the considered parameters and inform the development of a more accurate model.

5.5. ANALYSIS AND DISCUSSIONS

An extensive database of 519 RC deep beam specimens [1, 20, 26, 27, 29, 31, 32, 49-53, 57, 67-69, 103-127] (Table **5-1**) was used to evaluate the performance of the STM, and examine the effectiveness of existing approaches in determining the concrete effectiveness factors.

5.5.1. SUITABILITY OF MODELS

As discussed earlier a combination of arch and truss action can develop in beams with shear reinforcement and shear span to depth ratio between 1.0 and 2.0. The specimens within the database that satisfy these conditions (136 RC deep beams) were used to assess the accuracy of the STM and TM in predicting shear strength. The strut effectiveness factor was taken as equal to one at this stage of the comparative study. The results (Figure 5-2) show that TM is highly unconservative (only 5.2% safe predictions) and cannot be used for RC deep beams. Figure 5-2 shows that using STM generally leads to more conservative results and is more suitable for the design of RC deep beams

both with and without shear reinforcement. This agrees with the findings of other researchers [128, 129]. However, the result of STM can be further improved if an appropriate effectiveness factor is adopted.

Table 5-1 Summary of the RC deep beams in the database

	RC deep beams without shear reinforcement	RC deep beams with shear reinforcement
Number of the beams	295	224
Concrete strength (MPa)	11 to 87	14 to 90
Shear span to depth ratio	0.25 to 2.0	0.27 to 2.0
Effective depth (mm)	151 to 1750	160 to 1750
Main reinforcement ratio (%)	0.26 to 6.64	0.16 to 4.25
Vertical shear reinforcement ratio (%)	----	0 to 2.45
Horizontal shear reinforcement ratio (%)	----	0 to 3.17
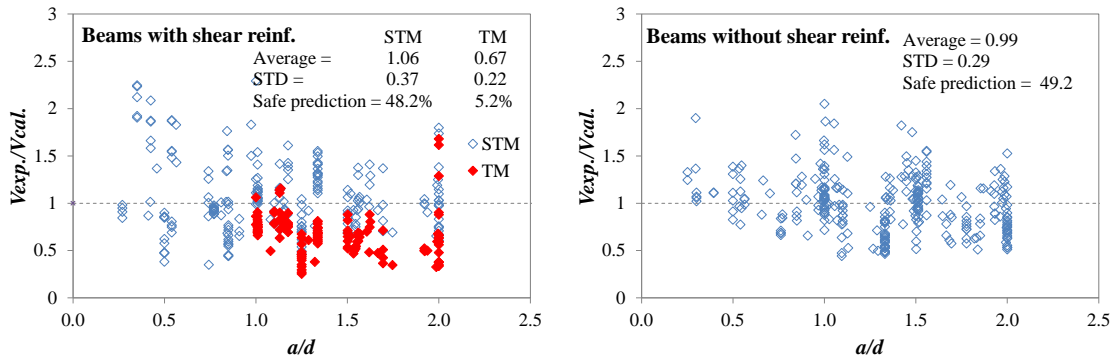
Figure 5-2-Shear strength prediction by STM and TM without using concrete effectiveness factor

5.5.2. EVALUATION OF EXISTING EFFECTIVENESS FACTORS

The eight different formulations for effectiveness factors presented in the previous section earlier are assessed in the following. The results are shown in Figure 5-3 and Figure 5-4; and the statistical analyses are summarized in Figure 5-5 and Figure 5-6 for RC deep beams with and without shear reinforcement, respectively. Overall, for all eight effectiveness factors the predictions for beams with shear reinforcement are more

conservative than those without shear reinforcement. The effectiveness factors proposed by Collins and Mitchell (Eq. 5.5), Vecchio and Collins (Eq. 5.7) and Modified Collins and Mitchell (Eq. 5.10) lead to very conservative results with large scatter. This is most probably due to the fact that, in these equations, the tensile strain in the concrete needs to be calculated based on the assumption that plane sections remain plane after bending. However, this assumption is far from accurate for deep beams. The effectiveness factor proposed by Marti (i.e. 0.6) [10] can lead to very unsafe results for RC deep beams without shear reinforcement, as the single factor proposed cannot account for all parameters. Additionally, experimental and numerical investigations conducted by the authors [130, 131] show that in many cases the effectiveness factor is lower than 0.6, especially for RC deep beams without shear reinforcement. Although the effectiveness factor proposed by Warwick and Foster (Eq. 5.11) accounts for the effect of concrete compressive strength and shear span to depth ratio, the non-uniform performance of this model shows that other parameters affect shear behaviour and their effect should be taken into account.

The models proposed by EC2, ACI 318-14 and Model Code 2010 also lead to very unsafe results especially for RC deep beams without shear reinforcement. This can be attributed again to the fact that these codes do not account for all the important influencing parameters such as shear span to depth ratio and shear reinforcement (EC2 and Model Code 2010); or concrete compressive strength and shear span to depth ratio (ACI 318-14).
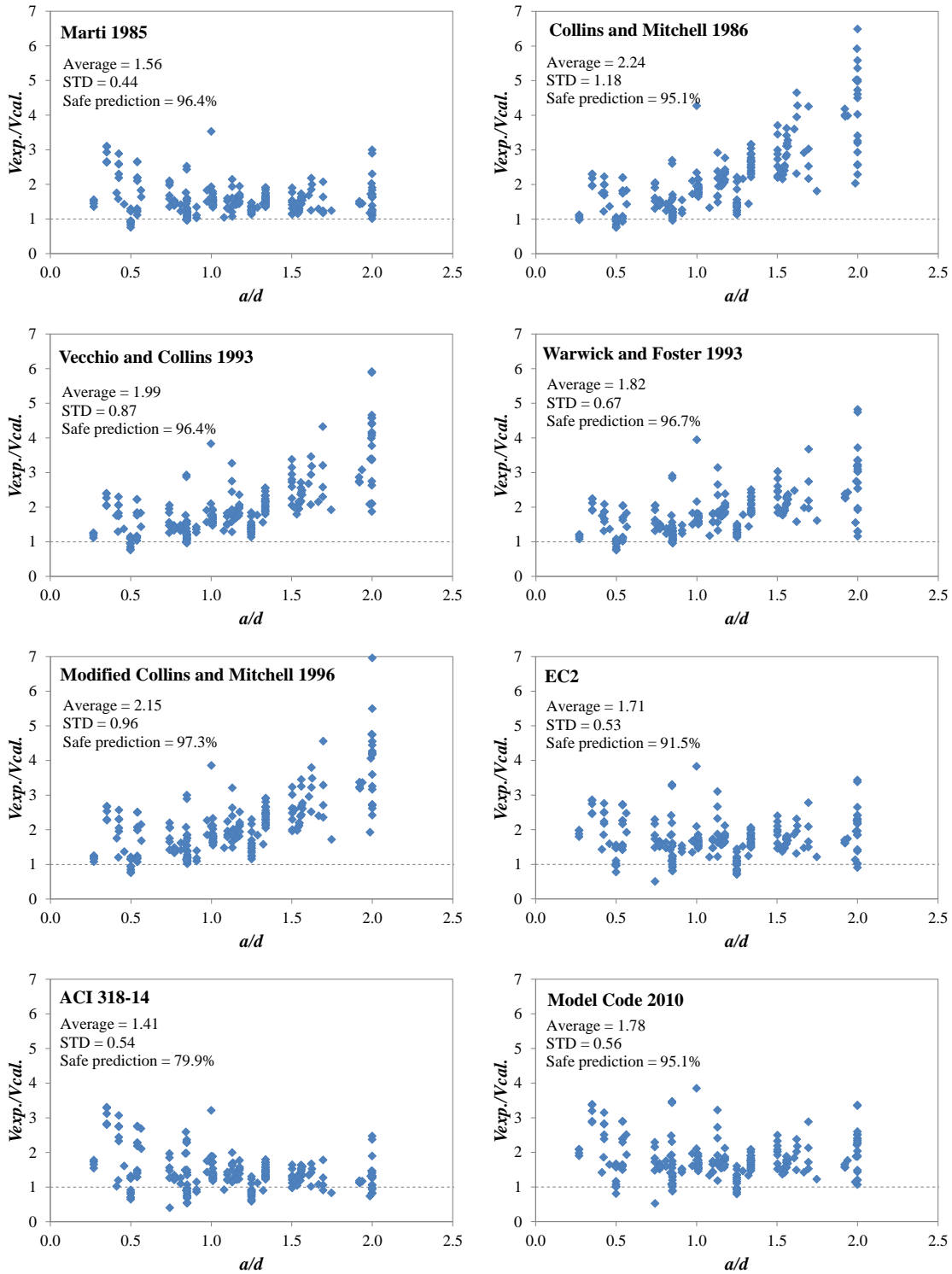
Figure 5-3-Effect of concrete effectiveness factor on shear strength prediction of RC deep beams with shear reinforcement by STM
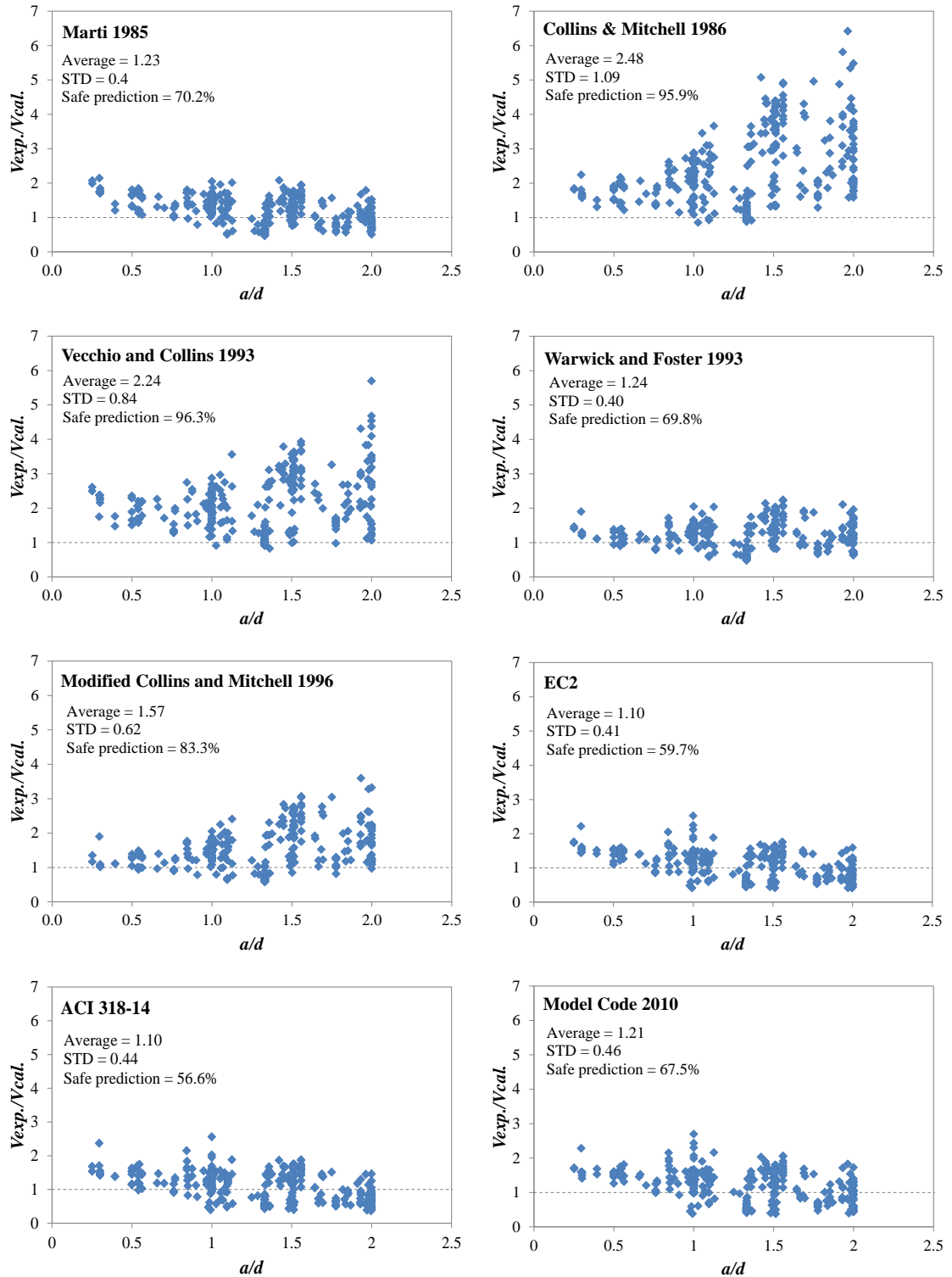
Figure 5-4-Effect of concrete effectiveness factor on shear strength prediction of RC deep beams without shear reinforcement by STM
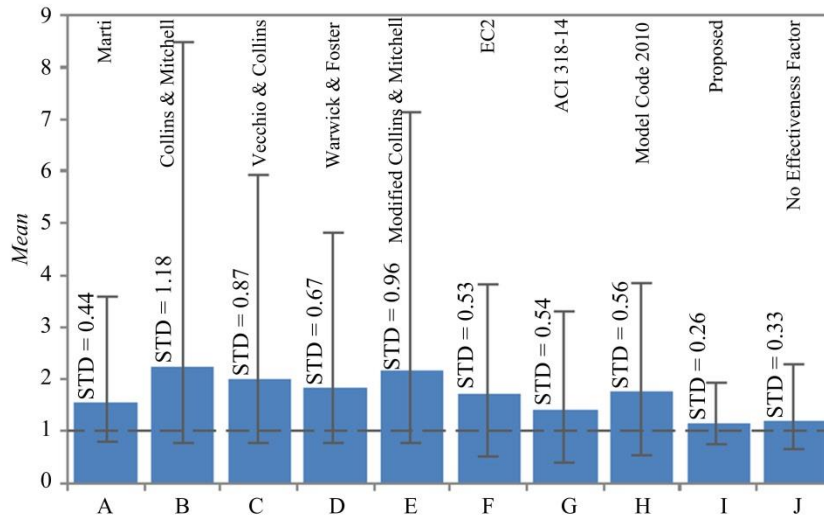
Figure 5-5-Statistical analysis of shear strength prediction of RC deep beams with shear reinforcement by STM
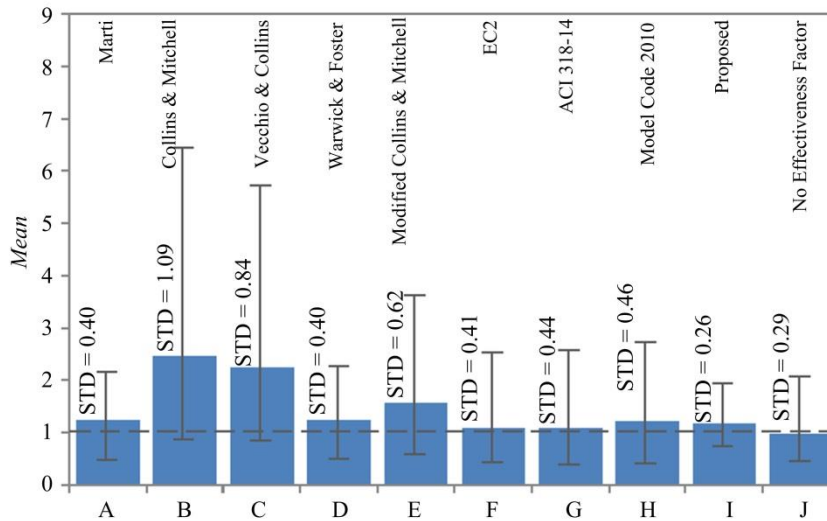
Figure 5-6-Statistical analysis of shear strength prediction of RC deep beams with shear reinforcement by STM

The safety of the above models was further checked by introducing the appropriate material partial safety factors or load factors. With the exception of the predictions by equations of Collins and Mitchell and Vecchio and Collins for RC deep beams without shear reinforcement, which are over conservative and uneconomic, all other models do not yield an adequate level of safety for all RC deep beams with and without shear reinforcement. The result of the analysis is summarised in Table 5-2. Therefore, a more

sophisticated effectiveness factor model that accounts for all influencing parameters and yields conservative and economic results is required for design purposes. This paper aims to propose new node strength factors and effectiveness factor that account for all influencing parameters and yield more accurate results.

Table 5-2-Percent of safe shear strength prediction by STM after application of safety factors

	Beams without shear reinforcement (295 beams)			Beams with shear reinforcement (224 beams)		
	Safe prediction (%)	Mean of safe results	Mean of unsafe results	Safe prediction (%)	Mean of safe results	Mean of unsafe results
Marti 1985	88.3	1.93	0.86	99.6	2.28	0.87
Collins and Mitchell 1986	100	4.14	---	99.6	3.33	0.87
Vecchio and Collins 1993	100	3.32	---	99.6	2.97	0.87
Warwick and Foster 1993	91.0	1.91	0.88	99.6	2.68	0.87
Modified Collins and Mitchell 1996	97.1	2.53	0.95	99.6	3.21	0.87
EC2	90.9	1.92	0.91	99.6	2.59	0.75
ACI 318-14	79.3	1.76	0.85	93.3	1.95	0.84
Model Code 2010	88.7	1.99	0.88	99.6	2.69	0.79
Proposed	100	1.74	---	100	1.62	---

5.6. PROPOSED EFFECTIVENESS FACTOR

Equations describing the development of biaxial stress fields, such as those included in the modified compression field theory [9] can be used to determine the effective compressive strength of concrete subjected to lateral tensile strain. Bazant and Xiang [132] derived a simple equation (Eq. 5.12) based on the theory of fracture mechanics to predict the compressive strength (σ_c) of a concrete specimen subjected to lateral tensile strain.

$$\sigma_c = \sqrt{2EG_f\,h/s}\,D^{-1/2} \tag{5.12}$$

where E and G_f are the modulus of elasticity and fracture energy of concrete, respectively; h is the width of the crack band, s is the spacing of cracks in the crack band and D is the width of the specimen.

Equation 5.12 can be used to estimate the effectiveness factor of an inclined strut. Model Code 2010 equations are used here to determine the modulus of elasticity and fracture energy of concrete and D is taken as the width of the strut (W_S). The effectiveness factor v (Eq. 5.13) can be expressed as the ratio between Eq. 5.12 and the uniaxial strength of the concrete (f_c) to obtain:

$$v = \sqrt{\frac{2EG_f}{W_s} \frac{h}{s}} \bigg/ f_c \qquad (5.13)$$

According to Bazant and Xiang [132], in the crack band the intact concrete between cracks behaves as columns of width s. The strain energy in the crack band releases due to buckling of these columns and failure occurs once the released energy reaches the fracture energy of the concrete. The presence of lateral tensile strain increases the crack width in the crack band which in turn increases the energy release rate and decreases the compressive capacity. This means that the value of h/s is directly affected by lateral tensile strain. Since the value of h/s needs to be determined by calibration of experimental results, the authors propose a more direct approach where h/s in Eq. 5.13 is replaced by lateral tensile strain and the equation needs to be calibrated by a factor (α) as shown in Eq. 5.14.

$$v = \alpha \sqrt{\frac{2EG_f}{W_s \varepsilon_1}} \bigg/ f_c \qquad (5.14)$$

Although lateral strain is a more rational quantity to use, it still needs to be quantified either by calculation or calibration of date.

5.6.1. LATERAL TENSILE STRAIN IN SHEAR SPAN

Experimental and numerical data from the finite element model developed and validated by the authors [130, 131] was used to determine the lateral tensile strain in the shear

span of RC deep beams. Figure 5-7 shows the effect of concrete compressive strength, shear span to depth ratio and effective depth on the lateral tensile strain obtained using finite element analysis for beams with and without shear reinforcement. It can be seen that shear span to depth ratio and effective depth influence the lateral tensile strain whilst concrete compressive strength has almost negligible effect. Therefore, in estimating the lateral tensile strain in the shear span of RC deep beams, shear span to depth ratio and effective depth need to be accounted for. For dimensional purposes, the effective member depth (d) can be normalized by the maximum aggregate size (d_a). Hence, based on best fit analysis, Eq. 5.15 is proposed to estimate the lateral tensile strains (ε_l) in the shear span of RC deep beams.
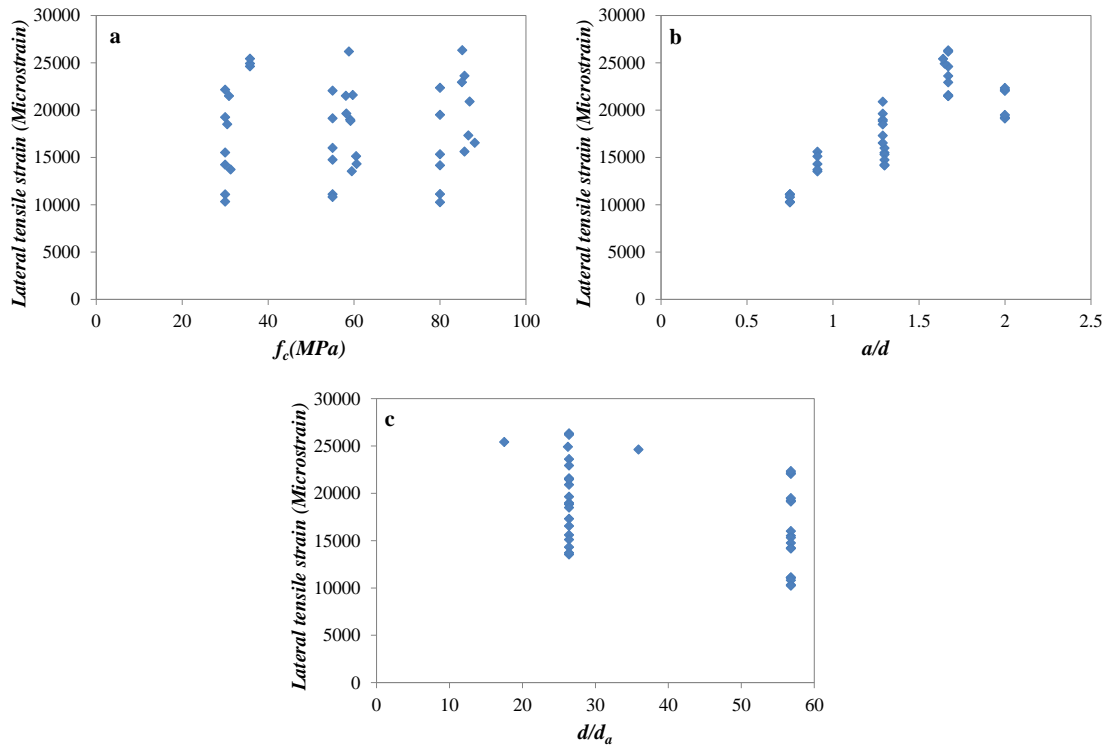
Figure 5-7-Effect of a) concrete strength, b) shear span to depth ratio and c) effective depth on the lateral tensile strain

$$\varepsilon_1 = 0.05 \frac{(a/d)^{0.5}}{(d/d_a)^{0.35}}$$

(5.15)

125

From a direct comparison with the finite element analysis results it can be seen in Figure 5-8 that this equation leads to a reasonable prediction of lateral tensile strain in the shear span of RC deep beams.
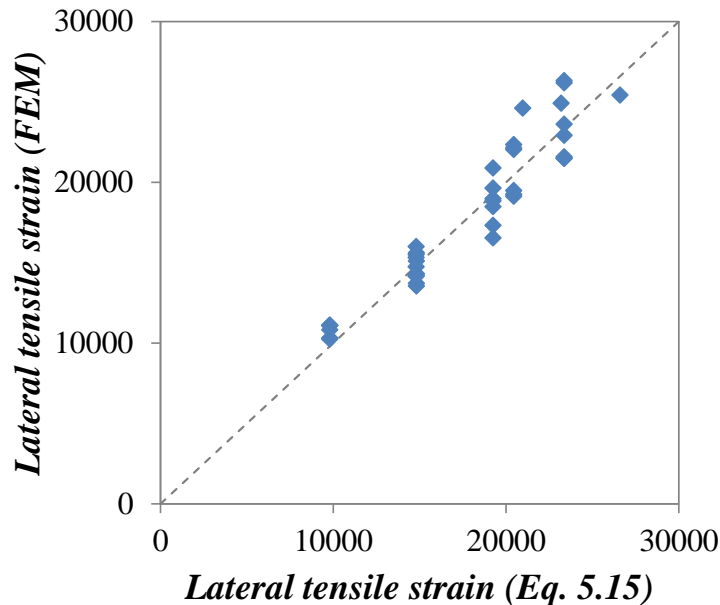
Figure 5-8-Estimating the lateral tensile strain by Eq. 5.15

5.6.2. DETERMINATION OF FACTOR α

Back analysis was adopted to determine the value of α in Eq. 14 from experimental and numerical data on RC deep beams. The finite element model was used to determine the maximum principal concrete compressive strength in the shear span of the beams (see Table 5-3 and Table 5-4). The effectiveness factor (v) was calculated as the ratio of the maximum principal compressive strength and uniaxial compressive strength of the concrete. To account for the effect of shear reinforcement, two different values of α need to be adopted as shown in Table 5-3 and Table 5-4 for RC deep beams with and without shear reinforcement. An average value of 400 can be used as α for RC deep beams without shear reinforcement or with shear reinforcement ratio less than 0.1%, whilst for RC deep beams with shear reinforcement ratio greater or equal to 0.1% a value of 450 can be used as α. In this context, the shear reinforcement can be taken either as the vertical or horizontal shear reinforcement or a combination thereof.

Table 5-3 Summary of finite element analysis of RC deep beams with shear reinforcement

Specimen	f_c (MPa)	a/d	d (mm)	Principal concrete strength (MPa)	α	
A2	85.7	1.67	330	28	435	
A3	85.1	1.67	330	29	451	
B2	86.6	1.29	330	32	462	
B3	88.1	1.29	330	34	489	
D2	59.7	1.67	330	24	410	
D3	58.1	1.67	330	25	430	
E2	59.1	1.29	330	26	416	
E3	59.2	1.29	330	29	463	
F2	60.6	0.91	330	34	488	
F3	59.5	0.91	330	34	490	
G1	30.9	1.67	330	23	467	Average = 452
G2	30.5	1.29	330	24	457	
G3	31.3	0.91	330	25	429	
BH-S-30	30	0.75	710	25	396	
BH-S-55	55	0.75	710	36	476	
BH-S-80	80	0.75	710	39	466	
BH-M-30	30	1.3	710	23	449	
BH-M-55	55	1.3	710	28	451	
BH-M-80	80	1.3	710	32	471	
BH-B-30	30	2	710	19	407	
BH-B-55	55	2	710	25	472	
BH-B-80	80	2	710	27	458	

Table 5-4 Summary of finite element analysis of RC deep beams without shear reinforcement

Specimen	f_c (MPa)	a/d	d (mm)	Principal concrete strength (MPa)	α	
A1	85.2	1.67	330	27	420	
B1	86.9	1.29	330	31	447	
C1	85.7	0.91	330	34	444	
D1	58.8	1.67	330	21	360	
E1	58.2	1.29	330	24	385	
F1	60.5	0.91	330	28	402	
H1	35.8	1.67	449	21	356	
H2	35.8	1.65	328	18	307	
H3	35.8	1.64	219	17	290	Average = 398
BN-S-30	30	0.75	710	23	365	
BN-S-55	55	0.75	710	32	431	
BN-S-80	80	0.75	710	38	451	
BN-M-30	30	1.3	710	22	421	
BN-M-55	55	1.3	710	25	413	
BN-M-80	80	1.3	710	30	434	
BN-B-30	30	2	710	18	385	
BN-B-55	55	2	710	23	423	
BN-B-80	80	2	710	26	436	

5.6.3. NODE STRENGTH FACTOR

An accurate estimation of node strengths is also crucial for safe design solutions. For the bottom node which is C-C-T, most codes of practice recommend using a strength which is lower than the uniaxial concrete strength due to presence of a tie in this node. In reality, concrete strength reduces due to the presence of lateral tensile strain and cracks. However, in this region there is no cracking, which means that the tensile stress is always below the concrete tensile strength. Hence, it is still safe to use the uniaxial compressive strength of the concrete without any reduction in estimating the strength of the node.

The strength of the top node (C-C-C) is expected to be higher than the uniaxial concrete strength because it is fully confined. Therefore, a factor with a value higher than one can be used to account for this confinement. Richart et al. [133] provide a simple equation (Eq.5.16) that can estimate the strength of the concrete when subjected to lateral compressive strength. This equation can be applied in the top node to calculate the node factor (Eq. 5.17) that needs to be used to estimate the effective strength.

$$f_{cc} = f_c + 4.1\sigma_l \tag{5.16}$$

Where f_{cc} and σ_l is confined concrete strength and lateral compressive stress, respectively. If the strut stress vf_c is used for σ_l and resolved in the vertical direction, the following node factor is developed

$$v_{Node} = (1 + 4.1v\sin\theta) \tag{5.17}$$

5.6.4. EVALUATION OF PROPOSED MODEL

The shear strength prediction according to the implementation of the STM using the proposed concrete effectiveness factor (including lateral tensile strain predictions) and the factors for estimating the strength of the nodes is shown in Figure 5-9 and summarized in Figure 5-5 and Figure 5-6 for RC deep beams with and without shear reinforcement, respectively. The use of the proposed model yields overall less conservative predictions with lower standard deviations. This can lead to more economical design solutions, yet maintaining an appropriate level of safety as shown in Table 5-2.
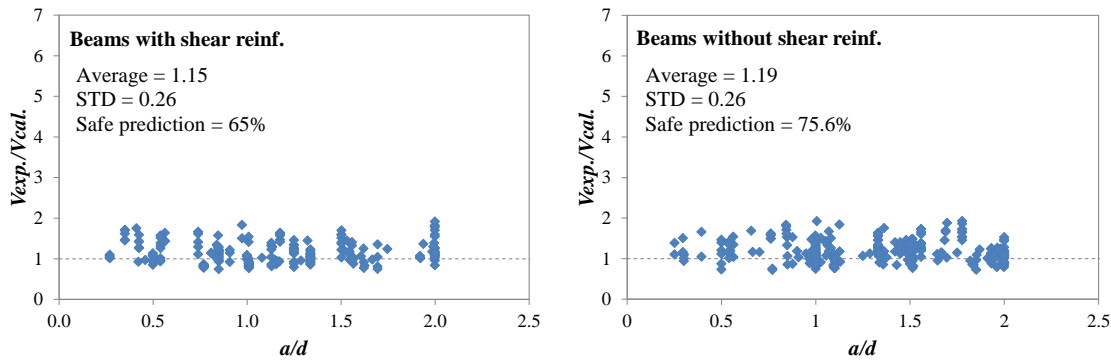
Figure 5-9-Shear strength prediction by STM with using the proposed concrete effectiveness factor

Figure 5-10 and Figure 5-11 show the effect of shear span to depth ratio, concrete compressive strength and member depth (i.e. size effect) on the performance of the three codes of practice discussed in this paper, along with the proposed effectiveness factor for RC deep beams with and without shear reinforcement, respectively. It can be seen that ACI 318-14 which neglects the influence of both shear span to depth ratio, concrete compressive strength and member depth, offer the less reliable predictions. The EC2 and Model Code 2010, though they include the effect of concrete compressive strength, do not sufficiently account for the effect of this parameter and they do not account for the effect of shear span to depth ratio, as evidenced by their variable degree of conservatism. The use of the proposed effectiveness factor accounts for the effect of these parameters more accurately and leads to a more uniform performance level for both RC deep beams with and without shear reinforcement.
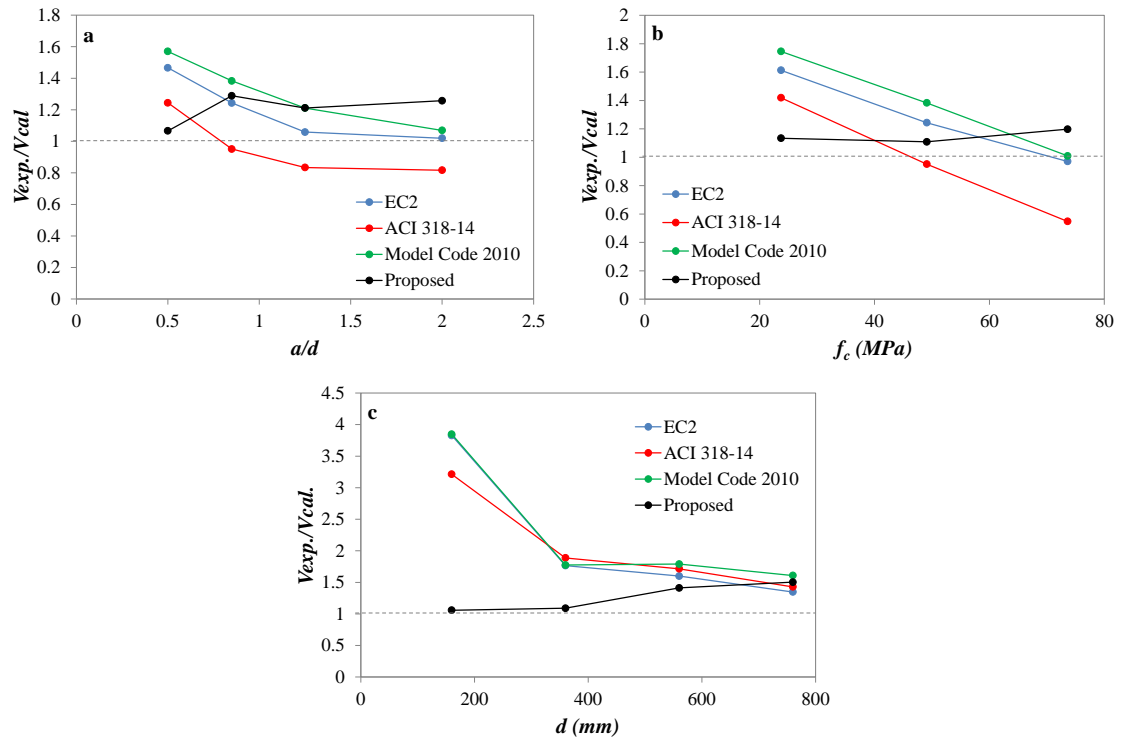
Figure 5-10-Effect of a) shear span to depth ratio b) concrete strength and c) depth on the performance of different effectiveness factor (with shear reinforcement)
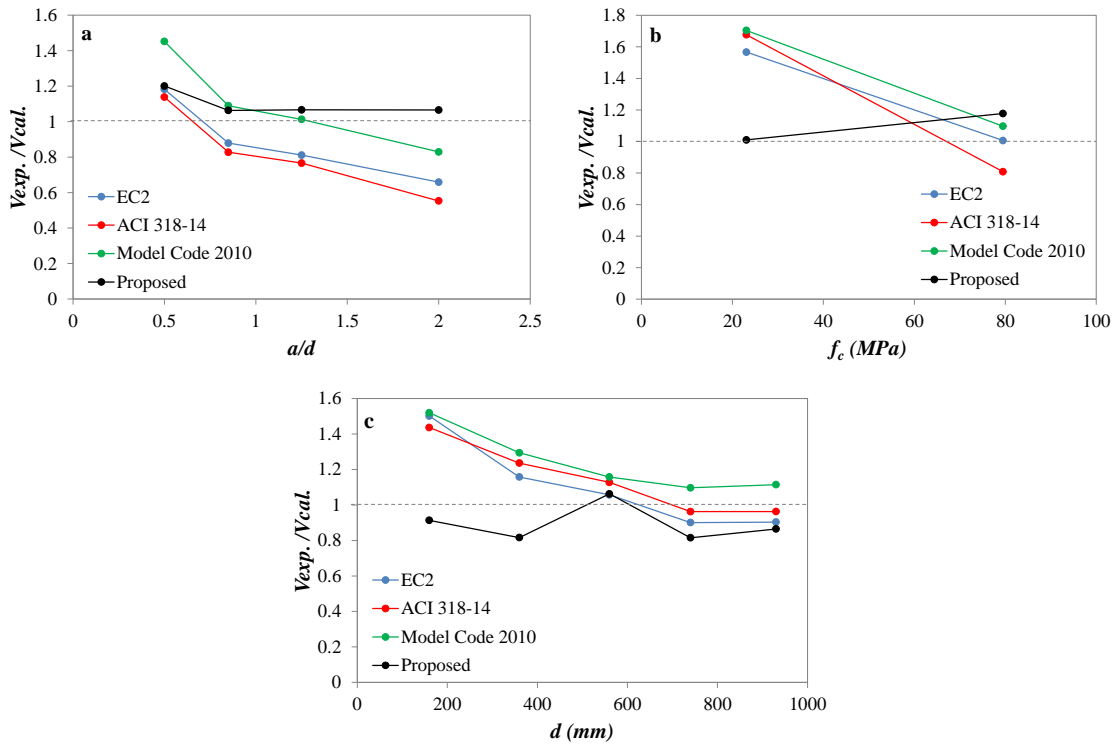
Figure 5-11-Effect of a) shear span to depth ratio b) concrete strength and c) depth on the performance of different effectiveness factor (No shear reinforcement)

5.7. CONCLUSIONS

The main conclusions of this research study can be summarized as follows:

1. A tie-arch mechanism is the main resisting mechanism in RC deep beams with and without shear reinforcement and can be best represented by the strut-and-tie model.

2. The selection of an appropriate strut-and-tie model and size of its elements is critical for accurate shear capacity predictions.

3. The effectiveness factor models based on the modified compression field theory show poor correlation against the experimental results, with a large scatter and high coefficients of variation.

132

4. The STM provision and the effectiveness factors of EC2, ACI 318-14 and Model Code 2010 do not ensure adequate safety levels (after application of safety factors) for RC deep beams without shear reinforcement.

5. A new model which utilises a concrete effectiveness factor based on predicted lateral strain is proposed. The use of the proposed model leads to less conservative yet safe predictions, and can accurately account for the effect of concrete compressive strength, shear span to depth ratio, shear reinforcement and member depth.

CHAPTER 6.   CONCLUSIONS AND RECOMMENDATIONS FOR FUTURE WORK

6.1. SUMMARY AND CONCLUSIONS

The main aim of this work was to develop better understanding of the behaviour and capacity of RC Deep beams. This was achieved through the use of an extensive experimental programme and numerical analysis. The results were used to develop a unified strut-and-tie model and propose an accurate and reliable effectiveness factor for designing RC deep beams. This chapter gives a brief summary of the work carried out in this study and reports the main conclusions.

6.1.1. EXPERIMENTAL PROGRAMME AND CODE COMPARISON

A total of 24 RC deep beams were tested in four-point bending to investigate the effect of concrete compressive strength, shear span to depth ratio, shear reinforcement and member depth on the shear behaviour and capacity of RC deep beams. Based on the results, the STM provisions of EC2, ACI318-14 and Model Code 2010 were evaluated, and the following conclusions can be drawn:

1. Shear span to depth ratio is the most important parameter that controls behaviour and shear capacity of RC deep beams.
2. Concrete compressive strength has more influence on the shear strength of deep beams than shear reinforcement. However, the presence of shear reinforcement is crucial in controlling crack propagation and providing ductility to deep beams.
3. There is a pronounced size effect on the average shear strength (V/bd) of deep beams; however, the first diagonal crack strength is not very size dependent.
4. The effectiveness factor is dominated by concrete compressive strength but it is also influenced by the shear span to depth ratio. ACI 318-14 provisions neglect

the effect of these two parameters in estimating the effective concrete strength of the inclined strut and as a result lead to unconservative predictions.

5. There is a difference of about 15% to 20% on the experimental effectiveness factor of deep beams with and without shear reinforcement. Amongst the models examined in this paper, ACI 318-14 is currently the only code of practice that accounts for the effect of shear reinforcement on the effectiveness factor. The EC2 and Model code 2010 should be modified to account for the effect of shear reinforcement on controlling crack growth.

6. Shear strength predictions by the STM with the provisions of both EC2 and Model Code 2010 are generally conservative; however, their conservatism reduces with increasing shear span to depth ratio because these two codes neglect the effect of shear span to depth ratio on the concrete effectiveness factor.

6.1.2. NUMERICAL ANALYSIS AND PARAMETRIC STUDY

An extensive numerical investigation was carried out using ABAQUS. The performance of the built-in smeared crack model and concrete damage plasticity model were examined and then the microplane M4 material model was implemented as a user subroutine in the program to better simulate the performance of RC deep beams. The microplane M4 model was validated against experimental results of 20 RC deep beams. A parametric study was then carried out to investigate the effect of shear span to depth ratio and concrete compressive strength for RC deep beams with and without shear reinforcement. Based on the results of the numerical investigation and parametric study, the following conclusions can be drawn:

1. The smeared crack and damage plasticity models are unable to realistically simulate the shear behaviour of RC deep beams. This is because these models cannot predict realistically shear deformation in discontinuity regions.

2. The implementation of the microplane material model M4 in ABAQUS led to reasonably accurate predictions of the overall behaviour of the RC deep beams analyzed; however, local strain values were generally underestimated because a

smeared approach is unable to realistically simulate the tension stiffening of the concrete.

3. Concrete compressive strength and shear span to depth ratio are the key parameter affecting the concrete effectiveness factor in the shear span of deep beams.

4. Minimum shear reinforcement can enable a better distribution of stresses within the shear span, control tensile strain and increase the effectiveness of the concrete by up to 15%.

5. An accurate model to estimate the effectiveness factor should include the effect of concrete strength, shear span to depth ratio and shear reinforcement.

6.1.3. STRUT-AND-TIE MODEL AND PROPOSED EFFECTIVENESS FACTOR

The performance of the different effectiveness factors for the inclined strut in the strut-and-tie model were evaluated against a database of experimental results of RC deep beams. On the basis of this analysis, a more reliable effectiveness factor model based on lateral tensile strain in the shear span was proposed to estimate the effective strength of inclined strut along with the node factors to predict the effective strength of the nodes. The main conclusions of this research study can be summarized as follows:

1. A tie-arch mechanism is the main resisting mechanism in RC deep beams with and without shear reinforcement and can be best represented by the strut-and-tie model.

2. The selection of an appropriate strut-and-tie model and size for its elements is critical for accurate shear capacity predictions.

3. The effectiveness factor models based on the modified compression field theory show poor correlation against the experimental results, with a large scatter and high coefficients of variation.

4. The STM provision and the effectiveness factors of EC2, ACI 318-14 and Model Code 2010 do not ensure adequate safety levels (after application of safety factors) for RC deep beams without shear reinforcement.

5. The use of the proposed model leads to less conservative yet safe predictions with the lowest standard deviations of 0.26 for both RC deep beams with and without shear reinforcement and can more accurately account for the effect of concrete compressive strength, shear span to depth ratio, shear reinforcement and member depth.

6.2. RECOMMENDATION FOR FUTURE WORK

Based on work conducted as part of this research programme the following recommendations for future work are reported:

1. More experimental work is required to investigate the effect of different parameters such as main flexural reinforcement ratio and type and distribution of loading on the behavior and capacity of RC deep beams.

2. More experimental work is needed to be done to investigate the effect of shear reinforcement on the size effect of RC deep beams.

3. The finite element model (using microplane model M4) needs to be further validated against experimental results, especially for RC slender beams as the shear resisting mechanisms are different from those developed in RC deep beams.

4. Mesh sensitivity techniques such as non-local or crack band model could be implemented in the microplane model M4 to yield more reliable results. These models can also better control crack propagation and compressive post peak behaviour.

5. The proposed effectiveness factors for strut-and-tie model need to be further validated using additional experimental work, including tests on more realistic elements such as T-beams and beams subjected to distributed load.

6. More sophisticated experimental work needs to be done on the distribution of strain/stress in the shear span and the depth of the compression zone in RC deep beams. This is to more realistically specify the size of both inclined and compression zone struts in the strut-and-tie model.

7. More research is required to examine the current shear provisions of EC2 for RC slender beams with shear reinforcement and assess/include the possible contribution of concrete to the total shear resistance.

REFERENCES

1.   Smith, K. and A. Vantsiotis. *Shear strength of deep beams*. in *ACI Journal Proceedings*. 1982. ACI.

2.   Collins, M.P., D. Mitchell, and E.C. Bentz, *Shear design of concrete structures.* The Structural Engineer Journal, 2008. 86(10): p. 32-39.

3.   British Standards Institution., *Eurocode 2: Design of Concrete Structures: Part 1-1: General Rules and Rules for Buildings*. 2004, British Standards Institution.

4.   ACI Committee, American Concrete Institute, and International Organization for Standardization, *Building Code Requirements for Structural Concrete (ACI 318M-14) and Commentary*. 2014, American Concrete Institute.

5.   Ritter, W., *Die Bauweise Hennebique (Hennebiques Construction Method).* Schweizerische Bauzeitung, 1899. 17: p. 41-43.

6.   Morsch, E., *Der eisenbetonbau, seine anwendung und theorie.* Wayss and Freytag, AG, Im Selbstverlag der Firma, Neustadt, AD Haardt, 1902: p. 118.

7.   Lampert, P. and B. Thurlimann, *Ultimate Strength and Design of Reinforced Concrete Beams in Torsion and Bending.* International Association for Bridge and Structural Engineering, 1971. 31(1): p. 107-131.

8.   Kupfer, H. and H. Bulicek, *A consistent model for the design of shear reinforcement in slender beams with I-or Box-shaped cross section.* Concrete shear in earthquake, 1992: p. 256-265.

9.   Vecchio, F.J. and M.P. Collins, *The modified compression-field theory for reinforced concrete elements subjected to shear.* ACI Journal Proceedings, 1986. 83(2).

10.   Marti, P. *Basic tools of reinforced concrete beam design*. in *ACI Journal Proceedings*. 1985. ACI.

11.   Marti, P., *Truss models in detailing.* Concrete International, 1985. 7(12): p. 66-73.

12.   Fib Bulletin No. 55., *Model Code 2010-first complete draft*. 2010, International Federation for Structural Concrete.

13.   Ashour, A. and K.-H. Yang, *Application of plasticity theory to reinforced concrete deep beams: a review.* Magazine of Concrete Research, 2008. 60(9): p. 657-664.

14.   Tuchscherer, R., D. Birrcher, C. Williams, D. Deschenes, and O. Bayrak, *Evaluation of Existing Strut-and-Tie Methods and Recommended Improvements.* ACI Structural Journal, 2014. 111(6).

15.   Arabzadeh, A., A. Rahaie, and R. Aghayari, *A simple strut-and-tie model for prediction of ultimate shear strength of rc deep beams.* International Journal of Civil Engineering, 2009. 7(3): p. 141-153.

16.   Kuchma, D., S. Yindeesuk, T. Nagle, J. Hart, and H.H. Lee, *Experimental validation of strut-and-tie method for complex regions.* ACI Structural Journal, 2008. 105(5).

17.   Sagaseta, J. and R. Vollum, *Shear design of short-span beams.* Magazine of Concrete Research, 2010. 62(4): p. 267-282.

18.   Collins, M.P., E.C. Bentz, and E.G. Sherwood, *Where is shear reinforcement required? Review of research results and design procedures.* ACI Structural Journal, 2008. 105(5).

19.   Brown, M.D. and O. Bayrak, *Design of deep beams using strut-and-tie models--part I: Evaluating US provisions.* ACI Structural Journal, 2008. 105(4).

20.   Kani, G.N.J., *How safe are our large reinforced concrete beams?* ACI journal, 1967. 64(3): p. 128-141.

21.   Taylor, H.P.J., *Shear Strength of Large Beams.* Journal of the Structural Division, 1972. 98(St 11): p. 2473-2490.

22.   Bazant, Z.P. and J.-K. Kim, *Size effect in shear failure of longitudinally reinforced beams.* ACI Journal, 1984. 81(5): p. 456-468.

23.   Shioya, T., M. Iguro, Y. Nojiri, H. Akiyama, and T. Okada, *Shear strength of large reinforced concrete beams.* ACI Special Publication, 1990. 118: p. 259-279.

24.   Bazant, Z.P. and M.T. Kazemi, *Size effect on diagonal shear failure of beams without stirrups.* ACI Structural Journal, 1991. 88(3): p. 268-276.

25.   Syroka-Korol, E. and J. Tejchman, *Experimental investigations of size effect in reinforced concrete beams failing by shear.* Engineering Structures, 2014. 58: p. 63-78.

26.   Walraven, J. and N. Lehwalter, *Size effects in short beams loaded in shear.* ACI Structural Journal, 1994. 91(5): p. 585-593.

27.   Tan, K. and H. Lu, *Shear behavior of large reinforced concrete deep beams and code comparisons.* ACI Structural Journal, 1999. 96(5): p. 836-845.

28.   Kotsovos, M.D. and M.N. Pavlović, *Size effects in beams with small shear span-to-depth ratios.* Computers & structures, 2004. 82(2): p. 143-156.

29.   Tan, K., G. Cheng, and H. Cheong, *Size effect in shear strength of large beams—behaviour and finite element modelling.* Magazine of Concrete Research, 2005. 57(8): p. 497-509.

30. Tan, K. and G. Cheng, *Size effect on shear strength of deep beams: Investigating with strut-and-tie model.* Journal of structural engineering, 2006. 132(5): p. 673-685.

31. Zhang, N. and K.-H. Tan, *Size effect in RC deep beams: Experimental investigation and STM verification.* Engineering structures, 2007. 29(12): p. 3241-3254.

32. Tan, K.-H., G.-H. Cheng, and N. Zhang, *Experiment to mitigate size effect on deep beams.* Magazine of Concrete Research, 2008. 60(10): p. 709-723.

33. Rashid, Y., *Ultimate strength analysis of prestressed concrete pressure vessels.* Nuclear engineering and design, 1968. 7(4): p. 334-344.

34. Chen, A.C. and W.-F. Chen, *Constitutive relations for concrete.* Journal of Engineering Mechanics, 1975. 101(ASCE# 11529 Proceeding).

35. Vermeer, P.A. and R. De Borst, *Non-associated plasticity for soils, concrete and rock.* HERON, 29 (3), 1984, 1984.

36. Hu, H.-T. and W.C. Schnobrich, *Nonlinear analysis of plane stress state reinforced concrete under short term monotonic loading*. 1988, University of Illinois Engineering Experiment Station. College of Engineering. University of Illinois at Urbana-Champaign.

37. Lubliner, J., J. Oliver, S. Oller, and E. Onate, *A plastic-damage model for concrete.* International Journal of solids and structures, 1989. 25(3): p. 299-326.

38. Ožbolt, J., Y. Li, and I. Kožar, *Microplane model for concrete with relaxed kinematic constraint.* International Journal of Solids and Structures, 2001. 38(16): p. 2683-2711.

39.   Bazant, Z.P., F.C. Caner, I. Carol, M.D. Adley, and S.A. Akers, *Microplane model M4 for concrete. I: Formulation with work-conjugate deviatoric stress.* Journal of Engineering Mechanics, 2000. 126(9): p. 944-953.

40.   Caner, F.C. and Z.P. Bazant, *Microplane model M4 for concrete. II: Algorithm and calibration.* Journal of Engineering Mechanics, 2000. 126(9): p. 954-961.

41.   Ozbolt, J. and Y.-J. Li, *Three-Dimensional Cyclic Analysis of Compressive Diagonal Shear Failure.* ACI Special Publication, 2001. 205(4): p. 61-80.

42.   Červenka, J., Z.P. Bažant, and M. Wierer, *Equivalent localization element for crack band approach to mesh‐sensitivity in microplane model.* International journal for numerical methods in engineering, 2005. 62(5): p. 700-726.

43.   Di Luzio, G., *A symmetric over-nonlocal microplane model M4 for fracture in concrete.* International journal of solids and structures, 2007. 44(13): p. 4418-4441.

44.   Wight, J.K. and J.G. MacGregor, *Reinforced Concrete: Mechanics and Design*. 6 ed. 2012: Pearson.

45.   Mitchell, D. and M.P. Collins. *Diagonal compression field theory-a rational model for structural concrete in pure torsion*. in *ACI Journal Proceedings*. 1974. ACI.

46.   Vecchio, F.J. and M.P. Collins, *Predicting the response of reinforced concrete beams subjected to shear using the modified compression field theory.* ACI Structural Journal, 1988. 85(3).

47.   Bentz, E.C., *Sectional analysis of reinforced concrete members.* PhD Thesis, Department of Civil Engineering, University of Toronto, 2000.

48.   Angelakos, D., E.C. Bentz, and M.P. Collins, *Effect of concrete strength and minimum stirrups on shear strength of large members.* ACI Structural Journal, 2001. 98(3).

49.   Mphonde, A.G. and G.C. Frantz. *Shear tests of high-and low-strength concrete beams without stirrups*. in *ACI Journal Proceedings*. 1984. ACI.

50.   Xie, Y., S.H. Ahmad, T. Yu, S. Hino, and W. Chung, *Shear ductility of reinforced concrete beams of normal and high-strength concrete.* ACI Structural Journal, 1994. 91(2).

51.   Tan, K.-H., F.-K. Kong, S. Teng, and L. Guan, *High-strength concrete deep beams with effective span and shear span variations.* ACI Structural Journal, 1995. 92(4).

52.   Oh, J.-K. and S.-W. Shin, *Shear strength of reinforced high-strength concrete deep beams.* ACI Structural Journal, 2001. 98(2).

53.   Leonhardt, F. and R. Walther, *The Stuttgart Shear Tests, 1961.* CACA Translation, 1964(111).

54.   Kim, J.-K. and Y.-D. Park, *Shear strength of reinforced high strength concrete beam without web reinforcement.* Magazine of concrete research, 1994. 46(166): p. 7-16.

55.   Rahal, K.N. and K.S. Al-Shaleh, *Minimum transverse reinforcement in 65 MPa concrete beams.* ACI Structural Journal, 2004. 101(6).

56.   Kawano, H. and H. Watanabe, *Shear strength of reinforced concrete columns– Effect of specimen size and load reversal.* Proceedings of the Second Italy-Japan Workshop on Seismic Design and Retrofit of Bridges, 1997: p. 141-154.

57.   Kong, P.Y. and B.V. Rangan, *Shear strength of high-performance concrete beams.* ACI Structural Journal, 1998. 95(6): p. 677-688.

58. Bazant, Z.P., Qiang Yu, Walter Gerstle, James Hanson, and J.W. Ju, *Justification of ACI 446 proposal for updating ACI code provisions for shear design of reinforced concrete beams.* ACI Structural Journal, 2007. 104(5).

59. Taylor, H.P.J., *Investigation of the forces carried across cracks in reinforced concrete beams in shear by interlock of aggregate*. 1970.

60. Walraven, J.C., *Fundamental analysis of aggregate interlock.* Journal of the Structural Division, 1981. 107(11): p. 2245-2270.

61. Yoon, Y.-S., W.D. Cook, and D. Mitchell, *Minimum shear reinforcement in normal, medium, and high-strength concrete beams.* ACI Structural journal, 1996. 93(5).

62. Collins, M.P. and D. Mitchell. *Rational Approach to Shear Design--The 1984 Canadian Code Provisions*. in *ACI Journal Proceedings*. 1986. ACI.

63. Mohammadhassani, M., M.Z. Jumaat, A. Ashour, and M. Jameel, *Failure modes and serviceability of high strength self compacting concrete deep beams.* Engineering Failure Analysis, 2011. 18(8): p. 2272-2281.

64. Haas, M., *Investigations on shear including the development of a material model for the FE analysis of cracked RC structures.* PhD Thesis, University of Sheffield, Sheffield, 1996.

65. Bazant, Z.P., *Fracturing truss model: Size effect in shear failure of reinforced concrete.* Journal of engineering mechanics, 1997. 123(12): p. 1276-1288.

66. Weibull, W., *A Statistical Theory of the Strength of Materials.* Royal Swedish Academy for Engineering Science, 1939. 151: p. 1-45.

67. Tan, K.-H., F.-K. Kong, S. Teng, and L.-W. Weng, *Effect of web reinforcement on high-strength concrete deep beams.* ACI Structural Journal, 1997. 94(5): p. 572-581.

68. Foster, S.J. and R.I. Gilbert, *Experimental studies on high-strength concrete deep beams.* ACI Structural Journal, 1998. 95(4): p. 382-390.

69. Yang, K.-H., H.-S. Chung, E.-T. Lee, and H.-C. Eun, *Shear characteristics of high-strength concrete deep beams without shear reinforcements.* Engineering structures, 2003. 25(10): p. 1343-1352.

70. Mihaylov, B.I., E.C. Bentz, and M.P. Collins, *Behavior of large deep beams subjected to monotonic and reversed cyclic shear.* ACI Structural Journal, 2010. 107(6): p. 726-734.

71. Lu, W.-Y., J. Lin, and H.-W. Yu, *Shear Strength of Reinforced Concrete Deep Beams.* ACI Structural Journal, 2013. 110(4): p. 671-680.

72. Birrcher, D.B., R.G. Tuchscherer, M. Huizinga, and O. Bayrak, *Depth Effect in Deep Beams.* ACI Structural Journal, 2014. 111(4): p. 731-740.

73. Bentz, E.C. and S. Buckley, *Repeating a classic set of experiments on size effect in shear of members without stirrups.* ACI structural journal, 2005. 102(6): p. 832-838.

74. Yang, K.-H. and A.F. Ashour, *Strut-and-tie model based on crack band theory for deep beams.* Journal of Structural Engineering, 2011. 137(10): p. 1030-1038.

75. Ismail, K.S. *Strength Prediction of Struts in High-Strength Reinforced Concrete Deep Beams by Strut-and-Tie Model*. University of Salahaddin-Hawler, 2009. MS.c

76. EN, B., *12390-3: 2009 (2009) Testing hardened concrete.* Making and curing specimens for strength tests. ISBN. 940137696.

77. ASTM, *Standard Test Methods and Definitions for Mechanical Testing of Steel Products—ASTM-A370*. 1997, American Society for Testing and Materials.

78.   Wight, J.K. and J.G. MacGregor, *Reinforced concrete: mechanics and design.* Pearson Education, Inc., Upper Saddle River, New Jersey, 2009. 7458: p. 1157.

79.   Mohammad, M., M.Z.B. Jumaat, M. Chemrouk, A. Ghasemi, S. Hakim, and R. Najmeh, *An experimental investigation of the stress-strain distribution in high strength concrete deep beams.* Procedia Engineering, 2011. 14: p. 2141-2150.

80.   ABAQUS, I., *Abaqus Version 6.9 Documentation.* Dassault Systemes. Velizy-Villacoublay; France, 2009.

81.   Aguilar, G., A.B. Matamoros, G.J. Parra-Montesinos, J.A. Ramírez, and J.K. Wight, *Experimental evaluation of design procedures for shear strength of deep reinforced concrete beams.* ACI Structural Journal, 2002. 99(4).

82.   Guadagnini, M. *Shear behaviour and design of FRP RC beams*. The University of Sheffield, 2002. PhD Thesis

83.   Taylor, G.I., *Plastic strain in metals.* Journal of the Institute of Metals, 1938. 62: p. 307-324.

84.   Batdorf, S.B. and B. Budiansky, *A mathematical theory of plasticity based on the concept of slip*. 1949: National Advisory Committee for Aeronautics.

85.   Bazant, Z.P. and P.G. Gambarova, *Crack Shear in Concrete: Crack Band Microplane Model.* Journal of Structural Engineering, 1984. 110(9): p. 2015-2035.

86.   Bazant, Z.P. and P.C. Prat, *Microplane model for brittle-plastic material: I. Theory.* Journal of Engineering Mechanics, 1988. 114(10): p. 1672-1688.

87.   Bazant, Z.P. and J. Ozbolt, *Nonlocal microplane model for fracture, damage, and size effect in structures.* Journal of Engineering Mechanics, 1990. 116(11): p. 2485-2505.

88.   Carol, I., P.C. Prat, and Z.P. Bažant, *New explicit microplane model for concrete: theoretical aspects and numerical implementation.* International Journal of Solids and Structures, 1992. 29(9): p. 1173-1191.

89.   Bazant, Z.P., Y. Xiang, and P.C. Prat, *Microplane model for concrete. I: stress-strain boundaries and finite strain.* Journal of Engineering Mechanics, 1996. 122(3): p. 245-254.

90.   Bazant, Z.P., Y. Xiang, M.D. Adley, P.C. Prat, and S.A. Akers, *Microplane model for concrete: II: data delocalization and verification.* Journal of Engineering Mechanics, 1996. 122(3): p. 255-262.

91.   Bažant, P. and B. Oh, *Efficient numerical integration on the surface of a sphere.* Journal of Applied Mathematics and Mechanics (ZAMM), 1986. 66(1): p. 37-49.

92.   Bažant, P. and B. Oh, *Efficient numerical integration on the surface of a sphere.* ZAMM-Journal of Applied Mathematics and Mechanics/Zeitschrift für Angewandte Mathematik und Mechanik, 1986. 66(1): p. 37-49.

93.   Slobbe, A., M. Hendriks, and J. Rots, *Systematic assessment of directional mesh bias with periodic boundary conditions: Applied to the crack band model.* Engineering Fracture Mechanics, 2013. 109: p. 186-208.

94.   Brown, M.D. and O. Bayrak, *Design of Deep Beams Using Strut-and-Tie Models--Part II: Design Recommendations.* ACI Structural Journal, 2008. 105(4).

95.   Park, J.-w. and D. Kuchma, *Strut-and-tie model analysis for strength prediction of deep beams.* ACI Structural Journal, 2007. 104(6).

96.   Tuchscherer, R.G., D.B. Birrcher, and O. Bayrak, *Experimental Examination of ACI 318 Strut and Tie Modeling Provisions.* ACI Special Publication, 2014. 296.

97. Brena, S.F. and N.C. Roy, *Evaluation of load transfer and strut strength of deep beams with short longitudinal bar anchorages.* ACI Structural Journal, 2009. 106(5).

98. Bakir, P. and H. Boduroğlu, *Mechanical behaviour and non-linear analysis of short beams using softened truss and direct strut & tie models.* Engineering structures, 2005. 27(4): p. 639-651.

99. Jirsa, J., J. Breen, and K. Bergmeister. *Experimental studies of nodes in strut-and-tie models*. in *IABSE Colloquium Stuttgart*. 1991.

100. Vecchio, F.J. and M.P. Collins, *Compression response of cracked reinforced concrete.* Journal of Structural Engineering, 1993. 119(12): p. 3590-3610.

101. Foster, S.J. and R.I. Gilbert, *The design of nonflexural members with normal and high-strength concretes.* ACI Structural Journal, 1996. 93(1).

102. Warwick, W. and S.J. Foster, *Investigation into the efficiency factor used in non-flexural reinforced concrete member design*. 1993: University of New South Wales.

103. Clark, A.P. *Diagonal tension in reinforced concrete beams*. in *ACI journal proceedings*. 1951. ACI.

104. Moody, K., I. Viest, R. Elstner, and E. Hognestad. *Shear Strength of Reinforced Concrete Beams Part 1-Tests of Simple Beams*. in *ACI journal proceedings*. 1954. ACI.

105. Moody, K., I. Viest, R. Elstner, and E. Hognestad. *Shear Strength of Reinforced Concrete Beams Part 2-Tests of Restrained Beams Without Web Reinforcement*. in *ACI Journal Proceedings*. 1955. ACI.

106. Morrow, J. and I.M. Viest. *Shear strength of reinforced concrete frame members without web reinforcement*. in *ACI Journal Proceedings*. 1957. ACI.

107.   Chang, T.S. and C.E. Kesler. *Static and fatigue strength in shear of beams with tensile reinforcement*. in *ACI Journal Proceedings*. 1958. ACI.

108.   Watstein, D. and R.G. Mathey. *Strains in beams having diagonal cracks*. in *ACI Journal Proceedings*. 1958. ACI.

109.   Rodriguez, J.J., A.C. Bianchini, I.M. Viest, and C.E. Kesler. *Shear Strength of Two-Span Continous Reinforced Concrete Beams*. in *ACI Journal Proceedings*. 1959. ACI.

110.   de Cossio, R.D. and C.P. Siess. *Behavior and strength in shear of beams and frames without web reinforcement*. in *ACI Journal Proceedings*. 1960. ACI.

111.   Mathey, R.G. and D. Watstein. *Shear strength of beams without web reinforcement containing deformed bars of different yield strengths*. in *ACI journal proceedings*. 1963. ACI.

112.   de Paiva, H.R. and C.P. Siess, *Strength and behavior of deep beams in shear.* ASCE Structural Journal, 1965. 91(ST5): p. 22.

113.   Krefeld, W.J. and C.W. Thurston. *Studies of the shear and diagonal tension strength of simply supported reinforced concrete beams*. in *ACI Journal Proceedings*. 1966. ACI.

114.   Ramakrishnan, V. and Y. Ananthanarayana. *Ultimate strength of deep beams in shear*. in *ACI Journal Proceedings*. 1968. ACI.

115.   Kong, F.-K., P.J. Robins, and D.F. Cole. *Web reinforcement effects on deep beams*. in *ACI Journal Proceedings*. 1970. ACI.

116.   Manuel, R.F., B.W. Slight, and G.T. Suter, *Deep beam behavior affected by length and shear span variations.* Am Concrete Inst Journal & Proceedings, 1971. 68(12).

150

117. Manuel, R., *Failure of deep beams.* ACI Special publication, 1974. 42: p. 15.

118. Niwa, J., K. Maekawa, and H. Okamura, *Non-linear Finite Element Analysis of Deep Beams.* Advanced Mechanics of Reinforced Concrete, IABSE Colloqium Delft Netherlands, 1981: p. 13.

119. Rogowsky, D.M., J.G. MacGregor, and S.Y. Ong. *Tests of reinforced concrete deep beams*. in *ACI Journal Proceedings*. 1986. ACI.

120. Subedi, N., A.E. Vardy, and N. Kubotat, *Reinforced concrete deep beams some test results.* Magazine of Concrete Research, 1986. 38(137): p. 206-219.

121. Ahmad, S.H. and D. Lue, *Flexure-shear interaction of reinforced high strength concrete beams.* ACI Structural Journal, 1987. 84(4).

122. Lehwalter, N. *Bearing Capacity of Concrete Compression Struts in Truss-Systems, Exemplified by the Case of Short Beams*. PhD thesis, Darmstadt, 1988.(in German), 1988.

123. Shin, S.-W., K.-S. Lee, J.-I. Moon, and S. Ghosh, *Shear strength of reinforced high-strength concrete beams with shear span-to-depth ratios between 1.5 and 2.5.* ACI Structural Journal, 1999. 96(4).

124. Adebar, P., *One-way shear strength of large footings.* Canadian journal of civil engineering, 2000. 27(3): p. 553-562.

125. Pendyala, R.S. and P. Mendis, *Experimental study on shear strength of high-strength concrete beams.* ACI Structural Journal, 2000. 97(4).

126. Lertsrisakulrat, T., J. Niwa, A. Yanagawa, and M. Matsuo. *Concept of concrete compressive fracture energy in RC deep beams without transverse reinforcement*. in *Transactions of the Japan Concrete Institute*. 2002.

127.   Seliem, H., A. Hosny, H. Dwairi, and S. Rizkalla, *Shear behavior of concrete beams reinforced with MMFX steel without web reinforcement.* NC State University Final Report, Project No. IS-06-08, 2006.

128.   Kani, M.W., M. W. Huggins, and R. R. Wittkopp, *Kani on shear in reinforced concrete*. 1979: Deptartment of Civil Engineering, University of Toronto.

129.   Tuchscherer, R.G., D.B. Birrcher, and O. Bayrak, *Strut-and-tie model design provisions.* PCI journal, 2011. 56(1): p. 155-170.

130.   Ismail, K.S., M. Guadagnini, and K. Pilakoutas, *Shear Behaviour and Size Effect of RC Deep Beams.* ACI Structural journal. Submitted, 2015.

131.   Ismail, K.S., M. Guadagnini, and K. Pilakoutas, *Numerical Investigation on the Shear strength of RC Deep Beams Using the Microplane Model.* Journal of Structural Engineering. Submitted, 2015.

132.   Bazant, Z.P. and Y. Xiang, *Size effect in compression fracture: splitting crack band propagation.* Journal of Engineering Mechanics, 1997. 123(2): p. 162-172.

133.   Richart, F.E., A. Brandtzaeg, and R.L. Brown, *A study of the failure of concrete under combined compressive stresses.* University of Illinois Bulletin; v. 26, no. 12, 1928.

134.   Laupa, A., C.P. Siess, and N.M. Newmark, *The shear strength of simple-span reinforced concrete beams without web reinforcement*. 1953, University of Illinois Engineering Experiment Station. College of Engineering. University of Illinois at Urbana-Champaign.

135.   Ferguson, P.M. *Some implications of recent diagonal tension tests*. in *ACI Journal Proceedings*. 1956. ACI.

136.   Sozen, M.A., E. Zwoyer, and C.P. Siess, *Investigation of prestressed concrete for highway bridges: Part I strength in shear of beams without web*

reinforcement. University of Illinois. Engineering Experiment Station. Bulletin; no. 452, 1959.

137.   Bower, J.E. and I.M. Viest. *Shear strength of restrained concrete beams without web reinforcement.* in *ACI Journal Proceedings.* 1960. ACI.

138.   de Cossio, R.D., *Discussion to 326 Report.* ACI Journal Proceedings, 1962. 59(11): p. 1323-1349.

139.   Rüsch, H., F.R. Haugli, and H. Mayer, *Schubversuche an stahlbeton-rechteckbalken mit gleichmassig verteilter belastung.* (in German) Deutcher Ausschuss fur Stahlbeton, 1962: p. 4-30.

140.   Bresler, B. and A.C. Scordelis. *Shear strength of reinforced concrete beams.* in *ACI Journal Proceedings.* 1963. ACI.

141.   Rajagopalan, K.S. and P.M. Ferguson, *Exploratory Shear Tests Emphasizing Percentage of Lightweight Steel.* ACI Journal Proceedings, 1968. 65(8): p. 634-638.

142.   Bhal, N.S. *Über den Einfluss der Balkenhöhe auf die Schubtragfähigkeit von einfeldrigen Stahlbetonbalken mit und ohne Schubbewehrung.* Stuttgart University, 1967. (in German) Ph.D. Thesis

143.   Taylor, H.P., *Shear stresses in reinforced concrete beams without shear reinforcement.* Cement and Concrete Association, Technical Report TRA 407, Wexham Springs, United Kingdom, 1968.

144.   Mattock, A.H., *Diagonal tension cracking in concrete beams with axial forces.* Journal of the Structural Division, 1969. 95(9): p. 1887-1900.

145.   Placas, A. and P.E. Regan. *Shear failure of reinforced concrete beams.* in *ACI Journal Proceedings.* 1971. ACI.

146. Aster, H. and R. Koch, *Schubtragfähigkeit dicker Stahlbetonplatten.* (in German) BETON-U STAHLBETONBAU, 1974. 69(11).

147. Chana, P., *Some aspects of modelling the behaviour of reinforced concrete under shear loading.* Cement and Concrete Association Technical Report No. 543. C&CA, Wexham Springs, United Kingdom, 1981(Monograph): p. 22pp.

148. Kwun, M., *Shear in RC beams without web reinforcement.* ASCE Journal of Structural Engineering, 1981. 107(5): p. 907-921.

149. Heger, F.J. and T.J. McGrath, *Design method for reinforced concrete pipe and box sections.* Simpson, Gumpertz & Heger Inc, 1982: p. 251pp.

150. Mphonde, A.G. and G.C. Frantz, *Shear tests of high-and low-strength concrete beams with stirrups.* ACI Special Publication, 1985. 87: p. 179-196.

151. Elzanaty, A.H., A.H. Nilson, and F.O. Slate. *Shear capacity of reinforced concrete beams using high-strength concrete*. in *ACI Journal Proceedings*. 1986. ACI.

152. Yasuo, M. and I. AKIRA, *Flexural and shear strength of reinforced high—strength lightweight concrete beams.* Transactions of the Japan Concrete Institute, 1986. 8: p. 267-274.

153. Mansur, M., K. Ong, and P. Paramasivam, *Shear strength of fibrous concrete beams without stirrups.* Journal of Structural Engineering, 1986. 112(9): p. 2066-2079.

154. Niwa, J., K. Yamada, K. Kokozawa, and M. Okamura, *Revaluation of the Equation for Shear Strength of Reinforced Concrete-Beams without Web Reinforcement.* Translation JSCE, 1987. 372/V-5.

155. Regan, P. and H. Rezai-Jorabi, *Shear resistance of one-way slabs under concentrated loads.* ACI Structural Journal, 1988. 85(2).

156. Johnson, M.K. and J.A. Ramirez, *Minimum shear reinforcement in beams with higher strength concrete.* ACI Structural Journal, 1989. 86(4).

157. Adebar, P. and M.P. Collins, *Shear strength of members without transverse reinforcement.* Canadian journal of civil engineering, 1996. 23(1): p. 30-41.

158. Thorenfeldt, E. and G. Drangsholt, *Shear capacity of reinforced high-strength concrete beams.* ACI Special Publication, 1990. 121.

159. Hallgren, M., *Flexural and shear capacity of reinforced high strength concrete beams without stirrups.* Licentiate degree, Royal Institute of Technology, Stockholm, Sweden,, 1994.

160. Jin-Keun, K. and P. Yon-Dong, *Shear strength of reinforced high strength concrete beam without web reinforcement.* Magazine of concrete research, 1994. 46(166): p. 7-16.

161. Matsui, Y., N. Kurihara, Y. Uchida, K. Rokugo, and W. Koyangi, *Shear capacity of rienforced high strength concrete beams without shear reinforcement.* Transactions of the Japan Concrete Institute, 1995. 17: p. 319-326.

162. Kawano, H. and H. Watanabe. *Shear strength of reinforced concrete columns-effect of specimen size and load reversal*. in *Proceedings of the Second Italy-Japan Workshop on Seismic Design and Retrofit of Bridges*. 1997.

163. Ghannoum, W.M. *Size effect on shear strength of reinforced concrete beams*. McGill University Montréal, Canada, 1998.

164. Islam, M., H. Pam, and A. Kwan, *Shear capacity of high-strength concrete beams with their point of inflection within the shear span.* Proceedings of the Institution of Civil Engineers: Structures and Buildings, 1998. 128(1): p. 91-99.

165. Collins, M.P. and D. Kuchma, *How safe are our large, lightly reinforced concrete beams, slabs, and footings?* ACI Structural Journal, 1999. 96(4).

166. Yoshida, Y. *Shear reinforcement for large lightly reinforced concrete members*. University of Toronto, 2000.

167. Cao, S., *Size effect and the influence of longitudinal reinforcement on the shear response of large reinforced concrete members.* Masters thesis, Department of Civil Engineering, University of Toronto, 2001.

168. Tariq, M. and J. Newhook. *Shear testing of FRP reinforced concrete without transverse reinforcement*. in *Proceedings, Annual Conference of the Canadian Society for Civil Engineering*. 2003.

169. Lubell, A., T. Sherwood, E. Bentz, and M. Collins, *Safe shear design of large, wide beams.* Concrete International, 2004. 26(1): p. 66-78.

170. Cladera, A. and A. Mari, *Experimental study on high-strength concrete beams failing in shear.* Engineering Structures, 2005. 27(10): p. 1519-1527.

171. El-Sayed, A., E. El-Salakawy, and B. Benmokrane, *Analytical Modeling of FRP-Reinforced Concrete Beams Failed in Shear.* 1st CSCE Specialyt Conference on Infrastructure Technologies, Manament and Policy, Toronto, Canada, FR-127-1-FR-127-10., 2005.

172. Sherwood, E.G., A.S. Lubell, E.C. Bentz, and M.P. Collins, *One-way shear strength of thick slabs and wide beams.* ACI Structural Journal, 2006. 103(6).

173. Lubell, A.S., *Shear in wide reinforced concrete members*. Vol. 68. 2006.

174. Uzel, A., B. Podgorniak, E.C. Bentz, and M.P. Collins, *Design of large footings for one-way shear.* ACI Structural Journal, 2011. 108(2).

175.   Roller, J.J. and H.G. Russel, *Shear strength of high-strength concrete beams with web reinforcement.* ACI Structural Journal, 1990. 87(2).

176.   Bazant, Z. and P. Prat, *Microplane model for brittle plastic material: II. Verification.* Journal of Engineering Mechanics, 1988. 114(10): p. 1689-1699.

APPENDIX A.   DATABASE

Table A-1-Slender beams without shear reinforcement

#	Author	Specimen	h (mm)	d (mm)	b (mm)	a (mm)	a/d	f_{ck} (MPa)	ρ	f_{yk} (MPa)	d_a (mm)	Top plate width (mm)	Bottom plate width (mm)	$V_{exp.}$ (kN)
1	Clark [103]	A0-1	457	404	203	914	2.26	21.5	0.0094	370	15	89	89	89.0
2		A0-2	457	408	203	914	2.24	26.0	0.0093	370	15	89	89	107.9
3	Laupa & Seiss [134]	S2	305	269	152	1295	4.81	26.9	0.0208	284	25	10	10	42.5
4		S3	305	265	152	1295	4.89	32.3	0.0252	410	25	10	10	53.1
5		S4	305	263	152	1295	4.92	30.8	0.0321	309	25	10	10	55.6
6		S5	305	262	152	1295	4.94	29.9	0.0411	315	25	10	10	49.8
7		S11	305	267	152	1295	4.85	14.8	0.0190	328	25	10	10	33.8
8		S13	305	262	152	1295	4.94	26.2	0.0411	304	25	10	10	49.8
9		T-3average	203	178	102	765	4.30	23.9	0.0316	359	25	10	10	19.6
10		T-5a	203	178	102	765	4.30	23.9	0.0219	317	25	10	10	22.2
11		T-5b	203	178	102	765	4.30	23.9	0.0219	317	25	10	10	22.7
12		T-5c	203	178	102	765	4.30	23.9	0.0219	317	25	10	10	23.1
13		T-6b	203	178	102	765	4.30	21.6	0.0140	331	25	10	10	19.3
14		T-12a	203	178	147	765	4.30	33.7	0.0220	359	25	10	10	35.6
15		T-12b	203	178	147	765	4.30	33.7	0.0220	359	25	10	10	33.8
16		T-12c	203	178	147	765	4.30	33.7	0.0220	359	25	10	10	32.0
17		T2-Ma	305	269	152	915	3.40	29.8	0.0139	331	25	10	10	42.3
18		T2-Mb	305	269	152	915	3.40	27.7	0.0139	331	25	10	10	44.5
19	Moody et al [104]	A-A1	350	262	178	800	3.05	30.3	0.0217	483	25	102	102	60.7
20		A-A2	350	267	178	800	3.00	31.0	0.0215	483	25	102	102	67.4
21		A-A3	350	268	178	800	2.99	31.0	0.0222	483	25	102	102	76.3
22		A-A4	350	270	178	800	2.96	31.5	0.0237	483	25	102	102	71.8
23		A-B1	350	267	178	800	3.00	21.2	0.0162	483	25	102	102	56.9
24		A-B2	350	268	178	800	2.99	21.6	0.0163	483	25	102	102	60.7
25		A-B3	350	270	178	800	2.96	19.2	0.0160	483	25	102	102	56.3
26		A-B4	350	272	178	800	2.94	16.8	0.0166	483	25	102	102	56.3
27		A-C1	350	268	178	800	2.99	6.3	0.0081	483	25	102	102	20.7

#	Author	Specimen	h (mm)	d (mm)	b (mm)	a (mm)	a/d	f_{ck} (MPa)	ρ	f_{yk} (MPa)	d_a (mm)	Top plate width (mm)	Bottom plate width (mm)	$V_{exp.}$ (kN)
28		A-C2	350	272	178	800	2.94	6.1	0.0083	483	25	102	102	25.1
29		A-C3	350	273	178	800	2.93	6.9	0.0080	483	25	102	102	26.0
30		A-C4	350	274	178	800	2.92	6.8	0.0082	483	25	102	102	25.8
31		B-B1	350	268	152	914	3.41	36.7	0.0189	483	25	203	203	58.5
32		B-B2	350	268	152	914	3.41	16.7	0.0189	483	25	203	203	36.3
33		B-B3	350	268	152	914	3.41	25.8	0.0189	483	25	203	203	53.0
34		B-B4	350	268	152	914	3.41	15.4	0.0189	483	25	203	203	41.2
35		B-B5	350	268	152	914	3.41	30.7	0.0189	483	25	203	203	52.7
36		B-B6	350	268	152	914	3.41	15.8	0.0189	483	25	203	203	35.2
37		B-B7	350	268	152	914	3.41	30.9	0.0189	483	25	203	203	51.9
38		B-B8	350	268	152	914	3.41	12.2	0.0189	483	25	203	203	31.8
39		B-B9	350	268	152	914	3.41	41.2	0.0189	483	25	203	203	54.1
40		B-B10	350	268	152	914	3.41	24.0	0.0189	483	25	203	203	49.6
41		B-B11	350	268	152	914	3.41	38.1	0.0189	483	25	203	203	60.8
42		B-B12	350	268	152	914	3.41	20.2	0.0189	483	25	203	203	48.9
43		B-B13	350	268	152	914	3.41	37.8	0.0189	483	25	203	203	56.3
44		B-B14	350	268	152	914	3.41	22.6	0.0189	483	25	203	203	43.9
45		B-B15	350	268	152	914	3.41	37.4	0.0189	483	25	203	203	51.9
46		B-B16	350	268	152	914	3.41	16.3	0.0189	483	25	203	203	38.5
47	Ferguson [135]	F2	210	189	101	610	3.23	29.3	0.0210	483	6	25	25	22.2
48	Morrow & Viest [106]	B28-A6	406	353	305	711	2.01	47.2	0.0383	483	6	102	102	334.7
49		B40-B4	406	368	305	1016	2.76	34.8	0.0185	483	6	102	102	157.6
50		B56-B2	406	368	305	1422	3.86	14.7	0.0185	483	6	102	102	103.2
51		B56-E2	406	368	305	1422	3.86	14.7	0.0058	483	6	102	102	82.7
52		B56-A4	406	375	305	1422	3.79	25.0	0.0241	483	6	102	102	140.9
53		B56-B4	406	368	305	1422	3.86	27.2	0.0185	483	6	102	102	125.4
54		B56-E4	406	368	305	1422	3.86	28.4	0.0124	483	6	102	102	112.1
55		B56-A6	406	356	305	1422	3.99	39.9	0.0379	483	6	102	102	181.1
56		B56-B6	406	372	305	1422	3.82	45.7	0.0183	483	6	102	102	139.8
57		B70-B2	406	365	305	1778	4.87	16.3	0.0186	483	6	102	102	93.1
58		B70-A4	406	368	305	1778	4.83	27.2	0.0246	483	6	102	102	136.4
59		B70-A6	406	356	305	1778	4.99	45.0	0.0383	483	6	102	102	182.1

#	Author	Specimen	h (mm)	d (mm)	b (mm)	a (mm)	a/d	f_{ck} (MPa)	ρ	f_{yk} (MPa)	d_a (mm)	Top plate width (mm)	Bottom plate width (mm)	$V_{exp.}$ (kN)
60		B84-B4	406	363	305	2134	5.88	27.2	0.0188	483	6	102	102	116.4
61		B113-B4	406	365	305	2870	7.86	32.6	0.0186	483	6	102	102	111.6
62	Chang & Kesler [107]	1A1	152	137	102	533	3.89	27.6	0.0289	328	25	64	64	19.9
63		1B1	152	137	102	330	2.41	27.6	0.0186	328	25	64	64	19.6
64		1C2	152	137	102	432	3.15	27.6	0.0237	328	25	64	64	19.6
65		1C2	152	137	102	432	3.15	27.6	0.0237	328	25	64	64	17.8
66		IIA1	152	137	102	432	3.15	17.7	0.0186	328	25	64	64	17.0
67		IIA2	152	137	102	432	3.15	17.7	0.0186	328	25	64	64	17.3
68		IIB1	152	137	102	533	3.89	17.7	0.0237	328	25	64	64	16.6
69		IIC1	152	137	102	330	2.41	17.7	0.0289	328	25	64	64	17.8
70		IIIA1	152	137	102	533	3.89	14.9	0.0237	328	25	64	64	17.0
71		IIIB1	152	137	102	432	3.15	14.9	0.0186	328	25	64	64	15.3
72		IIIB2	152	137	102	432	3.15	14.9	0.0186	328	25	64	64	15.5
73		IIIC1	152	137	102	330	2.41	14.9	0.0289	328	25	64	64	18.4
74		4-21a	152	137	102	483	3.53	38.6	0.0289	328	25	64	64	21.1
75		4-21b	152	137	102	483	3.53	38.6	0.0186	328	25	64	64	24.6
76		4-22a	152	137	102	483	3.53	31.9	0.0186	328	25	64	64	21.4
77		4-22b	152	137	102	483	3.53	31.7	0.0186	328	25	64	64	23.4
78		4-23a	152	137	102	483	3.53	32.2	0.0186	328	25	64	64	21.6
79		4-23b	152	137	102	483	3.53	32.2	0.0186	328	25	64	64	22.5
80		5-21a	152	137	102	483	3.53	32.2	0.0289	328	25	64	64	28.9
81		5-21b	152	137	102	483	3.53	32.2	0.0289	328	25	64	64	27.5
82		5-22a	152	137	102	483	3.53	31.2	0.0289	328	25	64	64	22.4
83		5-22b	152	137	102	483	3.53	31.2	0.0289	328	25	64	64	25.9
84		5-23a	152	137	102	483	3.53	32.1	0.0289	328	25	64	64	24.5
85		5-23b	152	137	102	483	3.53	32.1	0.0289	328	25	64	64	23.4
86	Rodriqez et al [109]	E3N1	368	318	152	813	2.56	25.2	0.0159	483	25	102	102	109.5
87		E3N2	368	318	152	813	2.56	23.3	0.0159	483	25	102	102	102.3
88		C3N1	368	318	152	813	2.56	23.1	0.0159	483	25	102	102	65.9
89		C3N2	368	318	154	813	2.56	22.7	0.0159	483	25	102	102	104.8
90		E2N1	368	318	157	1295	4.07	29.0	0.0159	483	25	102	102	55.3
91		E2N2	368	318	152	1295	4.07	20.8	0.0159	483	25	102	102	57.2

#	Author	Specimen	h (mm)	d (mm)	b (mm)	a (mm)	a/d	f_{ck} (MPa)	ρ	f_{yk} (MPa)	d_a (mm)	Top plate width (mm)	Bottom plate width (mm)	$V_{exp.}$ (kN)
92		E2N3	368	321	156	1295	4.03	23.0	0.0159	483	25	102	102	47.5
93		C2N1	368	318	156	1295	4.07	26.1	0.0159	483	25	102	102	54.6
94		C2N2	368	318	152	1295	4.07	18.6	0.0159	483	25	102	102	53.5
95	Sozen et al [136]	A.32.19	305	229	155	914	3.99	34.4	0.0032	1434	38	10	10	25.2
96		B.31.15	305	259	152	914	3.53	40.1	0.0059	1434	38	10	10	19.6
97		B.32.11	305	264	152	1372	5.20	36.0	0.0038	1434	38	10	10	24.2
98		B.32.19	305	259	152	914	3.53	29.9	0.0055	1434	38	10	10	23.4
99		B.32.31	305	259	152	914	3.53	18.8	0.0055	1434	38	10	10	16.9
100		B.32.34	305	257	152	914	3.56	17.3	0.0055	1434	38	10	10	21.5
101		B.32.41	305	269	152	914	3.40	22.6	0.0095	1434	38	10	10	35.6
102		B32.54	305	264	152	914	3.46	22.1	0.0124	1434	38	10	10	32.1
103	De Cassio & Seiss [110]	L-1	305	252	152	508	2.02	21.0	0.0336	303	25	152	152	116.1
104		L-2	305	252	152	762	3.02	21.5	0.0336	310	25	152	152	75.6
105		L-2A	305	252	152	762	3.02	36.7	0.0336	283	25	152	152	80.1
106		L-3	305	252	152	1016	4.03	28.0	0.0336	310	25	152	152	53.4
107		L-4	305	252	152	1270	5.04	25.8	0.0336	303	25	152	152	51.2
108		L-6	305	252	152	1778	7.06	30.6	0.0336	317	25	152	152	46.9
109		L-1R	305	252	152	508	2.02	21.0	0.0336	303	25	152	152	164.6
110		L-2R	305	252	152	762	3.02	21.5	0.0336	310	25	152	152	74.7
111		L-2aR	305	252	152	762	3.02	36.7	0.0336	283	25	152	152	92.5
112		L-3R	305	252	152	1016	4.03	28.0	0.0336	310	25	152	152	62.0
113		A-1	305	252	152	508	2.02	28.1	0.0098	459	25	305	305	73.4
114		A-2	305	254	152	762	3.00	31.5	0.0098	469	25	305	305	41.8
115		A-3	305	254	152	1016	4.00	19.4	0.0098	452	25	305	305	34.2
116		A-4	305	254	152	1270	5.00	26.8	0.0098	459	25	305	305	35.1
117		A-12	305	254	152	762	3.00	26.1	0.0333	314	25	305	305	58.9
118		A-13	305	254	152	1016	4.00	22.1	0.0333	393	25	305	305	46.9
119		A-14	305	254	152	1270	5.00	27.5	0.0333	364	25	305	305	54.7
120		A-15	305	254	152	1524	6.00	25.0	0.0333	332	25	305	305	49.4
121		D-15	305	252	152	559	2.22	26.6	0.0101	461	25	152	152	73.5
122		D-14	305	252	152	559	2.22	32.1	0.0101	462	25	152	152	76.9
123		D-16	305	252	152	559	2.22	39.7	0.0101	586	25	152	152	90.5

161

#	Author	Specimen	h (mm)	d (mm)	b (mm)	a (mm)	a/d	f_{ck} (MPa)	ρ	f_{yk} (MPa)	d_a (mm)	Top plate width (mm)	Bottom plate width (mm)	$V_{exp.}$ (kN)
124		D-13	305	252	152	699	2.77	19.2	0.0101	464	25	152	152	49.1
125		D-17	305	252	152	699	2.77	41.2	0.0101	586	25	152	152	59.7
126	Bower & Viest [137]	IA-1a	356	306	152	762	2.49	22.8	0.0159	324	6	102	102	59.2
127		IA-1b	356	314	152	762	2.43	30.0	0.0159	323	6	102	102	76.9
128		IIB-1	356	318	152	1067	3.36	24.7	0.0153	323	6	102	102	45.4
129		IIB-2	356	311	152	1219	3.92	20.9	0.0156	320	6	102	102	40.7
130		IIB-3	356	308	152	1372	4.45	19.7	0.0158	321	6	102	102	36.9
131		IA-2a	356	311	152	1016	3.27	24.8	0.0159	308	25	102	102	73.1
132		IA-2b	356	311	152	1016	3.27	24.4	0.0159	319	25	102	102	39.7
133		IA-3a	356	311	152	1270	4.08	27.7	0.0159	326	25	102	102	52.0
134		IA-3b	356	305	152	1270	4.16	24.5	0.0159	323	25	102	102	60.5
135		IA-4a	356	305	152	1524	5.00	22.8	0.0159	321	25	102	102	51.0
136		IA-4b	356	311	152	1524	4.90	21.9	0.0159	319	25	102	102	46.0
137		IA-5a	356	308	152	1270	4.12	23.9	0.0159	317	25	102	102	41.4
138		IA-5b	356	308	152	1270	4.12	21.5	0.0159	323	25	102	102	49.4
139		IA-6a	356	305	152	1016	3.33	21.5	0.0159	308	25	102	102	41.9
140		IA-6b	356	305	152	1016	3.33	24.3	0.0159	323	25	102	102	66.0
141		IA-7b	356	305	152	762	2.50	22.6	0.0159	317	25	102	102	57.0
142		IA-8a	356	311	152	1100	3.54	24.1	0.0159	307	25	102	102	49.4
143		IA-8b	356	305	152	1100	3.61	21.5	0.0159	319	25	102	102	57.1
144		IB-1	356	305	152	813	2.67	22.2	0.0159	326	25	102	102	56.7
145		IB-2	356	305	152	1016	3.33	21.2	0.0159	330	25	102	102	65.2
146		IB-3	356	305	152	1016	3.33	22.8	0.0159	319	25	102	102	60.2
147		IIa-1a	356	308	152	914	2.97	22.8	0.0159	319	25	102	102	61.7
148		IIa-1b	356	318	152	914	2.87	25.5	0.0159	324	25	102	102	93.7
149		IIa-2	356	312	152	1219	3.91	21.6	0.0159	319	25	102	102	67.3
150		IIA-3	356	312	152	1524	4.88	21.7	0.0159	320	25	102	102	51.5
151		IIA-4a	356	305	152	1829	6.00	20.0	0.0159	319	25	102	102	37.5
152		IIA-4b	356	292	152	1829	6.26	22.9	0.0159	323	25	102	102	42.5
153		IIA-5	356	292	152	2743	9.39	23.6	0.0159	323	25	102	102	40.8
154		IIA-8	356	292	152	2134	7.31	18.4	0.0159	307	25	102	102	36.4
155		IIA-9	356	292	152	2438	8.35	21.2	0.0159	328	25	102	102	42.3

#	Author	Specimen	h (mm)	d (mm)	b (mm)	a (mm)	a/d	f_{ck} (MPa)	ρ	f_{yk} (MPa)	d_a (mm)	Top plate width (mm)	Bottom plate width (mm)	$V_{exp.}$ (kN)
156	Leonhardt & Walther [53]	P2	162	142	503	490	3.45	13.4	0.0095	427	30	45	45	76.2
157		P3	162	142	502	490	3.45	13.4	0.0111	427	30	45	45	81.1
158		P4	165	145	500	490	3.38	14.5	0.0140	427	30	45	45	100.8
159		P5	165	145	503	490	3.38	13.4	0.0186	427	30	45	45	100.8
160		P8	168	148	502	490	3.31	24.9	0.0091	427	30	45	45	88.0
161		P9	166	146	500	490	3.36	24.9	0.0186	427	30	45	45	105.8
162		P10	122	102	503	350	3.43	12.4	0.0110	427	30	45	45	59.3
163		P11	203	183	498	630	3.44	13.7	0.0111	427	30	45	45	101.2
164		P12	162	142	501	350	2.46	12.6	0.0095	427	30	45	45	100.5
165		4L	320	270	190	670	2.48	32.4	0.0207	465	30	100	100	81.6
166		4R	320	270	190	670	2.48	32.4	0.0207	465	30	100	100	87.0
167		5I	320	270	190	810	3.00	32.4	0.0207	465	30	100	100	60.3
168		5r	320	270	190	810	3.00	32.4	0.0207	465	30	100	100	76.5
169		6I	320	270	190	1100	4.07	32.4	0.0207	465	30	100	100	60.8
170		6r	320	270	190	1100	4.07	32.4	0.0207	465	30	100	100	68.2
171		7-1	320	278	190	1390	5.00	33.9	0.0201	465	30	100	100	62.3
172		7-2	320	278	190	1390	5.00	33.9	0.0201	465	30	100	100	68.2
173		8-1	320	278	190	1668	6.00	34.0	0.0201	465	30	100	100	65.7
174		8-2	320	274	190	1644	6.00	34.0	0.0204	465	30	100	100	65.7
175		9-1	323	273	190	1890	6.92	34.9	0.0205	465	30	100	100	58.9
176		9-2	323	273	190	1890	6.92	36.0	0.0205	465	30	100	100	58.9
177		D1/1	80	70	50	210	3.00	35.1	0.0171	451	15	30	30	7.3
178		D1/2	80	70	50	210	3.00	35.1	0.0171	451	15	30	30	7.2
179		D2/1	160	140	100	420	3.00	31.3	0.0162	427	15	50	50	21.2
180		D2/2	160	140	100	420	3.00	31.3	0.0162	427	15	50	50	23.2
181		D3/1	240	210	150	630	3.00	33.8	0.0162	413	15	75	75	46.4
182		D3/2I	240	210	150	630	3.00	33.8	0.0162	413	15	75	75	42.9
183		D3/2r	240	210	150	630	3.00	33.8	0.0162	413	15	75	75	42.9
184		D4/1	320	280	200	840	3.00	34.6	0.0168	439	15	100	100	74.1
185		D4/2I	320	280	200	840	3.00	34.6	0.0168	439	15	100	100	71.3
186		D4/2r	320	280	200	840	3.00	34.6	0.0168	439	15	100	100	71.3
187		C1	180	150	100	450	3.00	38.3	0.0129	425	30	60	60	21.6

#	Author	Specimen	h (mm)	d (mm)	b (mm)	a (mm)	a/d	f_{ck} (MPa)	ρ	f_{yk} (MPa)	d_a (mm)	Top plate width (mm)	Bottom plate width (mm)	$V_{exp.}$ (kN)
188		C2	330	300	150	900	3.00	38.3	0.0128	425	30	80	80	64.7
189		C3	500	450	200	1350	3.00	38.3	0.0128	425	30	120	120	101.5
190		C4	670	600	225	1800	3.00	38.3	0.0128	425	30	120	120	152.1
191		EA1	320	270	190	750	2.78	22.2	0.0182	439	30	100	100	58.4
192		EA2	320	270	190	750	2.78	22.2	0.0178	490	30	100	100	74.6
193		E6	320	270	190	750	2.78	27.6	0.0247	426	30	100	100	91.2
194		13/1	323	273	190	625	2.29	37.3	0.0205	465	30	100	100	106.6
195		13/2	322	272	189	625	2.30	37.3	0.0207	465	30	100	100	106.7
196		14/1	323	273	190	750	2.75	36.2	0.0205	465	30	100	100	85.9
197		14/2	323	273	190	750	2.75	36.2	0.0205	465	30	100	100	86.3
198		15/1	322	272	190	1000	3.68	38.3	0.0205	465	30	100	100	80.9
199		15/2	323	273	189	1000	3.66	38.3	0.0206	465	30	100	100	86.0
200		16/1	323	273	190	1250	4.58	37.8	0.0205	465	30	100	100	84.2
201		16/2	324	274	189	1250	4.56	37.8	0.0205	465	30	100	100	83.7
202		17/2	324	274	189	1500	5.47	35.5	0.0205	465	30	100	100	77.6
203	de Cassio [138]	32-8E	102	83	321	332	4.00	23.2	0.0187	418	12	17	17	32.8
204		32-8F	102	83	319	330	3.98	21.2	0.0187	418	12	17	17	33.2
205		48-8F	102	83	479	331	3.99	27.9	0.0198	408	12	17	17	60.7
206		48-8E	102	82	479	329	4.01	26.7	0.0199	459	12	16	16	51
207		64-8F	102	83	639	332	4.00	30.4	0.0188	373	12	17	17	71.3
208		64-8E	102	87	639	347	3.99	31.2	0.0192	373	12	17	17	67.7
209		32-8D	102	84	320	336	4.00	21.2	0.0185	367	12	17	17	34.1
210		32-8C	102	82	319	326	3.98	23.2	0.0191	367	12	16	16	34.9
211		48-8D	102	84	479	336	4.00	26.6	0.0194	383	12	17	17	65
212		48-8C	102	83	483	332	4.00	25.2	0.0195	404	12	17	17	58.7
213		64-8C	102	82	640	328	4.00	28.5	0.0190	383	12	16	16	85.2
214		64-8D	102	81	640	324	4.00	28.5	0.0195	383	12	16	16	81.6
215		32-8A	102	81	322	324	4.00	23.7	0.0190	383	12	16	16	37.1
216		32-8B	102	81	317	325	4.01	23.7	0.0185	383	12	16	16	38
217		B32-8A	102	80	318	318	3.98	26.8	0.0281	403	12	16	16	49
218		B32-8B	102	80	318	320	4.00	26.8	0.0280	432	12	16	16	51.9
219		C32-8A	102	80	319	320	4.00	26.6	0.0195	394	12	16	16	41.2

#	Author	Specimen	h (mm)	d (mm)	b (mm)	a (mm)	a/d	f_{ck} (MPa)	ρ	f_{yk} (MPa)	d_a (mm)	Top plate width (mm)	Bottom plate width (mm)	$V_{exp.}$ (kN)
220		C32-8B	102	80	319	318	3.98	26.6	0.0195	394	12	16	16	42.2
221		48-8B	102	82	505	326	3.98	27.8	0.0198	399	12	16	16	65.3
222		48-8A	102	81	479	324	4.00	27.8	0.0201	410	12	16	16	62
223		64-8A	102	82	640	327	3.99	28.5	0.0190	397	12	16	16	87
224		64-8B	102	81	636	322	3.98	29.2	0.0194	440	12	16	16	85.5
225		A2.1-16.8A	203	168	21	450	2.68	34.6	0.0200	410	12	34	34	4.7
226		A2.1-16.8B	203	168	21	450	2.68	34.6	0.0200	410	12	34	34	4.7
227		A3-12A	152	122	30	325	2.66	28.5	0.0198	394	12	24	24	4.3
228		A3-12B	152	120	30	320	2.67	29	0.0197	394	12	24	24	4.2
229		A3-12C	152	122	30	325	2.66	28.5	0.0197	396	12	24	24	4.4
230		A4.25-17A	203	170	42	680	4.00	13.7	0.0200	408	12	34	34	5.3
231		A4.25-17B	203	172	42	688	4.00	13.7	0.0194	408	12	34	34	6
232		B3-12A	152	120	29	480	4.00	29	0.0200	394	12	24	24	4.8
233		B3-12B	152	120	30	480	4.00	29	0.0197	394	12	24	24	4
234		B4.25-17A	203	170	42	680	4.00	13.4	0.0200	408	12	34	34	5.5
235		B4.25-17B	203	170	42	680	4.00	13.7	0.0194	408	12	34	34	5.6
236		C4.25-17A	203	170	42	454	2.67	13.7	0.0196	421	12	34	34	6.7
237		C4.25-17B	203	170	42	454	2.67	13.7	0.0196	421	12	34	34	5.9
238		A4.7-14.7A	178	147	46	393	2.67	28.3	0.0208	436	12	29	29	9.6
239		A4.7-14.7B	178	147	46	393	2.67	28.3	0.0208	436	12	29	29	9.8
240		A4.25-8.5A	102	86	42	230	2.67	29.7	0.0197	397	12	17	17	5.6
241		A4.25-8.5B	102	86	42	231	2.69	29.7	0.0197	397	12	17	17	5.8
242		A4.25-8.5C	102	86	42	230	2.67	29.7	0.0197	397	12	17	17	5.8
243		A6-12A	152	121	60	323	2.67	29.7	0.0194	390	12	24	24	10.6
244		A6-12B	152	122	60	326	2.67	29.7	0.0192	390	12	24	24	10.5
245		A6-12C	152	120	60	321	2.68	29.7	0.0194	390	12	24	24	10.4
246		A8.5-17A	203	171	87	456	2.67	35	0.0192	392	12	34	34	23.5

#	Author	Specimen	h (mm)	d (mm)	b (mm)	a (mm)	a/d	f_{ck} (MPa)	ρ	f_{yk} (MPa)	d_a (mm)	Top plate width (mm)	Bottom plate width (mm)	$V_{exp.}$ (kN)
247		A8.5-17B	203	170	85	454	2.67	35	0.0196	392	12	34	34	23.9
248		A8.5-17C	203	170	86	454	2.67	33.9	0.0195	390	12	34	34	21
249		A10.4-13.9A	178	139	103	372	2.68	23.9	0.0197	440	12	28	28	21.5
250		A10.4-13.9B	178	140	103	374	2.67	23.9	0.0196	440	12	28	28	23.8
251		A12-12A	152	121	120	323	2.67	23.7	0.0195	402	12	24	24	27
252		A12-12B	152	122	120	326	2.67	29.2	0.0196	402	12	24	24	26
253		A12-12C	152	121	120	323	2.67	31	0.0195	402	12	24	24	23.8
254		A12-12D	152	120	120	320	2.67	31	0.0197	402	12	24	24	23.7
255		A14.7-9.8A	127	99	147	264	2.67	26.5	0.0196	450	12	20	20	22.8
256		A14.7-9.8B	127	99	146	263	2.66	26.5	0.0197	450	12	20	20	25.8
257		B12-6A	76	62	120	165	2.66	26	0.0288	434	12	12	12	16.4
258		B12-6B	76	63	120	168	2.67	26	0.0284	434	12	13	13	17.9
259		A12-6A	76	60	121	161	2.68	30	0.0144	392	12	12	12	17
260		A12-6B	76	62	120	165	2.66	30	0.0192	392	12	12	12	15.5
261		A12-6C	76	62	122	165	2.66	30	0.0190	392	12	12	12	15.7
262		A12-6D	76	61	120	163	2.67	24.1	0.0194	404	12	12	12	16.6
263		A12-6E	76	61	120	164	2.69	30.3	0.0193	404	12	12	12	18.6
264		D29.4-9.8A	127	100	290	400	4.00	24.6	0.0290	382	12	20	20	37.8
265		D29.4-9.8B	127	100	294	400	4.00	24.6	0.0290	382	12	20	20	34.3
266		D29.4-9.8C	127	98	293	392	4.00	24.6	0.0246	422	12	20	20	42.9
267		D29.4-9.8D	127	99	294	396	4.00	24.6	0.0292	422	12	20	20	47.5
268		A29.4-9.8A	127	99	293	264	2.67	27.2	0.0196	426	12	20	20	50.1
269		A29.4-9.8B	127	99	293	264	2.67	27.2	0.0196	426	12	20	20	52.5
270		C29.4-9.8A	127	99	294	264	2.67	14.9	0.0195	372	12	20	20	36.3
271		C29.4-9.8B	127	99	294	264	2.67	18	0.0195	372	12	20	20	43.4
272		B29.4-9.8A	127	98	294	392	4.00	25.6	0.0197	378	12	20	20	41.8
273		B29.4-9.8B	127	98	294	392	4.00	23.2	0.0197	378	12	20	20	45.9

#	Author	Specimen	h (mm)	d (mm)	b (mm)	a (mm)	a/d	f_{ck} (MPa)	ρ	f_{yk} (MPa)	d_a (mm)	Top plate width (mm)	Bottom plate width (mm)	$V_{exp.}$ (kN)
274		A.8.5-34A	406	341	85	910	2.67	28	0.0186	408	12	68	68	28.6
275		A.8.5-34B	406	340	87	909	2.67	25.8	0.0180	416	12	68	68	27.6
276		A50-25A	305	253	501	675	2.67	34.5	0.0181	399	12	51	51	188.7
277		A50-25B	305	252	502	674	2.67	34.1	0.0185	394	12	50	50	171.2
278	Ruesch et al. [139]	X	134	111	90	400	3.60	23.0	0.0265	481	30	10	10	14.6
279		Y	229	199	120	717	3.60	23.0	0.0265	407	30	10	10	30.1
280		Z	302	262	180	947	3.61	24.2	0.0264	412	30	10	10	54.7
281	Bresler & Scordelis [140]	0A-1	556	461	310	1753	3.80	22.6	0.0181	555	19	127	127	166.8
282		0A-2	561	466	305	2210	4.74	23.7	0.0227	555	19	127	127	177.9
283		0A-3	556	462	307	3124	6.76	37.6	0.0273	552	19	127	127	189.0
284	Mathey & Watstein [111]	IIIa-17	457	403	203	1524	3.78	29.2	0.0254	505	25	89	89	88.1
285		IIIa-18	457	403	203	1524	3.78	25.2	0.0254	505	25	89	89	80.7
286		Va-19	457	403	203	1524	3.78	23.5	0.0093	694	25	89	89	63.3
287		Va-20	457	403	203	1524	3.78	25.6	0.0093	694	25	89	89	65.9
288		VIb-21	457	403	203	1143	2.84	26.1	0.0084	707	25	89	89	71.4
289		VIb-22	457	403	203	1143	2.84	25.8	0.0084	707	25	89	89	62.4
290		VIb-23	457	403	203	1143	2.84	30.6	0.0084	707	25	89	89	75.1
291		VIa-24	457	403	203	1524	3.78	26.3	0.0047	696	25	89	89	54.5
292		VIa-25	457	403	203	1524	3.78	25.8	0.0047	696	25	89	89	49.9
293	Krefeld & Thurston [113]	II-4A3	457	390	203	915	2.35	30.6	0.0206	400	25	178	178	109.9
294		II-5A3	457	390	203	915	2.35	29.9	0.0309	400	25	178	178	170.4
295		II-11A2	381	314	152	915	2.91	30.2	0.0341	400	25	178	178	73.4
296		II-12A2	305	238	152	914	3.84	30.1	0.0450	400	25	178	178	64.1
297		III-18A2	381	316	152	915	2.90	19.3	0.0268	370	25	178	178	63.2
298		III-18B2	381	316	152	915	2.90	19.9	0.0268	370	25	178	178	72.1
299		III-18C2	381	316	152	915	2.90	22.6	0.0268	370	25	178	178	73.4
300		III-18D2	381	316	152	915	2.90	22.1	0.0268	370	25	178	178	60.0
301		IV-13A2	381	319	152	914	2.87	19.9	0.0080	379	25	178	178	48.5
302		IV-14A2	305	243	152	914	3.76	20.7	0.0105	379	25	178	178	35.1
303		IV-15A2	381	316	152	915	2.90	20.1	0.0134	370	25	178	178	45.8
304		IV-15B2	381	316	152	915	2.90	20.7	0.0134	370	25	178	178	52.0
305		IV-16A2	305	240	152	914	3.81	22.2	0.0177	370	25	178	178	41.8

167

#	Author	Specimen	h (mm)	d (mm)	b (mm)	a (mm)	a/d	f_{ck} (MPa)	ρ	f_{yk} (MPa)	d_a (mm)	Top plate width (mm)	Bottom plate width (mm)	$V_{exp.}$ (kN)
306		IV-17A2	305	243	152	914	3.76	22.0	0.0209	379	25	178	178	44.0
307		IV-18E2	381	316	152	915	2.90	19.8	0.0268	370	25	178	178	81.8
308		IV-19A2	305	240	152	914	3.81	20.6	0.0353	370	25	178	178	46.3
309		IV-20A2	305	238	152	914	3.84	21.0	0.0452	400	25	178	178	50.7
310		IV-21A2	305	238	203	914	3.84	19.9	0.0501	400	25	178	178	76.5
311		V-2AC	305	254	152	1219	4.80	23.0	0.0132	394	25	178	178	37.8
312		V-3AC	305	256	152	1219	4.76	20.8	0.0199	379	25	178	178	44.0
313		V-4AC	305	254	152	1219	4.80	16.5	0.0263	394	25	178	178	37.8
314		V-5AC	305	252	152	1219	4.84	18.3	0.0335	370	25	178	178	41.8
315		V-6AC	305	250	152	1220	4.88	22.8	0.0430	400	25	178	178	53.4
316		V-3CC	305	256	152	1523	5.95	20.5	0.0199	379	25	178	178	35.6
317		V-4CC	305	254	152	1524	6.00	20.6	0.0263	394	25	178	178	40.0
318		V-5CC	305	252	152	1524	6.05	20.3	0.0335	370	25	178	178	44.5
319		V-6CC	305	250	152	1524	6.10	20.6	0.0430	400	25	178	178	44.5
320		V-4EC	305	254	152	1829	7.20	21.2	0.0263	394	25	178	178	41.8
321		V-5GC	305	252	152	1828	7.25	19.5	0.0335	379	25	178	178	39.6
322		V-6EC	305	250	152	1828	7.31	19.1	0.0430	400	25	178	178	42.3
323		V-4GC	305	254	152	2134	8.40	21.0	0.0263	394	25	178	178	36.9
324		V-5GC	305	252	152	2133	8.46	21.9	0.0335	370	25	178	178	41.8
325		V-6GC	305	250	152	2133	8.53	21.4	0.0430	400	25	178	178	40.5
326		VII-6C	305	252	152	914	3.63	20.1	0.0335	370	25	178	178	51.2
327		VIII-3AAC	305	256	152	915	3.57	34.6	0.0199	379	25	178	178	55.6
328		VIII-4AAC	305	254	152	914	3.60	29.2	0.0263	394	25	178	178	57.8
329		VIII-5AAC	305	252	152	914	3.63	32.8	0.0335	370	25	178	178	56.9
330		VIII-6AAC	305	250	152	914	3.66	34.4	0.0430	400	25	178	178	60.0
331		VIII-3AC	305	256	152	1219	4.76	31.9	0.0199	379	25	178	178	53.4
332		VIII-4AC	305	254	152	1219	4.80	30.5	0.0263	394	25	178	178	53.8
333		VIII-5AC	305	252	152	1219	4.84	32.8	0.0335	370	25	178	178	54.3
334		VIII-6AC	305	250	152	1220	4.88	34.1	0.0430	400	25	178	178	59.2
335		VIII-4CC	305	254	152	1524	6.00	38.4	0.0263	394	25	178	178	52.5
336		VIII-5CC	305	252	152	1524	6.05	37.4	0.0335	370	25	178	178	57.4

#	Author	Specimen	h (mm)	d (mm)	b (mm)	a (mm)	a/d	f_{ck} (MPa)	ρ	f_{yk} (MPa)	d_a (mm)	Top plate width (mm)	Bottom plate width (mm)	$V_{exp.}$ (kN)
337		VIII-6CC	305	250	152	1524	6.10	38.4	0.0430	400	25	178	178	63.2
338		VIII-5EC	305	252	152	1828	7.25	37.4	0.0335	370	25	178	178	53.4
339		VIII-6EC	305	250	152	1828	7.31	33.8	0.0430	400	25	178	178	48.9
340		IX-3AAC	305	256	152	915	3.57	12.6	0.0199	379	25	178	178	40.5
341		IX-4AAC	305	254	152	914	3.60	12.9	0.0263	394	25	178	178	42.7
342		IX-5AAC	305	252	152	914	3.63	15.4	0.0335	370	25	178	178	50.3
343		IX-6AAC	305	250	152	914	3.66	13.4	0.0430	400	25	178	178	62.3
344		IX-3AC	305	256	152	1219	4.76	13.7	0.0199	379	25	178	178	36.9
345		IX-4AC	305	254	152	1219	4.80	12.9	0.0263	394	25	178	178	40.0
346		IX-5AC	305	252	152	1219	4.84	15.4	0.0335	370	25	178	178	43.6
347		IX-6AC	305	250	152	1220	4.88	12.4	0.0430	400	25	178	178	40.9
348		IX-3CC	305	256	152	1523	5.95	12.2	0.0199	379	25	178	178	31.1
349		IX-4CC	305	254	152	1524	6.00	17.1	0.0263	394	25	178	178	35.1
350		IX-5CC	305	252	152	1524	6.05	14.7	0.0335	370	25	178	178	34.2
351		IX-6CC	305	250	152	1524	6.10	13.7	0.0430	400	25	178	178	39.6
352		X-*-C	533	483	203	1525	3.16	16.8	0.0156	394	25	178	178	84.5
353		XI-*-PCa	305	250	152	1828	7.31	36.3	0.0430	400	25	178	178	53.4
354		XI-*-PCb	305	250	152	1828	7.31	36.3	0.0430	400	25	178	178	53.4
355		s-I-*-OCa	305	254	152	1524	6.00	35.7	0.0263	394	25	178	178	48.5
356		s-I-*-OCb	305	254	152	1524	6.00	39.0	0.0263	394	25	178	178	52.5
357		s-II-*-OCa	508	456	254	1830	4.01	38.3	0.0222	370	25	178	178	146.8
358		s-II-*-OCb	508	456	254	1830	4.01	38.3	0.0222	370	25	178	178	133.4
359	Kani [20]	25	305	271	152	543	2.00	25	0.0187	396	19	152	152	104.1
360		26	305	271	152	543	2.00	27	0.0187	396	19	152	152	78.1
361		27	305	271	152	678	2.50	30	0.0187	396	19	152	152	51.4
362		28	305	271	152	678	2.50	29	0.0187	396	19	152	152	54.3
363		29	305	271	152	1221	4.51	25	0.0187	350	19	152	152	42.9
364		30	305	271	152	1221	4.51	25	0.0187	350	19	152	152	46.3
365		35	305	269	155	953	3.54	26	0.0182	491	19	152	152	44.9
366		36	305	273	153	953	3.49	26	0.0182	491	19	152	152	51.6
367		40	152	140	152	747	5.35	26.4	0.0259	388	19	152	152	32.0

169

#	Author	Specimen	h (mm)	d (mm)	b (mm)	a (mm)	a/d	f_{ck} (MPa)	ρ	f_{yk} (MPa)	d_a (mm)	Top plate width (mm)	Bottom plate width (mm)	$V_{exp.}$ (kN)
368		41	152	141	152	340	2.41	27.2	0.0261	381	19	152	152	51.4
369		43	152	137	151	813	5.93	28.0	0.0273	392	19	152	152	29.1
370		45	152	133	151	272	2.05	25.5	0.0283	392	19	152	152	64.6
371		47	152	132	151	678	5.13	45.4	0.0284	392	19	152	152	28.2
372		48	152	133	151	678	5.09	24.8	0.0282	392	19	152	152	27.1
373		52	152	138	152	544	3.93	24.8	0.0269	392	19	152	152	28.9
374		55	152	135	150	406	3.02	25.1	0.0280	392	19	152	152	32.6
375		56	152	137	153	476	3.46	27.2	0.0267	403	19	152	152	28.0
376		57	152	139	153	747	5.39	26.4	0.0261	375	19	152	152	31.6
377		58	152	138	152	476	3.44	27.2	0.0266	417	19	152	152	28.9
378		59	152	140	154	373	2.67	26.6	0.0263	392	19	152	152	50.2
379		60	152	139	155	407	2.93	26.8	0.0264	392	19	152	152	39.3
380		81	305	274	153	1628	5.93	27.5	0.0276	343	19	152	152	51.2
381		83	305	271	156	814	3.00	27.4	0.0274	343	19	152	152	64.9
382		84	305	271	151	1085	4.00	27.4	0.0284	342	19	152	152	55.4
383		91	305	269	154	1628	6.06	27.4	0.0270	364	19	64	64	51.0
384		93	305	273	155	1763	6.46	30.3	0.0266	372	19	152	152	53.8
385		95	305	275	153	678	2.47	25.3	0.0275	338	19	152	152	72.7
386		96	305	275	153	1085	3.94	25.3	0.0276	335	19	64	64	56.3
387		97	305	276	152	815	2.95	27.2	0.0268	366	19	64	64	62.5
388		98	305	275	153	679	2.47	26.2	0.0268	366	19	152	152	76.3
389		99	305	272	152	679	2.50	26.2	0.0273	366	19	152	152	77.2
390		100	305	270	153	544	2.02	27.2	0.0275	366	19	64	64	111.9
391		61	610	542	156	1085	2.00	26.8	0.0255	349	19	76	76	163.2
392		63	610	543	154	2170	4.00	26.2	0.0277	352	19	64	64	93.2
393		64	610	541	156	4340	8.03	25.7	0.0275	352	19	64	64	79.0
394		65	610	552	150	3899	7.06	27.0	0.0282	374	19	152	152	112.3
395		66	610	541	156	3255	6.01	26.4	0.0275	352	19	64	64	90.7
396		71	610	544	155	1628	2.99	27.4	0.0266	373	19	229	229	102.1
397		74	610	523	152	1631	3.12	27.2	0.0284	366	19	152	152	107.6
398		75	610	524	152	1631	3.11	27.3	0.0284	367	19	152	152	107.9
399		76	610	518	152	1359	2.63	30.8	0.0287	372	19	64	64	114.8

#	Author	Specimen	h (mm)	d (mm)	b (mm)	a (mm)	a/d	f_{ck} (MPa)	ρ	f_{yk} (MPa)	d_a (mm)	Top plate width (mm)	Bottom plate width (mm)	$V_{exp.}$ (kN)
400		79	610	556	153	3805	6.84	26.1	0.0272	381	19	152	152	83.6
401		3042	1219	1095	154	2737	2.50	26.4	0.0270	375	19	229	229	236.9
402		3043	1219	1092	154	3277	3.00	27.0	0.0271	376	19	229	229	165.0
403		3044	1219	1097	152	4364	3.98	29.5	0.0272	376	19	229	229	159.0
404		3045	1219	1092	155	5461	5.00	28.3	0.0270	381	19	229	229	152.3
405		3046	1219	1097	155	8418	7.67	26.7	0.0270	360	19	229	229	154.1
406		3047	1219	1095	155	9495	8.67	26.7	0.0269	376	19	229	229	147.0
407		3061	1202	1091	154	3378	3.10	27.4	0.0080	345	19	152	152	97.5
408		102	305	269	153	543	2.02	25.3	0.0076	423	19	152	152	48.8
409		103	305	274	155	814	2.97	29.4	0.0074	423	19	152	152	38.8
410		104	305	269	154	1072	3.99	25.3	0.0076	423	19	152	152	33.6
411		105	305	272	152	679	2.50	26.2	0.0077	383	19	152	152	41.5
412		106	305	268	154	678	2.53	28.8	0.0076	422	19	152	152	44.6
413		107	305	267	154	1356	5.08	26.6	0.0076	422	19	152	152	25.7
414		111	305	272	154	678	2.49	27.0	0.0076	368	19	152	152	43.3
415		112	305	273	153	678	2.48	27.0	0.0076	368	19	152	152	39.4
416		114	305	270	153	544	2.01	25.5	0.0080	486	19	152	152	61.4
417		115	305	272	152	679	2.50	26.2	0.0077	383	19	152	152	45.3
418		116	305	271	152	815	3.01	26.4	0.0078	384	19	152	152	39.3
419		121	305	272	152	815	3.00	20.3	0.0185	330	19	152	152	49.0
420		122	305	276	150	1087	3.94	19.9	0.0184	343	19	152	152	38.8
421		123	305	271	155	1085	4.00	15.4	0.0179	346	19	152	152	37.8
422		124	305	271	154	1356	5.00	15.4	0.0180	345	19	152	152	32.0
423		126	305	272	155	814	2.99	16.3	0.0178	346	19	152	152	42.7
424		130	305	276	153	1467	5.32	18.0	0.0179	346	19	152	152	40.1
425		131	305	274	151	679	2.48	18.1	0.0185	401	19	152	152	49.6
426		132	305	271	154	679	2.51	18.6	0.0181	417	19	152	152	49.8
427		133	305	273	154	1359	4.98	19.9	0.0181	508	19	152	152	38.5
428		141	305	270	151	544	2.01	19.3	0.0081	382	19	152	152	48.7
429		143	305	274	154	1085	3.96	17.7	0.0074	428	19	152	152	30.2
430		147	305	287	152	678	2.36	16.8	0.0070	417	19	152	152	42.3
431		149	305	272	153	678	2.49	18.0	0.0078	380	19	152	152	43.7

#	Author	Specimen	h (mm)	d (mm)	b (mm)	a (mm)	a/d	f_ck (MPa)	ρ	f_yk (MPa)	d_a (mm)	Top plate width (mm)	Bottom plate width (mm)	V_exp. (kN)
432		150	305	273	153	678	2.48	18.0	0.0077	380	19	152	152	46.2
433		151	305	273	154	679	2.49	19.3	0.0078	382	19	152	152	35.6
434		152	305	270	149	815	3.02	19.7	0.0079	384	19	152	152	32.5
435		153	305	273	152	815	2.99	19.7	0.0076	384	19	152	152	32.8
436		163	305	273	156	678	2.48	35.4	0.0076	378	19	152	152	40.5
437		164	305	271	156	1085	4.00	33.8	0.0073	412	19	152	152	35.8
438		166	305	271	152	815	3.01	35.4	0.0078	377	19	152	152	40.3
439		179	305	264	153	678	2.57	32.3	0.0053	400	19	152	152	33.6
440		182	305	268	155	1356	5.06	33.9	0.0180	386	19	152	152	48.8
441		186	305	272	155	1085	3.99	35.1	0.0178	394	19	152	152	55.4
442		191	305	275	154	815	2.96	34.0	0.0180	497	19	152	152	53.1
443		193	305	278	153	678	2.44	34.6	0.0180	352	19	152	152	56.7
444		194	305	278	154	814	2.93	34.6	0.0180	352	19	152	152	51.2
445		195	305	275	153	1085	3.95	34.6	0.0182	352	19	152	152	47.3
446		196	305	269	154	1359	5.05	36.2	0.0185	380	19	152	152	51.2
447		197	305	274	150	679	2.48	36.0	0.0184	376	19	152	152	60.1
448		202	305	273	154	1628	5.96	33.9	0.0268	377	19	152	152	49.9
449		206	305	270	152	679	2.51	35.2	0.0273	381	19	152	152	100.3
450		208	305	275	157	1221	4.44	35.7	0.0268	379	19	152	152	60.1
451		210	305	272	154	679	2.50	35.2	0.0267	381	19	152	152	79.0
452		211	305	270	153	815	3.02	35.2	0.0273	381	19	152	152	57.2
453		212	305	273	155	815	2.99	35.2	0.0266	381	19	152	152	60.5
454		213	305	276	154	1223	4.43	36.7	0.0266	381	19	152	152	57.4
455		214	305	272	153	679	2.50	36.0	0.0271	412	19	152	152	82.0
456		215	305	274	154	679	2.48	36.0	0.0267	412	19	152	152	88.1
457		246	305	274	153	952	3.47	27.6	0.0051	400	19	152	152	25.4
458		248	305	282	153	678	2.40	27.6	0.0049	400	19	152	152	37.2
459		266	305	272	153	673	2.47	18.1	0.0050	396	19	152	152	32.5
460		267	305	269	153	949	3.53	20.7	0.0052	400	19	152	152	24.5
461		268	305	275	153	816	2.97	20.1	0.0049	396	19	152	152	27.2
462		271	305	269	611	1631	6.06	27.0	0.0275	377	19	152	152	217.2
463		272	305	271	611	1359	5.01	27.0	0.0273	377	19	152	152	227.8

#	Author	Specimen	h (mm)	d (mm)	b (mm)	a (mm)	a/d	f_{ck} (MPa)	ρ	f_{yk} (MPa)	d_a (mm)	Top plate width (mm)	Bottom plate width (mm)	$V_{exp.}$ (kN)
464		273	305	271	612	1087	4.01	27.2	0.0272	377	19	152	152	206.2
465	Rajagopalan & Ferguson [141]	S-1	311	259	154	1016	3.92	36.6	0.0143	655	13	50	50	35.6
466		S-2	311	265	154	1016	3.83	33.1	0.0098	655	13	50	50	37.4
467		S-3	311	267	152	1118	4.19	29.0	0.0081	524	13	50	50	31.1
468		S-4	311	268	152	1118	4.17	33.1	0.0063	524	13	50	50	28.0
469		S-5	311	262	152	1118	4.27	27.9	0.0053	1779	13	50	50	33.6
470		S-6	311	267	151	1118	4.19	31.0	0.0035	1779	13	50	50	27.4
471		S-7	311	268	152	1118	4.17	28.6	0.0025	1779	13	50	50	30.0
472		S-9	311	262	152	1118	4.27	25.1	0.0053	1779	13	50	50	24.5
473		S-12	311	268	153	1118	4.17	29.7	0.0025	1779	13	50	50	24.6
474		S-13	311	265	152	1118	4.22	23.7	0.0173	655	13	50	50	40.0
475		S-14	349	269	151	1119	4.16	29.8	0.0063	524	13	50	50	25.0
476		S-15	311	269	761	1119	4.16	33.0	0.0063	524	13	50	50	150.8
477	Bhal [142]	B1	350	297	240	900	3.03	23.2	0.0126	434	30	59	59	70.7
478		B2	650	600	240	1800	3.00	29.6	0.0126	434	30	120	120	119.5
479		B3	950	900	240	2700	3.00	27.5	0.0126	434	30	180	180	166.8
480		B4	1250	1200	240	3600	3.00	25.2	0.0126	434	30	240	240	185.2
481		B5	650	600	240	1800	3.00	26.6	0.0063	434	30	120	120	106.2
482		B6	650	600	240	1800	3.00	24.7	0.0063	430	30	120	120	114.1
483		B7	950	900	240	2700	3.00	27.2	0.0063	434	30	180	180	139.8
484		B8	950	900	240	2700	3.00	27.7	0.0063	430	30	180	180	127.5
485	Taylor [143]	1A	406	370	203	1118	3.02	28.9	0.0103	350	10	10	10	61.8
486		2A	406	370	203	1118	3.02	33.2	0.0155	350	10	10	10	91.6
487		1B	406	370	203	1118	3.02	28.9	0.0103	350	10	10	10	75.6
488		2B	406	370	203	1118	3.02	33.2	0.0155	350	10	10	10	100.5
489		3B	406	370	203	1118	3.02	31.6	0.0103	350	10	10	10	76.1
490		5A	406	370	203	914	2.47	29.9	0.0103	350	10	10	10	80.5
491		5B	406	370	203	914	2.47	29.9	0.0103	350	10	10	10	80.5
492	Mattock [144]	1	305	254	152	762	3.00	17.1	0.0103	400	19	10	10	36.5
493		3	305	254	152	762	3.00	46.9	0.0103	400	19	10	10	54.7
494		10	305	254	152	762	3.00	18.6	0.0310	400	19	10	10	56.0
495		15	305	254	152	1372	5.40	25.9	0.0103	400	19	10	10	31.1

173

#	Author	Specimen	h (mm)	d (mm)	b (mm)	a (mm)	a/d	f_{ck} (MPa)	ρ	f_{yk} (MPa)	d_a (mm)	Top plate width (mm)	Bottom plate width (mm)	$V_{exp.}$ (kN)
496		18	305	254	152	1372	5.40	18.1	0.0207	400	19	10	10	35.6
497		22	305	254	152	1372	5.40	16.1	0.0310	400	19	10	10	40.0
498		24	305	254	152	1372	5.40	29.2	0.0310	400	19	10	10	52.5
499	Placas & Regan [145]	R1	305	272	152	914	3.36	26.2	0.0098	621	19	10	10	44.9
500		R2	305	272	152	914	3.36	26.2	0.0146	621	19	10	10	47.1
501		R3	305	272	152	914	3.36	24.8	0.0146	621	19	10	10	44.9
502		R7	305	272	152	914	3.36	28.1	0.0146	621	19	10	10	54.3
503		D2	305	272	152	914	3.36	30.3	0.0146	621	19	10	10	52.5
504	Taylor [21]	A1	1000	930	400	2800	3.01	28.7	0.0135	420	38	186	186	358.4
505		A2	1000	930	400	2800	3.01	25.1	0.0135	420	19	186	186	328.4
506		B1	500	465	200	1400	3.01	24.2	0.0135	420	38	93	93	104.3
507		B2	500	465	200	1400	3.01	22.0	0.0135	420	19	93	93	87.3
508		B3	500	465	200	1400	3.01	28.4	0.0135	420	9	93	93	85.3
509		C1	250	233	100	700	3.00	22.7	0.0135	420	19	47	47	22.5
510		C2	250	233	100	700	3.00	22.7	0.0135	420	9	47	47	24.0
511		C3	250	233	100	700	3.00	24.4	0.0135	420	9	47	47	27.5
512		C4	250	233	100	700	3.00	18.5	0.0135	420	9	47	47	22.5
513		C5	250	233	100	700	3.00	19.9	0.0135	420	9	47	47	27.0
514		C6	250	233	100	700	3.00	25.6	0.0135	420	2	47	47	27.5
515		D1	150	139	60	420	3.02	28.4	0.0135	420	2	28	28	11.6
516		D2	150	139	60	420	3.02	28.4	0.0135	420	2	28	28	12.1
517		D3	150	139	60	420	3.02	28.4	0.0135	420	2	28	28	10.6
518		D4	150	139	60	420	3.02	28.4	0.0135	420	2	28	28	11.4
519	Aster & Koch [146]	11	539	500	1000	1825	3.65	24.6	0.0046	535	30	100	100	267.4
520		16	794	750	1000	2750	3.67	30.4	0.0042	536	30	150	150	406.7
521		2	281	250	1000	920	3.68	26.9	0.0064	554	30	50	50	218.0
522		12	540	500	1000	1825	3.65	27.3	0.0065	535	30	100	100	330.2
523		3	289	250	1000	920	3.68	27.3	0.0091	535	30	50	50	222.5
524		8	544	500	1000	2750	5.50	31.1	0.0063	535	30	100	100	287.1
525		9	544	500	1000	2750	5.50	19.9	0.0063	535	30	100	100	260.6

#	Author	Specimen	h (mm)	d (mm)	b (mm)	a (mm)	a/d	f_{ck} (MPa)	ρ	f_{yk} (MPa)	d_a (mm)	Top plate width (mm)	Bottom plate width (mm)	$V_{exp.}$ (kN)
526		10	544	500	1000	2750	5.50	20.0	0.0063	535	30	100	100	261.6
527		17	794	750	1000	2750	3.67	28.7	0.0042	535	30	150	150	363.5
528	Chana [147]	2.1a	406	356	203	1068	3.00	49.3	0.0169	414	20	10	10	96.0
529		2.1b	406	356	203	1068	3.00	49.3	0.0169	414	20	10	10	97.1
530		2.2a	406	356	203	1068	3.00	41.6	0.0169	414	10	10	10	87.4
531		2.2b	406	356	203	1068	3.00	41.6	0.0169	414	10	10	10	94.4
532		2.3a	406	356	203	1068	3.00	45.2	0.0169	414	20	10	10	99.4
533		2.3b	406	356	203	1068	3.00	45.2	0.0169	414	20	10	10	96.4
534		3.1a	203	177	100	531	3.00	34.5	0.0174	414	10	10	10	23.8
535		3.1b	203	177	100	531	3.00	34.5	0.0174	414	10	10	10	23.9
536		3.2a	203	177	100	531	3.00	36.8	0.0174	414	10	10	10	24.5
537		3.2b	203	177	100	531	3.00	36.8	0.0174	414	10	10	10	25.5
538		3.3a	203	177	100	531	3.00	40.1	0.0174	414	10	10	10	26.5
539		3.3b	203	177	100	531	3.00	40.1	0.0174	414	10	10	10	23.2
540		D1	203	177	100	531	3.00	31.6	0.0174	414	10	10	10	22.1
541		D2	203	177	100	531	3.00	32.4	0.0174	414	10	10	10	23.4
542		D3	203	177	100	531	3.00	44.7	0.0174	414	10	10	10	21.4
543		4.1a	127	106	60	318	3.00	30.9	0.0172	414	5	10	10	9.8
544		4.1b	127	106	60	318	3.00	30.9	0.0172	414	5	10	10	8.7
545		4.2a	127	106	60	318	3.00	30.9	0.0172	414	5	10	10	9.0
546		4.2b	127	106	60	318	3.00	30.9	0.0172	414	5	10	10	9.7
547		4.3a	127	106	60	318	3.00	52.2	0.0172	414	5	10	10	11.7
548		4.3b	127	106	60	318	3.00	52.2	0.0172	414	5	10	10	12.4
549		4.4a	127	106	60	318	3.00	52.2	0.0172	414	5	10	10	9.6
550		4.4b	127	106	60	318	3.00	52.2	0.0172	414	5	10	10	10.5
551		5.1a	203	170	200	510	3.00	40.3	0.0180	414	10	10	10	47.8
552		5.1b	203	170	200	510	3.00	40.3	0.0180	414	10	10	10	47.8
553		5.2a	203	170	200	510	3.00	39.6	0.0180	414	10	10	10	55.0
554		5.2b	203	170	200	510	3.00	39.6	0.0180	414	10	10	10	56.0
555		6.1	51	42	23	126	3.00	35.8	0.0170	414	2	10	10	2.1
556		6.2	51	42	23	126	3.00	38.0	0.0170	414	2	10	10	1.9
557		6.3	51	42	23	126	3.00	39.1	0.0170	414	2	10	10	2.1

175

#	Author	Specimen	h (mm)	d (mm)	b (mm)	a (mm)	a/d	f_ck (MPa)	ρ	f_yk (MPa)	d_a (mm)	Top plate width (mm)	Bottom plate width (mm)	V_exp. (kN)
558		6.4	51	42	23	126	3.00	60.0	0.0170	414	2	10	10	2.1
559		6.5	51	42	23	126	3.00	46.9	0.0170	414	2	10	10	2.6
560		6.6	51	42	23	126	3.00	64.0	0.0170	414	2	10	10	2.7
561		6.7	51	42	23	126	3.00	43.1	0.0170	414	2	10	10	2.4
562		6.8	51	42	23	126	3.00	42.6	0.0170	414	2	10	10	2.2
563		6.9	51	42	23	126	3.00	45.0	0.0170	414	2	10	10	2.3
564	Kwun [148]	4-C-1	248	226	152	686	3.04	46.6	0.0017	1167	19	10	10	19.9
565		4-C-2	248	226	152	686	3.04	45.0	0.0017	1167	19	10	10	47.8
566		3-S-1	305	255	154	762	2.99	37.2	0.0019	1641	19	10	10	28.9
567	Heger & McGrath [149]	SW9-0A	224	184	914	597	3.24	48.5	0.0062	603	19	50	50	167.6
568		SW9-0B	227	190	914	597	3.14	48.5	0.0060	603	19	50	50	155.5
569		SW9M-0A	225	187	914	597	3.19	48.5	0.0061	594	19	50	50	155.7
570		SW9M-0B	226	185	914	597	3.23	48.5	0.0062	594	19	50	50	174.3
571		SW9M-0B-15	226	174	914	381	2.19	48.5	0.0066	594	19	50	50	308.1
572		SW14-0A	227	191	914	597	3.13	49.0	0.0093	673	19	50	50	197.2
573		SW14-0B	226	186	914	597	3.21	49.0	0.0096	673	19	50	50	195.9
574		SW1B-0A	225	184	914	597	3.24	48.3	0.0124	633	19	50	50	202.6
575		SW1B-0B	225	180	914	597	3.32	48.3	0.0127	633	19	50	50	222.8
576	Mphonde & Frantz [150]	AO-3-3b	337	298	152	1067	3.58	21.3	0.0334	414	10	50	50	64.6
577		AO-3-3c	337	298	152	1067	3.58	27.8	0.0233	414	10	50	50	66.8
578		AO-7-3a	337	298	152	1067	3.58	38.6	0.0334	414	10	50	50	82.2
579		AO-7-3b	337	298	152	1067	3.58	42.7	0.0334	414	10	50	50	82.8
580		AO-11-3a	337	298	152	1067	3.58	76.9	0.0334	414	10	50	50	89.7
581		AO-11-3b	337	298	152	1067	3.58	76.6	0.0334	414	10	50	50	89.4
582		AO-15-3a	337	298	152	1067	3.58	83.4	0.0334	414	10	50	50	93.4
583		AO-15-3b	337	298	152	1067	3.58	96.1	0.0334	414	10	50	50	100.0
584		AO-15-3c	337	298	152	1067	3.58	94.2	0.0334	414	10	50	50	97.8
585		AO-3-2	337	298	152	740	2.48	21.1	0.0334	414	10	50	50	77.8
586		AO-7-2	337	298	152	740	2.48	46.3	0.0334	414	10	50	50	117.9
587		AO-11-2	337	298	152	740	2.48	81.3	0.0334	414	10	50	50	111.3

176

#	Author	Specimen	h (mm)	d (mm)	b (mm)	a (mm)	a/d	f_{ck} (MPa)	ρ	f_{yk} (MPa)	d_a (mm)	Top plate width (mm)	Bottom plate width (mm)	$V_{exp.}$ (kN)
588		AO-15-2a	337	298	152	740	2.48	85.9	0.0334	414	10	50	50	177.8
589		AO-15-2b	337	298	152	740	2.48	71.2	0.0334	414	10	50	50	205.8
590	Elzanaty et al. [151]	F7	305	268	178	1073	4.00	20.7	0.0060	434	13	10	10	33.7
591		F11	305	270	178	1080	4.00	20.7	0.0119	434	13	10	10	45.3
592		F12	305	268	178	1073	4.00	20.7	0.0244	434	13	10	10	55.7
593		F8	305	273	178	1092	4.00	40.0	0.0093	434	13	10	10	46.4
594		F13	305	270	178	1080	4.00	40.0	0.0119	434	13	10	10	46.6
595		F14	305	268	178	1073	4.00	40.0	0.0244	434	13	10	10	65.7
596		F1	305	270	178	1080	4.00	65.5	0.0119	434	13	10	10	58.7
597		F2	305	268	178	1073	4.00	65.5	0.0244	434	13	10	10	67.6
598		F10	305	267	178	1067	4.00	65.5	0.0321	434	13	10	10	79.0
599		F9	305	268	178	1073	4.00	79.3	0.0163	434	13	10	10	63.6
600		F15	305	268	178	1073	4.00	79.3	0.0244	434	13	10	10	68.6
601		F3	305	268	178	537	2.00	69.0	0.0119	434	13	10	10	85.3
602		F4	305	268	178	537	2.00	69.0	0.0244	434	13	10	10	129.6
603		F6	305	268	178	1610	6.01	63.4	0.0250	434	13	10	10	61.5
604	Rogowsky et al. [119]	BM1/2.0/T1	500	455	200	1000	2.20	43.2	0.0088	455	10	200	200	177.0
605	Muruyama & Iwabuchi [152]	N1	250	230	200	625	2.72	47.1	0.0168	343	19	90	90	97.1
606		N2	250	230	200	625	2.72	51.0	0.0168	343	19	90	90	83.4
607		NP1	250	230	200	775	3.37	47.2	0.0346	343	19	90	90	87.3
608		NP2	250	230	200	775	3.37	47.3	0.0346	343	19	90	90	112.8
609		NP3	250	230	200	775	3.37	49.2	0.0346	343	19	90	90	95.2
610		NS1	250	230	200	750	3.26	45.5	0.0279	343	19	90	90	93.2
611		NS2	250	230	200	750	3.26	46.8	0.0279	343	19	90	90	91.2
612		NS3	250	230	200	750	3.26	49.1	0.0346	343	19	90	90	86.3
613		NS4	250	230	200	750	3.26	50.5	0.0346	343	19	90	90	82.4
614		NL1	250	230	200	1000	4.35	46.9	0.0279	343	19	90	90	91.2
615		NL2	250	230	200	1000	4.35	43.9	0.0279	343	19	90	90	80.4
616		NL3	250	230	200	1000	4.35	43.5	0.0279	343	19	90	90	83.4
617		NL4	250	230	200	1000	4.35	47.9	0.0346	343	19	90	90	89.3
618		NL5	250	230	200	1000	4.35	47.1	0.0346	343	19	90	90	91.2
619	Mansur et al	A2	225	200	150	560	2.80	24.2	0.0134	463	20	10	10	45.0

177

#	Author	Specimen	h (mm)	d (mm)	b (mm)	a (mm)	a/d	f_{ck} (MPa)	ρ	f_{yk} (MPa)	d_a (mm)	Top plate width (mm)	Bottom plate width (mm)	$V_{exp.}$ (kN)
620	[153]	A3	225	200	150	720	3.60	24.2	0.0134	463	20	10	10	38.5
621		A4	225	200	150	880	4.40	24.2	0.0134	463	20	10	10	33.8
622	Ahmad & Lue [121]	A1	254	203	127	813	4.00	66.0	0.0393	414	12.7	10	10	28.9
623		A2	254	203	127	609	3.00	66.0	0.0393	414	12.7	10	10	34.5
624		A3	254	203	127	548	2.70	66.0	0.0393	414	12.7	10	10	34.5
625		A4	254	203	127	467	2.30	66.0	0.0393	414	12.7	10	10	46.7
626		A7	254	208	127	832	4.00	66.0	0.0177	414	12.7	10	10	23.4
627		A8	254	208	127	624	3.00	66.0	0.0177	414	12.7	10	10	24.5
628		A9	254	208	127	562	2.70	66.0	0.0177	414	12.7	10	10	40.0
629		A10	254	208	127	478	2.30	66.0	0.0177	414	12.7	10	10	41.1
630		B1	254	202	127	808	4.00	73.0	0.0504	414	12.7	10	10	24.9
631		B2	254	202	127	606	3.00	73.0	0.0504	414	12.7	10	10	34.5
632		B3	254	202	127	545	2.70	73.0	0.0504	414	12.7	10	10	50.0
633		B4	254	202	127	465	2.30	73.0	0.0504	414	12.7	10	10	71.6
634		B7	254	208	127	832	4.00	73.0	0.0225	414	12.7	10	10	22.2
635		B8	254	208	127	624	3.00	73.0	0.0225	414	12.7	10	10	23.4
636		B9	254	208	127	562	2.70	73.0	0.0225	414	12.7	10	10	40.0
637		B10	254	208	127	478	2.30	73.0	0.0225	414	12.7	10	10	32.0
638		C1	254	184	127	736	4.00	70.0	0.0664	414	12.7	10	10	27.1
639		C2	254	184	127	552	3.00	70.0	0.0664	414	12.7	10	10	37.8
640		C3	254	184	127	497	2.70	70.0	0.0664	414	12.7	10	10	34.5
641		C4	254	184	127	423	2.30	70.0	0.0664	414	12.7	10	10	44.5
642		C7	254	207	127	828	4.00	70.0	0.0326	414	12.7	10	10	22.7
643		C8	254	207	127	621	3.00	70.0	0.0326	414	12.7	10	10	22.2
644		C9	254	207	127	559	2.70	70.0	0.0326	414	12.7	10	10	22.7
645		C10	254	207	127	476	2.30	70.0	0.0326	414	12.7	10	10	28.5
646	Niwa et al. [154]	1	2100	2000	600	6000	3.00	27.1	0.0028	999	25	200	200	402.0
647		2	2100	2000	600	6000	3.00	26.2	0.0014	999	25	200	200	382.0
648		3	1100	1000	300	3000	3.00	24.6	0.0014	999	25	200	200	102.0
649	Regan & Rezai-Jorabi [155]	1.0	100	83	400	450	5.42	37.8	0.0166	670	10	100	100	62.5
650		2.0	100	83	600	450	5.42	37.8	0.0158	670	10	100	100	85.0
651		3.0	100	83	800	450	5.42	37.8	0.0154	670	10	100	100	97.5

#	Author	Specimen	h (mm)	d (mm)	b (mm)	a (mm)	a/d	f_{ck} (MPa)	ρ	f_{yk} (MPa)	d_a (mm)	Top plate width (mm)	Bottom plate width (mm)	$V_{exp.}$ (kN)
652		4.0	100	83	400	450	5.42	28.1	0.0166	670	10	100	100	54.5
653		5.0	100	83	600	450	5.42	28.1	0.0158	670	10	100	100	80.0
654		6.0	100	83	800	450	5.42	28.1	0.0154	670	10	100	100	96.5
655		10.0	100	83	400	450	5.42	33.4	0.0166	670	20	100	100	52.5
656		11.0	100	83	400	450	5.42	33.4	0.0166	670	20	100	100	55.0
657		12.0	100	83	600	450	5.42	33.4	0.0158	670	20	100	100	76.0
658		13.0	100	83	600	450	5.42	33.4	0.0158	670	20	100	100	79.5
659		14.0	100	83	800	450	5.42	31.0	0.0154	670	20	100	100	92.5
660		15.0	100	83	800	450	5.42	30.8	0.0154	670	20	100	100	85.0
661		16.0	100	83	800	450	5.42	31.2	0.0154	670	20	100	100	108.0
662		17.0	100	83	1000	450	5.42	31.0	0.0151	670	20	100	100	90.0
663		18.0	100	83	1000	450	5.42	31.2	0.0151	670	20	100	100	120.0
664		19.0	100	83	1000	450	5.42	29.0	0.0151	670	20	100	100	111.0
665		20.0	100	83	1000	450	5.42	30.8	0.0151	670	20	100	100	122.5
666		22.0	100	83	1200	450	5.42	37.0	0.0164	670	20	100	100	121.5
667		23.0	100	83	1200	450	5.42	35.4	0.0164	670	20	100	100	125.0
668		24.0	100	83	1200	450	5.42	38.6	0.0164	670	20	100	100	150.0
669		26.0	100	83	1200	450	5.42	29.7	0.0164	670	20	100	100	137.5
670		16R	100	83	800	450	5.42	31.2	0.0154	670	20	100	100	116.5
671		17R	100	83	1000	450	5.42	31.0	0.0151	670	20	100	100	137.5
672	Johnson & Ramirez [156]	6	610	539	305	1670	3.10	55.9	0.0249	525	19	102	102	316.3
673	Adebar & Collins [157]	ST1	310	278	360	1600	5.76	52.5	0.0157	539	19	10	10	127.5
674		ST2	310	278	360	1600	5.76	52.5	0.0157	539	19	10	10	118.7
675		ST3	310	278	290	1600	5.76	49.3	0.0195	539	19	10	10	107.7
676		ST16	210	178	290	1600	8.99	51.5	0.0304	539	19	10	10	75.1
677		ST17	410	378	290	1600	4.23	51.5	0.0137	539	19	10	10	118.9
678		ST23	310	278	290	1600	5.76	58.9	0.0099	539	19	10	10	89.9
679	Thorenfeldt & Drangshold	B11	250	221	150	663	3.00	54	0.0182	500	16	25	25	58.1

#	Author	Specimen	h (mm)	d (mm)	b (mm)	a (mm)	a/d	f_{ck} (MPa)	ρ	f_{yk} (MPa)	d_a (mm)	Top plate width (mm)	Bottom plate width (mm)	$V_{exp.}$ (kN)
680	[158]	B12	251	221	151	508	2.30	54	0.0182	500	16	25	25	70.8
681		B13	252	207	152	828	4.00	54	0.0324	500	16	25	25	70.5
682		B14	253	207	153	621	3.00	54	0.0324	500	16	25	25	82.6
683		B15	254	207	154	476	2.30	54	0.0324	500	16	25	25	107.1
684		B21	250	221	150	663	3.00	78	0.0182	500	16	25	25	67.9
685		B22	250	221	150	508	2.30	78	0.0182	500	16	25	25	102.7
686		B23	250	207	150	828	4.00	78	0.0324	500	16	25	25	77.8
687		B24	250	207	150	621	3.00	78	0.0324	500	16	25	25	82.6
688		B25	250	207	150	476	2.30	78	0.0324	500	16	25	25	175.8
689		B43	250	207	150	828	4.00	86	0.0324	500	16	25	25	86.2
690		B44	250	207	150	621	3.00	86	0.0324	500	16	25	25	107.2
691		B45	250	207	150	476	2.30	86	0.0324	500	16	25	25	148.3
692		B51	250	221	150	663	3.00	98	0.0182	500	16	25	25	56.2
693		B52	250	221	150	508	2.30	98	0.0182	500	16	25	25	77.7
694		B53	250	207	150	828	4.00	98	0.0324	500	16	25	25	76.8
695		B54	250	207	150	621	3.00	98	0.0324	500	16	25	25	77.7
696		B55	250	207	150	476	2.30	98	0.0324	500	16	25	25	156.1
697		B61	500	442	300	1326	3.00	78	0.0182	500	16	25	25	179.8
698		B61R	500	442	300	1326	3.00	78	0.0182	500	16	25	25	180.3
699		B62	500	442	300	1017	2.30	78	0.0182	500	16	25	25	438.7
700		B63	500	414	300	1656	4.00	78	0.0324	500	16	25	25	222.5
701		B63R	500	414	300	1656	4.00	78	0.0324	500	16	25	25	229.4
702		B64	500	414	300	1242	3.00	78	0.0324	500	16	25	25	280.7
703		B65	500	414	300	952	2.30	78	0.0324	500	16	25	25	576.3
704		B65R	500	414	300	952	2.30	78	0.0324	500	16	25	25	710.3
705	Bazant & Kazemi [24]	S1B4	51	41	38	123	3.00	47.0	0.0170	793	4.8	10	10	3.2
706		S1B5	51	41	38	123	3.00	47.0	0.0170	793	4.8	10	10	3.0
707		S1B6	51	41	38	123	3.00	47.0	0.0170	793	4.8	10	10	3.1
708		S1B7	101	81	38	243	3.00	47.0	0.0170	793	4.8	10	10	5.5
709		S1B8	101	81	38	243	3.00	47.0	0.0170	793	4.8	10	10	5.6
710		S1B9	101	81	38	243	3.00	47.0	0.0170	793	4.8	10	10	5.2
711		S1B10	204	163	38	489	3.00	47.0	0.0170	793	4.8	10	10	9.1

#	Author	Specimen	h (mm)	d (mm)	b (mm)	a (mm)	a/d	f_{ck} (MPa)	ρ	f_{yk} (MPa)	d_a (mm)	Top plate width (mm)	Bottom plate width (mm)	$V_{exp.}$ (kN)
712		S1B11	204	163	38	489	3.00	47.0	0.0170	793	4.8	10	10	9.8
713		S1B12	204	163	38	489	3.00	47.0	0.0170	793	4.8	10	10	10.1
714		S2B1	25	20	38	60	3.00	46.0	0.0160	793	4.8	10	10	2.1
715		S2B2	25	20	38	60	3.00	46.0	0.0160	793	4.8	10	10	2.4
716		S2B3	25	20	38	60	3.00	46.0	0.0160	793	4.8	10	10	2.3
717		S2B4	50	41	38	123	3.00	46.0	0.0160	793	4.8	10	10	2.9
718		S2B5	50	41	38	123	3.00	46.0	0.0160	793	4.8	10	10	2.7
719		S2B6	50	41	38	123	3.00	46.0	0.0160	793	4.8	10	10	3.2
720		S2B7	103	84	38	252	3.00	46.0	0.0160	793	4.8	10	10	5.4
721		S2B8	103	84	38	252	3.00	46.0	0.0160	793	4.8	10	10	5.0
722		S2B9	103	84	38	252	3.00	46.0	0.0160	793	4.8	10	10	4.4
723		S2B10	203	165	38	495	3.00	46.0	0.0160	793	4.8	10	10	7.3
724		S2B11	203	165	38	495	3.00	46.0	0.0160	793	4.8	10	10	8.4
725		S2B12	203	165	38	495	3.00	46.0	0.0160	793	4.8	10	10	8.2
726		S2B13	406	330	38	990	3.00	46.0	0.0160	793	4.8	10	10	10.3
727		S2B14	406	330	38	990	3.00	46.0	0.0160	793	4.8	10	10	11.3
728		S2B15	406	330	38	990	3.00	46.0	0.0160	793	4.8	10	10	9.3
729	Hallgren [159]	B90SB13-2-8	233	192	163	700	3.65	86.2	0.0217	630	18	10	10	82.5
730		B90SB14-2-8	235	194	158	700	3.61	86.2	0.0221	630	18	10	10	76.5
731		B90SB22-2-8	234	193	158	700	3.63	84.6	0.0222	630	18	10	10	75.5
732		B91SC2-2-62	237	196	155	700	3.57	61.8	0.0223	443	18	10	10	69.5
733		B91SC4-2-69	236	195	156	700	3.59	69.1	0.0223	443	18	10	10	74.0
734		B90SB17-2-4	232	191	157	700	3.66	44.9	0.0226	630	18	10	10	59.0
735		B90SB18-2-4	235	194	155	700	3.61	44.9	0.0225	630	18	10	10	63.0
736		B90SB21-2-8	235	194	155	700	3.61	84.6	0.0225	630	18	10	10	69.0
737		B91SC1-2-62	234	193	156	700	3.63	61.8	0.0225	443	18	10	10	71.0
738		B91SD1-4-61	247	194	156	700	3.61	60.8	0.0398	494	18	10	10	88.5
739		B91SD2-4-61	248	195	156	700	3.59	60.8	0.0396	494	18	10	10	90.0

181

#	Author	Specimen	h (mm)	d (mm)	b (mm)	a (mm)	a/d	f_{ck} (MPa)	ρ	f_{yk} (MPa)	d_a (mm)	Top plate width (mm)	Bottom plate width (mm)	$V_{exp.}$ (kN)
740		B91SD3-4-66	248	195	156	700	3.59	65.7	0.0396	494	18	10	10	81.5
741		B91SD4-4-66	248	195	155	700	3.59	65.7	0.0399	494	18	10	10	79.0
742		B91SD5-4-58	249	196	156	700	3.57	58.3	0.0394	494	18	10	10	78.0
743		B91SD6-4-58	249	196	150	700	3.57	58.3	0.0410	494	18	10	10	82.5
744		B90SB5-2-33	232	191	156	700	3.66	32.8	0.0228	651	18	10	10	56.0
745		B90SB6-2-33	235	194	156	700	3.61	32.8	0.0224	651	18	10	10	53.5
746		B90SB9-2-31	233	192	156	700	3.65	31.1	0.0226	651	18	10	10	49.0
747		B90SB10-2-3	234	193	157	700	3.63	31.1	0.0220	651	18	10	10	53.5
748	Kim & Park [160]	CTL-1	300	270	170	810	3.00	53.7	0.0187	477	25	10	10	71.1
749		CTL-2	300	270	170	810	3.00	53.7	0.0187	477	25	10	10	71.6
750		P1.0-1	300	272	170	816	3.00	53.7	0.0101	477	25	10	10	58.3
751		P1.0-2	300	272	170	816	3.00	53.7	0.0101	477	25	10	10	56.4
752		P3.4-1	300	267	170	801	3.00	53.7	0.0335	477	25	10	10	78.1
753		P3.4-2	300	267	170	801	3.00	53.7	0.0335	477	25	10	10	78.5
754		P4.6-1	300	255	170	765	3.00	53.7	0.0468	477	25	10	10	89.7
755		P4.6-2	300	255	170	765	3.00	53.7	0.0468	477	25	10	10	95.4
756		A4.5-1	300	270	170	1215	4.50	53.7	0.0187	477	25	10	10	66.6
757		A4.5-2	300	270	170	1215	4.50	53.7	0.0187	477	25	10	10	63.8
758		A6.0-1	300	270	170	1620	6.00	53.7	0.0187	477	25	10	10	59.2
759		A6.0-2	300	270	170	1620	6.00	53.7	0.0187	477	25	10	10	61.0
760		D142-1	170	142	170	426	3.00	53.7	0.0187	477	25	10	10	41.0
761		D142-2	170	142	170	426	3.00	53.7	0.0187	477	25	10	10	39.3
762		D550-1	620	550	300	1650	3.00	53.7	0.0188	477	25	10	10	226.1
763		D550-2	620	550	300	1650	3.00	53.7	0.0188	477	25	10	10	214.5
764		D915-1	1000	915	300	2745	3.00	53.7	0.0187	477	25	10	10	271.8
765		D915-2	1000	915	300	2745	3.00	53.7	0.0187	477	25	10	10	332.1
766	Walraven & Lehwalter [26]	A1	150	125	200	375	3.00	23	0.0083	440	16	31	31	31.5
767		A2	450	420	200	1260	3.00	23	0.0074	440	16	84	84	70.6
768		A3	750	720	200	2160	3.00	23	0.0079	440	16	144	144	100.8

#	Author	Specimen	h (mm)	d (mm)	b (mm)	a (mm)	a/d	f_{ck} (MPa)	ρ	f_{yk} (MPa)	d_a (mm)	Top plate width (mm)	Bottom plate width (mm)	$V_{exp.}$ (kN)
769	Xie et al. [50]	NNN-3	254	216	127	648	3.00	39.7	0.0207	421	19	15	15	36.7
770		NHN-3	254	216	127	648	3.00	104.2	0.0207	421	19	15	15	45.7
771	Matsui et al. [161]	A1	180	150	100	450	3.00	32.4	0.0265	367	19	10	10	27.5
772		A2	180	150	100	450	3.00	32.4	0.0265	367	19	10	10	31.9
773		B1	180	150	100	450	3.00	38.4	0.0265	367	19	10	10	29.3
774		B2	180	150	100	450	3.00	38.4	0.0265	367	19	10	10	30.7
775		C1	180	150	100	450	3.00	48.7	0.0265	367	19	10	10	29.6
776		C2	180	150	100	450	3.00	48.7	0.0265	367	19	10	10	32.3
777		D1	180	150	100	450	3.00	70.9	0.0265	367	19	10	10	33.4
778		D2	180	150	100	450	3.00	70.9	0.0265	367	19	10	10	33.9
779		E1	180	150	100	450	3.00	83.4	0.0265	367	19	10	10	38.3
780		E2	180	150	100	450	3.00	83.4	0.0265	367	19	10	10	42.5
781		F1	180	150	100	450	3.00	127.5	0.0265	367	19	10	10	34.4
782		F2	180	150	100	450	3.00	127.5	0.0265	367	19	10	10	48.1
783		L1	260	225	100	675	3.00	124.5	0.0255	403	19	10	10	69.7
784		L2	260	225	100	675	3.00	124.5	0.0255	403	19	10	10	42.5
785		M1	260	225	100	788	3.50	124.5	0.0255	403	19	10	10	43.4
786		M2	260	225	100	788	3.50	124.5	0.0255	403	19	10	10	43.8
787		N1	260	225	100	900	4.00	124.5	0.0255	403	19	10	10	41.3
788		N2	260	225	100	900	4.00	124.5	0.0255	403	19	10	10	38.8
789		S1	360	320	100	1080	3.38	127.5	0.0290	336	19	10	10	54.0
790		S2	360	320	100	1080	3.38	127.5	0.0290	336	19	10	10	83.1
791	Yoon et al. [61]	N1-S	750	655	375	2150	3.28	36.0	0.0288	400	20	150	150	249.0
792		M1-S	750	655	375	2150	3.28	67.0	0.0288	400	10	150	150	296.0
793		H1-S	750	655	375	2150	3.28	87.0	0.0288	400	10	150	150	327.0
794	Konig et al. [57]	s1.1	200	153	300	570	3.73	90.1	0.0134	660	16	50	50	70.1
795		s4.1	200	153	300	570	3.73	110.9	0.0134	660	16	50	50	74.2
796		s2.3	400	348	300	1230	3.53	93.7	0.0094	469	16	70	70	123.1
797		s3.3	800	746	300	2630	3.53	94.4	0.0083	487	16	149	149	192.8
798		s1.2	200	152	300	570	3.75	91.2	0.0221	517	16	50	50	75.8
799		s4.2	200	152	300	570	3.75	110.9	0.0221	517	16	50	50	90.3
800		s2.2	400	348	300	1230	3.53	91.3	0.0188	469	16	100	100	187.1

#	Author	Specimen	h (mm)	d (mm)	b (mm)	a (mm)	a/d	f_{ck} (MPa)	ρ	f_{yk} (MPa)	d_a (mm)	Top plate width (mm)	Bottom plate width (mm)	$V_{exp.}$ (kN)
801		s3.2	800	718	300	2556	3.56	93.7	0.0172	487	16	144	144	259.1
802		s1.3	200	146	300	570	3.90	93.7	0.0422	487	16	50	50	98.6
803		s4.3	200	146	300	570	3.90	110.9	0.0422	487	16	50	50	122.3
804		s2.4	400	328	300	1230	3.75	94.1	0.0376	487	16	66	66	229.8
805		s3.4	800	690	300	2630	3.81	94.1	0.0357	487	16	138	138	379.0
806	Kawano & Wantanabe [162]	A1A	330	300	105	900	3.00	24.8	0.0126	400	20	60	60	33.5
807		A1B	330	300	105	900	3.00	24.8	0.0126	400	20	60	60	29.5
808		A2A	570	500	176	1500	3.00	27.3	0.0136	400	20	100	100	82.5
809		A2B	570	500	176	1500	3.00	27.3	0.0136	400	20	100	100	101.5
810		A3A	1050	950	350	2850	3.00	20.7	0.0122	400	20	190	190	216.0
811		A3B	1050	950	350	2850	3.00	20.6	0.0122	400	20	190	190	237.5
812		A4A	2200	2000	600	6000	3.00	22.2	0.0120	400	40	400	400	610.5
813		A4B	2200	2000	600	6000	3.00	23.1	0.0120	400	40	400	400	560.0
814	Ghannoum [163]	N220-l	220	190	400	475	2.50	34.2	0.0120	433	20	100	100	103.6
815		N350-l	350	313	400	783	2.50	34.2	0.0120	477	20	100	100	157.9
816		N485-l	485	440	400	1100	2.50	34.2	0.0120	385	20	100	100	186.8
817		N960-l	960	889	400	2223	2.50	34.2	0.0120	385	20	100	100	360.2
818		N220-h	220	190	400	475	2.50	34.2	0.0200	433	20	100	100	122.7
819		N350-h	350	313	400	783	2.50	34.2	0.0200	477	20	100	100	178.4
820		N485-h	485	440	400	1100	2.50	34.2	0.0200	385	20	100	100	214.6
821		N960-h	960	889	400	2223	2.50	34.2	0.0200	385	20	100	100	379.7
822		H220-l	220	190	400	475	2.50	58.6	0.0120	433	10	100	100	105.8
823		H350-l	350	313	400	783	2.50	58.6	0.0120	477	10	100	100	157.1
824		H485-l	485	440	400	1100	2.50	58.6	0.0120	385	10	100	100	197.7
825		H960-l	960	889	400	2223	2.50	58.6	0.0120	385	10	100	100	310.4
826		H220-h	220	190	400	475	2.50	58.6	0.0200	433	10	100	100	135.3
827		H350-h	350	313	400	783	2.50	58.6	0.0200	477	10	100	100	189.5
828		H485-h	485	440	400	1100	2.50	58.6	0.0200	385	10	100	100	198.2
829		H960-h	960	889	400	2223	2.50	58.6	0.0200	385	10	100	100	331.1
830	Islam et al. [164]	M100-S0	250	203	150	800	3.94	83.3	0.0322	532	10	10	10	65.0
831		M100-S1	250	203	150	800	3.94	83.3	0.0322	532	10	10	10	107.7
832		M100-S2	250	203	150	800	3.94	83.3	0.0322	532	10	10	10	131.1

#	Author	Specimen	h (mm)	d (mm)	b (mm)	a (mm)	a/d	f_{ck} (MPa)	ρ	f_{yk} (MPa)	d_a (mm)	Top plate width (mm)	Bottom plate width (mm)	$V_{exp.}$ (kN)
833		M100-S3	250	203	150	800	3.94	83.3	0.0322	532	10	10	10	96.9
834		M100-S4	250	203	150	800	3.94	83.3	0.0322	532	10	10	10	80.7
835		M80-S0	250	203	150	800	3.94	72.2	0.0322	532	10	10	10	58.0
836		M80-S1	250	203	150	800	3.94	72.2	0.0322	532	10	10	10	117.3
837		M80-S2	250	203	150	800	3.94	72.2	0.0322	532	10	10	10	123.0
838		M80-S3	250	203	150	800	3.94	72.2	0.0322	532	10	10	10	115.4
839		M80-S4	250	203	150	800	3.94	72.2	0.0322	532	10	10	10	72.1
840		M60-S0	250	207	150	800	3.86	50.8	0.0202	554	10	10	10	45.5
841		M60-S1	250	207	150	800	3.86	50.8	0.0202	554	10	10	10	92.3
842		M60-S2	250	207	150	800	3.86	50.8	0.0202	554	10	10	10	103.8
843		M60-S3	250	207	150	800	3.86	50.8	0.0202	554	10	10	10	90.4
844		M60-S4	250	207	150	800	3.86	50.8	0.0202	554	10	10	10	51.9
845		M40-S0	250	205	150	800	3.90	34.4	0.0319	320	10	10	10	55.0
846		M40-S1	250	205	150	800	3.90	34.4	0.0319	320	10	10	10	84.6
847		M40-S2	250	205	150	800	3.90	34.4	0.0322	320	10	10	10	96.1
848		M40-S3	250	205	150	800	3.90	34.4	0.0319	320	10	10	10	80.7
849		M40-S4	250	205	150	800	3.90	34.4	0.0319	320	10	10	10	76.9
850		M25-S0	250	207	150	800	3.86	26.6	0.0202	350	10	10	10	47.5
851		M25-S1	250	207	150	800	3.86	26.6	0.0202	350	10	10	10	67.3
852		M25-S2	250	207	150	800	3.86	26.6	0.0202	350	10	10	10	94.2
853		M25-S3	250	207	150	800	3.86	26.6	0.0202	350	10	10	10	56.5
854		M25-S4	250	207	150	800	3.86	26.6	0.0202	350	10	10	10	65.4
855	Collins and Kuchma [165]	B100	1000	925	300	2700	2.92	36.0	0.0101	550	10	152	152	225.0
856		B100-R	1000	925	300	2700	2.92	36.0	0.0101	550	10	152	152	249.0
857		B100D	1000	925	300	2700	2.92	36.0	0.0119	550	10	152	152	320.0
858		B100H	1000	925	300	2700	2.92	98.0	0.0101	550	10	152	152	193.0
859		B100HE	1000	925	300	2700	2.92	98.0	0.0101	550	10	152	152	217.0
860		B100L	1000	925	300	2700	2.92	39.0	0.0101	483	10	152	152	223.0
861		B100L-R	1000	925	300	2700	2.92	39.0	0.0101	483	10	152	152	235.0
862		B100B	1000	925	300	2700	2.92	39.0	0.0101	550	10	152	152	204.0
863		BN100	1000	925	300	2700	2.92	37.2	0.0076	550	10	152	152	192.0
864		BND100	1000	925	300	2700	2.92	37.2	0.0105	550	10	152	152	258.0

#	Author	Specimen	h (mm)	d (mm)	b (mm)	a (mm)	a/d	f_{ck} (MPa)	ρ	f_{yk} (MPa)	d_a (mm)	Top plate width (mm)	Bottom plate width (mm)	$V_{exp.}$ (kN)
865		BH100	1000	925	300	2700	2.92	98.8	0.0076	550	10	152	152	193.0
866		BHD100	1000	925	300	2700	2.92	98.8	0.0105	550	10	152	152	278.0
867		BHD100 R	1000	925	300	2700	2.92	98.8	0.0105	550	10	152	152	334.0
868		BRL100	1000	925	300	2700	2.92	94.0	0.0050	550	10	152	152	163.0
869	Shin et al. [123]	MHB2.5-0	250	215	125	538	2.50	52.0	0.0377	414	19	45	45	56.4
870		HB2.5-0	250	215	125	538	2.50	73.0	0.0377	414	13	45	45	80.4
871	Adebar [124]	DF-1	1090	1000	500	2330	2.33	21.0	0.0042	550	20	150	150	429.0
872		DF-2	1090	1000	500	2330	2.33	18.4	0.0042	550	20	150	150	315.0
873		DF-2R	1090	1000	500	2330	2.33	18.4	0.0042	550	20	150	150	378.0
874		DF-3	1090	1000	500	2330	2.33	18.4	0.0042	550	20	150	150	329.0
875		DF-4	1090	1000	500	2330	2.33	25.5	0.0060	550	20	150	150	387.0
876		DF-5	1090	996	500	2400	2.41	25.5	0.0066	550	20	150	150	381.0
877		DF-6	1090	1000	500	2200	2.20	21.0	0.0098	550	20	200	200	771.0
878		DF-7	1090	1000	500	2330	2.33	20.6	0.0098	550	20	150	150	435.0
879		DF-8	1090	1000	500	2330	2.33	22.4	0.0098	550	20	150	150	531.0
880		DF-8R	1090	1000	500	2330	2.33	22.4	0.0098	550	20	150	150	579.0
881		DF-9	1090	1000	500	2330	2.33	31.7	0.0098	550	20	150	150	532.0
882		DF-10	1090	1000	500	2330	2.33	31.7	0.0098	550	20	150	150	524.0
883		DF-10R	1090	1000	500	2330	2.33	31.7	0.0098	550	20	150	150	605.0
884	Pendyala & Mendis [125]	2	160	140	80	700	5.00	34.0	0.0202	410	10	10	10	16.5
885		4	160	140	80	700	5.00	63.0	0.0202	410	10	10	10	16.0
886		6	160	140	80	700	5.00	87.0	0.0202	410	10	10	10	18.0
887	Yoshida [166]	YB2000/0	2000	1890	300	5400	2.86	33.6	0.0074	435	10	300	300	255.0
888	Angelakos et al. [48]	DB120	1000	925	300	2700	2.92	21.0	0.0101	550	10	152	152	179.0
889		DB130	1000	925	300	2700	2.92	32.0	0.0101	550	10	152	152	185.0
890		DB140	1000	925	300	2700	2.92	38.0	0.0101	550	10	152	152	180.0
891		DB165	1000	925	300	2700	2.92	65.0	0.0101	550	10	152	152	185.0
892		DB180	1000	925	300	2700	2.92	80.0	0.0101	550	10	152	152	172.0
893		DB230	1000	925	300	2700	2.92	32.0	0.0202	550	10	152	152	257.0
894		DB0.530	1000	925	300	2700	2.92	32.0	0.0050	550	10	152	152	165.0
895	Cao [167]	SB2003/0	2000	1890	300	5400	2.86	30.0	0.0036	435	10	300	300	224.0

186

#	Author	Specimen	h (mm)	d (mm)	b (mm)	a (mm)	a/d	f_{ck} (MPa)	ρ	f_{yk} (MPa)	d_a (mm)	Top plate width (mm)	Bottom plate width (mm)	$V_{exp.}$ (kN)
896		SB2 2012/0	2000	1890	300	5400	2.86	27.5	0.0152	435	10	300	300	402.0
897	Guadagnini [82]	SB40	250	224	150	750	3.35	42.8	0.0135	499	20	100	100	45.0
898		SB41	250	224	150	500	2.23	42.8	0.0135	499	20	100	100	67.5
899	Tariq & Newhook [168]	R-S007Na	400	346	160	950	2.75	37.3	0.0072	483	20	69	69	58.9
900		R-S007Nb	400	346	160	950	2.75	37.3	0.0072	483	20	69	69	63.3
901		R-S010N1	400	346	160	1150	3.32	43.2	0.0108	483	20	69	69	66.7
902		R-S010N2	400	346	160	1150	3.32	43.2	0.0108	483	20	69	69	62.2
903		R-S015N1	400	325	160	1150	3.54	34.1	0.0154	483	20	65	65	69.8
904		R-S015N2	400	325	160	1150	3.54	34.1	0.0154	483	20	65	65	70.5
905	Lubell et al. [169]	AT-1	1005	920	2010	2700	2.93	64.1	0.0794	460	10	152	152	1272.1
906	OSU test (2004)	37T	1219	1151	356	3353	2.91	31.8	0.0074	478	19	230	230	243.8
907	Rahal & Al-Shaleh [55]	A65-NTR	370	330	200	900	2.73	61.3	0.0216	483	12	10	10	125.0
908		B65-NTR	370	305	200	900	2.95	61.9	0.0389	483	12	10	10	170.0
909	Bentz & Buckley [73]	SBB1.1	103	84	104	248	2.95	33.0	0.0163	494	10	10	10	14.5
910		SBB1.2	103	84	105	248	2.95	33.0	0.0162	494	10	10	10	18.5
911		SBB1.3	103	84	104	248	2.95	33.0	0.0163	494	10	10	10	15.0
912		SBB2.1	206	168	106	495	2.95	30.0	0.0160	494	10	10	10	28.8
913		SBB2.2	206	168	105	495	2.95	30.0	0.0162	494	10	10	10	30.5
914		SBB2.3	206	166	106	495	2.98	30.0	0.0162	494	10	10	10	29.7
915		SBB3.1	378	333	105	990	2.97	34.0	0.0155	490	10	10	10	42.2
916		SBB3.2	378	333	101	990	2.97	34.0	0.0161	490	10	10	10	40.6
917		SBB3.3	378	333	101	990	2.97	34.0	0.0161	490	10	10	10	42.9
918	Cladera and Marí [170]	H50/1	400	359	200	1080	3.01	49.9	0.0224	500	12	150	150	99.7
919		H60/1	400	359	200	1080	3.01	60.8	0.0224	500	12	150	150	108.1
920		H75/1	400	359	200	1080	3.01	68.9	0.0224	500	12	150	150	99.9
921		H100/1	400	359	200	1080	3.01	87.0	0.0224	500	12	150	150	117.9
922	El-Sayed et al. [171]	SN-0.8	400	326	250	1000	3.07	50.0	0.0086	453	19	300	300	98.5
923		SN-1.2	400	326	250	1000	3.07	44.6	0.0123	460	19	300	300	116.5
924		SN-1.7	400	326	250	1000	3.07	43.6	0.0172	460	19	300	300	144.5

#	Author	Specimen	h (mm)	d (mm)	b (mm)	a (mm)	a/d	f_{ck} (MPa)	ρ	f_{yk} (MPa)	d_a (mm)	Top plate width (mm)	Bottom plate width (mm)	$V_{exp.}$ (kN)
925		SH-1.7	400	326	250	1000	3.07	62.0	0.0172	460	19	300	300	160.0
926	Sherwood et al. [172]	AT-2-250A	470	437	250	1295	2.96	37.7	0.0009	465	10	152	152	115.8
927		AT-2-250B	470	440	250	1295	2.94	38.5	0.0009	465	10	152	152	113.3
928		AT-2-1000A	470	440	1000	1295	2.94	39.0	0.0009	465	10	152	152	476.0
929		AT-2-1000B	470	437	1000	1295	2.96	37.9	0.0009	465	10	152	152	444.8
930		AT-2-3000	472	440	3000	1295	2.94	40.6	0.0009	465	10	152	152	1295.3
931		AT-3-A	338	307	696	1039	3.38	37.5	0.0009	448	10	152	152	239.3
932		AT-3-C	338	305	706	1039	3.41	37.1	0.0009	448	10	152	152	260.2
933		AT-3-B	338	305	701	1039	3.41	37.8	0.0009	448	10	152	152	254.8
934		AT-3-D	338	307	706	1039	3.38	37.1	0.0009	448	10	152	152	250.2
935	Lubell [173]	AW1	590	538	1170	1850	3.44	36.9	0.0079	467	10	305	305	585.0
936		AW4	590	506	1168	1850	3.66	39.9	0.0169	467	10	305	305	716.0
937		AW8	591	507	1169	1850	3.65	39.4	0.0169	467	10	152	152	789.0
938		AX6	338	288	703	1040	3.61	41.0	0.0173	467	10	152	152	281.0
939		AX7	335	287	704	1040	3.62	41.0	0.0104	413	10	152	152	249.0
940		AX8	339	289	705	1040	3.60	41.0	0.0172	467	10	152	152	272.0
941		AY1	467	434	249	1300	3.00	40.7	0.0033	900	10	152	152	85.0
942	Seliem et al [127]	G-2.7-32	915	850	460	2325	2.74	32.0	0.0072	468	19	230	230	284.6
943		M-2.7-32	915	850	460	2325	2.74	32.0	0.0044	865	19	230	230	327.6
944	Sherwood et al. [172]	L-10N1	1510	1400	300	4050	2.89	38.4	0.0083	452	10	152	152	265.0
945		L-10N2	1510	1400	300	4050	2.89	40.3	0.0083	452	10	152	152	242.0
946		L-10H	1510	1400	300	4050	2.89	73.6	0.0083	452	10	152	152	240.0
947		L-20N1	1510	1400	300	4050	2.89	31.4	0.0083	452	20	152	152	265.0
948		L-20N2	1510	1400	300	4050	2.89	33.2	0.0083	452	20	152	152	266.0
949		L-40N1	1510	1400	300	4050	2.89	28.1	0.0083	452	40	152	152	242.0
950		L-40N2	1510	1400	300	4050	2.89	28.5	0.0083	452	40	152	152	288.0
951		L-50N1	1510	1400	300	4050	2.89	41.0	0.0083	452	50	152	152	272.0
952		L-50N2	1510	1400	300	4050	2.89	40.1	0.0083	452	50	152	152	298.0
953		L-50N2R	1510	1400	300	4050	2.89	40.1	0.0083	452	50	152	152	323.0

#	Author	Specimen	h (mm)	d (mm)	b (mm)	a (mm)	a/d	f_{ck} (MPa)	ρ	f_{yk} (MPa)	d_a (mm)	Top plate width (mm)	Bottom plate width (mm)	$V_{exp.}$ (kN)
954		S-10N1	330	280	122	810	2.89	41.9	0.0083	494	10	30	30	36.6
955		S-10N2	330	280	122	810	2.89	41.9	0.0083	494	10	30	30	38.3
956		S-10H	330	280	122	810	2.89	77.3	0.0083	494	10	30	30	37.7
957		S-20N1	330	280	122	810	2.89	39.2	0.0083	494	20	30	30	39.1
958		S-20N2	330	280	122	810	2.89	38.1	0.0083	494	20	30	30	38.2
959		S-40N1	330	280	122	810	2.89	29.1	0.0083	494	40	30	30	41.8
960		S-40N2	330	280	122	810	2.89	29.1	0.0083	494	40	30	30	34.9
961		S-50N1	330	280	122	810	2.89	43.5	0.0083	494	50	30	30	38.5
962		S-50N2	330	280	122	810	2.89	43.5	0.0083	494	50	30	30	40.6
963	Uzel et al. [174]	AF8	1000	925	300	1994	2.16	33.8	0.0076	562	10	152	152	249.2

Table A-2-Slender beams with shear reinforcement

#	Author	Specimen	h (mm)	d (mm)	b (mm)	a (mm)	a/d	f_{ck} (MPa)	ρ	f_{yk} (MPa)	ρ_s	f_{yv} (MPa)	ρ_h	f_{yh} (Mpa)	d_a (mm)	Top plate width (mm)	Bottom plate width(mm)	Vexp. (kN)
1	Clark [103]	A1-1	457	380	203	914	2.41	24.7	0.031795	321	0.0038	331	0	0	15	89	89	222.5
2		A1-2	457	379	203	914	2.41	23.7	0.031834	321	0.0038	331	0	0	15	89	89	209.1
3		A1-3	457	379	203	914	2.41	23.4	0.031872	321	0.0038	331	0	0	15	89	89	222.5
4		A1-4	457	379	203	914	2.41	24.8	0.031834	321	0.0038	331	0	0	15	89	89	244.7
5		B1-1	457	379	203	762	2.01	23.4	0.031872	321	0.0037	331	0	0	15	89	89	278.8
6		B1-2	457	380	203	762	2.00	25.4	0.031757	321	0.0037	331	0	0	15	89	89	256.6
7		B1-3	457	379	203	762	2.01	23.7	0.031872	321	0.0037	331	0	0	15	89	89	284.8
8		B1-4	457	379	203	762	2.01	23.3	0.03191	321	0.0037	331	0	0	15	89	89	268.1
9		B1-5	457	380	203	762	2.01	24.6	0.031795	321	0.0037	331	0	0	15	89	89	241.4
10		B2-1	457	379	203	762	2.01	23.2	0.03191	321	0.0037	331	0	0	15	89	89	301.1
11		B2-3	457	380	203	762	2.00	24.9	0.031757	321	0.0037	331	0	0	15	89	89	334.9
12		D2-6	381	319	152	762	2.39	29.5	0.033768	321	0.0061	331	0	0	15	89	89	168.4
13		D2-7	381	317	152	762	2.40	28.4	0.033889	321	0.0061	331	0	0	15	89	89	157.3
14		D2-8	381	316	152	762	2.41	26.1	0.034053	321	0.0061	331	0	0	15	89	89	168.4
15		D4-1	381	317	152	762	2.41	27.4	0.033971	321	0.0049	331	0	0	15	89	89	168.4
16		D4-2	381	315	152	762	2.42	25.7	0.034094	321	0.0049	331	0	0	15	89	89	157.3
17		D4-3	381	312	152	762	2.44	22.1	0.034468	321	0.0049	331	0	0	15	89	89	165.1
18		D5-1	381	317	152	762	2.40	27.7	0.03393	321	0.0037	331	0	0	15	89	89	146.2
19		D5-2	381	318	152	762	2.40	29.0	0.033808	321	0.0037	331	0	0	15	89	89	157.3

#	Author	Specimen	h (mm)	d (mm)	b (mm)	a (mm)	a/d	f'c (MPa)	ρ	f_sk (MPa)	ρᵥ	f_yv (MPa)	ρₕ	f_sh (Mpa)	dₐ (mm)	Top plate width (mm)	Bottom plate width(mm)	Vexp. (kN)
20		D5-3	381	317	152	762	2.41	27.1	0.033971	321	0.0037	331	0	0	15	89	89	157.3
21	Krefeld & Thurston [113]	26-1	508	456	254	1829	4.01	40.1	0.02218	370	0.00146	341	0	0	25	178	178	103.4
22		29a-1	508	456	254	1829	4.01	38.8	0.02218	370	0.00097	341	0	0	25	178	178	79.8
23		29b-1	508	456	254	1829	4.01	37.7	0.02218	370	0.00097	341	0	0	25	178	178	80.1
24		213.5-1	508	456	254	1829	4.01	38.9	0.02218	370	0.00064	341	0	0	25	178	178	74.1
25		29a-2	508	456	254	1829	4.01	37.2	0.02218	370	0.00097	372	0	0	25	178	178	108.3
26		29b-2	508	456	254	1829	4.01	41.4	0.02218	370	0.00097	372	0	0	25	178	178	101.2
27		29c-2	508	456	254	1829	4.01	24.1	0.02218	370	0.00097	372	0	0	25	178	178	80.7
28		29d-2	508	456	254	1829	4.01	30.4	0.02218	370	0.00097	372	0	0	25	178	178	82.5
29		0.29	508	456	254	1829	4.01	48.5	0.02218	370	0.00097	372	0	0	25	178	178	103.2
30		29f-2	508	456	254	1829	4.01	41.8	0.02218	370	0.00097	372	0	0	25	178	178	117.2
31		29g-2	508	456	254	1829	4.01	15.7	0.02218	370	0.00097	372	0	0	25	178	178	75.0
32		213.5a-2	508	456	254	1829	4.01	37.0	0.02218	370	0.00064	372	0	0	25	178	178	80.7
33		218a-2	508	456	254	1829	4.01	37.6	0.02218	370	0.00048	372	0	0	25	178	178	82.1
34		29-3	508	456	254	1829	4.01	34.3	0.02218	370	0.00097	237	0	0	25	178	178	89.0
35		318-1	508	456	254	1829	4.01	40.6	0.02218	370	0.00048	517	0	0	25	178	178	110.1
36		321-1	508	456	254	1829	4.01	38.8	0.02218	370	0.00041	517	0	0	25	178	178	81.8
37		39-2	508	456	254	1829	4.01	37.1	0.02218	370	0.00097	352	0	0	25	178	178	124.3
38		313.5-2	508	456	254	1829	4.01	39.7	0.02218	370	0.00064	352	0	0	25	178	178	117.4
39		39-3	508	456	254	1829	4.01	42.7	0.02218	370	0.00097	276	0	0	25	178	178	119.9
40		313.5-3	508	456	254	1829	4.01	42.7	0.02218	370	0.00064	276	0	0	25	178	178	106.8
41		318-3	508	456	254	1829	4.01	43.0	0.02218	370	0.00048	276	0	0	25	178	178	87.4
42		321-3	508	456	254	1829	4.01	43.0	0.02218	370	0.00041	276	0	0	25	178	178	70.3
43	Smith and Vantsiotis [1]	4D1-13	356	305	102	613	2.01	16.1	0.019286	431	0.0042	437	0.0023	437.4	12.7	102	102	87.4
44	Johnson & Ramirez [156]	1	610	539	305	1670	3.10	36.4	0.024897	525	0.00144	479	0	0	19	102	102	191.6
45		2	610	539	305	1670	3.10	36.4	0.024897	525	0.00072	479	0	0	19	102	102	222.2
46		3	610	539	305	1670	3.10	72.3	0.024897	525	0.00072	479	0	0	19	102	102	281.2
47		4	610	539	305	1670	3.10	72.3	0.024897	525	0.00072	479	0	0	19	102	102	258.5
48		5	610	539	305	1670	3.10	55.9	0.024897	525	0.00144	479	0	0	19	102	102	263.0
49		7	610	539	305	1670	3.10	51.3	0.024897	525	0.00072	479	0	0	19	102	102	339.0
50		8	610	539	305	1670	3.10	51.3	0.024897	525	0.00072	479	0	0	19	102	102	383.2
51	Roller & Russell [175]	S1	635	559	356	1397	2.50	120.1	0.015879	472	0.0074	407	0	0	12.7	150	200	297.8
52		S2	679	559	356	1397	2.50	120.1	0.028884	431	0.0043	448	0	0	12.7	150	200	1099.3
53		S3	718	559	356	1397	2.50	120.1	0.043326	431	0.0088	458	0	0	12.7	150	200	1657.9
54		S4	718	559	356	1397	2.50	120.1	0.057768	431	0.0125	458	0	0	12.7	150	200	1943.4
55		S5	743	559	356	1397	2.50	120.1	0.066994	460	0.0175	458	0	0	12.7	150	200	2238.5

190

#	Author	Speci men	h (mm)	d (mm)	b (mm)	a (mm)	a/d	f_{ck} (MPa)	ρ	f_{sk} (MPa)	ρ_v	f_{yw} (MPa)	ρ_h	f_{sh} (Mpa)	d_a (mm)	Top plate width (mm)	Bottom plate width(mm)	Vexp. (kN)
56		S6	870	762	457	2286	3.00	72.0	0.016506	464	0.00082	445	0	0	12.7	150	200	665.2
57		S7	870	762	457	2286	3.00	72.0	0.018189	483	0.00158	445	0	0	12.7	150	200	787.7
58		S8	870	762	457	2286	3.00	125.0	0.018189	483	0.00082	445	0	0	12.7	150	200	482.7
59		S9	870	762	457	2286	3.00	125.0	0.022735	483	0.00158	445	0	0	12.7	150	200	749.3
60		S10	870	762	457	2286	3.00	125.0	0.02751	464	0.00233	445	0	0	12.7	150	200	1172.0
61	Xie et al. [50]	NNW-3	254	203	127	609	3.00	42.9	0.032032	421	0.0049	324	0	0	19	15	15	87.0
62		NHW-3	254	198	127	594	3.00	103.4	0.045156	421	0.0051	324	0	0	19	15	15	102.4
63		NHW-3a	254	198	127	594	3.00	94.8	0.045156	421	0.0065	324	0	0	19	15	15	108.2
64		NHW-3b	254	198	127	594	3.00	108.7	0.045156	421	0.0078	324	0	0	19	15	15	122.5
65		NHW-4	254	198	127	792	4.00	104.1	0.045156	421	0.0051	324	0	0	19	15	15	93.7
66	Yoon et al. [61]	N1-N	750	655	375	2150	3.28	36.0	0.02878	400	0.00081	430	0	0	20	150	150	457.0
67		N2-S	750	655	375	2150	3.28	36.0	0.02878	400	0.00081	430	0	0	20	150	150	363.0
68		N2-N	750	655	375	2150	3.28	36.0	0.02878	400	0.00116	430	0	0	20	150	150	483.0
69		M1-N	750	655	375	2150	3.28	67.0	0.02878	400	0.00081	430	0	0	10	150	150	405.0
70		M2-S	750	655	375	2150	3.28	67.0	0.02878	400	0.00116	430	0	0	10	150	150	552.0
71		M2-N	750	655	375	2150	3.28	67.0	0.02878	400	0.00163	430	0	0	10	150	150	689.0
72		H1-N	750	655	375	2150	3.28	87.0	0.02878	400	0.00081	430	0	0	10	150	150	483.0
73		H2-S	750	655	375	2150	3.28	87.0	0.02878	400	0.0014	430	0	0	10	150	150	598.0
74		H2-N	750	655	375	2150	3.28	87.0	0.02878	400	0.00233	430	0	0	10	150	150	721.0
75	Kong & Rangan [57]	S1-1	350	292	250	730	2.50	63.6	0.028027	452	0.00157	569	0	0	7	100	100	228.3
76		S1-2	350	292	250	730	2.50	63.6	0.028027	452	0.00157	569	0	0	7	100	100	208.3
77		S1-3	350	292	250	730	2.50	63.6	0.028027	452	0.00157	569	0	0	7	100	100	206.1
78		S1-4	350	292	250	730	2.50	63.6	0.028027	452	0.00157	569	0	0	7	100	100	277.9
79		S1-5	350	292	250	730	2.50	63.6	0.028027	452	0.00157	569	0	0	7	100	100	253.3
80		S1-6	350	292	250	730	2.50	63.6	0.028027	452	0.00157	569	0	0	7	100	100	224.1
81		S2-1	350	292	250	730	2.50	72.5	0.028027	452	0.00105	569	0	0	7	100	100	260.3
82		S2-2	350	292	250	730	2.50	72.5	0.028027	452	0.00126	569	0	0	7	100	100	232.5
83		S2-3	350	292	250	730	2.50	72.5	0.028027	452	0.00157	569	0	0	7	100	100	253.3
84		S2-4	350	292	250	730	2.50	72.5	0.028027	452	0.00157	569	0	0	7	100	100	219.4
85		S2-5	350	292	250	730	2.50	72.5	0.028027	452	0.00209	569	0	0	7	100	100	282.1
86		S3-1	350	297	250	740	2.49	67.4	0.016593	450	0.00101	632	0	0	7	100	100	209.2
87		S3-2	350	297	250	740	2.49	67.4	0.016593	450	0.00101	632	0	0	7	100	100	178.0
88		S3-3	350	293	250	730	2.49	67.4	0.027932	452	0.00101	632	0	0	7	100	100	228.6
89		S3-4	350	293	250	730	2.49	67.4	0.027932	452	0.00101	632	0	0	7	100	100	174.9
90		S3-5	350	299	250	720	2.41	67.4	0.036923	442	0.00101	632	0	0	7	100	100	296.6
91		S3-6	350	299	250	720	2.41	67.4	0.036923	442	0.00101	632	0	0	7	100	100	282.9
92		S4-1	600	542	250	1300	2.40	87.3	0.030199	452	0.00157	569	0	0	7	100	100	354.0

#	Author	Specimen	h (mm)	d (mm)	b (mm)	a (mm)	a/d	f_{ck} (MPa)	ρ	f_{sk} (MPa)	ρ_v	f_{yv} (MPa)	ρ_h	f_{sh} (Mpa)	d_a (mm)	Top plate width (mm)	Bottom plate width(mm)	Vexp. (kN)
93		S4-2	500	444	250	1070	2.41	87.3	0.029586	433	0.00157	569	0	0	7	100	100	572.8
94		S4-3	400	346	250	830	2.40	87.3	0.028486	450	0.00157	569	0	0	7	100	100	243.4
95		S4-4	350	292	250	730	2.50	87.3	0.028027	452	0.00157	569	0	0	7	100	100	258.1
96		S4-6	250	198	250	500	2.53	87.3	0.027879	442	0.00157	569	0	0	7	100	100	202.9
97		S5-1	350	292	250	880	3.01	89.4	0.028027	452	0.00157	569	0	0	7	100	100	241.7
98		S5-2	350	292	250	800	2.74	89.4	0.028027	452	0.00157	569	0	0	7	100	100	259.9
99		S5-3	350	292	250	730	2.50	89.4	0.028027	452	0.00157	569	0	0	7	100	100	243.8
100		S6-3	350	293	250	800	2.73	68.9	0.027932	452	0.00101	632	0	0	7	100	100	178.4
101		S6-4	350	293	250	800	2.73	68.9	0.027932	452	0.00101	632	0	0	7	100	100	214.4
102		S6-5	350	299	250	790	2.64	68.9	0.036923	442	0.00101	632	0	0	7	100	100	297.0
103		S6-6	350	299	250	790	2.64	68.9	0.036923	442	0.00101	632	0	0	7	100	100	287.2
104		S7-1	350	294	250	970	3.30	74.8	0.04468	433	0.00105	569	0	0	7	100	100	217.2
105		S7-2	350	294	250	970	3.30	74.8	0.04468	433	0.00126	569	0	0	7	100	100	205.4
106		S7-3	350	294	250	970	3.30	74.8	0.04468	433	0.00157	569	0	0	7	100	100	246.5
107		S7-4	350	294	250	970	3.30	74.8	0.04468	433	0.00196	569	0	0	7	100	100	273.6
108		S7-5	350	294	250	970	3.30	74.8	0.04468	433	0.00224	569	0	0	7	100	100	304.4
109		S7-6	350	294	250	970	3.30	74.8	0.04468	433	0.00262	569	0	0	7	100	100	310.6
110		S8-1	350	292	250	730	2.50	74.6	0.028027	452	0.00105	569	0	0	7	100	100	272.1
111		S8-2	350	292	250	730	2.50	74.6	0.028027	452	0.00126	569	0	0	7	100	100	250.9
112		S8-3	350	292	250	730	2.50	74.6	0.028027	452	0.00157	569	0	0	7	100	100	309.6
113		S8-4	350	292	250	730	2.50	74.6	0.028027	452	0.00157	569	0	0	7	100	100	265.8
114		S8-5	350	292	250	730	2.50	74.6	0.028027	452	0.00196	569	0	0	7	100	100	289.2
115		S8-6	350	292	250	730	2.50	74.6	0.028027	452	0.00224	569	0	0	7	100	100	283.9
116	Collins and Kuchma [165]	BM100	1000	925	300	2700	2.92	47.0	0.007568	550	0.00078	508	0	0	10	152	152	342.0
117		BM100D	1000	925	300	2700	2.92	47.0	0.01045	550	0.00078	508	0	0	10	152	152	461.0
118	Shin et al. [123]	MHB 2.5-25	250	215	125	538	2.50	52.0	0.037693	414	0.0025	414	0	0	19	45	45	98.6
119		MHB 2.5-50	250	215	125	538	2.50	52.0	0.037693	414	0.0047	414	0	0	19	45	45	138.7
120		MHB 2.5-75	250	215	125	538	2.50	52.0	0.037693	414	0.0071	414	0	0	19	45	45	159.4
121		MHB 2.5-100	250	215	125	538	2.50	52.0	0.037693	414	0.0094	414	0	0	19	45	45	164.2
122		HB2.5-25	250	215	125	538	2.50	73.0	0.037693	414	0.0024	414	0	0	13	45	45	115.6
123		HB2.5-50	250	215	125	538	2.50	73.0	0.037693	414	0.0047	414	0	0	13	45	45	148.9
124		HB2.5-75	250	215	125	538	2.50	73.0	0.037693	414	0.0071	414	0	0	13	45	45	166.9
125		HB2.5-100	250	215	125	538	2.50	73.0	0.037693	414	0.0094	414	0	0	13	45	45	183.8
126	Yoshida [166]	YB2000/4	2000	1890	300	5400	2.86	33.6	0.007407	435	0.00078	470	0	0	10	300	300	674.0
127		YB2000/6	2000	1890	300	5400	2.86	35.9	0.007407	435	0.00071	465	0	0	10	300	300	550.0

#	Author	Specimen	h (mm)	d (mm)	b (mm)	a (mm)	a/d	f_{ck} (MPa)	ρ	f_{sk} (MPa)	ρ_r	f_w (MPa)	ρ_b	f_{sh} (Mpa)	d_a (mm)	Top plate width (mm)	Bottom plate width(mm)	Vexp. (kN)
128		YB2000/9	2000	1890	300	5400	2.86	36.4	0.007407	435	0.00071	468	0	0	10	300	300	472.0
129	Angelakos et al. [48]	DB0.530M	1000	925	300	2700	2.92	32.0	0.005045	550	0.00078	508	0	0	10	152	152	263.0
130		DB120M	1000	925	300	2700	2.92	21.0	0.01009	550	0.00078	508	0	0	10	152	152	282.0
131		DB140M	1000	925	300	2700	2.92	38.0	0.01009	550	0.00078	508	0	0	10	152	152	277.0
132		DB165M	1000	925	300	2700	2.92	65.0	0.01009	550	0.00078	508	0	0	10	152	152	452.0
133		DB180M	1000	925	300	2700	2.92	80.0	0.01009	550	0.00078	508	0	0	10	152	152	395.0
134	Cao [167]	SB2003/6	2000	1890	300	5400	2.86	30.8	0.0036	435	0.00071	483	0	0	10	300	300	350.0
135		SB201 2/6	2000	1890	300	5400	2.86	27.5	0.015196	435	0.00071	483	0	0	10	300	300	635.0
136	Rahal & Al-Shaleh [55]	A65-200	370	325	200	900	2.77	60.9	0.021938	483	0.00141	240	0	0	12	10	10	175.0
137		A65-140	370	325	200	900	2.77	62.1	0.021938	483	0.00201	240	0	0	12	10	10	150.0
138		A65-110	370	325	200	900	2.77	60.9	0.021938	483	0.00257	240	0	0	12	10	10	188.0
139		A65-95	370	325	200	900	2.77	62.1	0.021938	483	0.00297	240	0	0	12	10	10	220.0
140		B65-200	370	300	200	900	3.00	64.3	0.039548	483	0.00141	240	0	0	12	10	10	195.0
141		B65-160	370	300	200	900	3.00	65.1	0.039548	483	0.00176	240	0	0	12	10	10	208.0
142		B65-140	370	300	200	900	3.00	65.1	0.039548	483	0.00201	240	0	0	12	10	10	235.0
143		B65-125	370	300	200	900	3.00	66.4	0.039548	483	0.00226	240	0	0	12	10	10	242.0
144		B65-110	370	300	200	900	3.00	66.4	0.039548	483	0.00257	240	0	0	12	10	10	270.0
145	Cladera and Marí [170]	H50/2	400	353	200	1080	3.06	49.9	0.022776	500	0.0011	530	0	0	12	150	150	177.6
146		H50/3	400	351	200	1080	3.08	49.9	0.022906	500	0.00239	540	0	0	12	150	150	242.1
147		H50/4	400	351	200	1080	3.08	49.9	0.029886	500	0.00239	540	0	0	12	150	150	246.3
148		H50/5	400	359	200	1080	3.01	49.9	0.022396	500	0	0	0.0045	540	12	150	150	129.7
149		H60/2	400	353	200	1080	3.06	60.8	0.022776	500	0.0014	530	0	0	12	150	150	179.7
150		H60/3	400	351	200	1080	3.08	60.8	0.022906	500	0.00239	530	0	0	12	150	150	258.8
151		H60/4	400	351	200	1080	3.08	60.8	0.029886	500	0.00239	530	0	0	12	150	150	308.7
152		H75/2	400	353	200	1080	3.06	68.9	0.022776	500	0.0014	530	0	0	12	150	150	203.9
153		H75/3	400	351	200	1080	3.08	68.9	0.022906	500	0.00239	530	0	0	12	150	150	269.4
154		H75/4	400	351	200	1080	3.08	68.9	0.029886	500	0.00239	530	0	0	12	150	150	255.2
155		H100/2	400	353	200	1080	3.06	87.0	0.022776	500	0.0017	530	0	0	12	150	150	225.6
156		H100/3	400	351	200	1080	3.08	87.0	0.022906	500	0.00239	540	0	0	12	150	150	253.6
157		H100/4	400	351	200	1080	3.08	87.0	0.029886	500	0.00239	540	0	0	12	150	150	266.5
158		H100/5	400	359	200	1080	3.01	87.0	0.022396	500	0	0	0.0045	540	12	150	150	140.1

193

Table A-3-Deep beams without shear reinforcement

#	Author	Specimen	h (mm)	d (mm)	b (mm)	a (mm)	a/d	f_{ck} (MPa)	ρ	f_{yk} (MPa)	d_a (mm)	Top plate width (mm)	Bottom plate width (mm)	$V_{exp.}$ (kN)
1	Moody et al. [104]	III-24a	610	533	178	831	1.56	17.8	0.0272	483	25	203	203	296.5
2		III-24b	610	533	178	831	1.56	20.6	0.0272	483	25	203	203	303.2
3		III-25a	610	533	178	831	1.56	24.3	0.0346	483	25	203	203	267.6
4		III-25b	610	533	178	831	1.56	17.2	0.0346	483	25	203	203	289.8
5		III-26a	610	533	178	831	1.56	21.7	0.0425	483	25	203	203	421.1
6		III-26b	610	533	178	831	1.56	20.6	0.0425	483	25	203	203	396.6
7		III-27a	610	533	178	831	1.56	21.4	0.0272	483	25	203	203	347.7
8		III-27b	610	533	178	831	1.56	22.9	0.0272	483	25	203	203	356.6
9		III-28a	610	533	178	831	1.56	23.3	0.0346	483	25	203	203	303.2
10		III-28b	610	533	178	831	1.56	22.4	0.0346	483	25	203	203	341.0
11		III-29a	610	533	178	831	1.56	21.7	0.0425	483	25	203	203	389.9
12		III-29b	610	533	178	831	1.56	25.0	0.0425	483	25	203	203	436.6
13	Moody et al. [105]	I-g	381	298	178	406	1.36	30.6	0.0095	483	25	203	203	133.4
14		I-h	381	298	178	406	1.36	24.4	0.0147	483	25	203	203	132.0
15		I-i	381	305	178	406	1.33	22.9	0.0210	483	25	203	203	146.8
16		I-2b	381	305	178	406	1.33	18.8	0.0376	483	25	203	203	140.9
17		I-3b	381	305	178	406	1.33	20.5	0.0476	483	25	203	203	149.7
18		I-j	381	305	178	406	1.33	33.4	0.0147	483	25	203	203	155.7
19		I-k	381	305	178	406	1.33	26.6	0.0210	483	25	203	203	161.6
20		I-4a	381	305	178	406	1.33	29.8	0.0286	483	25	203	203	148.3
21		I-4b	381	305	178	406	1.33	27.9	0.0286	483	25	203	203	162.0
22		I-5a	381	305	178	406	1.33	28.0	0.0376	483	25	203	203	177.9
23		I-5b	381	305	178	406	1.33	27.9	0.0376	483	25	203	203	163.1
24		I-6a	381	305	178	406	1.33	31.4	0.0476	483	25	203	203	170.5
25		I-6b	381	305	178	406	1.33	24.6	0.0476	483	25	203	203	177.9
26		I-I	381	305	178	406	1.33	35.2	0.0147	483	25	203	203	158.6
27		I-m	381	305	178	406	1.33	30.3	0.0210	483	25	203	203	155.7
28		I-7a	381	305	178	406	1.33	33.0	0.0286	483	25	203	203	170.5
29		I-7b	381	305	178	406	1.33	34.5	0.0286	483	25	203	203	178.3

#	Author	Specimen	h (mm)	d (mm)	b (mm)	a (mm)	a/d	f_{ck} (MPa)	ρ	f_{yk} (MPa)	d_a (mm)	Top plate width (mm)	Bottom plate width (mm)	$V_{exp.}$ (kN)
30		I-8a	381	305	178	406	1.33	33.0	0.0376	483	25	203	203	215.0
31		I-8b	381	305	178	406	1.33	32.3	0.0376	483	25	203	203	163.1
32		I-9a	381	305	178	406	1.33	36.3	0.0476	483	25	203	203	192.7
33		I-9b	381	305	178	406	1.33	32.1	0.0476	483	25	203	203	192.7
34		I-n	381	305	178	406	1.33	36.1	0.0147	483	25	203	203	175.0
35		I-o	381	305	178	406	1.33	34.8	0.0210	483	25	203	203	189.8
36		I-p	381	305	178	406	1.33	41.2	0.0286	483	25	203	203	197.2
37		I-q	381	305	178	406	1.33	33.7	0.0376	483	25	203	203	192.7
38		I-r	381	305	178	406	1.33	40.9	0.0476	483	25	203	203	207.6
39		II-18a	610	533	178	406	0.76	15.0	0.0282	483	25	203	203	326.2
40		II-19a	610	533	178	406	0.76	20.9	0.0346	483	25	203	203	357.3
41		II-19b	610	533	178	406	0.76	22.3	0.0346	483	25	203	203	394.7
42		II-20a	610	533	178	406	0.76	19.9	0.0425	483	25	203	203	348.4
43		II-20b	610	533	178	406	0.76	20.4	0.0425	483	25	203	203	369.2
44		IV-g	381	305	178	610	2.00	23.4	0.0095	483	25	203	203	80.1
45		IV-h	381	305	178	610	2.00	25.9	0.0147	483	25	203	203	89.0
46		IV-i	381	305	178	610	2.00	24.1	0.0210	483	25	203	203	86.4
47		IV-j	381	305	178	610	2.00	24.8	0.0286	483	25	203	203	105.5
48		IV-k	381	305	178	610	2.00	25.0	0.0376	483	25	203	203	111.8
49		IV-I	381	305	178	610	2.00	27.0	0.0476	483	25	203	203	102.9
50		V-b	381	305	178	406	1.33	26.0	0.0147	483	25	203	203	194.9
51		V-d	381	305	178	406	1.33	24.8	0.0286	483	25	203	203	213.4
52		V-f	381	305	178	406	1.33	23.3	0.0476	483	25	203	203	210.5
53		VI-a	381	305	178	542	1.78	28.2	0.0095	483	25	203	203	102.7
54		VI-b	381	305	178	542	1.78	28.7	0.0147	483	25	203	203	172.1
55		VI-c	381	305	178	542	1.78	24.7	0.0210	483	25	203	203	146.8
56		VI-d	381	305	178	542	1.78	26.9	0.0286	483	25	203	203	157.5
57		VI-e	381	305	178	542	1.78	28.4	0.0376	483	25	203	203	170.8
58		VI-f	381	305	178	542	1.78	38.4	0.0210	483	25	203	203	186.8
59		VI-g	381	305	178	542	1.78	38.1	0.0286	483	25	203	203	173.5
60		VI-h	381	305	178	542	1.78	36.6	0.0376	483	25	203	203	206.8

#	Author	Specimen	h (mm)	d (mm)	b (mm)	a (mm)	a/d	f_{ck} (MPa)	ρ	f_{yk} (MPa)	d_a (mm)	Top plate width (mm)	Bottom plate width (mm)	$V_{exp.}$ (kN)
61		VI-i	381	305	178	542	1.78	41.5	0.0476	483	25	203	203	194.8
62	Morrow & Viest [106]	B14-E2	410	375	305	356	0.95	12.7	0.0057	483	6	102	102	278.0
63		B14-A4	406	362	305	356	0.98	22.6	0.0250	483	6	102	102	511.5
64		B14-B4	406	368	305	356	0.97	26.3	0.0185	483	6	102	102	500.4
65		B14-E4	406	368	305	356	0.97	28.9	0.0124	483	6	102	102	511.5
66		B14-A6	406	356	305	356	1.00	45.4	0.0383	483	6	102	102	900.7
67		B14-B6	406	368	305	356	0.97	46.8	0.0185	483	6	102	102	778.4
68		B21-B2	406	367	305	533	1.45	13.9	0.0186	483	6	102	102	238.5
69		B21-E2	406	375	305	533	1.42	11.3	0.0057	483	6	102	102	211.7
70		B21-A4	406	368	305	533	1.45	29.8	0.0246	483	6	102	102	523.1
71		B21-B4	406	368	305	533	1.45	27.1	0.0185	483	6	102	102	396.4
72		B21-E4	406	365	305	533	1.46	24.2	0.0124	483	6	102	102	423.0
73		B21-E4R	406	368	305	533	1.45	31.9	0.0124	483	6	102	102	434.2
74		B21-F4	406	370	305	533	1.44	31.4	0.0117	483	6	102	102	467.6
75		B21-A6	406	356	305	533	1.50	45.3	0.0383	483	6	102	102	578.8
76		B21-B6	406	375	305	533	1.42	45.5	0.0182	483	6	102	102	578.7
77		B28-B2	406	362	305	711	1.96	14.7	0.0188	483	6	102	102	201.2
78		B28-E2	406	372	305	711	1.91	13.7	0.0057	483	6	102	102	130.0
79		B28-A4	406	368	305	711	1.93	27.5	0.0246	483	6	102	102	323.5
80		B28-B4	406	368	305	711	1.93	32.3	0.0185	483	6	102	102	256.8
81		B28-E4	406	368	305	711	1.93	33.1	0.0124	483	6	102	102	267.9
82		B28-B6	406	368	305	711	1.93	43.9	0.0185	483	6	102	102	323.5
83	Chang & Kesler [107]	IIIA2	152	137	102	254	1.85	14.9	0.0237	328	25	64	64	20.7
84	Watstein & Mathey [108]	B-18-1	457	404	203	610	1.51	25.4	0.0305	267	25	89	89	311.4
85		C-18-1	457	404	203	610	1.51	25.6	0.0185	490	25	89	89	289.1
86		C-18-2	457	404	203	610	1.51	26.4	0.0188	466	25	89	89	311.4
87		D-18-1	457	404	203	610	1.51	25.7	0.0117	724	25	89	89	266.9
88		D-18-2	457	404	203	610	1.51	27.0	0.0116	669	25	89	89	266.9
89		E-18-1	457	404	203	610	1.51	22.4	0.0075	686	25	89	89	220.8

#	Author	Specimen	h (mm)	d (mm)	b (mm)	a (mm)	a/d	f_{ck} (MPa)	ρ	f_{yk} (MPa)	d_a (mm)	Top plate width (mm)	Bottom plate width (mm)	$V_{exp.}$ (kN)
90		E-18-2	457	404	203	610	1.51	26.7	0.0075	688	25	89	89	222.4
91	Rodriqez et al. [109]	E6N1	368	318	152	432	1.36	22.1	0.0159	483	25	102	102	211.1
92		E6N2	368	318	154	432	1.36	17.9	0.0159	483	25	102	102	162.5
93		E6N3	368	318	154	432	1.36	22.7	0.0159	483	25	102	102	184.6
94		C6N1	368	321	156	432	1.35	26.1	0.0159	483	25	102	102	210.4
95		C6N2	368	318	152	432	1.36	22.1	0.0159	483	25	102	102	151.8
96		C6N3	368	314	154	432	1.38	21.7	0.0159	483	25	102	102	184.8
97	de Cassio & Seiss [110]	A-11	305	254	152	508	2.00	28.3	0.0333	341	25	305	305	103.4
98		D-5	305	276	152	419	1.52	25.8	0.0135	361	25	152	152	90.5
99	Leonhardt & Walther [53]	1	320	270	190	270	1.00	32.4	0.0207	465	30	100	100	388.5
100		2	320	270	190	400	1.48	32.4	0.0207	465	30	100	100	260.0
101		3	320	270	190	540	2.00	32.4	0.0207	465	30	100	100	147.2
102		GA1	320	270	190	500	1.85	22.3	0.0182	439	30	100	100	89.5
103		GA2	320	270	190	500	1.85	22.3	0.0178	490	30	100	100	106.0
104		G6	320	270	190	500	1.85	26.1	0.0247	426	30	100	100	143.6
105		11/1	340	290	190	375	1.29	38.1	0.0193	465	30	100	100	165.8
106		11/2	346	296	190	375	1.27	38.1	0.0189	465	30	100	100	177.0
107		12/1	323	273	190	500	1.83	36.8	0.0205	465	30	100	100	144.4
108		12/2	322	272	189	500	1.84	36.7	0.0207	465	30	100	100	114.6
109	Mathey & Watstein [111]	I-1	457	403	203	610	1.51	25.4	0.0305	267	25	89	89	312.9
110		II-3	457	403	203	610	1.51	21.9	0.0188	466	25	89	89	261.8
111		II-4	457	403	203	610	1.51	26.4	0.0188	466	25	89	89	312.9
112		III-5	457	403	203	610	1.51	25.7	0.0185	490	25	89	89	288.5
113		III-6	457	403	203	610	1.51	25.6	0.0185	490	25	89	89	290.7
114		IV-7	457	403	203	610	1.51	24.1	0.0186	443	25	89	89	290.8
115		IV-8	457	403	203	610	1.51	24.9	0.0186	443	25	89	89	304.0
116		V-9	457	403	203	610	1.51	23.1	0.0116	698	25	89	89	224.0
117		V-10	457	403	203	610	1.51	27.0	0.0116	698	25	89	89	268.4
118		VI-11	457	403	203	610	1.51	25.4	0.0117	698	25	89	89	224.0
119		VI-12	457	403	203	610	1.51	25.7	0.0117	698	25	89	89	268.4
120		V-13	457	403	203	610	1.51	22.4	0.0075	712	25	89	89	222.4

#	Author	Specimen	h (mm)	d (mm)	b (mm)	a (mm)	a/d	f_{ck} (MPa)	ρ	f_{yk} (MPa)	d_a (mm)	Top plate width (mm)	Bottom plate width (mm)	$V_{exp.}$ (kN)
121		V-14	457	403	203	610	1.51	26.7	0.0075	712	25	89	89	224.0
122		VI-15	457	403	203	610	1.51	25.5	0.0075	712	25	89	89	179.5
123		VI-16	457	403	203	610	1.51	22.8	0.0075	712	25	89	89	188.6
124	de Pavia and Siess [112]	G23S-11	330	305	51	203	0.67	24.6	0.0083	463	10	98	98	89.8
125		G33S-11	229	203	76	203	1.00	23.3	0.0167	463	10	98	98	85.3
126		G34S-11	229	203	76	203	1.00	35.2	0.0167	463	10	98	98	109.8
127		G43S-11	178	152	102	203	1.34	24.2	0.0167	463	10	98	98	76.9
128		G44S-11	178	152	102	203	1.34	37.0	0.0167	463	10	98	98	83.6
129	Kani [20]	24	305	271	152	407	1.50	27.9	0.0187	396	19	152	152	182.0
130		46	152	136	151	272	2.00	25.5	0.0276	392	19	152	152	69.0
131		53	152	132	151	136	1.03	47.4	0.0284	392	19	152	152	155.2
132		54	152	136	151	136	1.00	26.7	0.0276	392	19	152	152	157.7
133		94	305	273	153	543	1.99	25.3	0.0277	352	19	152	152	110.5
134		67	610	528	157	543	1.03	30.3	0.0275	407	19	152	152	547.8
135		69	610	542	155	543	1.00	27.4	0.0267	373	19	229	229	585.4
136		72	610	549	152	1087	1.98	24.8	0.0271	384	19	152	152	196.8
137		3041	1219	1097	152	2195	2.00	26.9	0.0272	377	19	432	432	326.0
138		109	305	271	153	407	1.50	25.0	0.0076	457	19	152	152	71.9
139		113	305	274	152	408	1.49	25.5	0.0077	486	19	152	152	87.2
140		129	305	275	155	407	1.48	17.6	0.0178	348	19	152	152	143.3
141		134	305	273	154	544	1.99	17.4	0.0181	419	19	152	152	59.9
142		135	305	274	149	544	1.99	17.4	0.0186	411	19	152	152	76.8
143		142	305	276	156	544	1.97	19.3	0.0077	382	19	152	152	58.3
144		148	305	274	152	408	1.49	19.9	0.0079	382	19	152	152	79.9
145		162	305	272	153	543	2.00	34.3	0.0077	377	19	152	152	59.0
146		174	305	272	153	270	0.99	36.4	0.0051	396	19	152	152	106.5
147		178	305	269	153	407	1.51	34.5	0.0052	400	19	152	152	67.2
148		181	305	272	154	543	2.00	33.9	0.0179	390	19	152	152	95.2

#	Author	Specimen	h (mm)	d (mm)	b (mm)	a (mm)	a/d	f_{ck} (MPa)	ρ	f_{yk} (MPa)	d_a (mm)	Top plate width (mm)	Bottom plate width (mm)	$V_{exp.}$ (kN)
149		184	305	271	154	407	1.50	35.1	0.0180	394	19	152	152	163.3
150		188	305	277	153	543	1.96	33.1	0.0176	384	19	152	152	92.6
151		199	305	273	152	544	1.99	36.0	0.0183	410	19	152	152	76.8
152		201	305	274	155	272	0.99	35.2	0.0265	381	19	152	152	253.7
153		204	305	275	152	543	1.97	34.8	0.0269	369	19	152	152	147.1
154		205	305	275	153	544	1.98	35.2	0.0266	381	19	152	152	125.5
155		249	305	276	153	270	0.98	28.0	0.0049	376	19	152	152	104.1
156		250	305	274	152	406	1.48	28.0	0.0050	376	19	152	152	62.8
157		251	305	276	154	544	1.97	26.2	0.0048	391	19	152	152	41.9
158		265	305	269	153	407	1.51	18.1	0.0052	400	19	152	152	53.0
159		269	305	274	154	270	0.99	18.1	0.0049	396	19	152	152	89.0
160		270	305	273	152	542	1.99	20.1	0.0050	396	19	152	152	41.4
161	Ramakrishnan & Ananthanarayana [114]	C1	381	343	76	241	0.70	21.5	0.0076	320	19	76	76	90.1
162		K1'-R	381	343	79	345	1.01	13.7	0.0026	320	19	76	76	39.4
163	Manuel et al. [116]	1	457	406	102	122	0.30	33.8	0.0097	410	19	152	152	444.8
164		2	457	406	102	122	0.30	35.2	0.0097	410	19	152	152	444.8
165		3	457	406	102	122	0.30	30.1	0.0097	392	19	152	152	367.0
166		4	457	406	102	122	0.30	31.9	0.0097	410	19	152	152	400.3
167	Manuel [117]	1	457	406	102	102	0.25	31.7	0.0063	308	19	152	152	389.2
168		4	457	406	102	102	0.25	31.7	0.0097	404	19	152	152	453.7
169		5	457	406	102	203	0.50	31.7	0.0097	401	19	152	152	402.5
170		7	457	406	102	203	0.50	36.9	0.0138	432	19	152	152	487.1
171		10	457	406	102	366	0.90	38.1	0.0188	374	19	152	152	293.6
172		11	457	406	102	432	1.06	32.3	0.0188	374	19	152	152	273.6
173	Niwa & Maekawa [118]	T1	300	228	100	200	0.88	35.8	0.0600	364	19	140	140	314.5
174		T2	600	507	100	200	0.39	54.7	0.0300	389	19	100	100	514.0
175		T3	300	228	100	200	0.88	13.1	0.0300	364	19	100	100	114.0
176		T4	600	507	100	150	0.30	13.1	0.0300	389	19	140	140	212.5
177		T5	600	507	100	200	0.39	66.6	0.0600	389	19	140	140	881.5
178		T6	600	507	100	150	0.30	35.8	0.0600	389	19	100	100	577.5

#	Author	Specimen	h (mm)	d (mm)	b (mm)	a (mm)	a/d	f_{ck} (MPa)	ρ	f_{yk} (MPa)	d_a (mm)	Top plate width (mm)	Bottom plate width (mm)	$V_{exp.}$ (kN)
179		T7	300	228	100	150	0.66	59.9	0.0600	364	19	100	100	446.0
180	Smith and Vantsiotis [1]	0A0-44	356	305	102	235	0.77	20.5	0.0193	431	13	102	102	159.5
181		0A0-48	356	305	102	235	0.77	20.9	0.0193	431	13	102	102	156.1
182		0B0-49	356	305	102	308	1.01	21.7	0.0193	431	13	102	102	149.0
183		0C0-50	356	305	102	408	1.34	20.7	0.0193	431	13	102	102	115.7
184	Mphonde & Frantz [49]	AO-3-1	337	298	152	448	1.50	23.1	0.0334	414	10	50	50	116.1
185		AO-15-1a	337	298	152	448	1.50	79.5	0.0334	414	10	50	50	275.7
186	Rogowsky & MacGregor [119]	BM1/1.0/T2	1000	950	200	1000	1.05	26.1	0.0095	380	10	200	200	699.0
187		BM1A/1.0	1000	950	200	1000	1.05	26.4	0.0095	367	10	200	200	600.0
188		BM1/1.5/T1	800	535	200	1000	1.87	42.4	0.0112	455	10	200	200	303.0
189	Ahmad & Lue [121]	A5	254	203	127	406	2.00	66.0	0.0393	414	13	10	10	83.4
190		A11	254	208	127	416	2.00	66.0	0.0177	414	13	10	10	37.8
191		A12	254	208	127	208	1.00	66.0	0.0177	414	13	10	10	111.2
192		B5	254	202	127	404	2.00	73.0	0.0504	414	13	10	10	53.4
193		B6	254	202	127	202	1.00	73.0	0.0504	414	13	10	10	102.8
194		B11	254	208	127	416	2.00	73.0	0.0225	414	13	10	10	61.2
195		B12	254	208	127	208	1.00	73.0	0.0225	414	13	10	10	106.8
196		C6	254	184	127	184	1.00	70.0	0.0664	414	13	10	10	82.0
197		C11	254	207	127	414	2.00	70.0	0.0326	414	13	10	10	53.4
198		C12	254	207	127	207	1.00	70.0	0.0326	414	13	10	10	122.3
199	Lehwalter [122]	V111	1000	930	250	465	0.50	16.8	0.0066	420	16	232	232	849.0
200		V122	1000	930	250	465	0.50	15.8	0.0066	420	32	232	232	642.0
201		V221	1000	930	250	930	1.00	20.4	0.0108	420	16	232	232	588.0
202		V222	1000	930	250	930	1.00	15.4	0.0108	420	32	232	232	430.0
203		V311	1000	930	250	1395	1.50	17.0	0.0169	420	16	232	232	369.0
204		V321	1000	930	250	1395	1.50	16.9	0.0169	420	32	232	232	387.0
205		V322	1000	930	250	1395	1.50	15.0	0.0169	420	32	232	232	375.0
206		V611	200	160	250	80	0.50	19.9	0.0085	420	16	40	40	221.0
207		V811	200	160	250	240	1.50	20.6	0.0190	420	16	40	40	140.0

#	Author	Specimen	h (mm)	d (mm)	b (mm)	a (mm)	a/d	f_{ck} (MPa)	ρ	f_{yk} (MPa)	d_a (mm)	Top plate width (mm)	Bottom plate width (mm)	$V_{exp.}$ (kN)
208	Walraven & Lehwaalter [26]	V011	400	360	250	360	1.00	16.1	0.0113	420	8	90	90	226.0
209		V012	400	360	250	360	1.00	21.8	0.0113	420	8	90	90	322.0
210		V013	400	360	250	360	1.00	22.1	0.0113	420	8	90	90	344.0
211		V014	400	360	250	360	1.00	24.3	0.0113	420	8	90	90	425.0
212		V021	400	360	250	360	1.00	13.9	0.0113	420	16	90	90	220.0
213		V023	400	360	250	360	1.00	20.1	0.0113	420	16	90	90	347.0
214		V024	400	360	250	360	1.00	25.2	0.0113	420	16	90	90	396.0
215		V031	400	360	250	360	1.00	20.0	0.0113	420	32	90	90	323.0
216		V032	400	360	250	360	1.00	18.2	0.0113	420	32	90	90	318.0
217		V033	400	360	250	360	1.00	19.8	0.0113	420	32	90	90	246.0
218		V034	400	360	250	360	1.00	26.4	0.0113	420	32	90	90	437.0
219		V711	200	160	250	160	1.00	18.1	0.0152	420	16	40	40	165.0
220		V022	400	360	250	360	1.00	19.9	0.0113	420	16	90	90	270.0
221		V511	600	560	250	560	1.00	19.8	0.0112	420	16	140	140	350.0
222		V411	800	740	250	740	1.00	19.4	0.0110	420	16	185	185	395.0
223		V211	1000	930	250	930	1.00	20.0	0.0108	420	16	233	233	505.0
224	Xie et al. [50]	NNN-1	254	216	127	216	1.00	47.0	0.0207	421	19	15	15	155.8
225		NNN-2	254	216	127	432	2.00	41.4	0.0207	421	19	15	15	56.6
226	Tan et al. [51]	I-1/0.75	500	443	110	375	0.85	56.3	0.0258	499	10	110	110	500.0
227		II-1/1.00	500	443	110	500	1.13	77.6	0.0258	499	10	110	110	255.0
228		III-1/1.50	500	443	110	750	1.69	77.6	0.0258	499	10	110	110	185.0
229	Shin et al. [123]	MHB1.5-0	250	215	125	323	1.50	52.0	0.0377	414	19	45	45	112.9
230		MHB2.0-0	250	215	125	430	2.00	52.0	0.0377	414	19	45	45	87.9
231		HB1.5-0	250	215	125	323	1.50	73.0	0.0377	414	13	45	45	142.2
232		HB2.0-0	250	215	125	430	2.00	73.0	0.0377	414	13	45	45	99.4
233	Tan & Lu [27]	1-500/0.50	500	444	140	250	0.56	49.1	0.0260	520	10	140	140	850.0
234		1-500/0.75	500	444	140	375	0.84	42.5	0.0260	520	10	140	140	700.0

201

#	Author	Specimen	h (mm)	d (mm)	b (mm)	a (mm)	a/d	f_{ck} (MPa)	ρ	f_{yk} (MPa)	d_a (mm)	Top plate width (mm)	Bottom plate width (mm)	$V_{exp.}$ (kN)
235		1-500/1.00	500	444	140	500	1.13	37.4	0.0260	520	10	140	140	570.0
236	Pendyala & Mendis [125]	3	160	140	80	280	2.00	63.0	0.0202	410	10	10	10	31.0
237		5	160	140	80	280	2.00	87.0	0.0202	410	10	10	10	35.0
238	Adebar [124]	DF-11	1090	1000	250	2000	2.00	19.5	0.0084	550	20	150	150	330.0
239		DF-14	1090	1000	250	1750	1.75	19.5	0.0084	550	20	150	150	409.0
240		DF-15	1090	962	250	1751	1.82	20.3	0.0175	550	20	150	150	330.0
241		DF-16	1090	1000	250	1430	1.43	20.3	0.0084	550	20	150	150	380.0
242	Oh and Shin [52]	N4200	560	500	130	425	0.85	23.7	0.0156	415	16	180	130	265.2
243		H4100	560	500	130	250	0.50	49.1	0.0156	415	16	180	130	642.2
244		H4200	560	500	130	425	0.85	49.1	0.0156	415	16	180	130	401.1
245		H4300	560	500	130	625	1.25	49.1	0.0156	415	16	180	130	337.4
246		H4500	560	500	130	1000	2.00	49.1	0.0156	415	16	180	130	112.5
247	Lertsrisakulrat et al. [126]	D200	250	200	150	200	1.00	38.4	0.0191	1026	13	50	50	214.2
248		D400	450	400	150	400	1.00	35.5	0.0169	1004	13	100	100	285.3
249		D600	650	600	150	600	1.00	40.8	0.0176	1006	13	150	150	424.5
250	Yang et al. [69]	L5-40	400	355	160	200	0.56	31.4	0.0101	804	19	100	100	446.9
251		L5-60	600	555	160	300	0.54	31.4	0.0097	804	19	100	100	535.1
252		L5-60R	600	555	160	300	0.54	31.4	0.0097	804	19	100	100	479.2
253		L5-75	750	685	160	375	0.55	31.4	0.0105	804	19	100	100	596.8
254		L5-100	1000	935	160	500	0.53	31.4	0.0090	577	19	100	100	582.1
255		L10-40	400	355	160	400	1.13	31.4	0.0101	804	19	100	100	192.1
256		L10-40R	400	355	160	400	1.13	31.4	0.0101	804	19	100	100	311.6
257		L10-60	600	555	160	600	1.08	31.4	0.0097	804	19	100	100	375.3
258		L10-75	750	685	160	750	1.09	31.4	0.0105	804	19	100	100	271.5
259		L10-75R	750	685	160	750	1.09	31.4	0.0105	804	19	100	100	330.3
260		L10-100	1000	935	160	1000	1.07	78.5	0.0090	577	19	100	100	543.9
261		UH5-40	400	355	160	200	0.56	78.5	0.0101	804	19	100	100	733.0
262		UH5-60	600	555	160	300	0.54	78.5	0.0097	804	19	100	100	823.2

202

#	Author	Specimen	h (mm)	d (mm)	b (mm)	a (mm)	a/d	f_{ck} (MPa)	ρ	f_{yk} (MPa)	d_a (mm)	Top plate width (mm)	Bottom plate width (mm)	$V_{exp.}$ (kN)
263		UH5-75	750	685	160	375	0.55	78.5	0.0105	804	19	100	100	1010.4
264		UH5-100	1000	935	160	500	0.53	78.5	0.0090	577	19	100	100	1029.0
265		UH10-40	400	355	160	375	1.06	78.5	0.0101	804	19	100	100	498.8
266		UH10-40R	400	355	160	375	1.06	78.5	0.0101	804	19	100	100	385.1
267		UH10-60	600	555	160	600	1.08	78.5	0.0097	804	19	100	100	573.3
268		UH10-75	750	685	160	750	1.09	78.5	0.0105	804	19	100	100	338.1
269		UH10-75R	750	685	160	750	1.09	78.5	0.0105	804	19	100	100	360.6
270		UH10-100	1000	935	160	1000	1.07	78.5	0.0090	577	19	100	100	769.3
271	Tan et al. [29]	1-500/1.5	500	444	140	750	1.69	41.8	0.0260	620	15	150	150	340.0
272		2-1000/1.5	1000	884	140	1500	1.70	39.4	0.0260	620	15	150	150	470.0
273		3-1400/1.5	1400	1243	140	2100	1.69	44.1	0.0260	620	15	150	150	690.0
274		4-1750/1.5	1750	1559	140	2625	1.68	43.4	0.0260	620	15	150	150	470.0
275	Seliem et al. [127]	G-1.9-51	915	850	460	1640	1.93	51.0	0.0072	468	19	230	230	744.1
276		M-1.9-51	915	850	460	1640	1.93	51.0	0.0044	865	19	230	230	788.6
277		M-1.9-38	915	850	460	1640	1.93	38.0	0.0044	865	19	230	230	690.6
278	Zhang and Tan [31]	2DB35	350	314	80	345	1.10	27.4	0.0125	469	10	53	53	85.0
279		2DB50	500	459	80	505	1.10	32.4	0.0115	500	10	75	75	135.5
280		2DB70	700	650	80	715	1.10	24.8	0.0128	508	10	105	105	155.5
281		2DB100	1000	926	80	1019	1.10	30.6	0.0126	508	10	150	150	241.5
282		3DB35b	350	314	80	345	1.10	27.4	0.0125	469	10	53	53	85.0
283		3DB50b	500	454	115	499	1.10	28.3	0.0128	508	10	75	75	167.0
284		3DB70b	700	642	160	706	1.10	28.7	0.0122	520	10	105	105	360.5
285		3DB100b	1000	904	230	994	1.10	29.3	0.012	540	10	150	150	672.0

#	Author	Specimen	h (mm)	d (mm)	b (mm)	a (mm)	a/d	f_{ck} (MPa)	ρ	f_{yk} (MPa)	d_a (mm)	Top plate width (mm)	Bottom plate width (mm)	$V_{exp.}$ (kN)
286	Tan et al. [32]	*1-500/0.75	500	444	140	375	0.84	42.5	0.0260	530	15	150	150	700.0
287		*2-1000/0.75	1000	884	140	750	0.85	32.7	0.0260	530	15	150	150	650.0
288		*3-1400/0.75	1400	1243	140	1050	0.84	36.2	0.0260	530	15	150	150	950.0
289		*4-1750/0.75	1750	1559	140	1313	0.84	40.4	0.0260	530	15	150	150	1240.0
290	Current Research	A1	400	330	100	550	1.67	85.2	0.0365	364	13	100	100	176.6
291		D1	400	330	100	550	1.67	58.2	0.0365	364	13	100	100	148.2
292		E1	400	330	100	425	1.29	58.2	0.0365	364	13	100	100	207.5
293		F1	400	330	100	300	0.91	60.5	0.0365	364	13	100	100	270.8
294		H2	375	328	150	540	1.65	35.8	0.0138	500	15	80	80	158.0
295		H3	250	219	150	360	1.64	35.8	0.0138	500	15	80	80	127.0

Table A-4-Deep beams with shear reinforcement

#	Author	Specimen	h (mm)	d (mm)	b (mm)	a (mm)	a/d	f_{ck} (MPa)	ρ	f_{sk} (MPa)	ρ_r	f_{sv} (MPa)	ρ_h	f_{sh} (MPa)	d_a (mm)	Top plate width (mm)	Bottom plate width(mm)	$V_{exp.}$ (kN)
1	Clark [103]	B2-2	457	382	203	762	2.00	26.3	0.0316	321	0.0037	331	0	0	15	89	89	322.2
2		B6-1	457	393	203	762	1.94	42.1	0.0307	321	0.0037	331	0	0	15	89	89	379.3
3		C1-1	457	391	203	610	1.56	25.7	0.0206	321	0.0034	331	0	0	15	89	89	277.7
4		C1-2	457	391	203	610	1.56	26.3	0.0206	321	0.0034	331	0	0	15	89	89	311.1
5		C1-3	457	389	203	610	1.57	22.0	0.0207	321	0.0034	331	0	0	15	89	89	254.9
6		C1-4	457	394	203	610	1.55	29.0	0.0204	321	0.0034	331	0	0	15	89	89	285.9
7		C2-1	457	389	203	610	1.57	23.7	0.0207	321	0.0069	331	0	0	15	89	89	289.9
8		C2-2	457	390	203	610	1.56	25.0	0.0206	321	0.0069	331	0	0	15	89	89	301.1
9		C2-4	457	392	203	610	1.55	27.0	0.0205	321	0.0069	331	0	0	15	89	89	288.2
10		C3-1	457	376	203	610	1.62	14.1	0.0214	321	0.0034	331	0	0	15	89	89	223.7
11		C3-2	457	375	203	610	1.63	13.8	0.0215	321	0.0034	331	0	0	15	89	89	200.3
12		C3-3	457	376	203	610	1.62	13.9	0.0214	321	0.0034	331	0	0	15	89	89	188.1
13		C4-1	457	379	203	610	1.61	24.5	0.0318	321	0.0034	331	0	0	15	89	89	309.3
14		C6-2	457	395	203	610	1.54	45.2	0.0306	321	0.0034	331	0	0	15	89	89	423.8

#	Author	Specimen	h (mm)	d (mm)	b (mm)	a (mm)	a/d	f_{ck} (MPa)	ρ	f_{sk} (MPa)	ρ_v	f_{yv} (MPa)	ρ_h	f_{sh} (MPa)	d_a (mm)	Top plate width (mm)	Bottom plate width(mm)	Vexp. (kN)
15		C6-3	457	395	203	610	1.54	44.7	0.0306	321	0.0034	331	0	0	15	89	89	434.9
16		C6-4	457	396	203	610	1.54	47.6	0.0305	321	0.0034	331	0	0	15	89	89	428.6
17		D1-1	457	397	203	457	1.15	20.2	0.0162	335	0.0046	331	0	0	15	89	89	310.1
18		D1-3	457	395	203	457	1.16	20.6	0.0163	335	0.0046	331	0	0	15	89	89	286.6
19		D2-1	457	395	203	457	1.16	21.4	0.0163	335	0.0061	331	0	0	15	89	89	298.9
20		D2-2	457	397	203	457	1.15	23.9	0.0162	335	0.0061	331	0	0	15	89	89	321.2
21		D3-1	457	390	203	457	1.17	28.2	0.0247	335	0.0092	331	0	0	15	89	89	394.9
22		D4-1	457	394	203	457	1.16	23.1	0.0163	335	0.0122	331	0	0	15	89	89	312.2
23		D1-6	381	317	152	610	1.92	27.7	0.0339	321	0.0046	331	0	0	15	89	89	174.7
24		D1-7	381	317	152	610	1.92	28.0	0.0339	321	0.0046	331	0	0	15	89	89	179.2
25		D1-8	381	317	152	610	1.92	27.8	0.0339	321	0.0046	331	0	0	15	89	89	185.8
26		E1-2	381	319	152	635	1.99	30.2	0.0337	321	0.0073	331	0	0	15	89	89	221.8
27	Moody et al. [104]	III-30	610	533	178	831	1.56	25.0	0.0425	483	0.0052	483	0	0	25	203	203	478.2
28		III-31	610	533	178	831	1.56	25.0	0.0425	483	0.0052	483	0	0	25	203	203	507.1
29	Kong et al. [115]	B1-30	762	724	76	254	0.35	21.5	0.0052	287	0.0245	280	0	0	10	76	76	238.9
30		B1-25	635	597	76	254	0.43	24.6	0.0063	287	0.0245	280	0	0	10	76	76	224.2
31		B1-20	508	470	76	254	0.54	21.2	0.0080	287	0.0245	280	0	0	10	76	76	189.5
32		B1-15	381	343	76	254	0.74	21.2	0.0109	287	0.0245	280	0	0	10	76	76	164.1
33		B1-10	254	216	76	254	1.18	21.7	0.0174	287	0.0245	280	0	0	10	76	76	89.4
34		B2-30	762	724	76	254	0.35	19.2	0.0052	287	0.0086	303	0	0	10	76	76	249.1
35		B2-25	635	597	76	254	0.43	18.6	0.0063	287	0.0086	303	0	0	10	76	76	224.2
36		B2-20	508	470	76	254	0.54	19.9	0.0080	287	0.0086	303	0	0	10	76	76	215.3
37		B2-15	381	343	76	254	0.74	22.8	0.0109	287	0.0086	303	0	0	10	76	76	139.7
38		B2-10	254	216	76	254	1.18	20.1	0.0174	287	0.0086	303	0	0	10	76	76	99.6
39		B3-30	762	724	76	254	0.35	22.6	0.0052	287	0	0	0.0245	280	10	76	76	276.2
40		B3-25	635	597	76	254	0.43	21.0	0.0063	287	0	0	0.0245	280	10	76	76	225.5
41		B3-20	508	470	76	254	0.54	19.2	0.0080	287	0	0	0.0245	280	10	76	76	207.7
42		B3-15	381	343	76	254	0.74	21.9	0.0109	287	0	0	0.0245	280	10	76	76	159.2
43		B3-10	254	216	76	254	1.18	22.6	0.0174	287	0	0	0.0245	280	10	76	76	86.3
44		B4-30	762	724	76	254	0.35	22.0	0.0052	287	0	0	0.0086	303	10	76	76	242.0
45		B4-25	635	597	76	254	0.43	21.0	0.0063	287	0	0	0.0086	303	10	76	76	201.1
46		B4-20	508	470	76	254	0.54	20.1	0.0080	287	0	0	0.0086	303	10	76	76	180.6
47		B4-15	381	343	76	254	0.74	22.0	0.0109	287	0	0	0.0086	303	10	76	76	109.4
48		B4-10	254	216	76	254	1.18	22.6	0.0174	287	0	0	0.0086	303	10	76	76	95.6
49		B5-30	762	724	76	254	0.35	18.6	0.0052	287	0.0061	280	0.0061	280	10	76	76	239.3
50		B5-25	635	597	76	254	0.43	19.2	0.0063	287	0.0061	280	0.0061	280	10	76	76	208.2
51		B5-20	508	470	76	254	0.54	20.1	0.0080	287	0.0061	280	0.0061	280	10	76	76	172.6
52		B5-15	381	343	76	254	0.74	21.9	0.0109	287	0.0061	280	0.0061	280	10	76	76	127.2

205

#	Author	Specimen	h (mm)	d (mm)	b (mm)	a (mm)	a/d	f_{ck} (MPa)	ρ	f_{sh} (MPa)	ρ_v	f_{sv} (MPa)	ρ_h	f_{sh} (MPa)	d_a (mm)	Top plate width (mm)	Bottom plate width(mm)	Vexp. (kN)
53		B5-10	254	216	76	254	1.18	22.6	0.0174	287	0.0061	280	0.0061	280	10	76	76	97.8
54	Smith and Vantsiotis [1]	1A1-10	356	305	102	235	0.77	18.7	0.0193	431	0.0028	437	0.0023	437	13	102	102	161.2
55		1A3-11	356	305	102	235	0.77	18.0	0.0193	431	0.0028	437	0.0045	437	13	102	102	148.3
56		1A4-12	356	305	102	235	0.77	16.1	0.0193	431	0.0028	437	0.0068	437	13	102	102	141.2
57		1A4-51	356	305	102	235	0.77	20.6	0.0193	431	0.0028	437	0.0068	437	13	102	102	170.9
58		1A6-37	356	305	102	235	0.77	21.1	0.0193	431	0.0028	437	0.0091	437	13	102	102	184.1
59		2A1-38	356	305	102	235	0.77	21.7	0.0193	431	0.0063	437	0.0023	437	13	102	102	174.5
60		2A3-39	356	305	102	235	0.77	19.8	0.0193	431	0.0063	437	0.0045	437	13	102	102	170.6
61		2A4-40	356	305	102	235	0.77	20.3	0.0193	431	0.0063	437	0.0068	437	13	102	102	171.9
62		2A6-41	356	305	102	235	0.77	19.1	0.0193	431	0.0063	437	0.0091	437	13	102	102	161.9
63		3A1-42	356	305	102	235	0.77	18.4	0.0193	431	0.0125	437	0.0023	437	13	102	102	161.0
64		3A3-43	356	305	102	235	0.77	19.2	0.0193	431	0.0125	437	0.0045	437	13	102	102	172.7
65		3A4-45	356	305	102	235	0.77	20.8	0.0193	431	0.0125	437	0.0068	437	13	102	102	178.5
66		3A6-46	356	305	102	235	0.77	19.9	0.0193	431	0.0125	437	0.0091	437	13	102	102	168.1
67		1BI-01	356	305	102	308	1.01	20.1	0.0193	431	0.0024	437	0.0023	437	13	102	102	147.5
68		1 B3-29	356	305	102	308	1.01	20.1	0.0193	431	0.0024	437	0.0045	437	13	102	102	143.6
69		1B4-30	356	305	102	308	1.01	20.8	0.0193	431	0.0024	437	0.0068	437	13	102	102	150.3
70		1B6-31	356	305	102	308	1.01	19.5	0.0193	431	0.0024	437	0.0091	437	13	102	102	153.3
71		2BI-05	356	305	102	308	1.01	17.2	0.0193	431	0.0042	437	0.0023	437	13	102	102	129.0
72		2B3-06	356	305	102	308	1.01	17.0	0.0193	431	0.0042	437	0.0045	437	13	102	102	131.2
73		2B4-07	356	305	102	308	1.01	17.5	0.0193	431	0.0042	437	0.0068	437	13	102	102	126.1
74		2B4-52	356	305	102	308	1.01	21.8	0.0193	431	0.0042	437	0.0068	437	13	102	102	149.9
75		2B6-32	356	305	102	308	1.01	19.8	0.0193	431	0.0042	437	0.0091	437	13	102	102	145.2
76		3B1-08	356	305	102	308	1.01	16.2	0.0193	431	0.0063	437	0.0023	437	13	102	102	130.8
77		3B1-36	356	305	102	308	1.01	20.4	0.0193	431	0.0077	437	0.0023	437	13	102	102	159.0
78		3B3-33	356	305	102	308	1.01	19.0	0.0193	431	0.0077	437	0.0045	437	13	102	102	158.4
79		3B4-34	356	305	102	308	1.01	19.2	0.0193	431	0.0077	437	0.0068	437	13	102	102	155.0
80		3B6-35	356	305	102	308	1.01	20.7	0.0193	431	0.0077	437	0.0091	437	13	102	102	166.1
81		4B1-09	356	305	102	308	1.01	17.1	0.0193	431	0.0125	437	0.0023	437	13	102	102	153.5
82		1C1-14	356	305	102	408	1.34	17.2	0.0193	431	0.0018	437	0.0023	437	13	102	102	119.0
83		1C3-02	356	305	102	408	1.34	18.9	0.0193	431	0.0018	437	0.0045	437	13	102	102	123.4
84		1C4-15	356	305	102	408	1.34	22.7	0.0193	431	0.0018	437	0.0068	437	13	102	102	131.0
85		1C6-16	356	305	102	408	1.34	19.0	0.0193	431	0.0018	437	0.0091	437	13	102	102	122.3
86		2C1-17	356	305	102	408	1.34	19.9	0.0193	431	0.0031	437	0.0023	437	13	102	102	124.1
87		2C3-03	356	305	102	408	1.34	16.2	0.0193	431	0.0031	437	0.0045	437	13	102	102	133.6
88		2C3-27	356	305	102	408	1.34	16.3	0.0193	431	0.0031	437	0.0045	437	13	102	102	115.3
89		2C4-18	356	305	102	408	1.34	20.4	0.0193	431	0.0031	437	0.0068	437	13	102	102	124.5
90		2C6-19	356	305	102	408	1.34	20.8	0.0193	431	0.0031	437	0.0091	437	13	102	102	124.1

206

#	Author	Specimen	h (mm)	d (mm)	b (mm)	a (mm)	a/d	f_{ck} (MPa)	ρ	f_{sk} (MPa)	ρ_v	f_{yv} (MPa)	ρ_h	f_{sh} (MPa)	d_a (mm)	Top plate width (mm)	Bottom plate width (mm)	$V_{exp.}$ (kN)
91		3C1-20	356	305	102	408	1.34	21.0	0.0193	431	0.0056	437	0.0023	437	13	102	102	140.8
92		3C3-21	356	305	102	408	1.34	16.6	0.0193	431	0.0056	437	0.0045	437	13	102	102	125.0
93		3C4-22	356	305	102	408	1.34	18.3	0.0193	431	0.0056	437	0.0068	437	13	102	102	127.7
94		3C6-23	356	305	102	408	1.34	19.0	0.0193	431	0.0056	437	0.0091	437	13	102	102	137.2
95		4C1-24	356	305	102	408	1.34	19.6	0.0193	431	0.0077	437	0.0023	437	13	102	102	146.6
96		4C3-04	356	305	102	408	1.34	18.6	0.0193	431	0.0063	437	0.0045	437	13	102	102	128.6
97		4C3-28	356	305	102	408	1.34	19.2	0.0193	431	0.0077	437	0.0045	437	13	102	102	152.3
98		4C4-25	356	305	102	408	1.34	18.5	0.0193	431	0.0077	437	0.0068	437	13	102	102	152.6
99		4C6-26	356	305	102	408	1.34	21.2	0.0193	431	0.0077	437	0.0091	437	13	102	102	159.5
100	Subedi & et al. [120]	1A2	500	450	100	190	0.42	37.0	0.0089	493	0.0024	454	0.0051	454	15	100	150	375.0
101		1B2	500	450	100	690	1.53	37.0	0.0089	493	0.0022	454	0.0051	454	15	100	150	169.5
102		1C2	900	850	100	390	0.46	35.5	0.0116	330	0.0021	454	0.0036	454	15	100	150	485.0
103		1D2	900	850	100	1290	1.52	35.5	0.0116	330	0.0021	454	0.0036	454	15	100	150	231.0
104		2C1	900	850	100	350	0.41	34.9	0.0027	334	0.0021	438	0.0036	438	15	100	150	303.0
105		3 E1	500	450	100	334	0.74	52.0	0.0016	479	0.0036	211	0.0027	211	15	100	150	90.0
106	Walraven & Lehwalter [26]	V711/4	200	160	250	160	1.00	19.5	0.0150	420	0.0013	420	0	0	16	40	40	207.0
107		V711/4	400	360	250	360	1.00	18.2	0.0113	420	0.0013	420	0	0	16	90	90	317.0
108		V511/4	600	560	250	565	1.01	18.7	0.0112	420	0.0014	420	0	0	16	140	140	465.0
109		V411/4	800	760	250	740	0.97	17.0	0.0107	420	0.0017	420	0	0	16	185	185	467.0
110		V711/4	200	160	250	160	1.00	19.6	0.0150	420	0.0035	420	0	0	16	40	40	380.0
111		V022/3	400	360	250	360	1.00	19.6	0.0113	420	0.0035	420	0	0	16	90	90	380.0
112		V511/3	600	560	250	565	1.01	21.3	0.0112	420	0.0033	420	0	0	16	140	140	580.0
113		V411/3	800	760	250	740	0.97	19.8	0.0107	420	0.0033	420	0	0	16	185	185	665.0
114	Tan et al. [51]	A-0.27-2.15	500	463	110	125	0.27	58.8	0.0123	505	0.0048	375	0	0	10	110	110	675.0
115		A-0.27-3.23	500	463	110	125	0.27	61.6	0.0123	505	0.0048	375	0	0	10	110	110	630.0
116		A-0.27-4.30	500	463	110	125	0.27	53.9	0.0123	505	0.0048	375	0	0	10	110	110	640.0
117		A-0.27-5.38	500	463	110	125	0.27	57.3	0.0123	505	0.0048	375	0	0	10	110	110	630.0
118		B-0.54-2.15	500	463	110	250	0.54	56.0	0.0123	505	0.0048	375	0	0	10	110	110	468.0
119		B-0.54-3.23	500	463	110	250	0.54	45.7	0.0123	505	0.0048	375	0	0	10	110	110	445.0
120		B-0.54-4.30	500	463	110	250	0.54	53.9	0.0123	505	0.0048	375	0	0	10	110	110	500.0
121		B-0.54-5.38	500	463	110	250	0.54	53.0	0.0123	505	0.0048	375	0	0	10	110	110	480.0
122		C-0.81-2.15	500	463	110	375	0.81	51.2	0.0123	505	0.0048	375	0	0	10	110	110	403.0
123		C-0.81-3.23	500	463	110	375	0.81	44.0	0.0123	505	0.0048	375	0	0	10	110	110	400.0
124		D-1.08-2.15	500	463	110	500	1.08	48.2	0.0123	505	0.0048	375	0	0	10	110	110	270.0
125		E-1.62-3.23	500	463	110	750	1.62	50.6	0.0123	505	0.0048	375	0	0	10	110	110	220.0
126	Tan et al. [67]	I-3/0.75	500	443	110	375	0.85	59.2	0.0258	499	0	0	0.0159	353	10	110	110	1120.0
127		I-4/0.75	500	443	110	375	0.85	63.8	0.0258	499	0	0	0.0159	447	10	110	110	1160.0
128		II-2N/1.00	500	443	110	500	1.13	77.6	0.0258	499	0.0143	353	0	0	10	110	110	1040.0

207

#	Author	Specimen	h (mm)	d (mm)	b (mm)	a (mm)	a/d	f_{ck} (MPa)	ρ	f_{sk} (MPa)	ρ_v	f_{sv} (MPa)	ρ_h	f_{sh} (MPa)	d_a (mm)	Top plate width (mm)	Bottom plate width(mm)	Vexp. (kN)
129		II-3/1.00	500	443	110	500	1.13	78.0	0.0258	499	0	0	0.0159	353	10	110	110	780.0
130		II-4/1.00	500	443	110	500	1.13	86.3	0.0258	499	0	0	0.0159	447	10	110	110	660.0
131		II-5/1.00	500	443	110	500	1.13	86.3	0.0258	499	0	0	0.0317	447	10	110	110	940.0
132		III-2N/1.50	500	443	110	750	1.69	77.6	0.0258	499	0.0143	353	0	0	10	110	110	670.0
133		III-3/1.50	500	443	110	750	1.69	78.0	0.0258	499	0	0	0.0159	353	10	110	110	400.0
134		III-4/1.50	500	443	110	750	1.69	86.3	0.0258	499	0	0	0.0159	447	10	110	110	380.0
135		III-5/1.50	500	443	110	750	1.69	86.3	0.0258	499	0	0	0.0317	447	10	110	110	530.0
136	Foster and Gilbert [68]	B2.0-1	700	624	125	825	1.32	83.0	0.0242	440	0.0066	590	0.0037	590	10	250	250	795.0
137	Kong & Rangan [57]	S5-4	350	292	250	580	1.99	89.4	0.0280	452	0.0016	569	0	0	7	100	100	476.7
138		S5-5	350	292	250	510	1.75	89.4	0.0280	452	0.0016	569	0	0	7	100	100	573.4
139	Shin et al. [123]	MHB1.5-25	250	215	125	323	1.50	52.0	0.0377	414	0.0045	414	0	0	19	45	45	156.4
140		MHB1.5-50	250	215	125	323	1.50	52.0	0.0377	414	0.0091	414	0	0	19	45	45	208.0
141		MHB1.5-75	250	215	125	323	1.50	52.0	0.0377	414	0.0136	414	0	0	19	45	45	239.7
142		MHB1.5-100	250	215	125	323	1.50	52.0	0.0377	414	0.0181	414	0	0	19	45	45	257.5
143		MHB2.0-25	250	215	125	430	2.00	52.0	0.0377	414	0.0032	414	0	0	19	45	45	110.7
144		MHB2.0-50	250	215	125	430	2.00	52.0	0.0377	414	0.0065	414	0	0	19	45	45	173.9
145		MHB2.0-75	250	215	125	430	2.00	52.0	0.0377	414	0.0097	414	0	0	19	45	45	185.4
146		MHB2.0-100	250	215	125	430	2.00	52.0	0.0377	414	0.0129	414	0	0	19	45	45	193.2
147		HB1.5-25	250	215	125	323	1.50	73.0	0.0377	414	0.0045	414	0	0	13	45	45	214.2
148		HB1.5-50	250	215	125	323	1.50	73.0	0.0377	414	0.0091	414	0	0	13	45	45	246.2
149		HB1.5-75	250	215	125	323	1.50	73.0	0.0377	414	0.0136	414	0	0	13	45	45	265.8
150		HB1.5-100	250	215	125	323	1.50	73.0	0.0377	414	0.0181	414	0	0	13	45	45	280.3
151		HB2.0-25	250	215	125	430	2.00	73.0	0.0377	414	0.0032	414	0	0	13	45	45	142.7
152		HB2.0-50	250	215	125	430	2.00	73.0	0.0377	414	0.0065	414	0	0	13	45	45	195.9
153		HB2.0-75	250	215	125	430	2.00	73.0	0.0377	414	0.0097	414	0	0	13	45	45	230.1
154		HB2.0-100	250	215	125	430	2.00	73.0	0.0377	414	0.0129	414	0	0	13	45	45	242.1
155	Tan & Lu [27]	2-1000/0.50	1000	884	140	500	0.57	31.2	0.0260	520	0.0012	414	0.0012	414	10	140	140	875.0
156		2-1000/0.75	1000	884	140	740	0.84	32.7	0.0260	520	0.0012	414	0.0012	414	10	140	140	650.0
157		2-1000/1.00	1000	884	140	1000	1.13	30.8	0.0260	520	0.0012	414	0.0012	414	10	140	140	435.0
158		3-1400/0.50	1400	1251	140	705	0.56	32.8	0.0260	520	0.0012	414	0.0012	414	10	140	140	1175.0
159		3-1400/0.75	1400	1251	140	1050	0.84	36.2	0.0260	520	0.0012	414	0.0012	414	10	140	140	950.0
160		3-1400/1.00	1400	1251	140	1420	1.14	35.3	0.0260	520	0.0012	414	0.0012	414	10	140	140	800.0
161		4-1750/0.75	1750	1559	140	1320	0.85	40.4	0.0260	520	0.0012	414	0.0012	414	10	140	140	1240.0
162		4-1750/1.00	1750	1559	140	1760	1.13	44.8	0.0260	520	0.0012	414	0.0012	414	10	140	140	1000.0
163	Pendyala & Mendis [125]	8	160	140	80	280	2.00	33.0	0.0202	410	0.005	370	0	0	10	10	10	34.0
164		12	160	140	80	280	2.00	69.0	0.0202	410	0.005	370	0	0	10	10	10	48.5
165		14	160	140	80	280	2.00	32.0	0.0202	410	0.0034	370	0	0	10	10	10	43.0
166		15	160	140	80	280	2.00	61.0	0.0202	410	0.0034	370	0	0	10	10	10	44.0

#	Author	Specimen	h (mm)	d (mm)	b (mm)	a (mm)	a/d	f_{ck} (MPa)	ρ	f_{sk} (MPa)	ρ_v	f_{yv} (MPa)	ρ_h	f_{sh} (MPa)	d_a (mm)	Top plate width (mm)	Bottom plate width(mm)	Vexp. (kN)
167		18	160	140	80	280	2.00	91.0	0.0202	410	0.0034	370	0	0	10	10	10	46.0
168		20	160	140	80	280	2.00	83.0	0.0202	410	0.0034	370	0	0	10	10	10	44.0
169		21	160	140	80	280	2.00	36.0	0.0202	410	0.005	370	0	0	10	10	10	46.5
170	Oh and Shin [52]	N42A2	560	500	130	425	0.85	23.7	0.0156	415	0.0012	415	0.0043	415	16	180	130	284.1
171		N42B2	560	500	130	425	0.85	23.7	0.0156	415	0.0022	415	0.0043	415	16	180	130	377.0
172		N42C2	560	500	130	425	0.85	23.7	0.0156	415	0.0034	415	0.0043	415	16	180	130	357.5
173		H41A2(1)	560	500	130	250	0.50	49.1	0.0156	415	0.0012	415	0.0043	415	16	180	130	713.1
174		H41B2	560	500	130	250	0.50	49.1	0.0156	415	0.0022	415	0.0043	415	16	180	130	705.9
175		H41C2	560	500	130	250	0.50	49.1	0.0156	415	0.0034	415	0.0043	415	16	180	130	708.5
176		H42A2(1)	560	500	130	425	0.85	49.1	0.0156	415	0.0012	415	0.0043	415	16	180	130	488.2
177		H42B2(1)	560	500	130	425	0.85	49.1	0.0156	415	0.0022	415	0.0043	415	16	180	130	456.3
178		H42C2(1)	560	500	130	425	0.85	49.1	0.0156	415	0.0034	415	0.0043	415	16	180	130	420.6
179		H43A2(1)	560	500	130	625	1.25	49.1	0.0156	415	0.0012	415	0.0043	415	16	180	130	347.1
180		H43B2	560	500	130	625	1.25	49.1	0.0156	415	0.0022	415	0.0043	415	16	180	130	380.9
181		H43C2	560	500	130	625	1.25	49.1	0.0156	415	0.0034	415	0.0043	415	16	180	130	402.4
182		H45A2	560	500	130	1000	2.00	49.1	0.0156	415	0.0012	415	0.0043	415	16	180	130	210.6
183		H45B2	560	500	130	1000	2.00	49.1	0.0156	415	0.0022	415	0.0043	415	16	180	130	237.3
184		H45C2	560	500	130	1000	2.00	49.1	0.0156	415	0.0034	415	0.0043	415	16	180	130	235.3
185		H41A2(2)	560	500	120	250	0.50	50.6	0.0129	415	0.0013	415	0.0047	415	16	180	130	490.2
186		H41A3	560	500	120	250	0.50	50.6	0.0129	415	0.0013	415	0.0094	415	16	180	130	454.8
187		H42A2(2)	560	500	120	425	0.85	50.6	0.0129	415	0.0013	415	0.0047	415	16	180	130	392.4
188		H42B2(2)	560	500	120	425	0.85	50.6	0.0129	415	0.0024	415	0.0047	415	16	180	130	360.6
189		H42C2(2)	560	500	120	425	0.85	50.6	0.0129	415	0.0037	415	0.0047	415	16	180	130	373.8
190		H43A0	560	500	120	625	1.25	50.6	0.0129	415	0.0013	415	0	415	16	180	130	313.6
191		H43A1	560	500	120	625	1.25	50.6	0.0129	415	0.0013	415	0.0023	415	16	180	130	260.4
192		H43A2(2)	560	500	120	625	1.25	50.6	0.0129	415	0.0013	415	0.0047	415	16	180	130	276.6
193		U41A0	560	500	120	250	0.50	73.6	0.0129	415	0.0013	415	0	415	16	180	130	438.0
194		U41A1	560	500	120	250	0.50	73.6	0.0129	415	0.0013	415	0.0023	415	16	180	130	541.8
195		U41A2	560	500	120	250	0.50	73.6	0.0129	415	0.0013	415	0.0047	415	16	180	130	548.4
196		U41A3	560	500	120	250	0.50	73.6	0.0129	415	0.0013	415	0.0094	415	16	180	130	546.6
197		U42A2	560	500	120	425	0.85	73.6	0.0129	415	0.0013	415	0.0047	415	16	180	130	417.6
198		U42B2	560	500	120	425	0.85	73.6	0.0129	415	0.0024	415	0.0047	415	16	180	130	410.4
199		U42C2	560	500	120	425	0.85	73.6	0.0129	415	0.0037	415	0.0047	415	16	180	130	408.0
200		U43A0	560	500	120	625	1.25	73.6	0.0129	415	0.0013	415	0	415	16	180	130	291.0
201		U43A1	560	500	120	625	1.25	73.6	0.0129	415	0.0013	415	0.0023	415	16	180	130	310.2
202		U43A2	560	500	120	625	1.25	73.6	0.0129	415	0.0013	415	0.0047	415	16	180	130	338.4
203		N33A2	560	500	130	625	1.25	23.7	0.0156	415	0.0012	415	0.0043	415	16	180	130	228.2
204		N43A2	560	500	130	625	1.25	23.7	0.0156	415	0.0012	415	0.0043	415	16	180	130	254.8

209

#	Author	Specimen	h (mm)	d (mm)	b (mm)	a (mm)	a/d	f_{ck} (MPa)	ρ	f_{sh} (MPa)	ρ_r	f_{sv} (MPa)	ρ_h	f_{sh} (MPa)	d_a (mm)	Top plate width (mm)	Bottom plate width(mm)	Vexp. (kN)
205		N53A2	560	500	130	625	1.25	23.7	0.0156	415	0.0012	415	0.0043	415	16	180	130	270.4
206		H31A2	560	500	130	250	0.50	49.1	0.0156	415	0.0012	415	0.0043	415	16	180	130	745.6
207		H32A2	560	500	130	425	0.85	49.1	0.0156	415	0.0012	415	0.0043	415	16	180	130	529.8
208		H33A2	560	500	130	625	1.25	49.1	0.0156	415	0.0012	415	0.0043	415	16	180	130	377.7
209		H51A2	560	500	130	250	0.50	49.1	0.0156	415	0.0012	415	0.0043	415	16	180	130	702.0
210		H52A2	560	500	130	425	0.85	49.1	0.0156	415	0.0012	415	0.0043	415	16	180	130	567.5
211		H53A2	560	500	130	625	1.25	49.1	0.0156	415	0.0012	415	0.0043	415	16	180	130	362.7
212	Zhang and Tan [31]	1DB35bw	350	313	80	344	1.10	25.9	0.0125	469	0.004	426	0	0	10	53	53	99.5
213		1DB50bw	500	454	115	499	1.10	27.4	0.0128	505	0.0039	426	0	0	10	75	75	186.5
214		1DB70bw	700	642	160	706	1.10	28.3	0.0122	522	0.0045	370	0	0	10	105	105	427.0
215		1DB100bw	1000	904	230	994	1.10	28.7	0.0120	540	0.0041	455	0	0	10	150	150	775.0
216	Tan et al. [32]	1-500/0.75W	500	444	140	375	0.84	30.7	0.0260	530	0.0038	250	0.0082	511	15	150	150	335.5
217		2-1000/0.75W	1000	884	140	750	0.85	37.6	0.0260	530	0.0038	250	0.008	511	15	150	150	801.5
218		3-1400/0.75W	1400	1243	140	1050	0.84	37.2	0.0260	530	0.0041	250	0.0084	511	15	150	150	1052.0
219		4-1750/0.75W	1750	1559	140	1313	0.84	35.3	0.0260	530	0.0038	250	0.0089	511	15	150	150	1305.0
220	Current Research	F2	400	330	100	300	0.91	60.6	0.0365	364	0.0067	448	0.0022	577	13	100	100	353.2
221		F3	400	330	100	300	0.91	59.5	0.0365	364	0.0143	448	0.0022	577	13	100	100	373.8
222		G1	400	330	100	550	1.67	30.9	0.0365	364	0.0056	448	0.0022	577	13	100	100	146.2
223		G2	400	330	100	425	1.29	30.5	0.0365	364	0.0059	448	0.0022	577	13	100	100	186.0
224		G3	400	330	100	300	0.91	31.3	0.0365	364	0.0067	448	0.0022	577	13	100	100	244.3

APPENDIX B.   EXPERIMENTAL METHODOLOGY

B.1. INTRODUCTION

Understanding the behaviour of disturbed regions (D-regions) in structural members, such as deep beams, has been a challenging issue for many decades and the problem is still not solved totally. To gain better understanding and explore the effect of different design parameters on the behaviour and ultimate shear capacity of reinforced concrete deep beams a two-phase experimental programme was employed.

The experimental work of this study can be categorised in two phases. In the first phase, 21 reinforced concrete deep beams were tested under two point loads in the structural laboratory at Salahaddin University\Hawler in Iraq [75]. The parameters were investigated in this phase were shear span to depth ratio, concrete compressive strength and amount of shear reinforcement. The second phase comprises testing three geometrically similar reinforced concrete deep beams with different sizes under four points bending in the heavy structural laboratory at The University of Sheffield in the UK. The main parameter investigated in this phase was depth of the member.

This chapter presents full description of the test specimens, mechanical properties of the utilised materials, specimen design and construction, test setup and instrumentation.

B.2. PHASES OF THE EXPERIMENTAL PROGRAMME

B.2.1. PHASE I

This phase of experimental programme consists of testing 21 reinforced concrete deep beams in four points bending. All the beams were loaded up to failure; however, beams C2 and C3 (Table **B-1**) did not fail because there failure loads were higher than the ultimate loading capacity of the testing machine [75].

B.2.1.1. Investigated Parameters

In order to know the effect of different design parameters on the behaviour and shear capacity of reinforced concrete deep beams, 21 reinforced concrete deep beams were designed in such a way that only one parameter was changed in each beam for easier comparison between the beams and knowing the influence of each parameter separately.

B.2.1.2. Concrete Compressive Strength

Due to direct transferring the applied load to the support by arch action, concrete compressive strength plays a significant role on the overall behaviour and ultimate shear capacity of deep beams. To analyse the influence of this parameter, this research was aimed to investigate the effect of varying the concrete compressive strength on the shear performance of reinforced concrete deep beams. The targeted concrete compressive strength was designed to range between 30 to 85MPa.

B.2.1.3. Shear Span to Depth Ratio

Shear span to depth ratio is one of the parameters that need to investigate because it has a great influence on the behaviour and shear capacity of reinforced concrete deep beams. Changing shear span to depth ratio will lead to change in the efficiency of arch action mechanism, which is the main shear transfer mechanism of RC deep beams, in transferring shear stresses. Therefore, three different shear spans were used to result in three different shear spans to depth ratio. Specimens in group A, D and beam G1 had a shear span of 550mm which resulted in 1.67 shear span to depth ratio. For group B, E and beam G2 shear span was 425mm and resulted in 1.29 shear span to depth ratio. Group C, F and beam G3 had a shear span of 300mm which resulted in shear span to depth ratio of 0.91.

B.2.1.4. Web Reinforcement

Web reinforcement was another investigated parameter in the current phase of the experimental programme. Both vertical and horizontal web reinforcement were utilised. Three different vertical shear reinforcements were used ranged from 0 to 1.26% and two horizontal shear reinforcements were used ranged from 0 to 0.215%. The reason behind

focusing more on vertical shear reinforcement that horizontal is because it was proven in past researches that vertical shear links has greater influence on the capacity of reinforced concrete deep beams than horizontal shear reinforcement and the effect of horizontal shear reinforcement becomes obvious almost only in deep beams with shear span to depth ratio less than one [1].

B.2.2. SPECIMENS

B.2.2.1. Description of the Specimens

All the specimens had identical cross-section which was 400mm deep and 100mm wide, and the same length of 1800mm with centre to centre span of 1400mm. The location of two point loads was changed to give different shear spans. The details are given in Table **B-1**.

The beams were divided into seven groups; with the exception of group G, the only parameters changed within each group was amount of web reinforcement, while the shear span to depth ratio and concrete compressive strength were held constant. To know the effect of shear span to depth ratio or concrete compressive strength beams in different groups but with the same amount of web reinforcement should be compared. All three specimens in group G had the same concrete compressive strength and amount of web reinforcement but shear span to depth ratio was changed.

The main longitudinal reinforcement of all specimens was identical and consisted of six 16mm diameter deformed bar distributed in three layers, two bars in each layer, with a clear concrete cover of 25mm. All six bars were hooked at both ends to prevent bond failure at the two ends of the beams. The top reinforcement consisted of two 12mm diameter bar with the clear cover to the top of the beam of 25mm. The vertical shear reinforcement was a closed stirrups used in different spacing as explained in Table B-1 and two 6mm diameter were used as a horizontal shear reinforcement for beams with web reinforcement.

B.2.2.2. Construction

Wooden moulds were used for the casting of specimens. A very thin layer of de-moulding agent was applied to the mould before casting and the reinforcement cage, which constructed according to the drawings shown in Figure B-1, were placed and fixed in its position to control the designated clear cover. The mould was put in a horizontal direction on a vibrating table. Concrete was put in layers and each layers vibrated then the final surface was levelled. The control cubes and cylinders were cast together with the specimens. The beams and the control specimens were kept covered with wet hessian and polythene sheets for 28 days after casting. Figure B-2 shows different stages of the construction process.

Table B-1 Details and Properties of Tested Beams

No	Spec.	L mm	b mm	h mm	d mm	a mm	a/d	$f'c$ Mpa	V.Shear Reinf		H.Shear Reinf
1	A1	1400	100	400	330	550	1.67	85	0	0	0
2	A2	1400	100	400	330	550	1.67	85	0.0056	ϕ8@180	0.00215
3	A3	1400	100	400	330	550	1.67	85	0.0126	ϕ8@80	0.00215
4	B1	1400	100	400	330	425	1.29	85	0	0	0
5	B2	1400	100	400	330	425	1.29	85	0.0059	ϕ8@170	0.00215
6	B3	1400	100	400	330	425	1.29	85	0.0134	ϕ8@75	0.00215
7	C1	1400	100	400	330	300	0.91	85	0	0	0
8	C2	1400	100	400	330	300	0.91	85	0.0067	ϕ8@150	0.00215
9	C3	1400	100	400	330	300	0.91	85	0.0144	ϕ8@70	0.00215
10	D1	1400	100	400	330	550	1.67	60	0	0	0
11	D2	1400	100	400	330	550	1.67	60	0.0056	ϕ8@180	0.00215
12	D3	1400	100	400	330	550	1.67	60	0.0126	ϕ8@80	0.00215
13	E1	1400	100	400	330	425	1.29	60	0	0	0
14	E2	1400	100	400	330	425	1.29	60	0.0059	ϕ8@170	0.00215
15	E3	1400	100	400	330	425	1.29	60	0.0134	ϕ8@75	0.00215
16	F1	1400	100	400	330	300	0.91	60	0	0	0
17	F2	1400	100	400	330	300	0.91	60	0.0067	ϕ8@150	0.00215
18	F3	1400	100	400	330	300	0.91	60	0.0144	ϕ8@70	0.00215
19	G1	1400	100	400	330	550	1.67	30	0.0056	ϕ8@180	0.00215
20	G2	1400	100	400	330	425	1.29	30	0.0059	ϕ8@170	0.00215
21	G3	1400	100	400	330	300	0.91	30	0.0067	ϕ8@150	0.00215
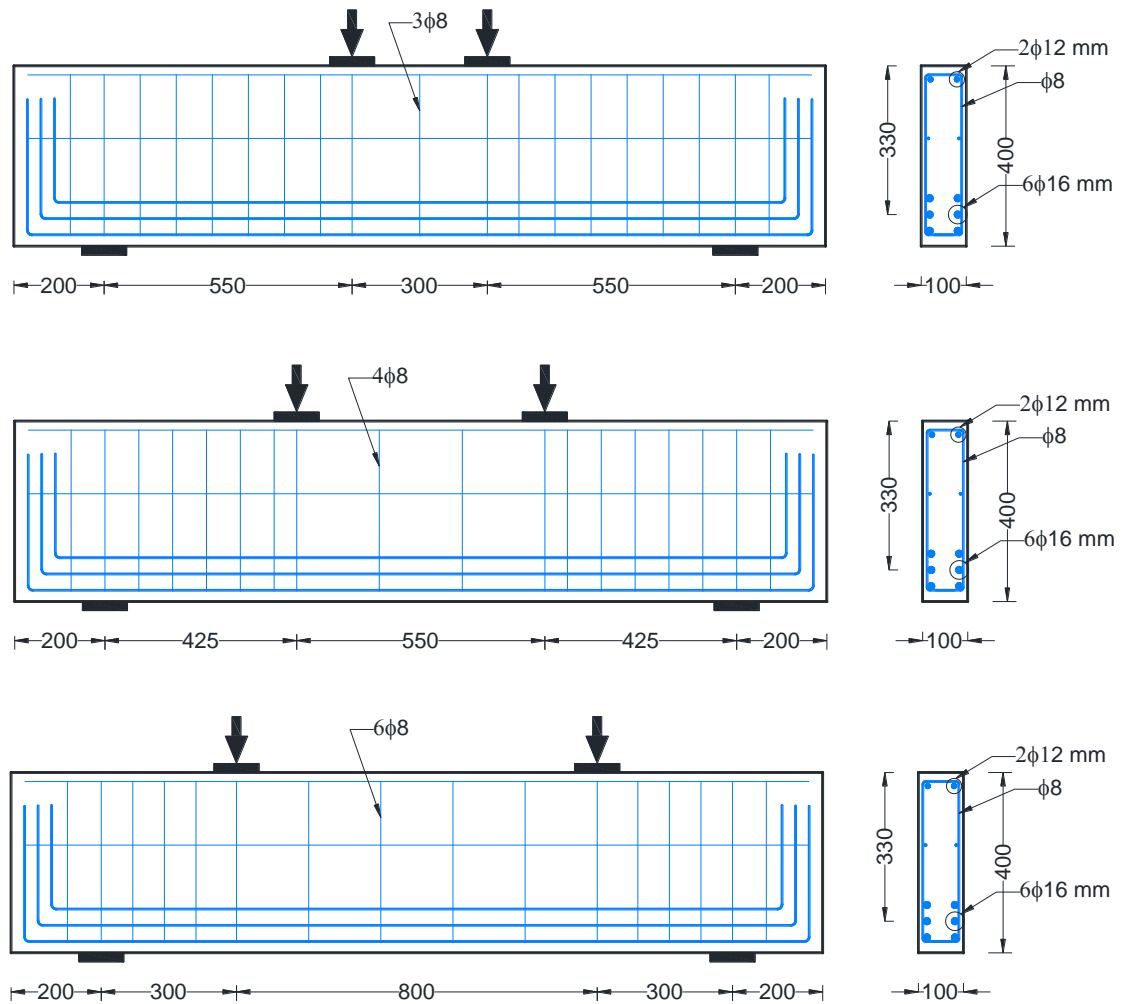
Figure B-1 Dimensions and reinforcement details of Specimens of Phase I

B.2.3. MATERIAL

B.2.3.1. Concrete

Since the preparation of high-strength concrete needs high quality of materials and number of specimens were 21, it was difficult to order ready-mix concrete and cast all specimens together. It was decided to use electrical concrete mixer that was available in the laboratory to cast the specimens. Different mix proportions were used to get different concrete strength and in case of high strength concrete, super-plasticizer was used to increase the workability. Maximum aggregate size for all the mixes was 12.5mm and ordinary Portland cement was utilised. Table B-1 shows the concrete mixes and

their targeted concrete compressive strength. The compressive strength of the concrete was measured by testing standard cubes (150 x 150 mm) according to BS 1881-116 (1983a). The cylinder compressive strength was then calculated as a 85% of the cube compressive strength. The concrete tensile strength was evaluated from splitting tests of standard cylinders (150 x 300 mm) according to BS 1881-117 (1983b).

Table B-2 Concrete mixes and their properties

No	Mix proportion By weight	W/C %	Super-plasticizer Litre/100 kg cement	Targeted compressive strength MPa
1	1.8 : 1.2 : 1	26	1	85
2	1.8 : 1.2 : 1	36	0.5	60
2	1 : 3 : 4	62	0	30

Figure B-2 Construction process

B.2.3.2. Steel Reinforcement

Four sizes of steel reinforcement were used in constructing reinforcement cage of the specimens. The main reinforcement consisted of deformed 16mm bars and the top reinforcement consisted of deformed 12mm bars. Vertical shear reinforcement consisted of 8mm deformed bars as a form of closed stirrups and horizontal shear reinforcement consisted of 6mm deformed bars. Direct tension tests were performed on three samples of each diameter to determine the mechanical properties of the rebars. Table B-3 shows areas and mechanical properties of all reinforcement.

Table B-3 Details and mechanical properties of reinforcing bars

Size mm	Area mm^2	Yield strength f_y ,MPa	Ultimate strength f_u, MPa
6	28	577	660
8	50	448	693
12	113	404	635
16	199	364	550

B.2.4. INSTRUMENTATION AND TESTING PROCEDURE

All the specimens were tested in four points bending using universal testing machine with a capacity of 100ton. A rigid steel beam was used to support the specimen. The test specimens were loaded symmetrically using two point loads and the load was applied to the specimen through a stiff steel beam positioned on the top of the specimen and reacting against the specimen, the distance between the two point loads was changed according to the drawing shown in Figure B-1 to give different shear spans.

Various measurements were taken to capture the local and global response of the tested beams by using different types of instrumentations. The measurement can be arranged into four groups: applied load, mid-span displacement, end rotation and steel strain.

The load was applied at increments of 20kN. At each load increment, the mid-span deflection of the beam was measured by dial gauge transducers. Inclinometers were

used to measure the end rotations of the beams. Crack propagation was monitored and marked at each load increment by visual inspection.

Steel strains in both longitudinal and transverse reinforcement were measured at each load increment using 10mm electrical strain gauges which were positioned at selected locations.

B.3. PHASE II

The main objective of the tests carried out in this phase of experimental programme was to investigate the effect of member depth on the shear behaviour of reinforced concrete deep beams. Changing depth of the members while holding other design parameters constant, offers key information about influence of size effect on the shear capacity and overall behaviour of reinforced concrete deep beams. To achieve this purpose, the only design parameter varied in this phase of experimental programme was depth of the member. In the following sub-sections the description of the specimens, material, instrumentation and test procedure of this phase will be discussed in detail.

B.3.1. TEST SPECIMENS

B.3.1.1. Specimen design

In all three specimens, all parameters were identical except the beam depth. The depth was varied from 250 to 500mm which gives the size ratio of 1:1.5:2. The width of the beams was deliberately kept constant at 150mm as it is not expected to change the size effect [24, 31]. Other reason behind the width of the beams to be kept constant is to mitigate the phenomenon called wall effect, which happens when the surface of the specimen has less aggregate content than the interior; this causes the fracture energy to be different near the surface than it is in the interior [24].

Since the specimens were designed to fail in shear, high percentage of main flexural reinforcement ratio was used to prevent flexural failure prematurely ends the test. The main flexural reinforcement ratio was 1.4% for all three specimens; however, different

bar sizes were used to keep reinforcement ratio identical for all the specimens. Figure B-3 shows the reinforcement detail and the dimensions of all three beams.
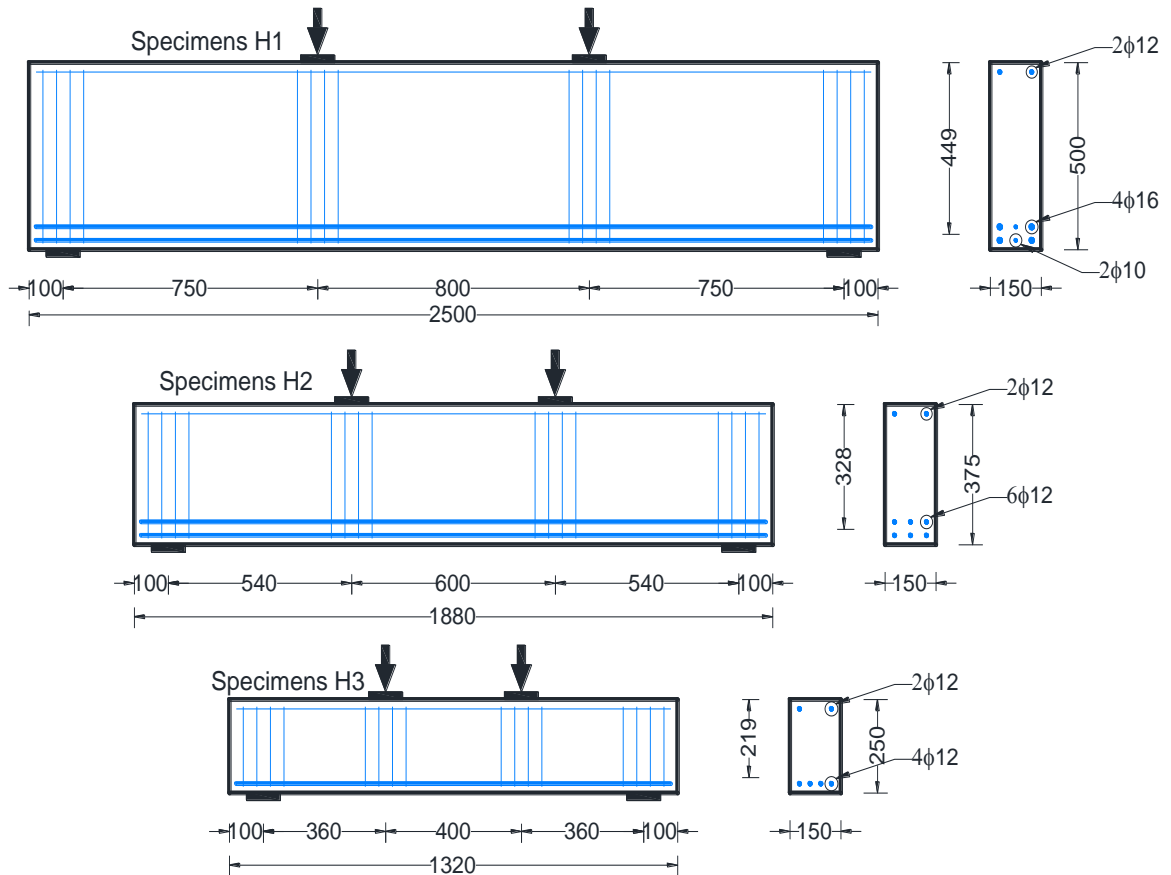
Figure B-3 Dimensions and reinforcement detail of the specimens

B.3.1.2. Specimen Construction

The construction of the specimens was started by cutting the reinforcement into specified length for each specimen. Before the assemblage of steel cages, the positions of strain gauges were accurately located on each bar and more details are given in strain gauge sub-section. Since all three specimens were without shear reinforcement, stirrups were only used in the support and loading regions to prevent local concrete crushing around this area. All the main flexural reinforcement was welded to the support stirrups to prevent bond failure at the end of the beams. Plastic ties were used to build the steel cage. Figure B-4 shows the assembled reinforcement cages for all three beams.

Figure B-4 Reinforcement cages for the tested beams

Steel moulds were utilized for casting of the beams. The moulds were cleaned and the inner surfaces were covered with a very thin layer of de-moulding agent to facilitate de-moulding after casting. The reinforcement cages were positioned inside the steel mould as shown in Figure B-5 and to guarantee the correct positioning and covers, plastic spacers were used. Since the specimens had different length, wood spacers were used to specify the length of the beams.

The specimens were cast all together in heavy structural laboratory at the University of Sheffield using ready-mix concrete which was supplied by a local supplier. The concrete was placed in two layers of approximately the same thickness and vibrated using an electrical poker vibrator as shown in Figure B-6.

Figure B-5 The reinforcement cage positioned inside the steel mould

After casting, the surfaces of the specimens were levelled to remove irregularities in geometries. The specimens were covered with wet hessian and polyethylene for seven days before removing from the mould. After that, the specimens were kept in the standard laboratory temperature until the day of testing.

Figure B-6 Specimens casting

221

B.3.2. MATERIALS

B.3.2.1. Concrete

Since the concrete compressive strength was constant for all three specimens, ready-mix concrete was order from local supplier with a targeted concrete compressive strength of 35MPa.

To determine the properties of the concrete, cylinders and prisms along with main specimens were casted, cured and tested. The compressive strength of the concrete was determined by performing compression test on standard 150x300mm cylinders according to BS EN 12390-3 [76] and concrete tensile strength was determined by doing splitting tensile test on the 150x300mm standard cylinders according to BS EN 12390-3 [76] along with performing four points bending for 100x100x500mm prisms. Table B-4 shows the average results from testing cylinders and prisms.

Table B-4 Average concrete compressive and tensile strength of specimens

Compressive strength (MPa)	Tensile strength from cylinders (MPa)	Tensile strength from prisms (MPa)
35.8	3.1	4.2

B.3.2.2. Steel Reinforcement

All reinforcement used in this phase of experimental programme had nominal yield strength of 500MPa. Different rebar sizes were used according to the drawing shown in the Figure B-3.

B.3.3. INSTRUMENTATIONS

B.3.3.1. Strain Gauges

To measure the strain development in the main longitudinal and compression reinforcement of the specimens throughout the loading history, strain gauges were located at specified locations on the reinforcements. Before the assemblage of the steel

cage of each specimen, the location of the strain gauge was marked accurately according to the drawing shown in Figure B-7. The marked location of each strain gauge was ground by using different grades of metal files and the final surface was smoothed. The smoothed surface was slightly wider than the gauge's width; however, extra care was taken to take as little material off the bars surface as possible so to prevent mechanical performance and the cross-sectional area being affected. After the surface was prepared and well cleaned, the gauge was attached using cement glue, and then external twisted wire was soldered to each strain gauge through a terminal positioned at the end of each strain gauge. The wires were bundled together and ran along the longitudinal reinforcement to the end of the beam. The strain gauges and the terminals were protected by a waterproof rubber sealant which provided by the strain gauge manufacturer as shown in the Figure B-8.

Different numbers of strain gauges were utilized in different specimens depending on the length of shear span of the specimen. The number of strain gauges was chosen in such a way that to take into consideration the possibility of strain gauges malfunctioning during casting, and the bond between concrete and reinforcing bars. Since two different rebar sizes were used in the main flexural reinforcement for beam H1, the strain gauges were positioned on both bar size in the exact same location to monitor the variability in strain development in each of them. The other two specimens, because the bar size was identical, the strain gauges were positioned only on one bar of the bars used as a main flexural reinforcement. To monitor the strain progress in the compression reinforcement, three strain gauges, one strain gauge in the mid-span and one strain gauge in each shear span, were positioned on the compression reinforcement for all three specimens.
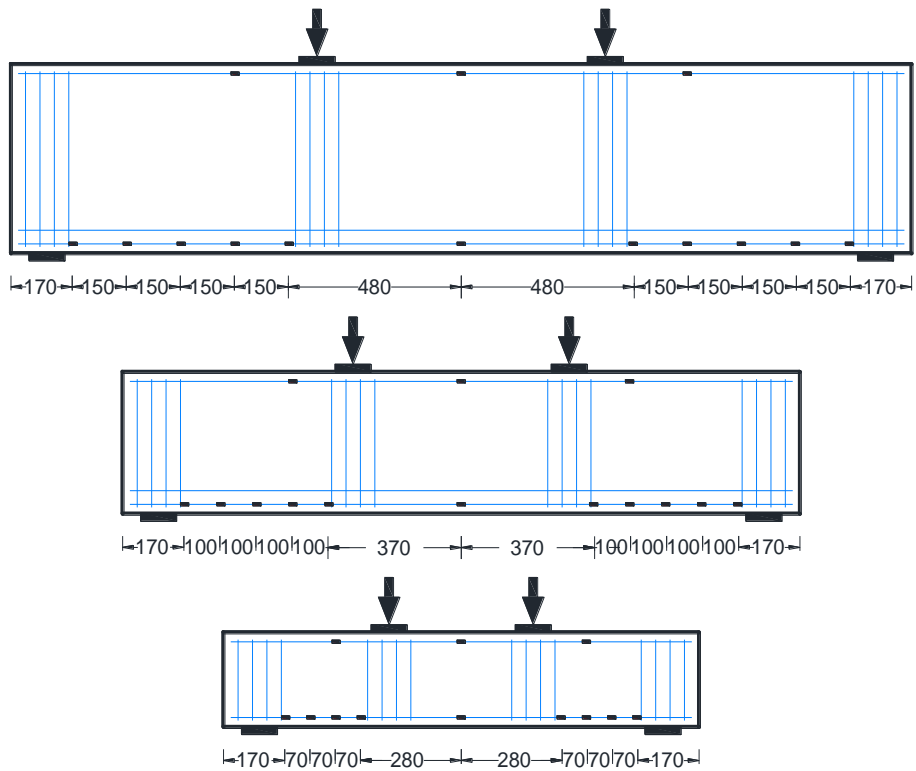
Figure B-7 Distribution of the strain gauges
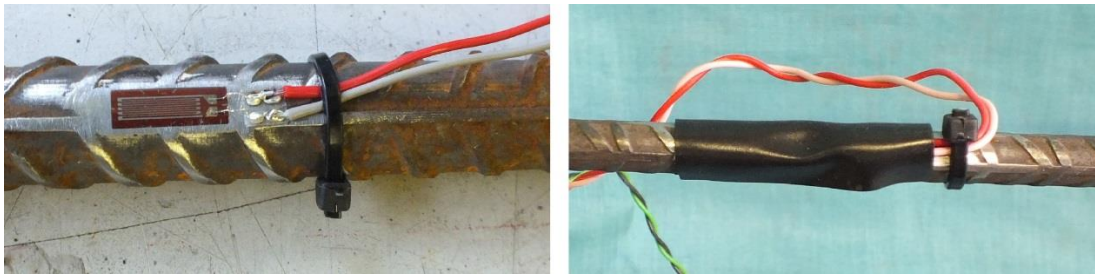
Figure B-8 Strain gauge and its waterproof rubber sealant

B.3.3.2. LVDT

A total of five Linear Variable Differential Transformer transducers (LVDT) were used to monitor deflection of the specimens throughout loading history. The location of LVDTs included mid-span point, under point loads and mid-length of shear span. To measure the pure deflection of the beam, a yoke support system were built and fitted on the beam body. The yoke system were fixed at both ends of the beam, the centre line of

the yoke support coincided with the centre line of the beam support. The bar that held the LVDTs in the yoke system could rotate at both ends and slide in one end. This system could exclude the support displacement and any other displacement that did not come from the beam.

B.3.3.3. Concrete Strain

The strain of the concrete was measured in each loading step by using demec gauges. The demec points were attached to the selected locations on the concrete surface and the original distance between the points was 100mm at the beginning of the test, then the relative movements between the points were recorded in each loading step by using mechanical dial gauge.

First specimen was tested in the phase II of experimental programme was beam H3. Two different patterns were used to measure the concrete strain in the shear span of that specimen to investigate which pattern is more accurate and gives better insight into the shear behaviour of the specimen. The patterns were according to the drawings shown in Figure B-9. After the test completed, it was found that the pattern one (Figure B-9 a) gave better information about the shear strain development in the shear span. Thus, pattern one was employed for the rest of the specimens. Another reason for not using both patterns for all three specimens, because it was time consuming and the applied load had to be hold. This probably includes the creep effect and the final result would be affected.
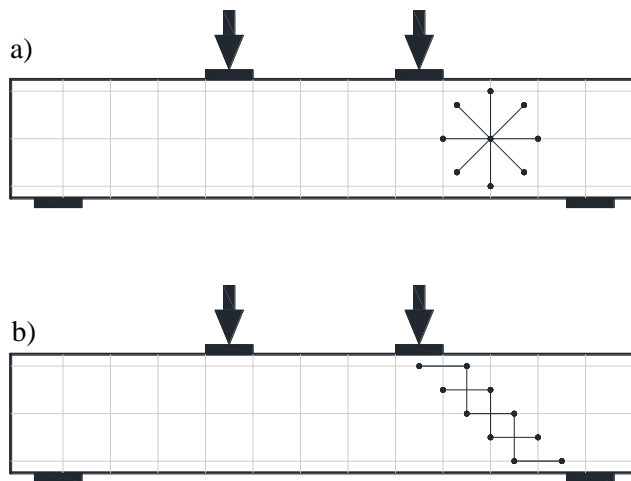
Figure B-9 Demec point patterns a) Pattern one, b) Pattern two

B.3.4. EXPERIMENTAL SETUP

One day before testing, the specimen was white-washed and 100x100mm grids were drawn over the side surface of the specimen to mark the crack propagation during testing and to facilitate crack location and propagation in the photos after finishing the test.

The specimen was positioned in a rigid steel frame system; different steel frames were used depending on the predicted ultimate shear capacity of the beam. For beam H3, a steel frame was used as shown in Figure B-10 and the load was applied by means of a 250 kN servo controlled hydraulic actuator which could be controlled in either load or displacement control manner. The actuator was operated by an Electronic Control Unit that was connected to a data acquisition system (ORION). The total load was distributed to two loading points through a stiff steel distributor. At each loading point, the applied load was transferred to the top surface of the by through a 40mm diameter steel roller which was supported by 100mm wide steel plate. The head of the actuator had a large spherical hinge that allowing free rotation of the top loading beam and restraining its translation in the horizontal direction. At the bottom, the beam was seated on two steel plates at both ends and the plates were supported through two steel rollers. To guarantee free elongation of the specimen and to simulate the actual simply supported system, one

of the supports allowed both rotation and horizontal movements while the other one only allowed rotation.
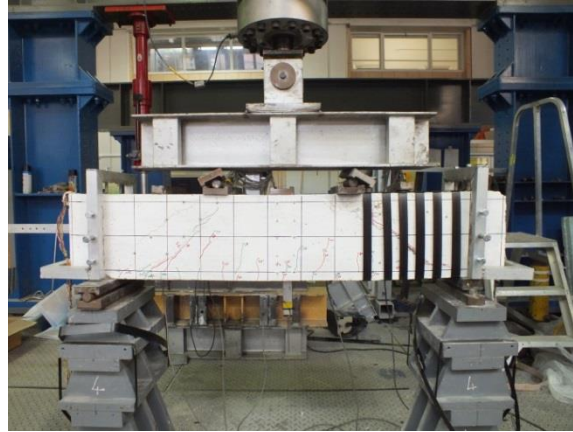
Figure B-10 Testing of beam H3

Since the ultimate predicted failure load of other two specimens, beam H1 and H2, was higher than the ultimate capacity of the actuator which was 250kN, other loading apparatus had to be utilized. For that purpose, a 2000kN universal testing machine was employed to test both beams (Figure B-11). The testing arrangement was exactly identical to the arrangements used for beam H3; however, the only difference between these two testing system was the universal testing machine could be controlled only in load control mode.

Figure B-11 Testing of beam H1

B.3.5. TESTING PROCEDURE

The testing was initiated by applying the load in increments of 5 or 10kN, depending on the ultimate predicted failure load of the specimen. The beam H3 was tested by using 250 kN servo controlled hydraulic actuator in the displacement control mode. At each 5 kN, the picture was taken, while other readings such as concrete strain and and the width of critical cracks was measured using a micrometre with an accuracy of 0.02mm and crack developments were marking at every 20kN increment. The strain gauge readings, applied load and the displacement were recorded automatically by the data acquisition system (ORION) at every two seconds throughout the loading history.

For the other two specimens which were tested using the 2000 kN universal testing machine. The testing procedure was the same but the loading was applied in load control mode. In these two tests the picture were taken at each 20 kN increment because it was found in the first test that pictures cannot capture the changes happening on 5 kN increments.

All three specimens were loaded up to a serviceability limit after that unloaded, then reloaded subsequently until the total failure load was reached.

B.4. TEST RESULTS

B.4.1. BEAM A1
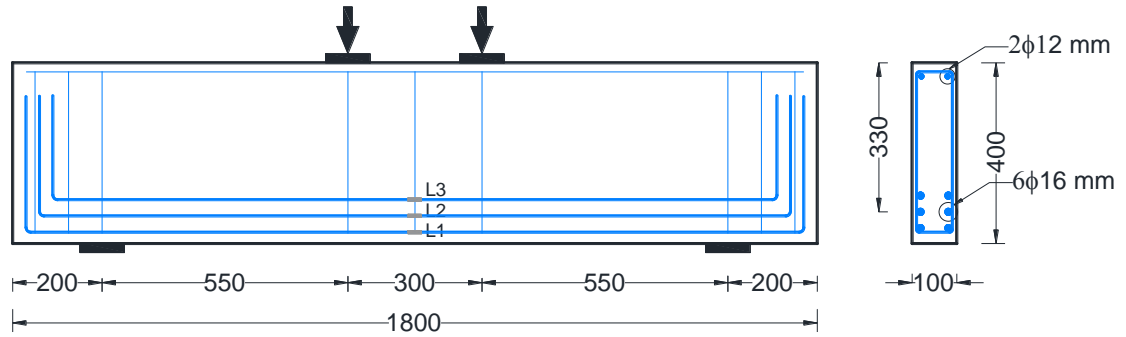
Figure B-12-General layout and reinforcement for beam A1
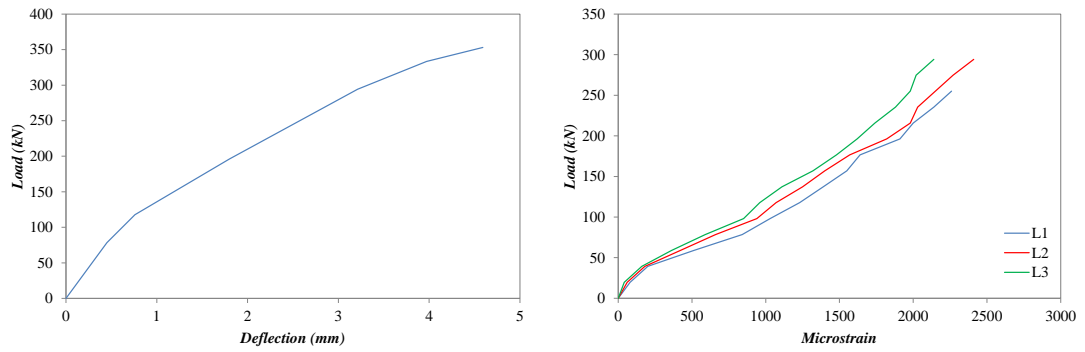
Figure B-13-Load-deflection response and strain in the flexural reinforcing bars of beam A1
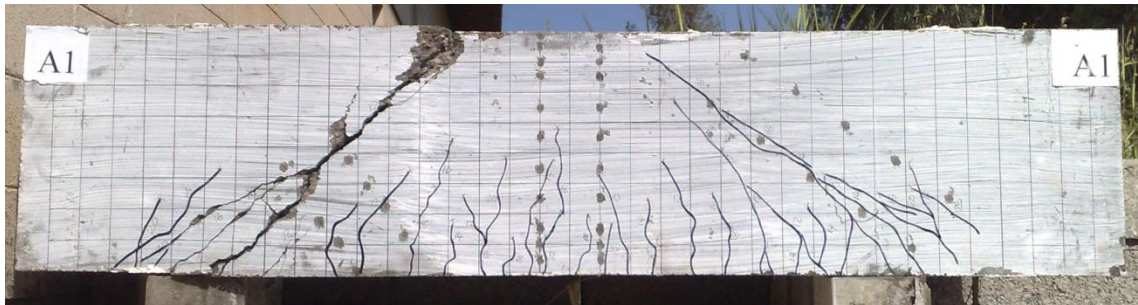
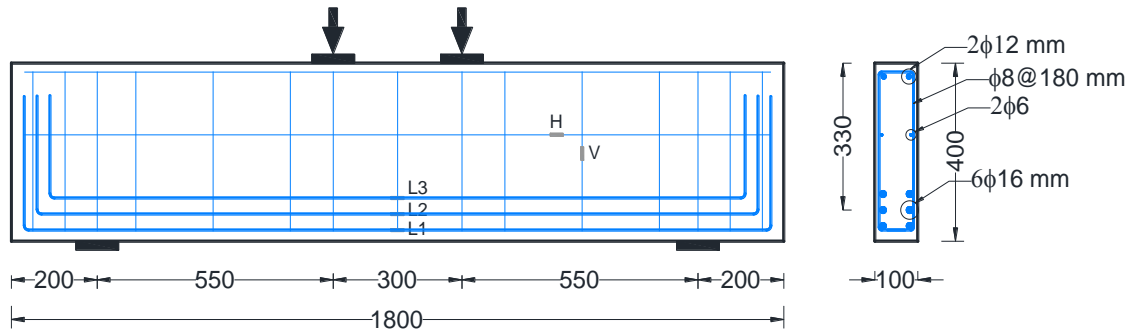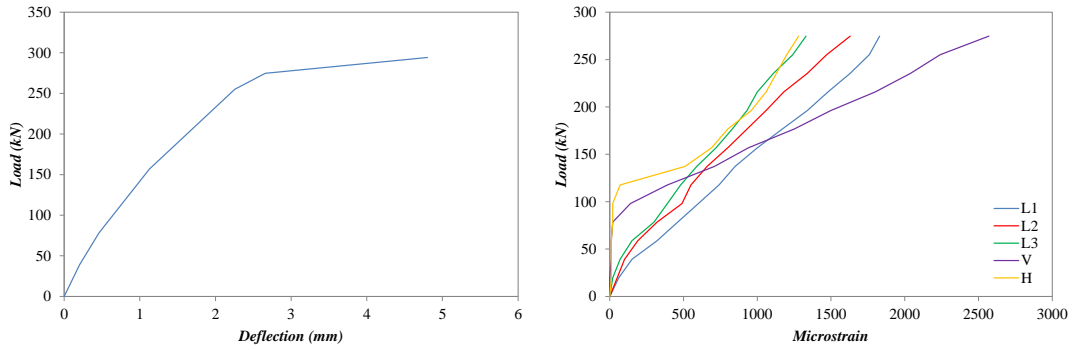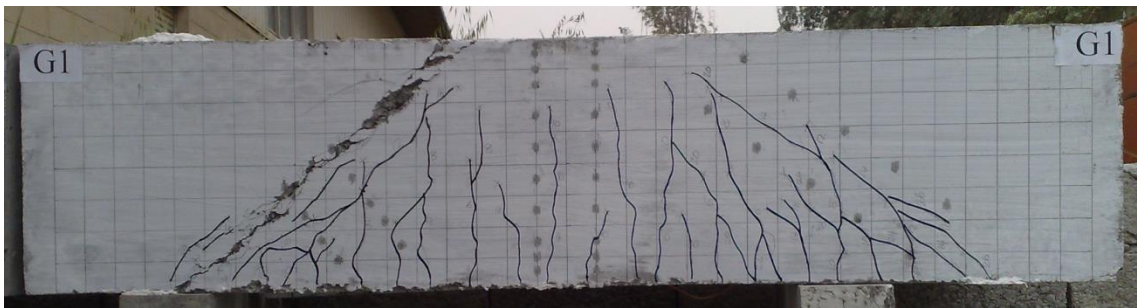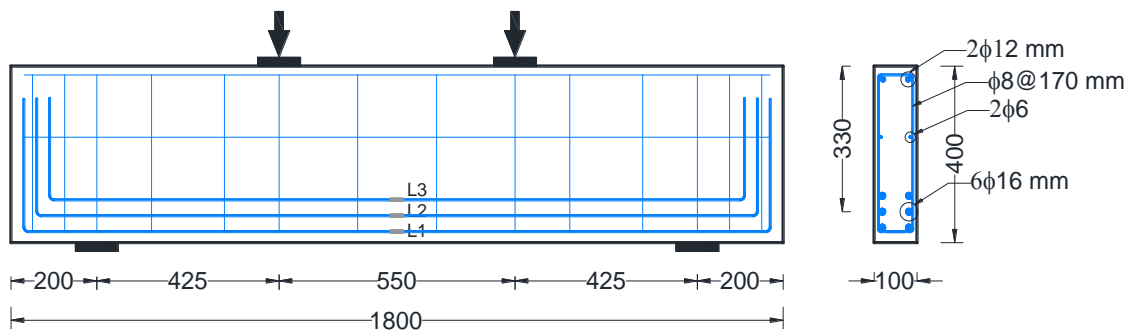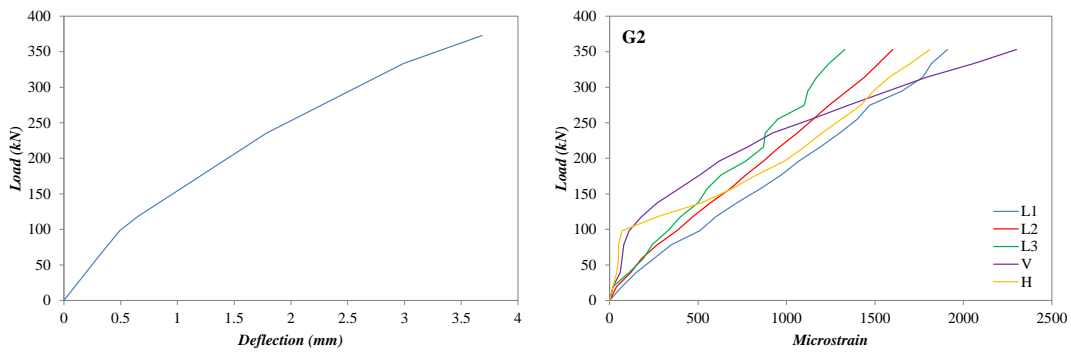**Figure B-14-Crack pattern after failure of beam A1**

B.4.2. BEAM A2
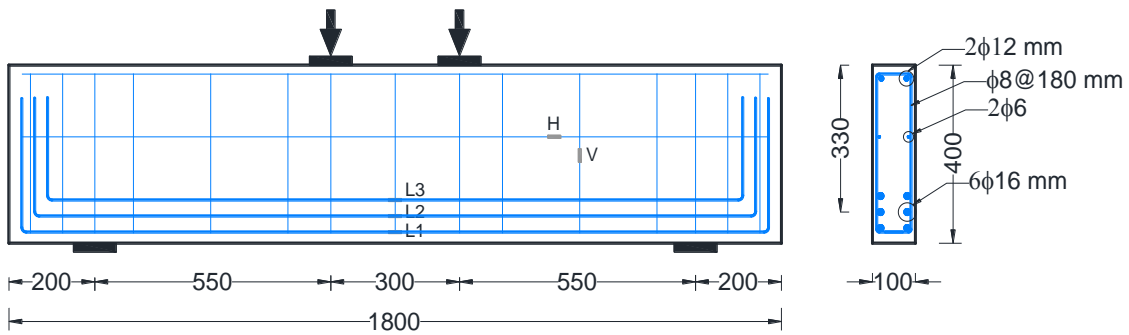
Figure B-15-General layout and reinforcement for beam A2
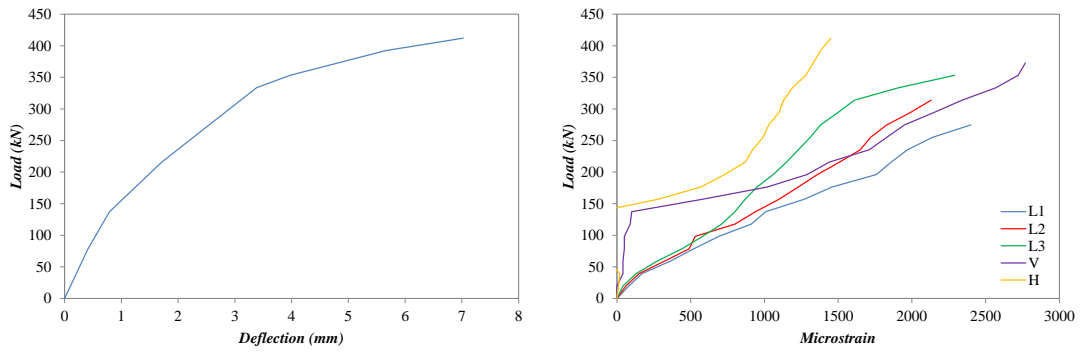
Figure B-16-Load-deflection response and strain in the flexural and shear reinforcing bars of beam A2
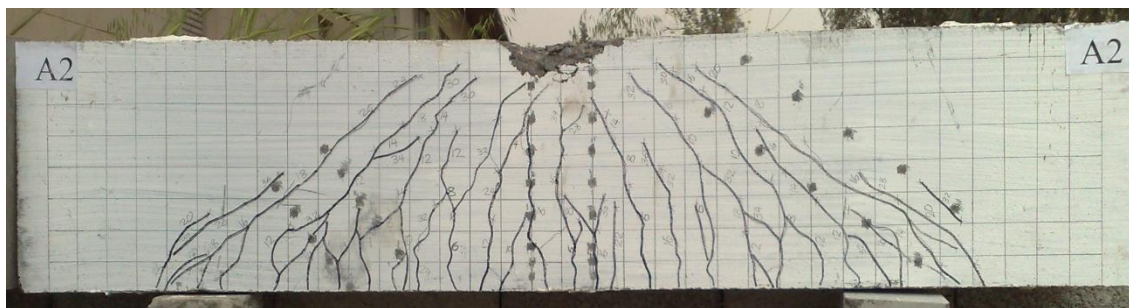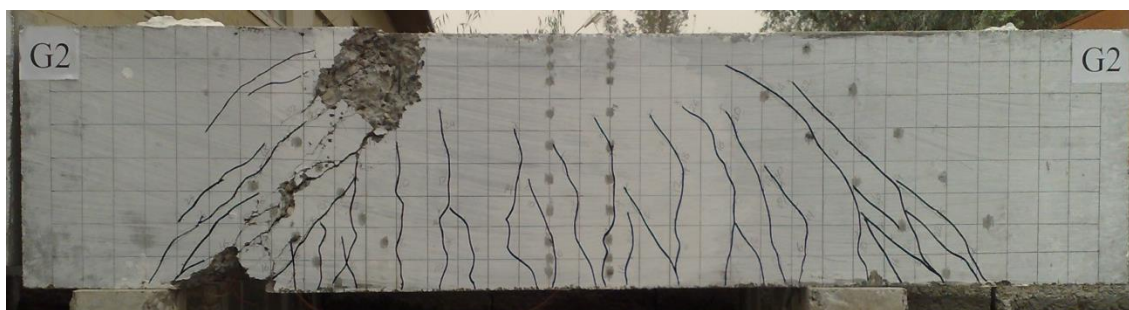

Figure B-17-Crack pattern after failure of beam A2
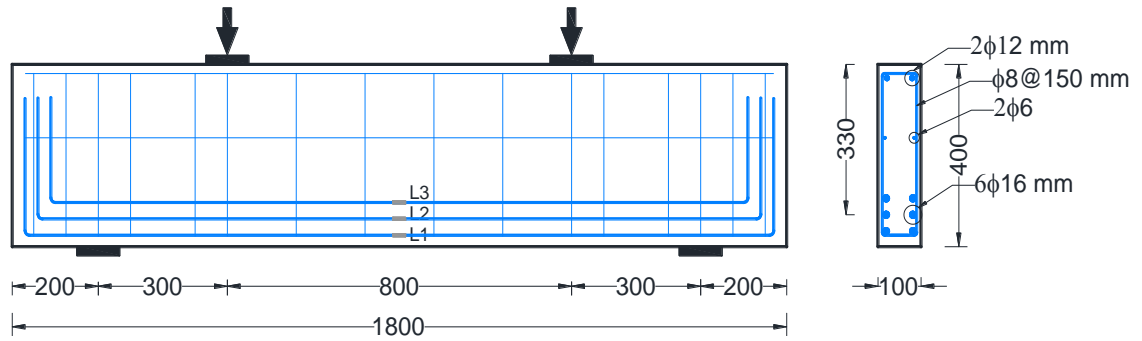
230

B.4.3. BEAM A3
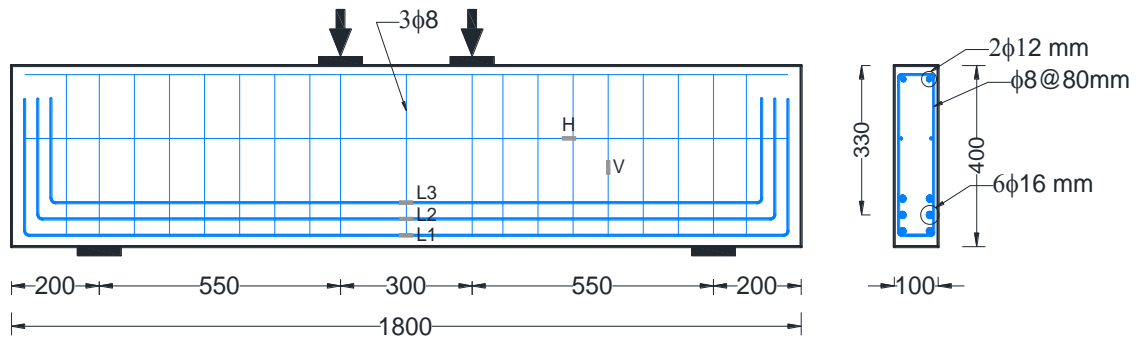
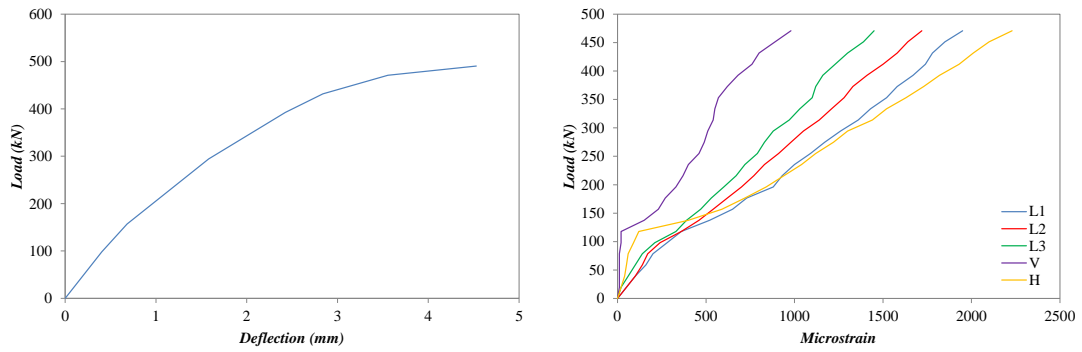**Figure B-18-General layout and reinforcement for beam A3**
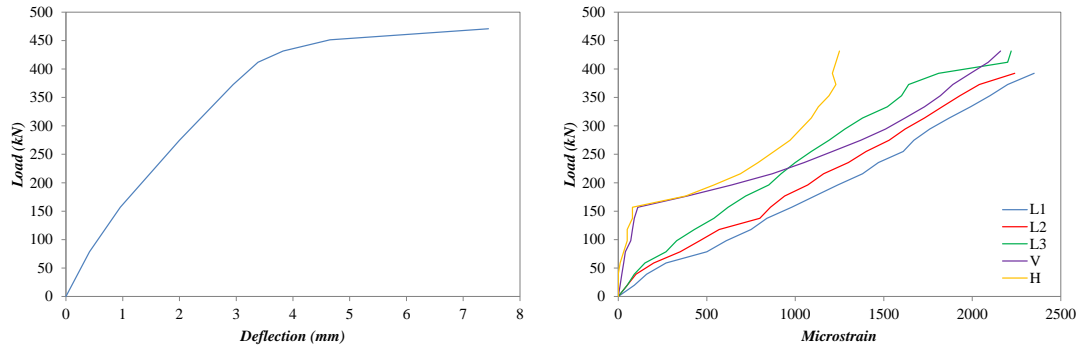
Figure B-19-Load-deflection response and strain in the flexural and shear reinforcing bars of beam A3
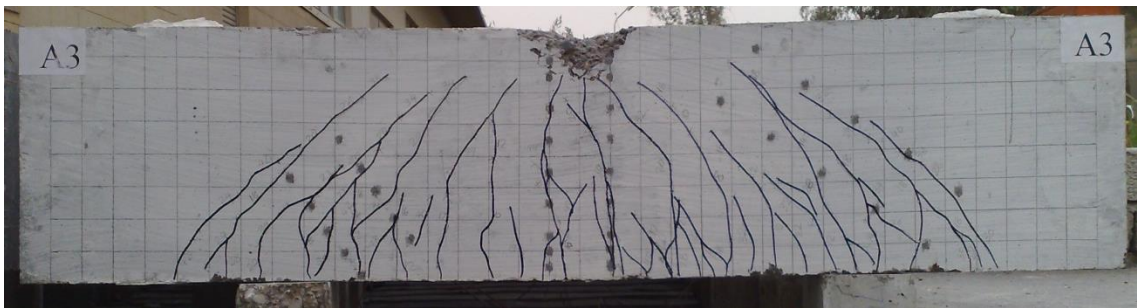
Figure B-20-Crack pattern after failure of beam A3

231

B.4.4. BEAM B1
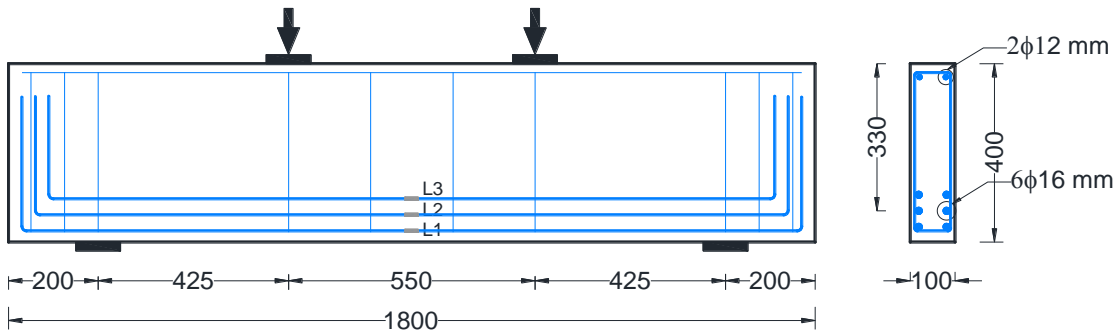
Figure B-21-General layout and reinforcement for beam B1
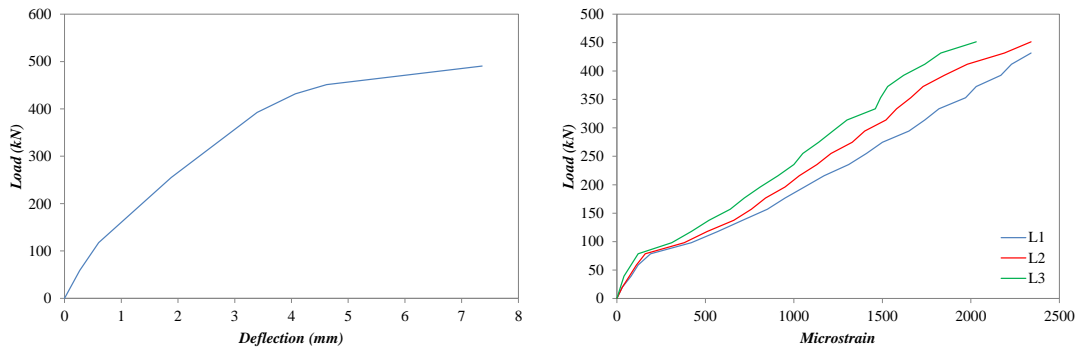
Figure B-22-Load-deflection response and strain in the flexural reinforcing bars of beam B1

Figure B-23-Crack pattern after failure of beam B1

B.4.5. BEAM B2
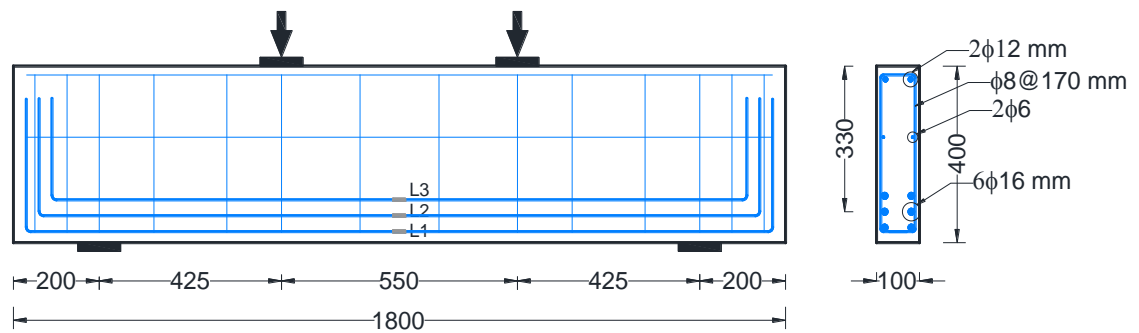
Figure B-24-General layout and reinforcement for beam B2
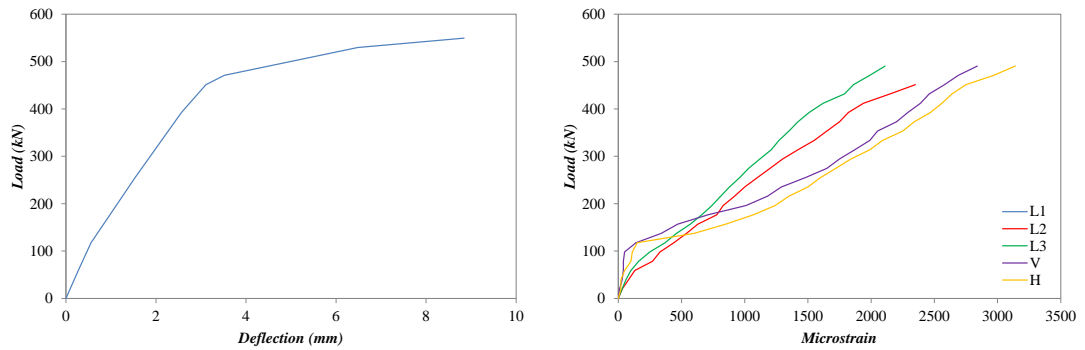
Figure B-25-Load-deflection response and strain in the flexural and shear reinforcing bars of beam B2
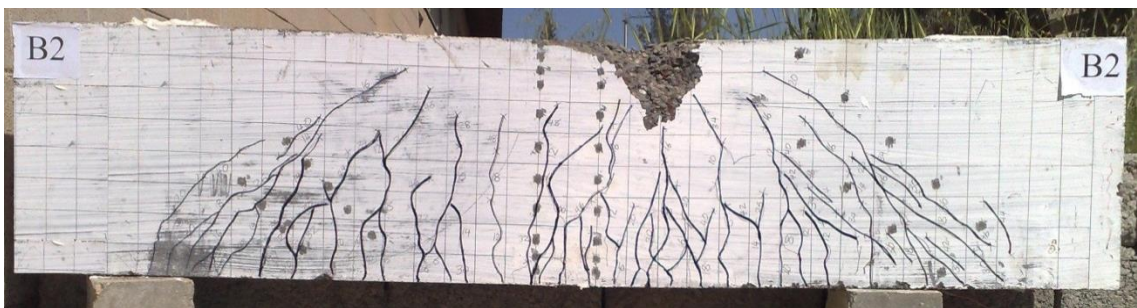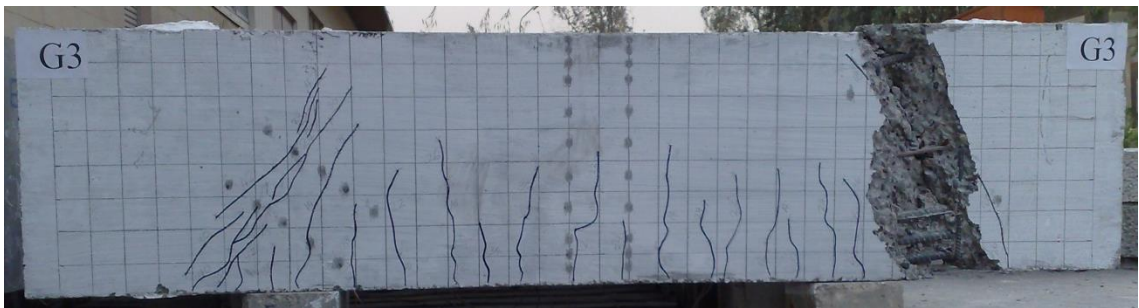

Figure B-26-Crack pattern after failure of beam B2

B.4.6. BEAM B3
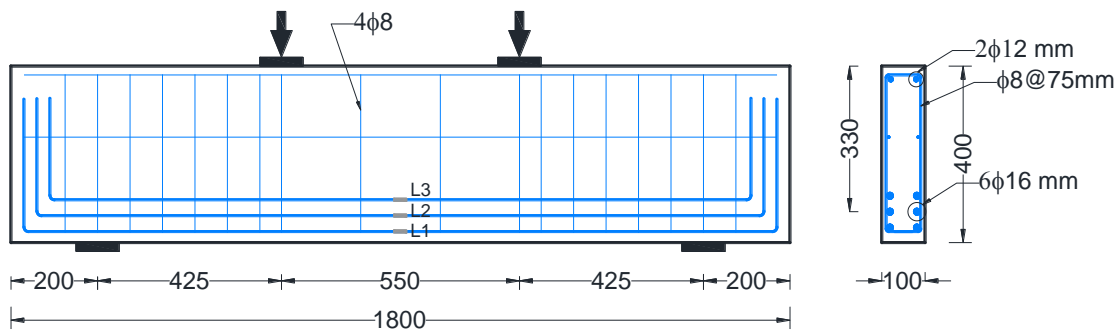
Figure B-27-General layout and reinforcement for beam B3
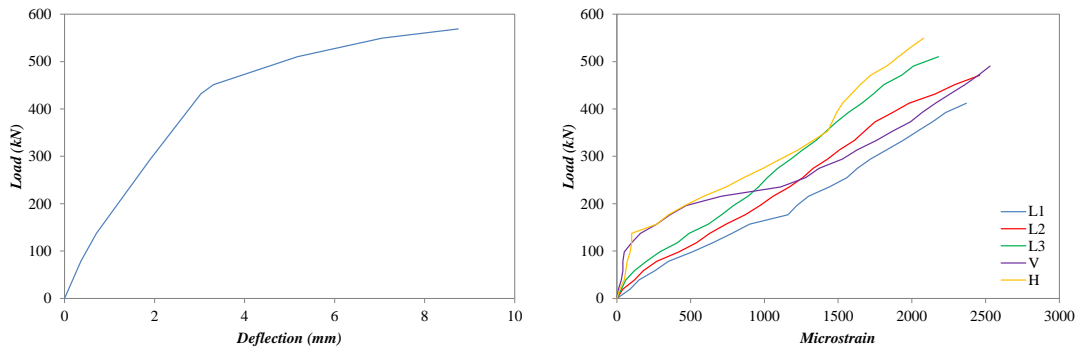
Figure B-28-Load-deflection response and strain in the flexural and shear reinforcing bars of beam B3
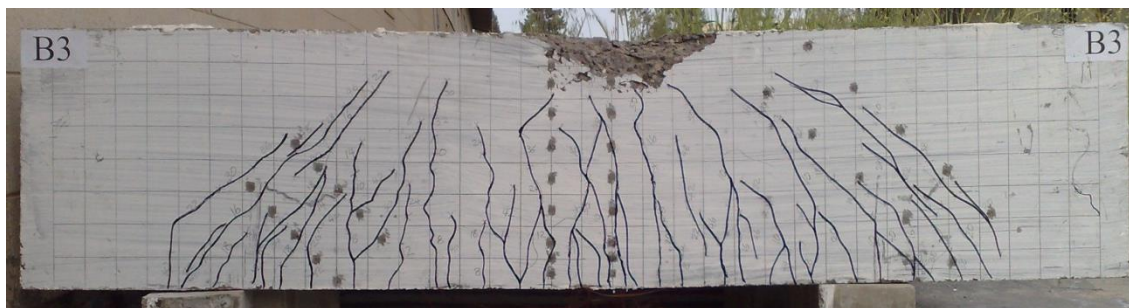
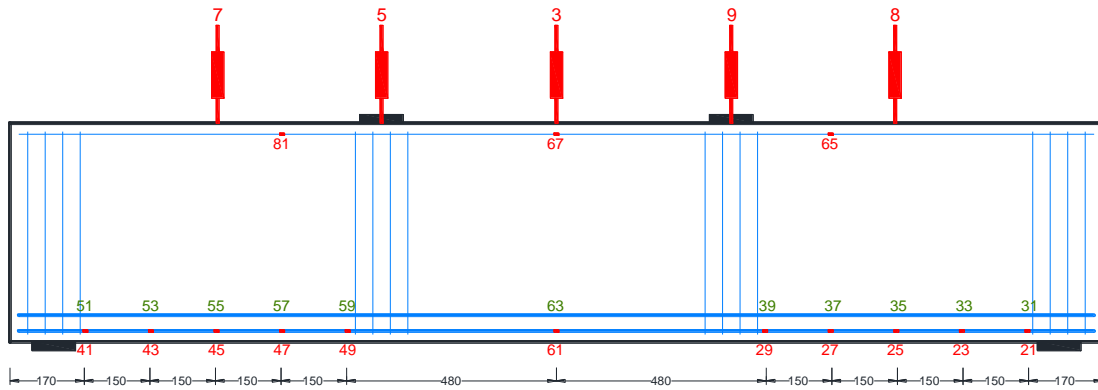**Figure B-29-Crack pattern after failure of beam B3**

B.4.7. BEAM C1
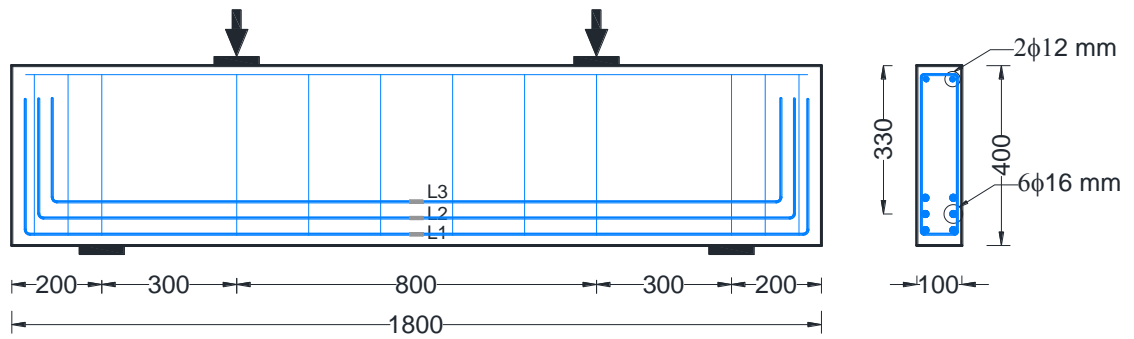
Figure B-30-General layout and reinforcement for beam C1
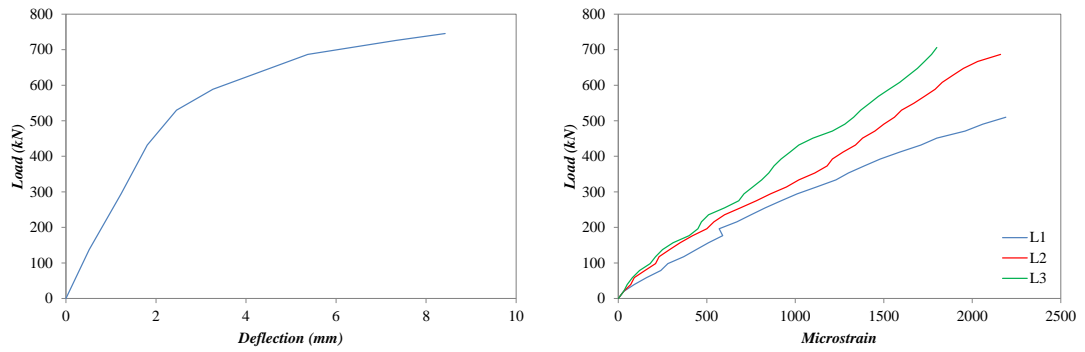
Figure B-31-Load-deflection response and strain in the flexural reinforcing bars of beam C1
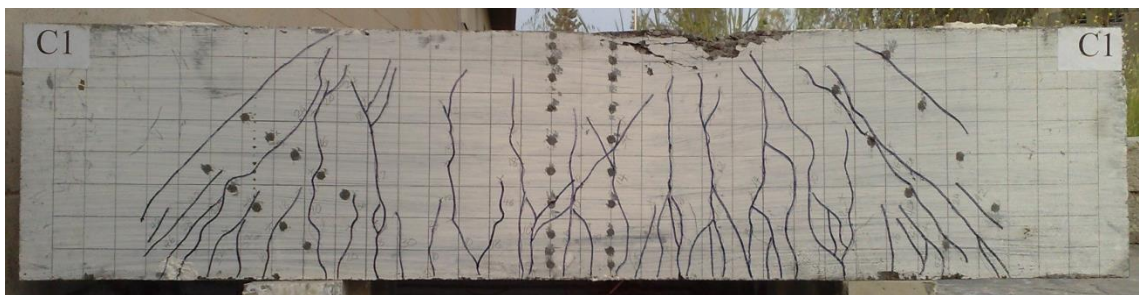
Figure B-32-Crack pattern after failure of beam C1

B.4.8. BEAM C2
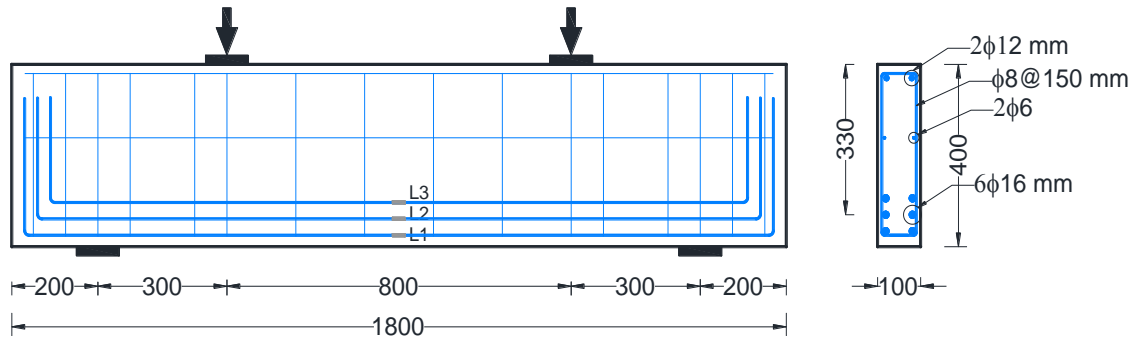
Figure B-33-General layout and reinforcement for beam C2
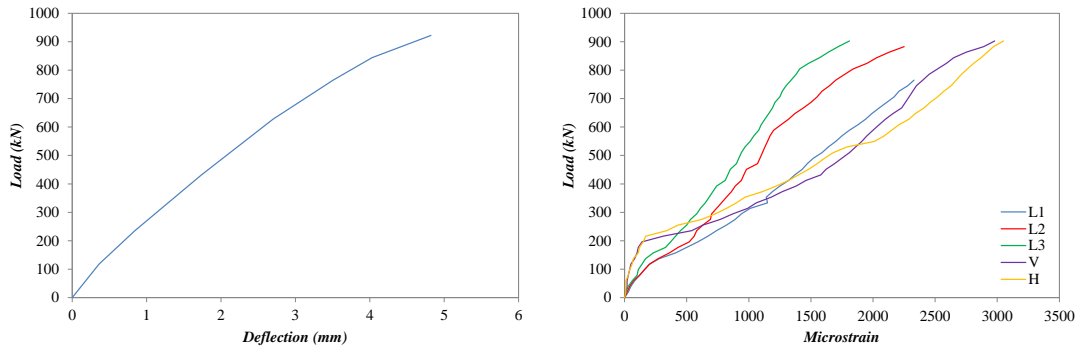
Figure B-34-Load-deflection response and strain in the flexural and shear reinforcing bars of beam C2
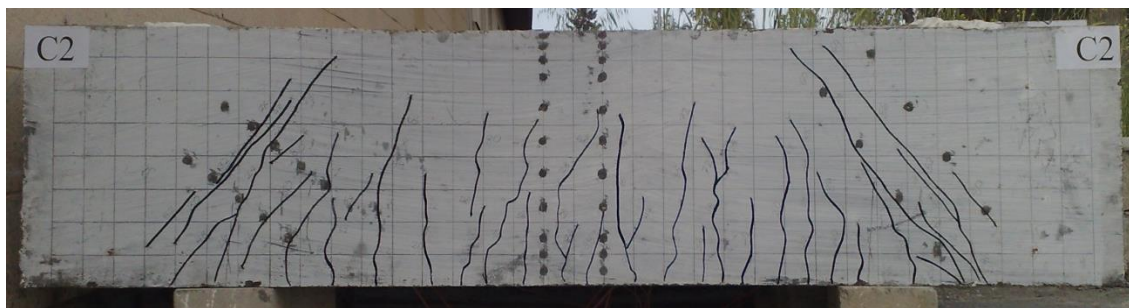
Figure B-35-Crack pattern of beam C2

236

B.4.9. BEAM C3
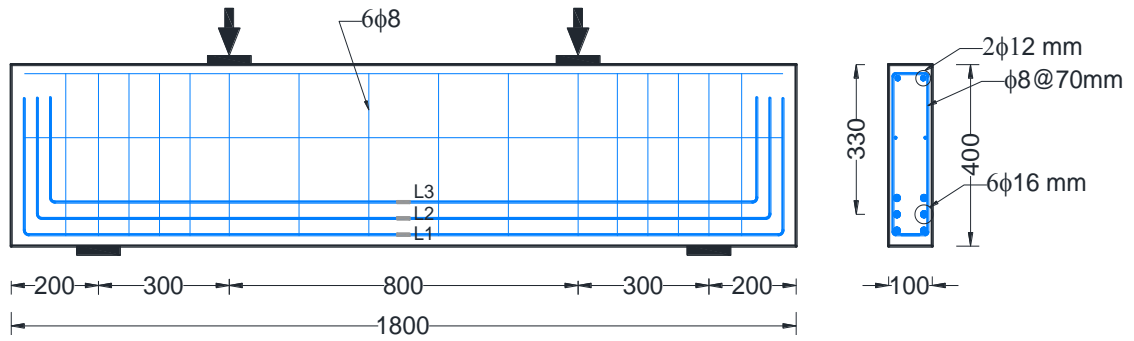
Figure B-36-General layout and reinforcement for beam C3
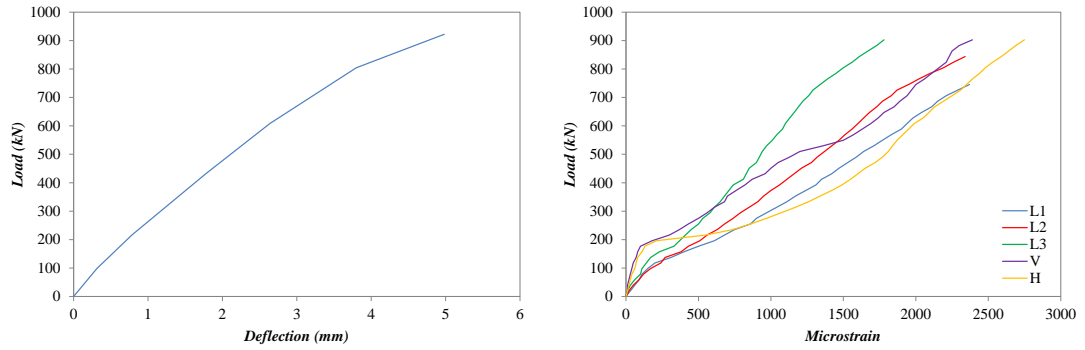
Figure B-37-Load-deflection response and strain in the flexural and shear reinforcing bars of beam C3
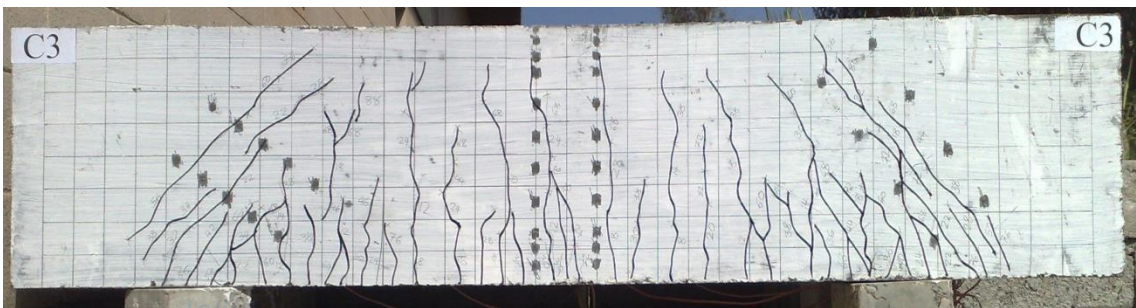
Figure B-38-Crack pattern of beam C3

B.4.10.   BEAM D1
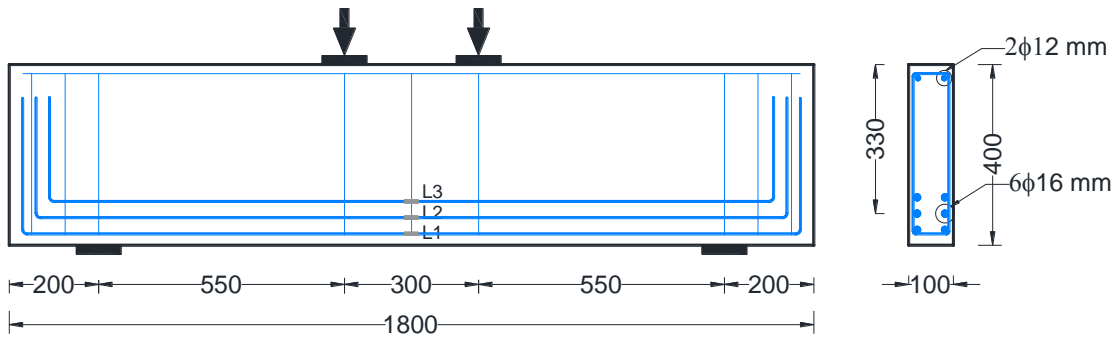
Figure B-39-General layout and reinforcement for beam D1
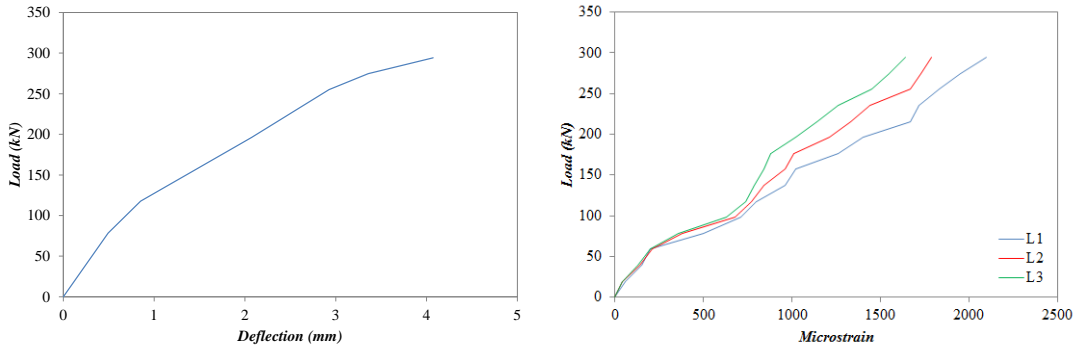
Figure B-40-Load-deflection response and strain in the flexural reinforcing bars of beam D1
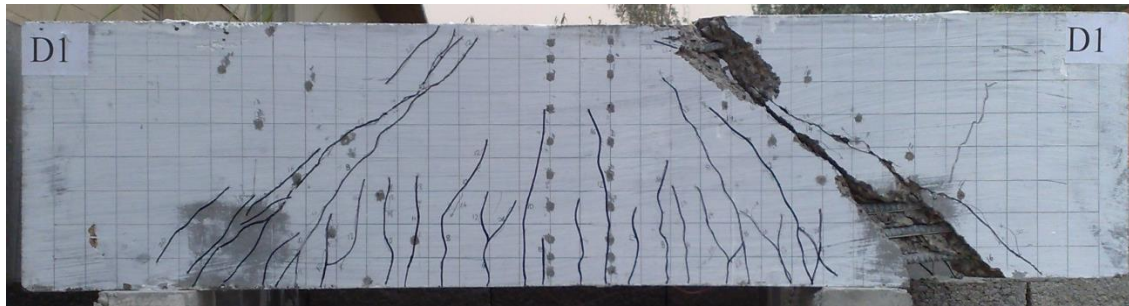
Figure B-41-Crack pattern after failure of beam D1

B.4.11.   BEAM D2
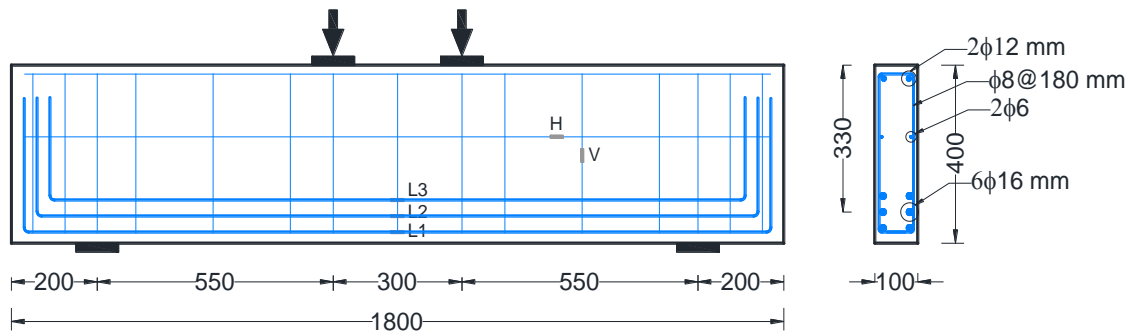
Figure B-42-General layout and reinforcement for beam D2
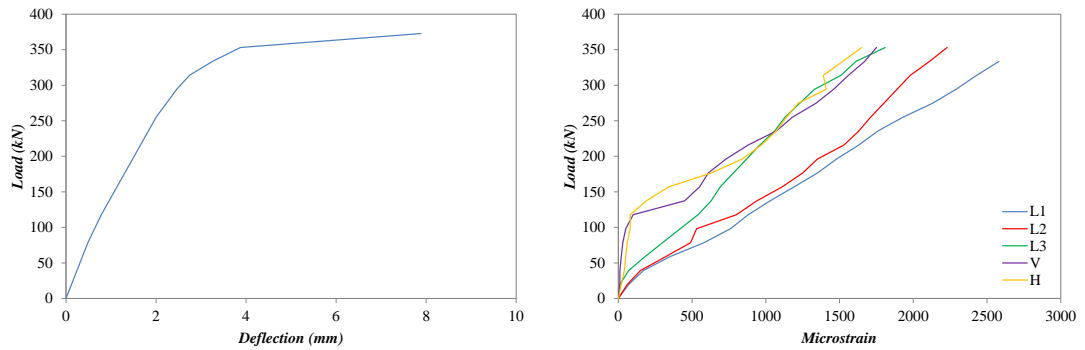
Figure B-43-Load-deflection response and strain in the flexural and shear reinforcing bars of beam D2
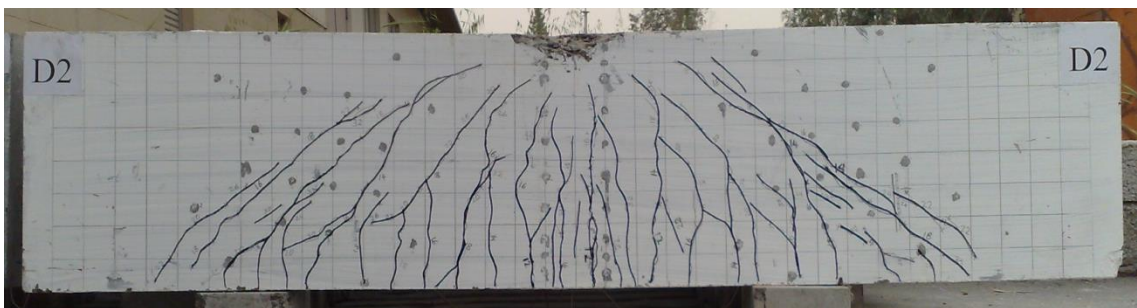
Figure B-44-Crack pattern after failure of beam D2

239

B.4.12.   BEAM D3
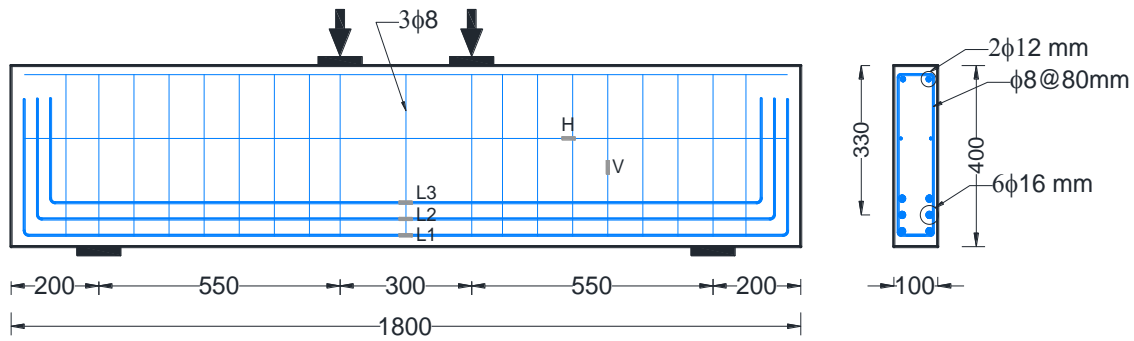
Figure B-45-General layout and reinforcement for beam D3
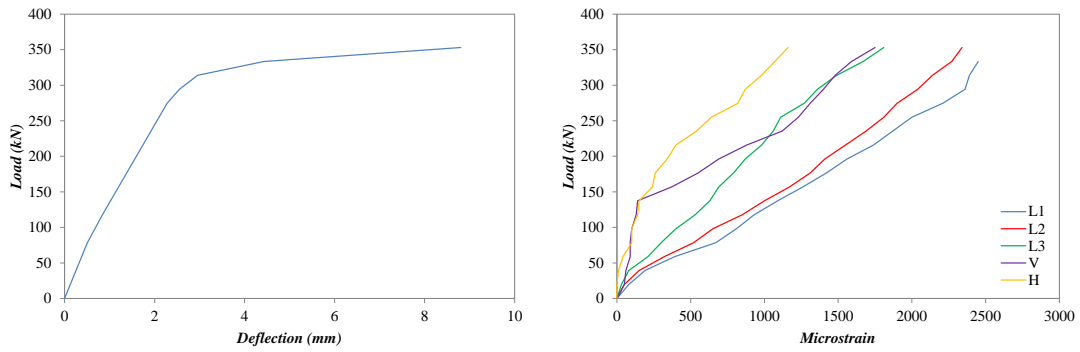
Figure B-46-Load-deflection response and strain in the flexural and shear reinforcing bars of beam D3

Figure B-47-Crack pattern after failure of beam D3

B.4.13.   BEAM E1
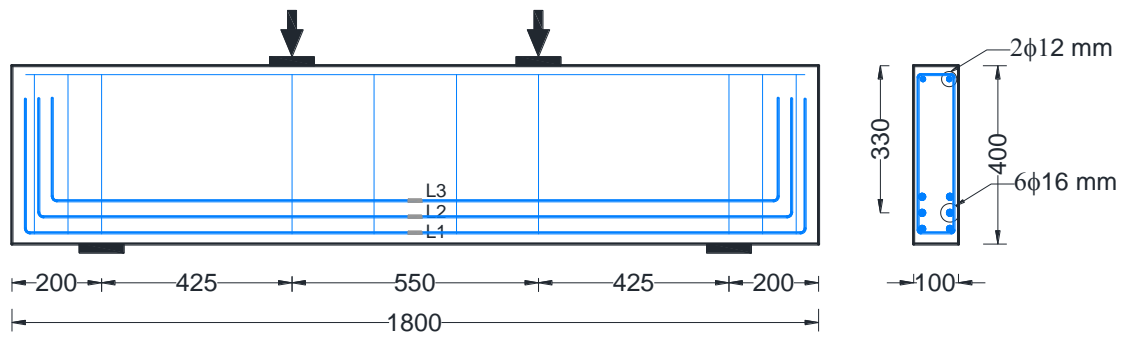
Figure B-48-General layout and reinforcement for beam E1
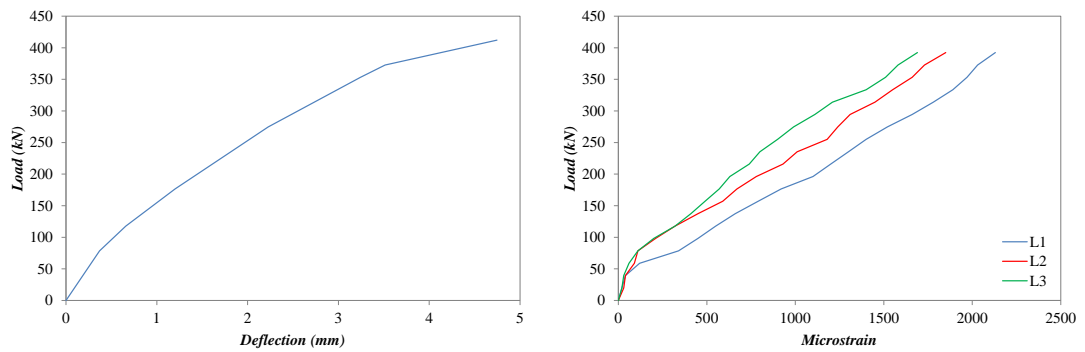
Figure B-49-Load-deflection response and strain in the flexural reinforcing bars of beam E1
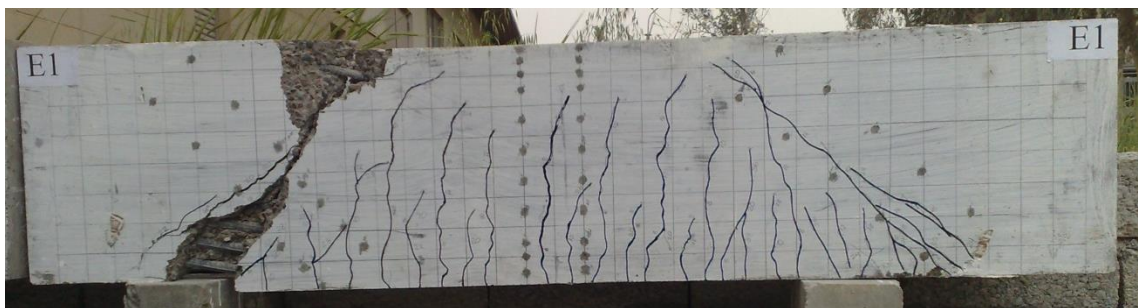
Figure B-50-Crack pattern after failure of beam E1

B.4.14.   BEAM E2
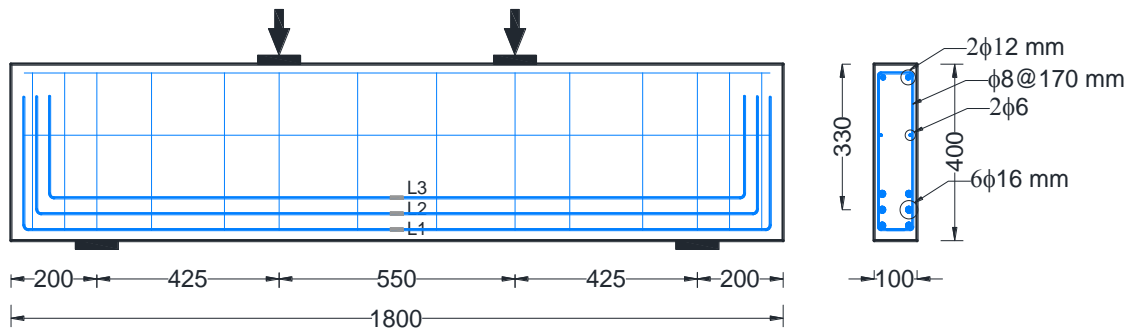
Figure B-51-General layout and reinforcement for beam E2
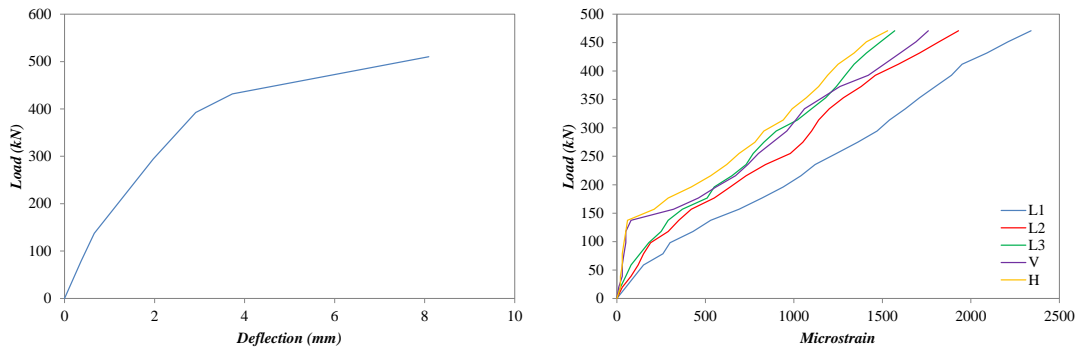
Figure B-52-Load-deflection response and strain in the flexural and shear reinforcing bars of beam E2
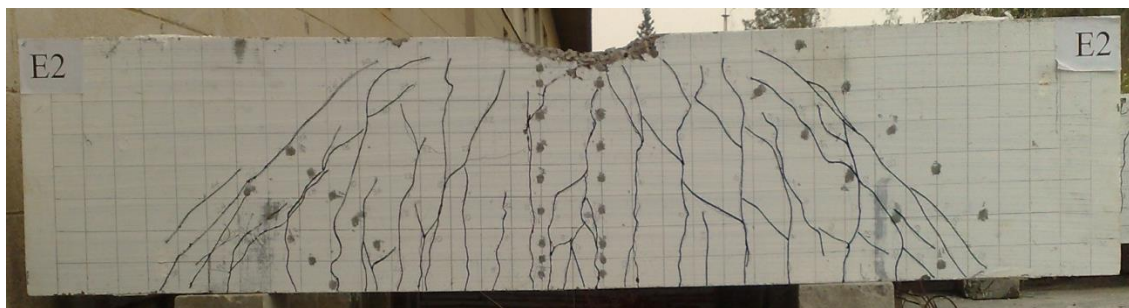
Figure B-53-Crack pattern after failure of beam E2

242

B.4.15.   BEAM E3
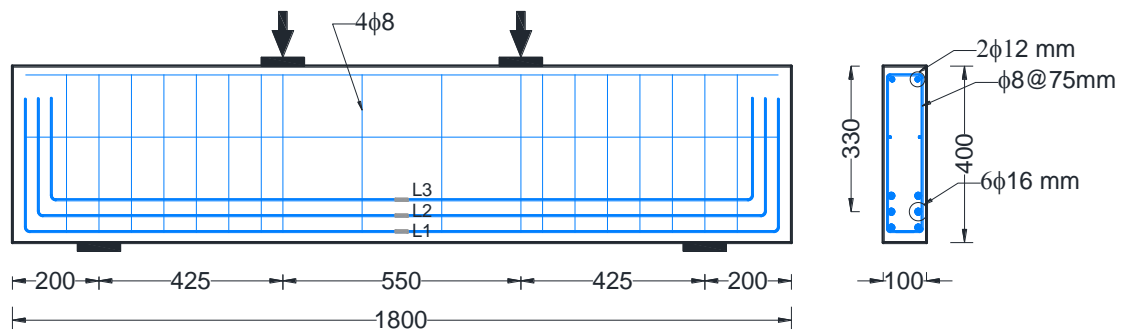
Figure B-54-General layout and reinforcement for beam E3
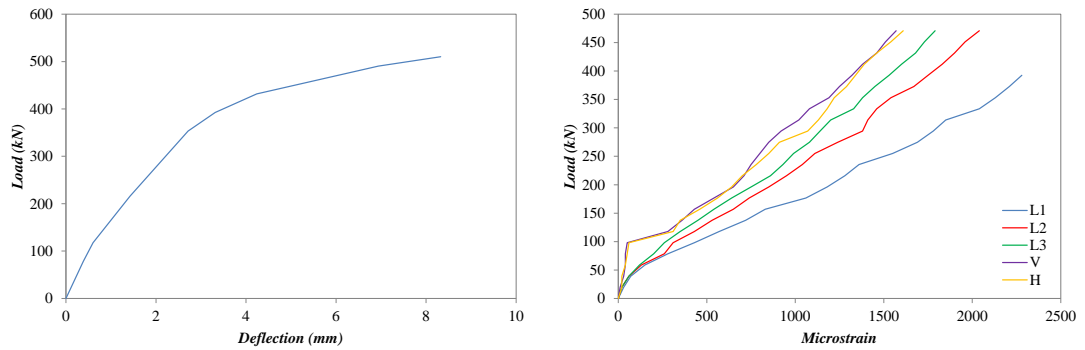
Figure B-55-Load-deflection response and strain in the flexural and shear reinforcing bars of beam E3
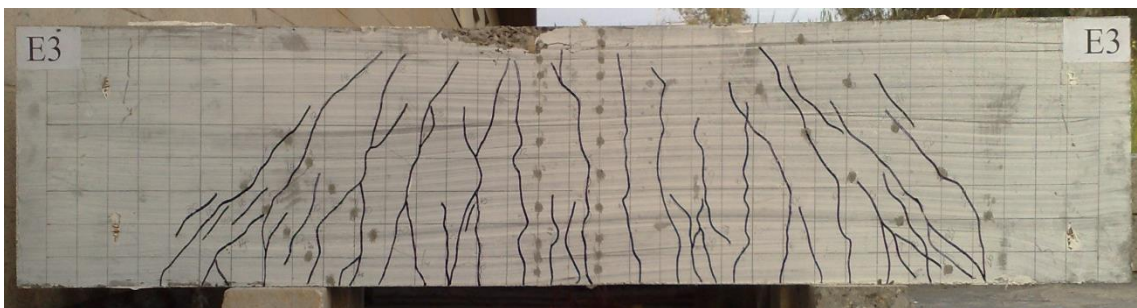
Figure B-56-Crack pattern after failure of beam E3

B.4.16.   BEAM F1
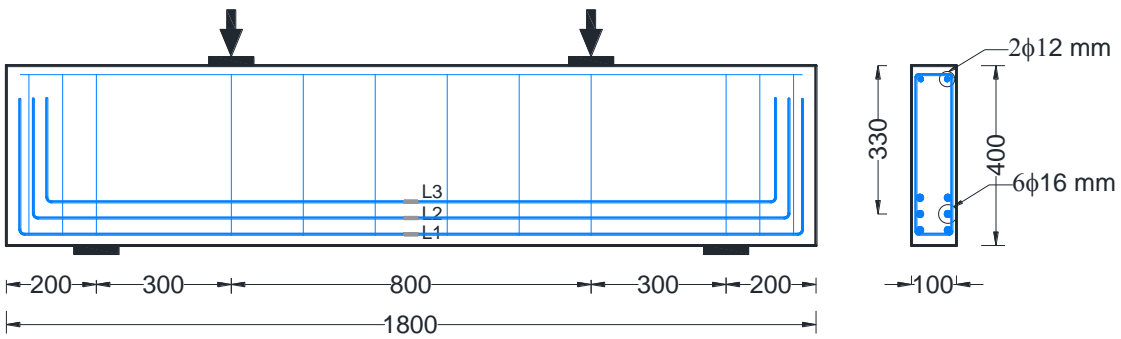
Figure B-57-General layout and reinforcement for beam F1
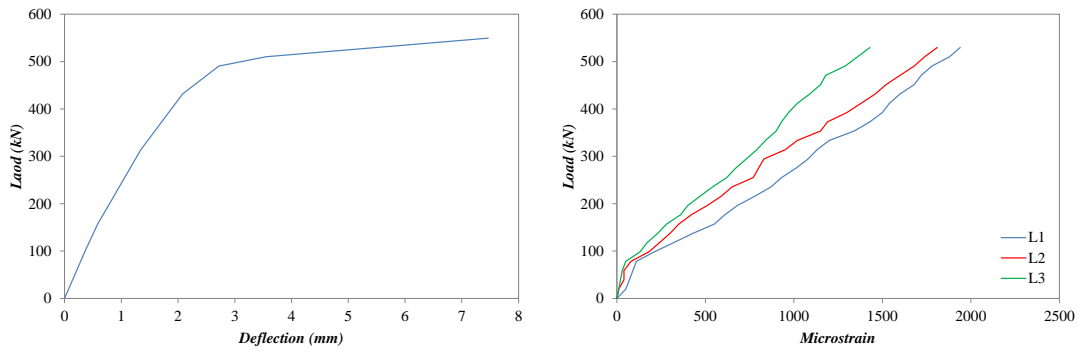
Figure B-58-Load-deflection response and strain in the flexural reinforcing bars of beam F1
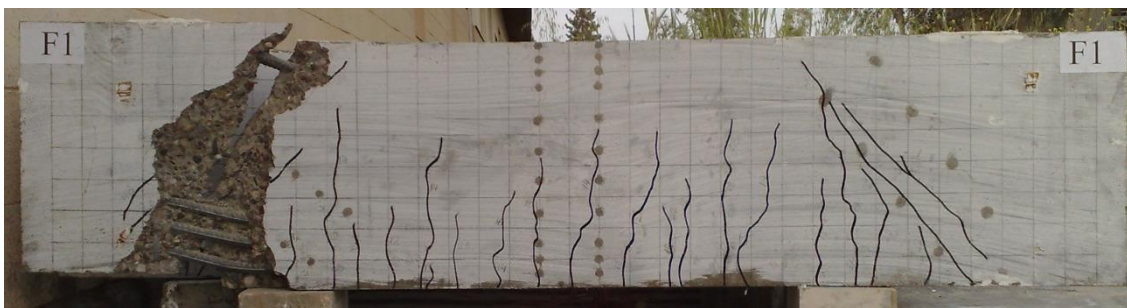
Figure B-59-Crack pattern after failure of beam F1

B.4.17.   BEAM F2
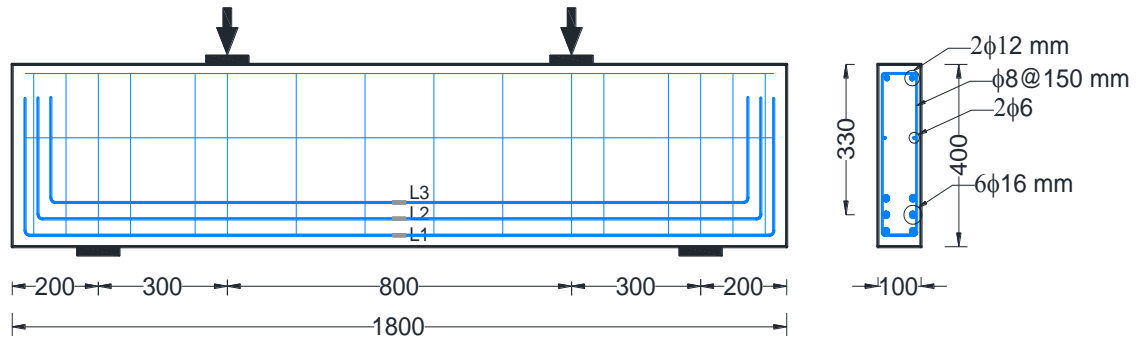
Figure B-60-General layout and reinforcement for beam F2
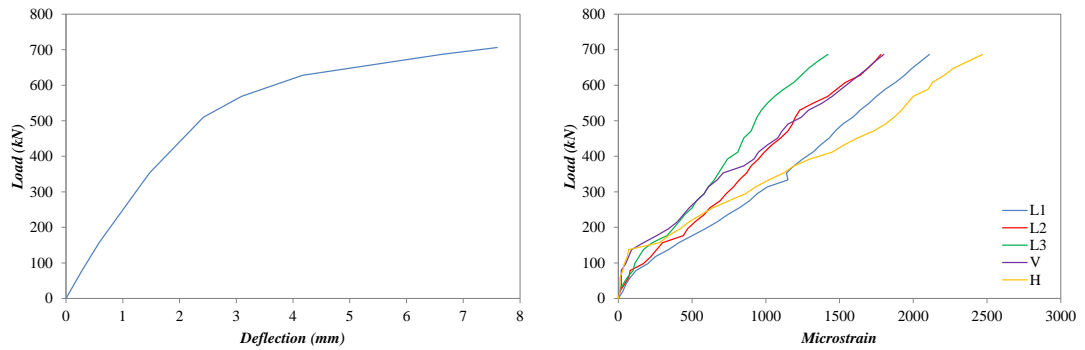
Figure B-61-Load-deflection response and strain in the flexural and shear reinforcing bars of beam F2
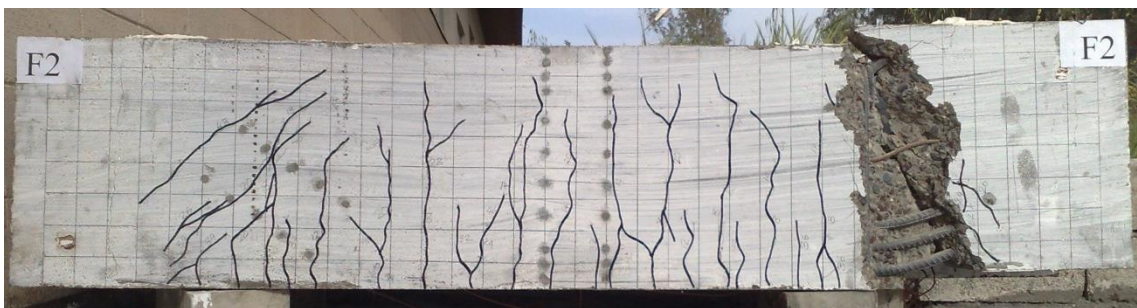
Figure B-62-Crack pattern after failure of beam F2

B.4.18.   BEAM F3
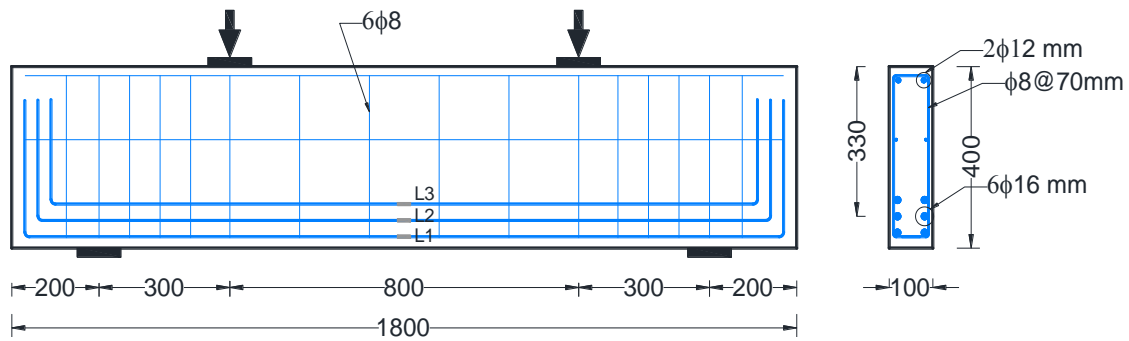
Figure B-63-General layout and reinforcement for beam F3
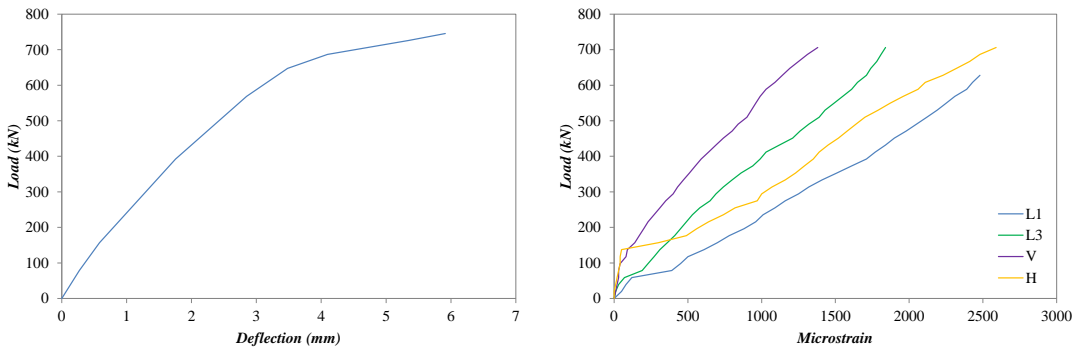
Figure B-64-Load-deflection response and strain in the flexural and shear reinforcing bars of beam F3
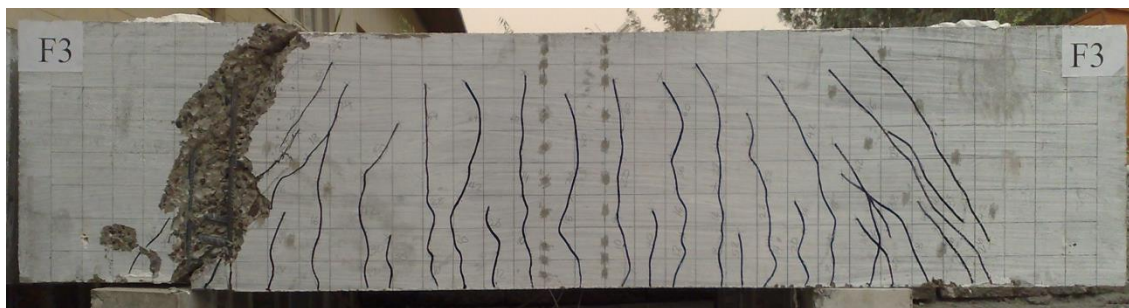
Figure B-65-Crack pattern after failure of beam F3

246

B.4.19.   BEAM G1

Figure B-66-General layout and reinforcement for beam G1

Figure B-67-Load-deflection response and strain in the flexural and shear reinforcing bars of beam G1

Figure B-68-Crack pattern after failure of beam G1

247

B.4.20.   BEAM G2

Figure B-69-General layout and reinforcement for beam G2

Figure B-70-Load-deflection response and strain in the flexural and shear reinforcing bars of beam G2

Figure B-71-Crack pattern after failure of beam G2

B.4.21.   BEAM G3

Figure B-72-General layout and reinforcement for beam G3

Figure B-73-Load-deflection response and strain in the flexural and shear reinforcing bars of beam G3

Figure B-74-Crack pattern after failure of beam G3

B.4.22.   BEAM H1

Figure B-75 Channel definition for LVDTs and internal strain-gauges
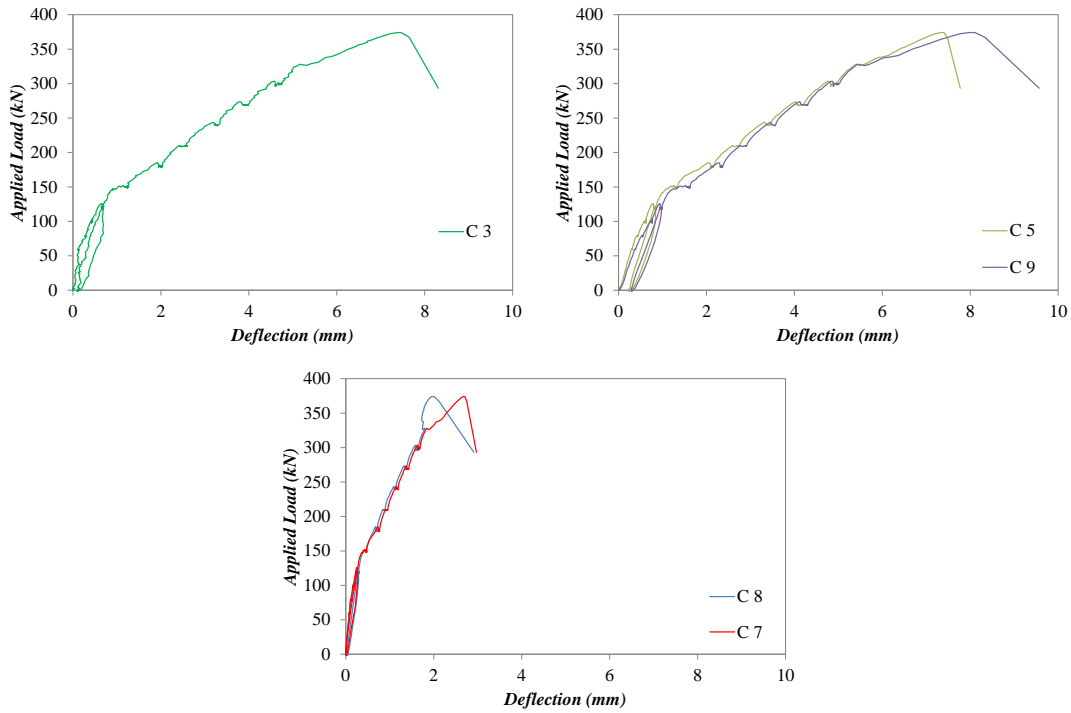
Figure B-76 Load-deflection responses
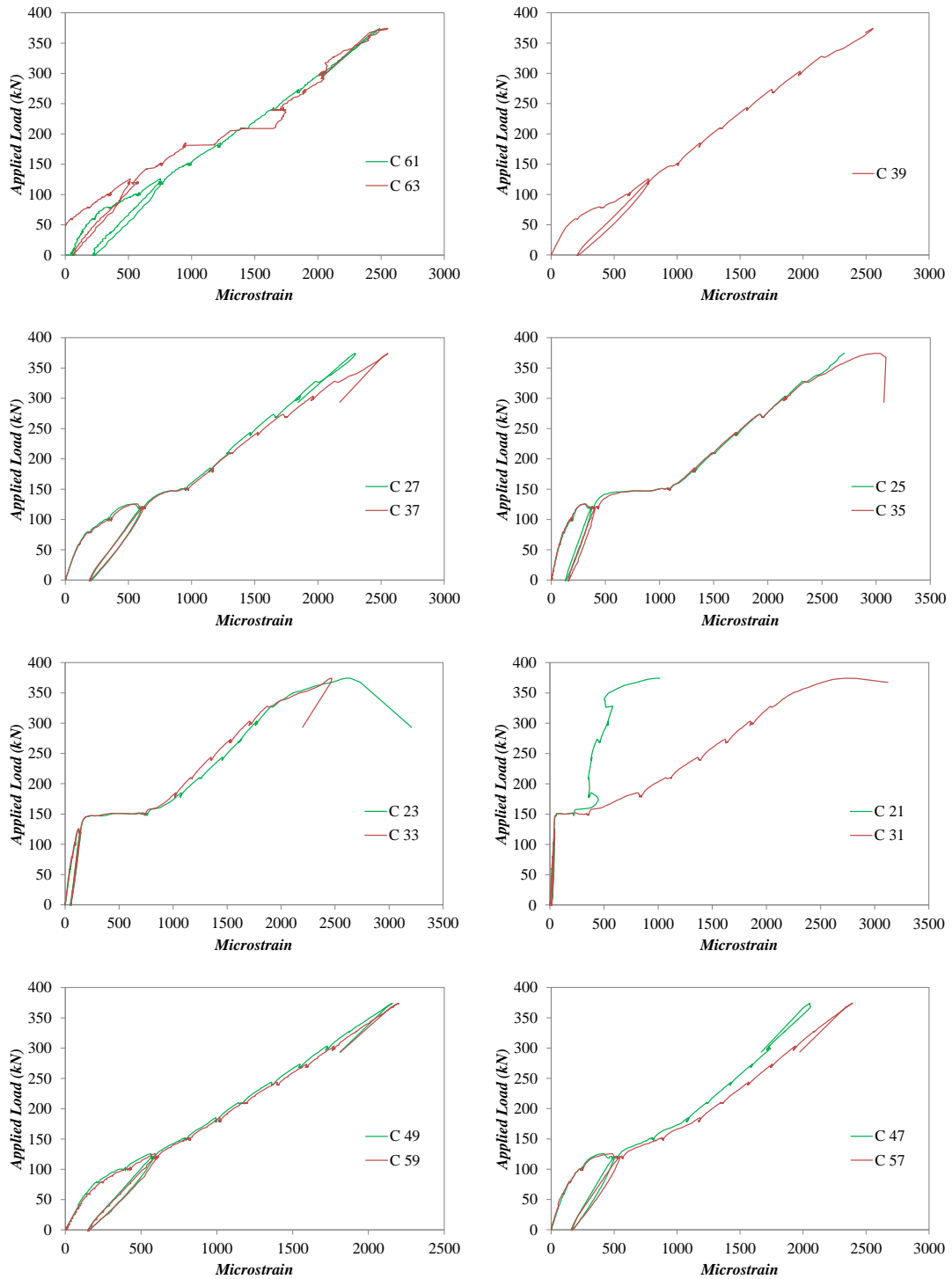
Figure B-77 Strain along the flexural reinforcing bars
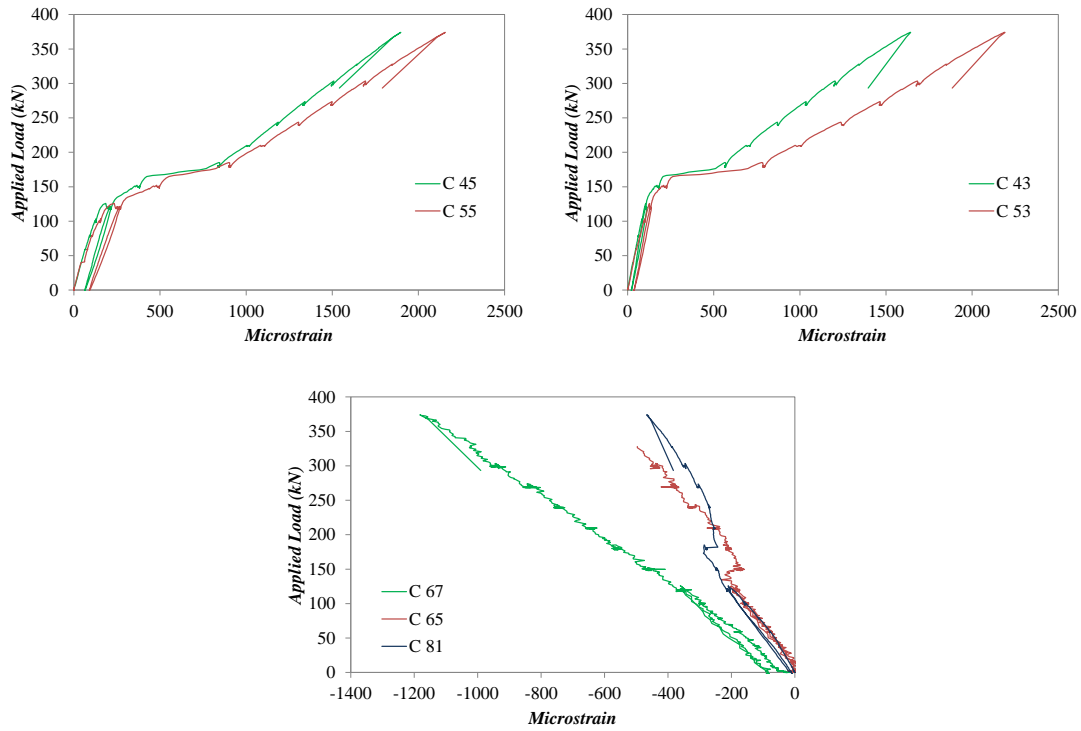
Figure B-77 Continued
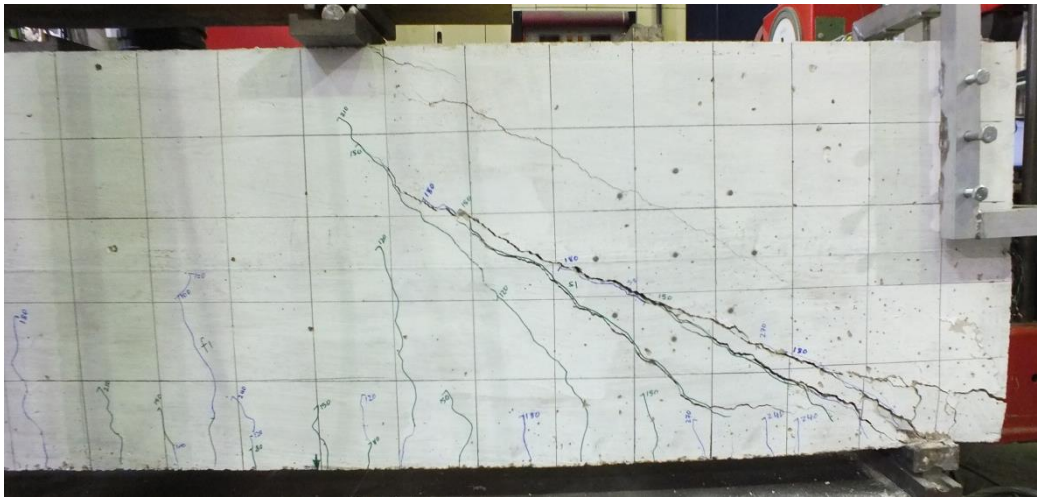
Figure B-78 Crack pattern after failure of beam H1

B.4.23.   BEAM H2
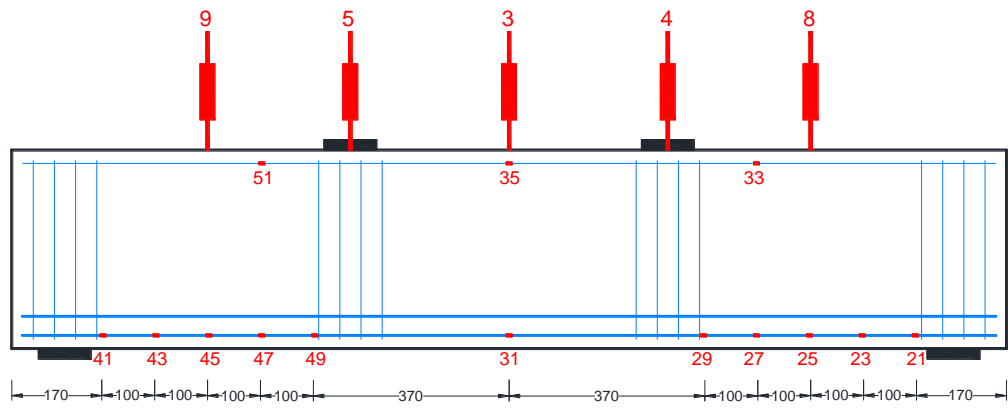
Figure B-79 Channel definition for LVDTs and internal strain-gauges
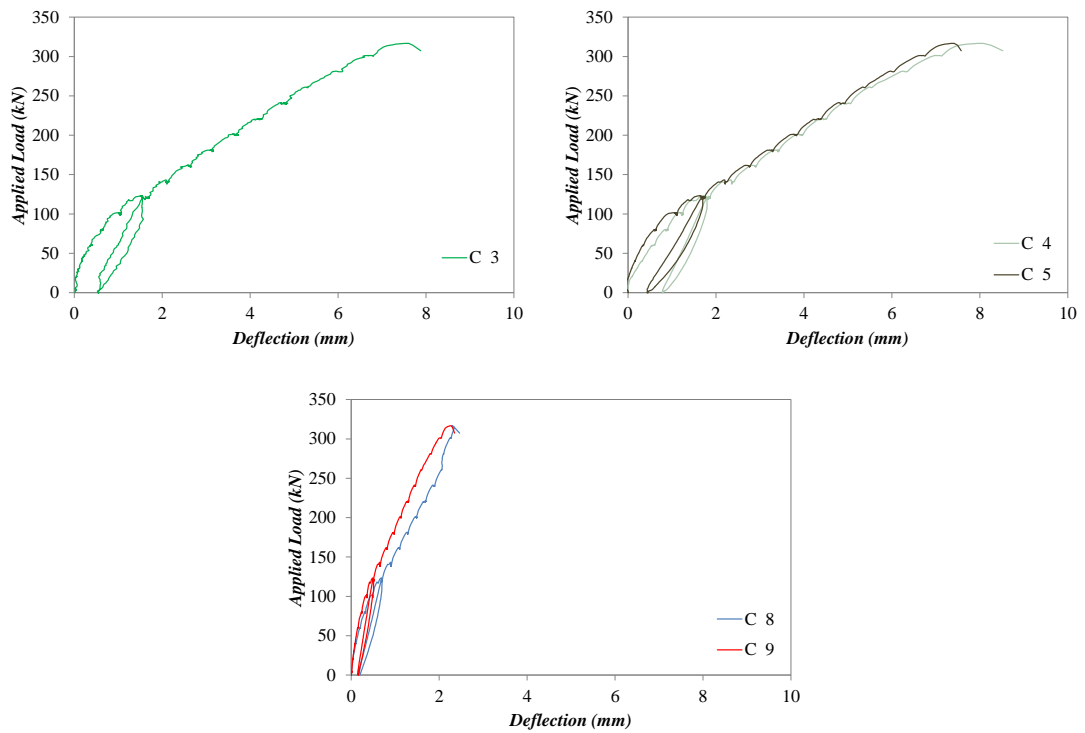
Figure B-80 Load-deflection responses
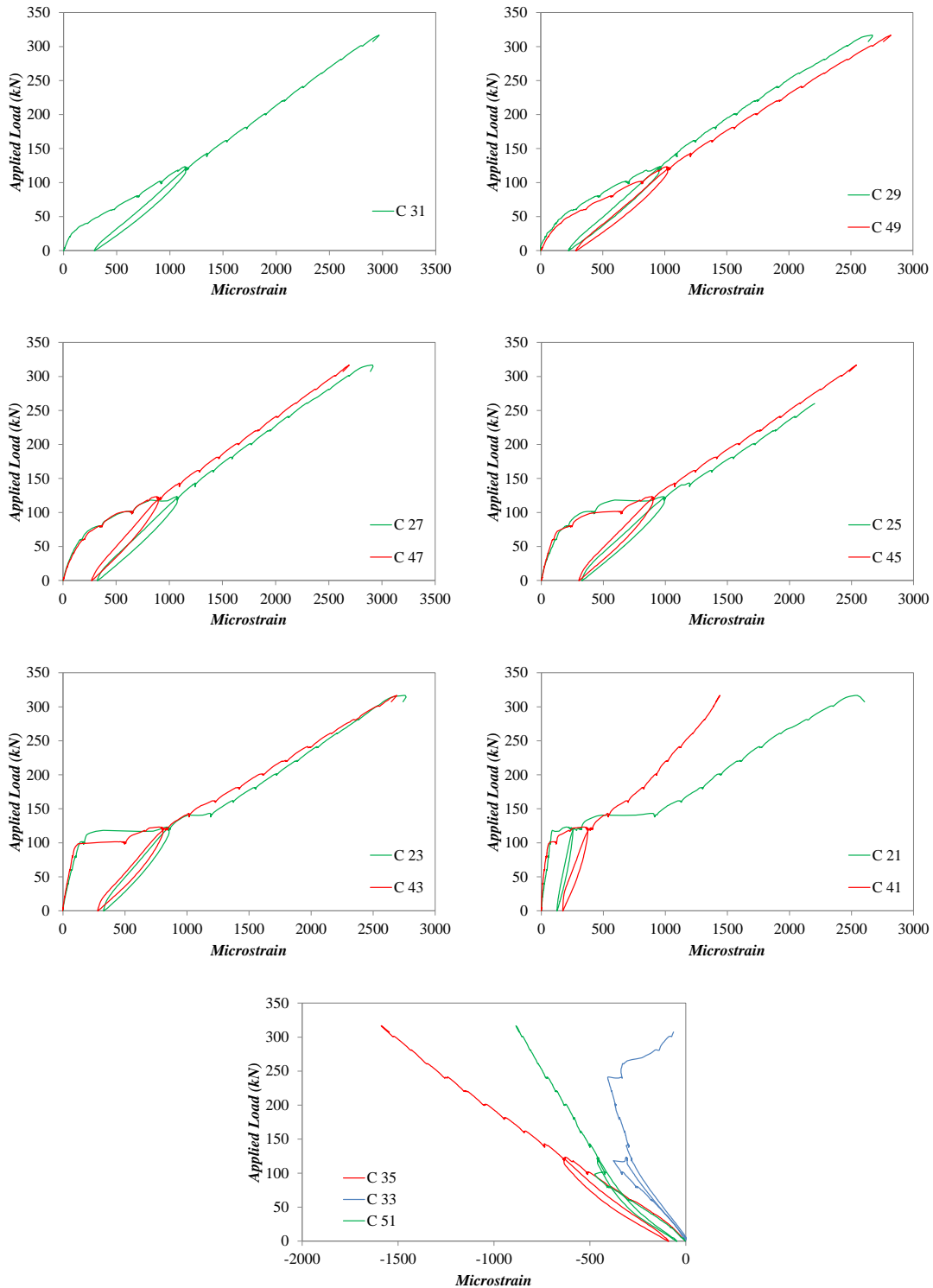
Figure B-81 Strain along the flexural reinforcing bars
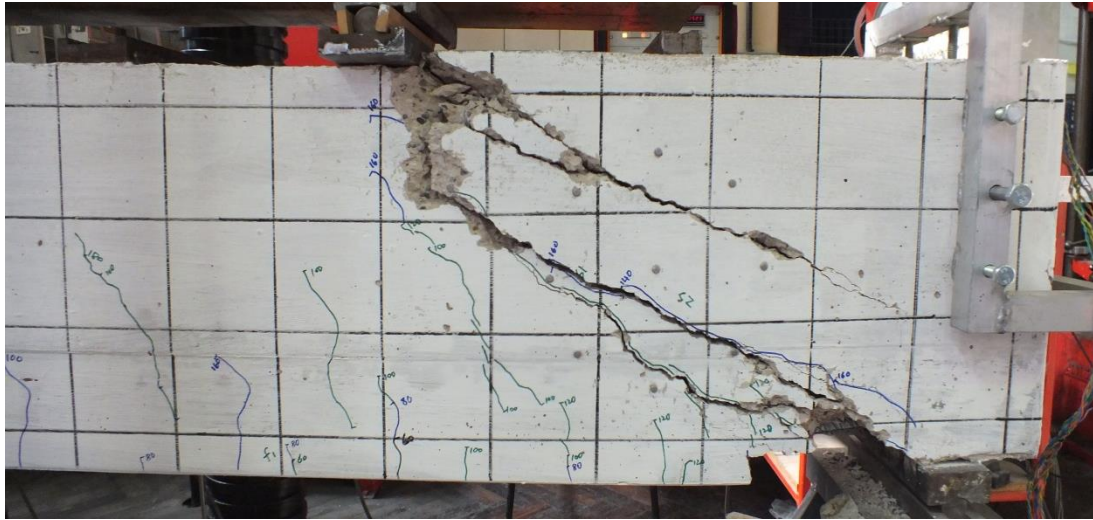
Figure B-82 Crack pattern after failure of beam H2

B.4.24.   BEAM H3
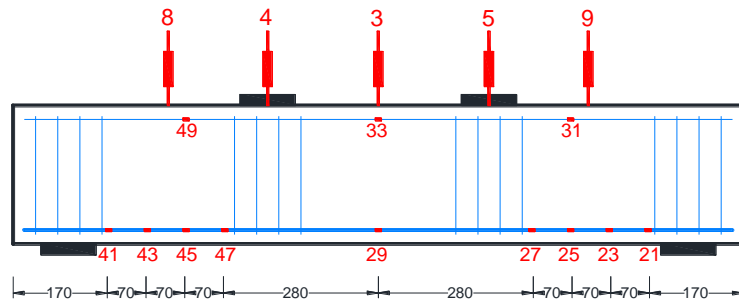
Figure B-83 Channel definition for LVDTs and internal strain-gauges
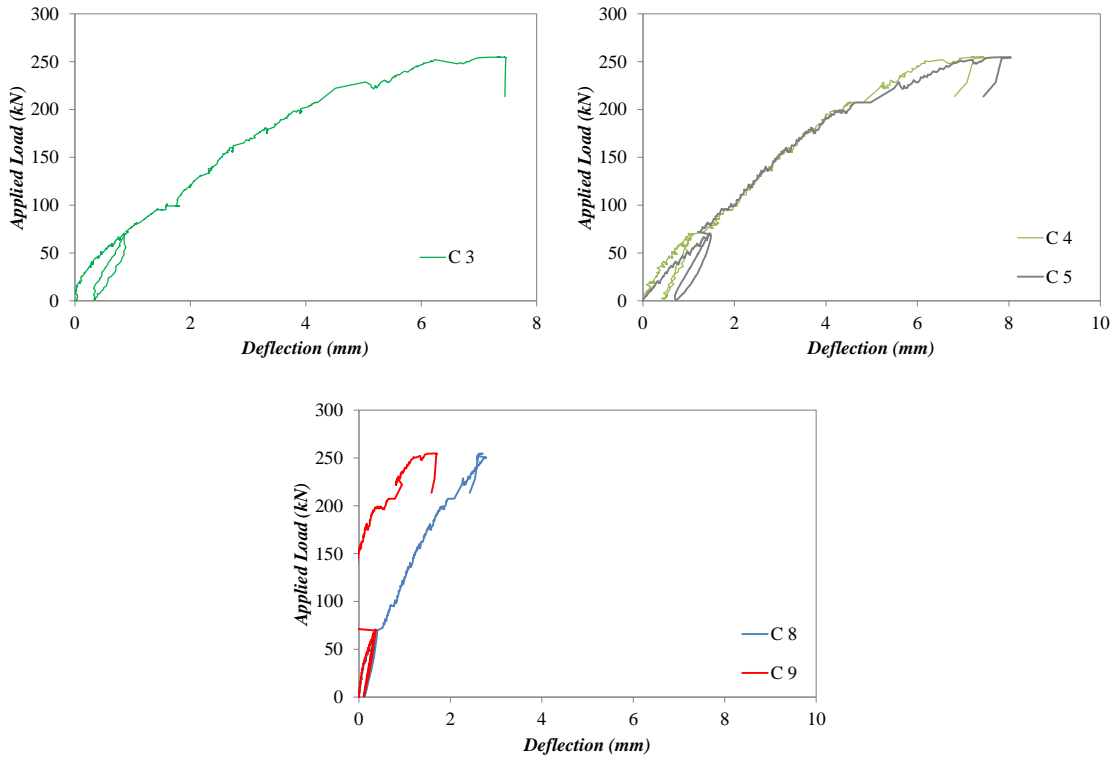
Figure B-84 Load-deflection responses
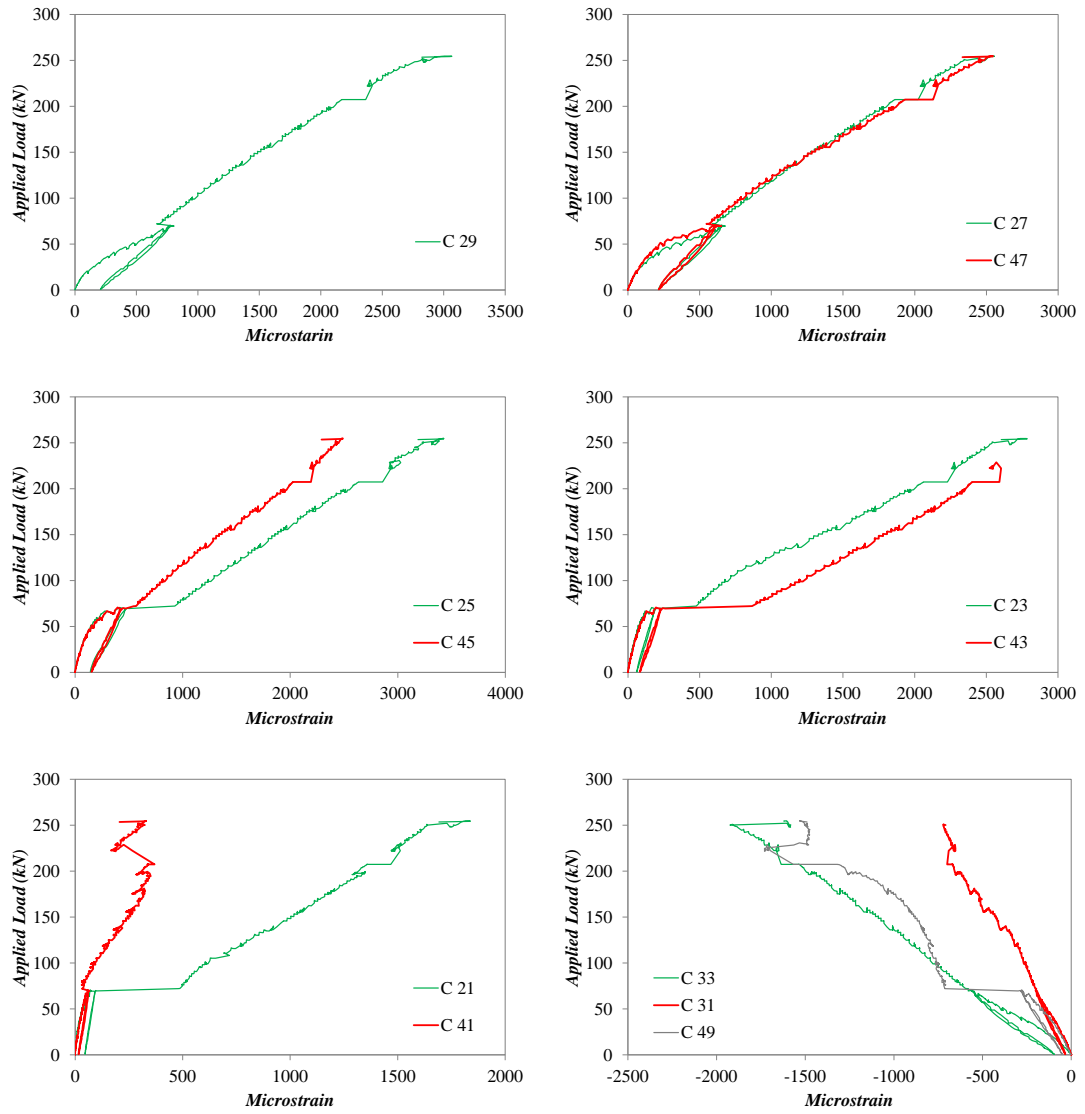
Figure B-85 Strain along the flexural reinforcing bars

APPENDIX C.   NUMERICAL RESULTS

C.1. EVALUATION OF CONCRETE MATERIAL MODELS AVAILABLE IN ABAQUS
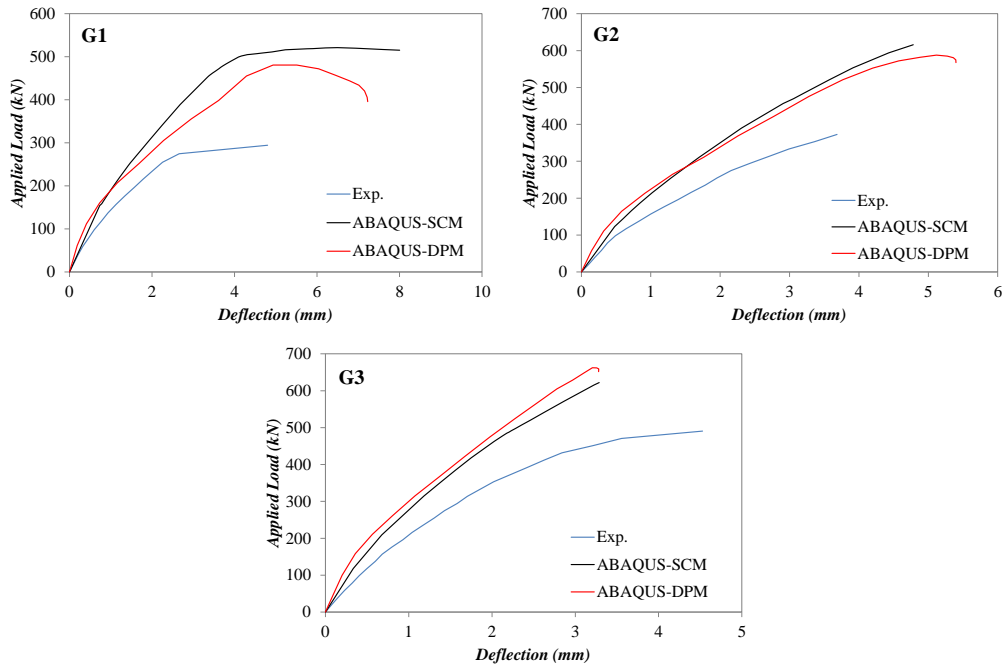
Figure C-1 Experimental and predicted load–deflection curves of specimens G1, G2 and G3
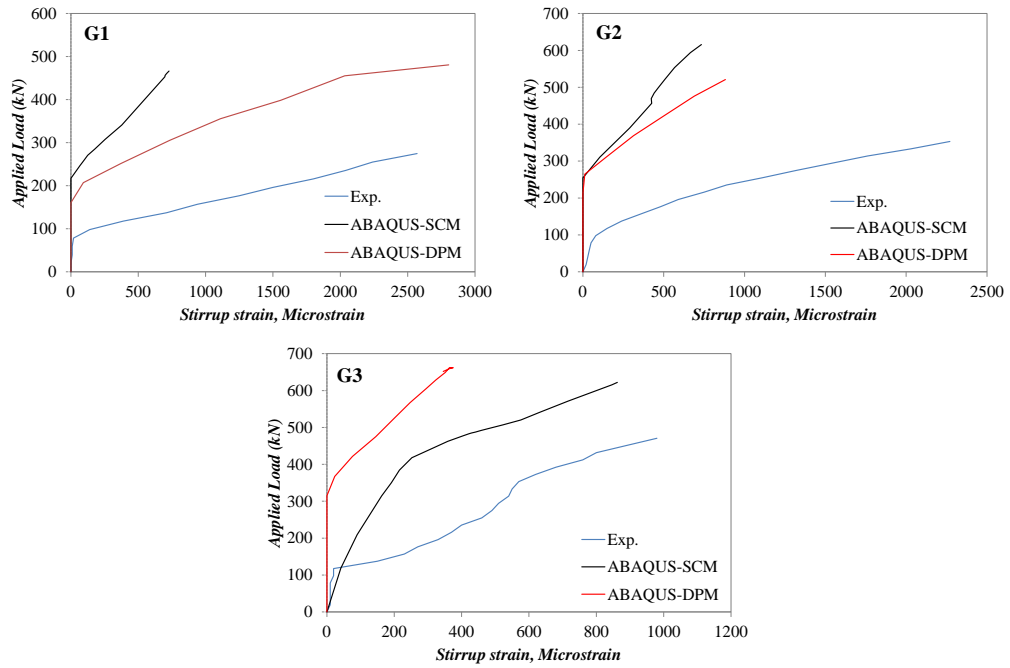
Figure C-2 Experimental and predicted stirrup strain of specimens G1, G2 and G3
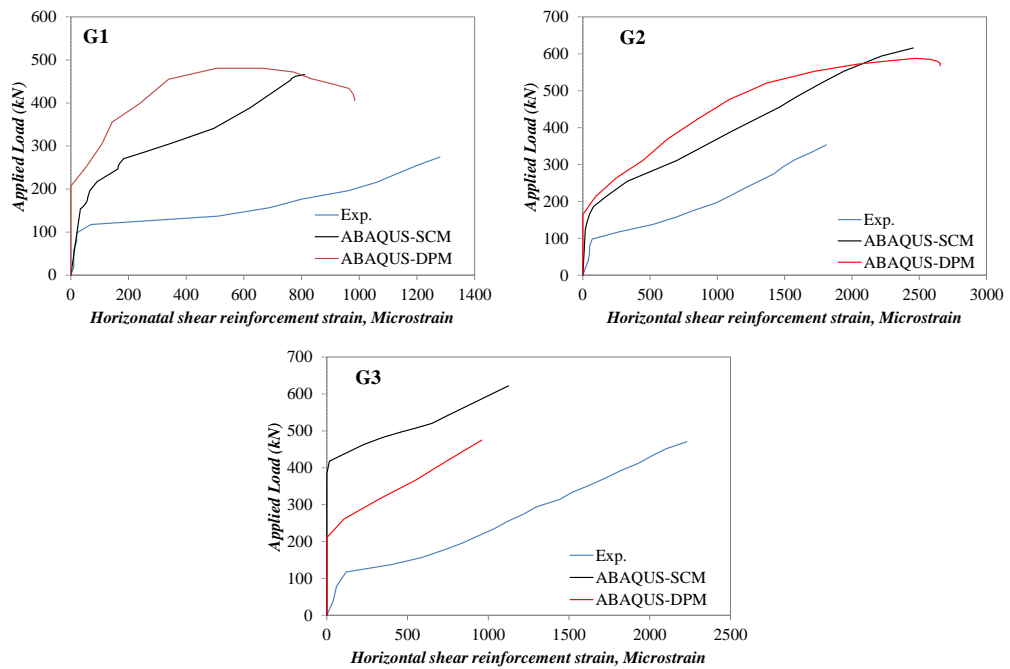
Figure C-3 Experimental and predicted horizontal shear reinforcement strain of

specimens G1, G2 and G3

C.2. MICROPLANE MATERIAL MODEL M4 FOR CONCRETE

The microplane material model is a macroscopic material model that defines the relation between the stress and strain vectors on planes of various orientations (microplanes). These microplanes can be assumed as cracked planes or weak planes, such as the contact faces between aggregate particles in concrete. The basic idea of the microplane model can be traced back to the pioneering idea of Tayler [83] which was later developed by Batdorf and Budianski [84] for polycrystalline metals and became known as the slip theory of plasticity. This model was later extended by Bazant and co-workers [39, 40, 43, 85-90] who added extra features to better represent the behaviour of quasi brittle materials, including concrete. These features can be briefly summarized as follows:

- The static micro-macro constraint should be replaced by kinematic micro-macro constraint to stabilize the postpeak strain softening. That is the strain vectors on microplanes are the projection of the strain tensors.
- Elastic strain is included at the microplane level instead of adding it at the macro level. This is due to replacing the static micro-macro constraint with the kinematic.
- The principle of virtual work is used instead of simple superposition of the microplane stresses to relate the stresses on the microplane, which can have any possible orientation, to the stress at macro level.

Since the kinematic constraint is used, the microplane strain vector ε_{Ni} is determined as the projection of the strain tensor ε_{ij}. The normal strain ε_N and both shear strains ε_M, ε_L on the microplane can then be found according to the following equations:

$$\varepsilon_N = N_{ij}\varepsilon_{ij}, \quad \varepsilon_M = M_{ij}\varepsilon_{ij}, \quad \varepsilon_L = L_{ij}\varepsilon_{ij} \tag{C-1}$$

where $N_{ij}=n_in_j$, $M_{ij}=(m_in_j+m_jn_i)/2$ and $L_{ij}=(l_in_j+l_jn_i)/2$ and n,m and l are direction cosines, their values of which can be found elsewhere [91].

Bazant et al. [39] calculated the stress at the continuum level from the microplane stresses applying principle of virtual work (Eq.C-2), which can be approximated by optimal Gaussian integration for a spherical surface (Eq.C-3).

$$\frac{2\pi}{3}\sigma_{ij}\delta\varepsilon_{ij} = \int_{\Omega}(\sigma_N\delta\varepsilon_N + \sigma_L\delta\varepsilon_L + \sigma_M\delta\varepsilon_M)d\Omega \tag{C-2}$$

$$\sigma_{ij} = \frac{3}{2\pi}\int_{\Omega}s_{ij}d\Omega \approx 6\sum_{\mu=1}^{N_m}w_\mu s_{ij}^{(\mu)}; \text{ with } s_{ij} = \sigma_N N_{ij} + \sigma_L L_{ij} + \sigma_M M_{ij} \tag{C-3}$$

The constitutive law of microplane M4 is characterized by an elastic stress-strain relationship up to a defined set of limits, which is called stress-strain boundaries, followed by a strain softening behaviour. The stresses are never allowed to exceed the boundaries, however, traveling along the boundaries is allowed if the strain increment and the total stress have the same sign, otherwise, unloading occurs.

Bazant and co-workers [39, 40] split the normal stress and strain components into volumetric and deviatoric parts ($\sigma_N=\sigma_V+\sigma_D$ and $\varepsilon_N=\varepsilon_V+\varepsilon_D$) to realistically model the compression failure and to control the value of Poisson's ratio. The incremental stress-strain relations are expressed as

$$d\sigma_V = E_V d\varepsilon_V, \quad d\sigma_D = E_D d\varepsilon_D, \quad d\sigma_M = E_T d\varepsilon_M, \quad d\sigma_L = E_T d\varepsilon_L \tag{C-4}$$

where E_V, E_D and E_T are microplane elastic moduli and can be written as

$$E_V = E/(1-2v), \quad E_D = 5E/[(1-2v)(2+3\eta)], \quad E_V = \eta E_D \tag{C-5}$$

where E is Young's modulus, v is Poison's ratio and η is 1.0 [176]. The above microplane elastic moduli can be used in the case of loading as well as reloading. Additionally, they can be used for unloading if the sign of $\sigma\Delta\varepsilon$ is positive. Otherwise stiffness degradation occurs and the value of tangential stiffness moduli (Eq. C-6 to C-9) should be used for unloading.

For ε_V>0 and σ_V>0 $E_V^U(-\varepsilon_V,-\sigma_V)=E_V\left(\dfrac{c_{15}}{c_{15}-\varepsilon_V}+\dfrac{\sigma_V}{c_{15}c_{16}E_V}\varepsilon_V\right)$ (C-6)

For ε_V>0 and σ_V>0 $E_V^U(\varepsilon_V,\sigma_V)=\min\left[\sigma_V(\varepsilon_V)/\varepsilon_V,E_V\right]$ (C-7)

$E_D^U=(1-c_{17})E_D+c_{17}E_D^S;\ E_D^S=E_D\ \text{if}\ \sigma_D\varepsilon_D\le 0;\ \text{else}\ E_D^S=\min\left(\sigma_D/\varepsilon_D,E_D\right)$ (C-8)

$E_T^U=(1-c_{17})E_T+c_{17}E_T^S;\ E_T^S=E_T\ \text{if}\ \sigma_T\varepsilon_T\le 0;\ \text{else}\ E_T^S=\min\left(\sigma_T/\varepsilon_T,E_T\right)$ (C-9)

where c_{15}, c_{16} and c_{17} are fixed dimensionless parameters.

The following stress-strain boundaries (Eq.C-10) were introduced by Bazant and co-workers to realistically simulate the behaviour of concrete and to capture its strain softening,:

$$\sigma_N\le F_N(\varepsilon_N),\quad F_V^-(\varepsilon_V)\le\sigma_V\le F_v^+(\varepsilon_v),\quad F_D^-(\varepsilon_D)\le\sigma_D\le F_D^+(\varepsilon_D),$$
$$|\sigma_M|\le F_T(\sigma_N,\varepsilon_V),\quad |\sigma_L|\le F_T(\sigma_N,\varepsilon_V)$$ (C-10)

where F_N, F_V, F_D and F_T are normal, volumetric, deviatoric and tangential boundaries, respectively, and they can be found through the following equations:

$$F_N(\varepsilon_N)=Ek_1c_1\exp\left(-\frac{\langle\varepsilon_N-k_1c_1c_2\rangle}{k_1k_5c_3+\langle-c_4(\sigma_V/E_V)\rangle}\right)$$ (C-11)

$$F_V^-(-\varepsilon_V)=-Ek_1k_3\exp\left(-\frac{\varepsilon_V}{k_1k_4}\right)\qquad \text{if}\ \sigma_V<0$$ (C-12)

$$F_v^+(\varepsilon_v)=\frac{E_vk_1c_{13}}{[1+(c_{14}/k_1)\langle\varepsilon_v-k_1c_{13}\rangle]^2}\qquad \text{if}\ \sigma_V>0$$ (C-13)

$$F_D^+(\varepsilon_D)=\frac{Ek_1c_5}{1+\left(\dfrac{\langle\varepsilon_D-k_1c_5c_6\rangle}{k_1c_7c_{18}}\right)^2}\qquad \text{if}\ \sigma_D>0$$ (C-14)

$$F_D^-(-\varepsilon_D) = \frac{Ek_1c_8}{1 + \left(\dfrac{\langle -\varepsilon_D - k_1c_8c_9 \rangle}{k_1c_7}\right)^2} \qquad \text{if } \sigma_D<0 \qquad\qquad \text{(C-15)}$$

$$F_T(-\sigma_N) = \frac{E_Tk_1k_2c_{10}\langle -\sigma_N + \sigma_N^0 \rangle}{E_Tk_1k_2 + c_{10}\langle -\sigma_N + \sigma_N^0 \rangle} \qquad\qquad \text{(C-16)}$$

where

$$\sigma_N^0 = \frac{E_Tk_1c_{11}}{1 + c_{12}\langle \varepsilon_v \rangle} \qquad\qquad \text{(C-17)}$$

The Macaulay brackets can be defined as $\langle x \rangle = Max(x,0)$. k_i (k_1, k_2, k_3 and k_4) and c_i ($c_1, c_2 ... c_{18}$) are adjustable and fixed material parameters, respectively.

The value of adjustable and fixed material parameters are as follow [43]:

$k_1=0.0003$	$k_2=200.0$	$k_3=15.0$	$k_4=100.0$		
$c_1=0.30$	$c_2=2.76$	$c_3=4.0$	$c_4=70.0$	$c_5=2.50$	$c_6=1.30$
$c_7=15$	$c_8=2.00$	$c_9=1.30$	$c_{10}=0.73$	$c_{11}=0.20$	$c_{12}=7000$
$c_{13}=0.20$	$c_{14}=0.50$	$c_{15}=0.02$	$c_{16}=0.01$	$c_{17}=0.40$	$c_{18}=1.01$

C.3. VUMAT CODE

```fortran
c VUMAT CODE
      subroutine vumat(
c Read only
     1 nblock, ndir, nshr, nstatev, nfieldv, nprops, lanneal,
     2 stepTime, totalTime, dt, cmname, coordMp, charLength,
     3 props, density, strainInc, relSpinInc,
     4 tempOld, stretchold, defgradold, fieldold,
     5 stressOld, stateOld, enerInternOld, enerInelasOld,
     6 tempNew, stretchNew, defgradNew, fieldNew,
c Write only
     7 stressNew, stateNew, enerInternNew, enerInelasNew)
c
      include 'vaba_param.inc'
c
      dimension props(nprops), density(nblock), coordMp(nblock,*),
     1 charLength(*), strainInc(nblock,ndir+nshr),
     2 relSpinInc(*), tempOld(*),
     3 stretchOld(nblock,ndir+nshr),
     4 defgradOld(*),
     5 fieldOld(*), stressOld(nblock,ndir+nshr),
     6 stateOld(nblock,nstatev), enerInternOld(nblock),
     7 enerInelasOld(nblock), tempNew(*),
     8 stretchNew(nblock,ndir+nshr),
     8 defgradNew(*),
     9 fieldNew(*),
     1 stressNew(nblock,ndir+nshr), stateNew(nblock,nstatev),
     2 enerInternNew(nblock), enerInelasNew(nblock)
c
      character*80 cmname
c
      real dstrain(nblock,6), strainold(nblock,6),
     1volstrainold(nblock), dvolstrain(nblock), volstrainnew(nblock),
     2volstressold(nblock), volstress(nblock), nbstressvol(nblock),
     3pbstressvol(nblock), volstress1(nblock), sn(3,3), dsn(3,3),
     4nstrainold(21), dnstrain(21), nstrainnew(nblock,21),
     5devstrainold(nblock,21), devstrainnew(nblock,21),
     6ddevstrain(nblock,21), devstressold(nblock,21),
     7devstress(nblock,21), pbdevstress(nblock,21),
     8nbdevstress(nblock,21), devstress1(nblock,21)
c
      real norstress(nblock,21), bnorstress(nblock,21),
     1norstressnew(nblock,21),volstress2(nblock), volstressnew(nblock),
     2devstressnew(nblock,21), mstrainold(21), lstrainold(21),
     3dmstrain(21), dlstrain(21), mstrainnew(nblock,21),
     4lstrainnew(nblock,21), mstressold(nblock,21),
     5lstressold(nblock,21), mstress1(nblock,21), lstress1(nblock,21),
     6tstrainnew(nblock,21), dtstrain(nblock,21), tstress1(nblock,21),
     7rm(nblock,21), rl(nblock,21), mstress2(nblock,21),
     8lstress2(nblock,21), tstress2(nblock,21), btstress(nblock,21)
c
      real tstressnew(nblock,21), mstressnew(nblock,21),
     1lstressnew(nblock,21), sd1(nblock), sd2(nblock),
```

```
     2sd3(nblock), sd4(nblock), sd5(nblock), sd6(nblock),
     3f(21), sigmano(nblock,21), norstresss(nblock,21),
     4norstressnews(nblock,21), norstressnewns(nblock,21),
     5norstressns(nblock,21), norstressnsold(nblock,21),
     6tstressold(nblock,21),volstressn(nblock),tstrainold(nblock,21),
     7prinmax(nblock,21)
c

      real N(21,3),M(21,3), L(21,3), W(21), delta(nblock,6)
      real ev1,ev2,evn,ev,ed1,mbd1,mbd2,ed,eds,mbn1,mbn2,en,mbf,sina,
     1fsigma,mbfi,fi,et1,mbt1,min,zi,mbt2,et,ets,mbv
c

      parameter(c1=0.3, c2=2.76, c3=4.0, c4=70, c5=2.5, c6=1.3,
     1c7=15, c8=2.0, c9=1.3, c10=0.73, c11=0.2, c12=7000, c13=0.20,
     2c14=0.5, c15=0.02, c16=0.01, c17=0.4, c18=1.0, u=1,
     3pi=3.141592654)
c

      do 100 km = 1,nblock
c
c   Weights and direction cosines for the 21-points integration formula
      n(1,1)=1
      N(1,2)=0
      N(1,3)=0
      N(2,1)=0
      N(2,2)=1
      N(2,3)=0
      N(3,1)=0
      N(3,2)=0
      N(3,3)=1
      N(4,1)=0.707106781
      N(4,2)=0.707106781
      N(4,3)=0
      N(5,1)=0.707106781
      N(5,2)=-0.707106781
      N(5,3)=0
      N(6,1)=0.707106781
      N(6,2)=0
      N(6,3)=0.707106781
      N(7,1)=0.707106781
      N(7,2)=0.0
      N(7,3)=-0.707106781
      N(8,1)=0
      N(8,2)=0.707106781
      N(8,3)=0.707106781
      N(9,1)=0.0
      N(9,2)=0.707106781
      N(9,3)=-0.707106781
      N(10,1)=0.387907304
      N(10,2)=0.387907304
      N(10,3)=0.836095597
      N(11,1)=0.387907304
      N(11,2)=0.387907304
      N(11,3)=-0.836095597
      N(12,1)=0.387907304
      N(12,2)=-0.387907304
      N(12,3)=0.836095597
```

265

```
          N(13,1)=0.387907304
          N(13,2)=-0.387907304
          N(13,3)=-0.836095597
          N(14,1)=0.387907304
          N(14,2)=0.836095597
          N(14,3)=0.387907304
          N(15,1)=0.387907304
          N(15,2)=0.836095597
          N(15,3)=-0.387907304
          N(16,1)=0.387907304
          N(16,2)=-0.836095597
          N(16,3)=0.387907304
          N(17,1)=0.387907304
          N(17,2)=-0.836095597
          N(17,3)=-0.387907304
          N(18,1)=0.836095597
          N(18,2)=0.387907304
          N(18,3)=0.387907304
          N(19,1)=0.836095597
          N(19,2)=0.387907304
          N(19,3)=-0.387907304
          N(20,1)=0.836095597
          N(20,2)=-0.387907304
          N(20,3)=0.387907304
          N(21,1)=0.836095597
          N(21,2)=-0.387907304
          N(21,3)=-0.387907304
C
          M(1,1)=0.0
          M(1,2)=-1.0
          M(1,3)=0.0
          M(2,1)=1.0
          M(2,2)=0.0
          M(2,3)=0.0
          M(3,1)=1.0
          M(3,2)=0.0
          M(3,3)=0.0
          M(4,1)=0.0
          M(4,2)=0.0
          M(4,3)=-1.0
          M(5,1)=0.0
          M(5,2)=0.0
          M(5,3)=-1.0
          M(6,1)=0.707106781186547
          M(6,2)=0.0
          M(6,3)=-0.707106781186547
          M(7,1)=0.0
          M(7,2)=-1.0
          M(7,3)=0.0
          M(8,1)=0.0
          M(8,2)=0.707106781186547
          M(8,3)=-0.707106781186547
          M(9,1)=0.0
          M(9,2)=-0.707106781186547
          M(9,3)=-0.707106781186547
```

```
          M(10,1)=0.707106781186547
          M(10,2)=-0.707106781186547
          M(10,3)=0.0
          M(11,1)=0.707106781186547
          M(11,2)=-0.707106781186547
          M(11,3)=0.0
          M(12,1)=-0.707106781186547
          M(12,2)=-0.707106781186547
          M(12,3)=0.0
          M(13,1)=-0.907124939317685
          M(13,2)=0.0
          M(13,3)=-0.420861431433062
          M(14,1)=0.707106781186547
          M(14,2)=0.0
          M(14,3)=-0.707106781186547
          M(15,1)=-0.707106781186547
          M(15,2)=0.0
          M(15,3)=-0.707106781186547
          M(16,1)=0.0
          M(16,2)=0.420861431433062
          M(16,3)=0.907124939317685
          M(17,1)=0.0
          M(17,2)=-0.420861431433062
          M(17,3)=-0.907124939317685
          M(18,1)=0.0
          M(18,2)=0.707106781186547
          M(18,3)=-0.707106781186547
          M(19,1)=0.420861431433062
          M(19,2)=-0.907124939317685
          M(19,3)=0.0
          M(20,1)=0.0
          M(20,2)=0.707106781186547
          M(20,3)=0.707106781186547
          M(21,1)=-0.420861431433062
          M(21,2)=0.0
          M(21,3)=-0.907124939317685
C
          L(1,1)=0.0
          L(1,2)=0.0
          L(1,3)=0.0
          L(2,1)=0.0
          L(2,2)=0.0
          L(2,3)=0.0
          L(3,1)=0.0
          L(3,2)=0.0
          L(3,3)=0.0
          L(4,1)=0.0
          L(4,2)=0.0
          L(4,3)=0.0
          L(5,1)=0.0
          L(5,2)=0.0
          L(5,3)=0.0
          L(6,1)=0.5
          L(6,2)=0.0
          L(6,3)=-0.5
```

267

```
        L(7,1)=0.0
        L(7,2)=0.0
        L(7,3)=0.0
        L(8,1)=0.0
        L(8,2)=0.5
        L(8,3)=-0.5
        L(9,1)=0.0
        L(9,2)=-0.5
        L(9,3)=0.5
        L(10,1)=0.274291885177568
        L(10,2)=-0.274291885177568
        L(10,3)=0.0
        L(11,1)=0.274291885177568
        L(11,2)=-0.274291885177568
        L(11,3)=0.0
        L(12,1)=-0.274291885177568
        L(12,2)=0.274291885177568
        L(12,3)=0.0
        L(13,1)=-0.351880389662664
        L(13,2)=0.0
        L(13,3)=0.351880389662664
        L(14,1)=0.274291885177568
        L(14,2)=0.0
        L(14,3)=-0.274291885177568
        L(15,1)=-0.274291885177568
        L(15,2)=0.0
        L(15,3)=0.274291885177568
        L(16,1)=0.0
        L(16,2)=-0.351880389662664
        L(16,3)=0.351880389662664
        L(17,1)=0.0
        L(17,2)=0.351880389662664
        L(17,3)=-0.351880389662664
        L(18,1)=0.0
        L(18,2)=0.274291885177568
        L(18,3)=-0.274291885177568
        L(19,1)=0.351880389662664
        L(19,2)=-0.351880389662664
        L(19,3)=0.0
        L(20,1)=0.0
        L(20,2)=-0.274291885177568
        L(20,3)=0.274291885177568
        L(21,1)=-0.351880389662664
        L(21,2)=0.0
        L(21,3)=0.351880389662664
C
        W(1)=0.0265214244093
        W(2)=0.0265214244093
        W(3)=0.0265214244093
        W(4)=0.0199301476312
        W(5)=0.0199301476312
        W(6)=0.0199301476312
        W(7)=0.0199301476312
        W(8)=0.0199301476312
        W(9)=0.0199301476312
```

```
      W(10)=0.0250712367487
      W(11)=0.0250712367487
      W(12)=0.0250712367487
      W(13)=0.0250712367487
      W(14)=0.0250712367487
      W(15)=0.0250712367487
      W(16)=0.0250712367487
      W(17)=0.0250712367487
      W(18)=0.0250712367487
      W(19)=0.0250712367487
      W(20)=0.0250712367487
      W(21)=0.0250712367487
c Constants
      E=props(1)
      nu=props(2)
      k1=props(3)
      k2=props(4)
      k3=props(5)
      k4=props(6)
      k5=props(7)
      k6=props(8)
c strain increment (dstrain) at the begining of new material point
      dstrain(km,1)=straininc(km,1)
      dstrain(km,2)=straininc(km,2)
      dstrain(km,3)=straininc(km,3)
      dstrain(km,4)=straininc(km,4)
c strain (Strainold)in the previous material point
      strainold(km,1)=stateOld(km,1)
      strainold(km,2)=stateold(km,2)
      strainold(km,3)=stateold(km,3)
      strainold(km,4)=stateold(km,4)
c starting of new increment
      statenew(km,1)=dstrain(km,1)+strainold(km,1)
      statenew(km,2)=dstrain(km,2)+strainold(km,2)
      statenew(km,3)=dstrain(km,3)+strainold(km,3)
      statenew(km,4)=dstrain(km,4)+strainold(km,4)
c
      volstrainold(km)=stateold(km,7)
      dvolstrain(km)=(dstrain(km,1)+dstrain(km,2)+dstrain(km,3))/3.0
      volstrainnew(km)=volstrainold(km)+dvolstrain(km)
      statenew(km,7)=volstrainnew(km)
      volstressold(km)=stateold(km,8)
c
      ev1=props(1)/(1.0-2.0*Props(2))
      evd=props(1)*props(5)/props(6)*exp(-volstrainnew(km)/(props(3)*
     1props(6)))
      evn=amax1(ev1,evd)
c checking for unloading
      if(volstressold(km).lt.00.and.volstrainold(km).lt.0.0.and.
     1dvolstrain(km).gt.0.0)then
        evn=ev1*((c15/(c15-volstrainold(km))+
     1   (volstressold(km)/(c15*c16*ev1)*volstrainold(km))))
      endif
      if(volstressold(km).gt.00.and.volstrainold(km).gt.0.0.and.
     1dvolstrain(km).lt.0.0)then
```

```fortran
      evn=amin1((volstressold(km)/volstrainold(km)),ev1)
      endif
      volstress(km)=volstressold(km)+evn*dvolstrain(km)
c volumetric bounderies
      nbstressvol(km)=-props(1)*props(3)*props(5)*
     1(exp((-volstrainnew(km))/(props(3)*props(6))))
      if((volstrainnew(km)-props(3)*c13).gt. 0.0)then
        mbv=volstrainnew(km)-props(3)*c13
        else
          mbv=0.0
      endif
      pbstressvol(km)=evn*props(3)*c13/((1+(c14/props(3))*mbv)**2)
c
      if(volstress(km).lt.nbstressvol(km))then
        volstress1(km)=nbstressvol(km)
        elseif(volstress(km).gt.pbstressvol(km))  then
        volstress1(km)=pbstressvol(km)
      else
        volstress1(km)=volstress(km)
      endif
      volstressn(km)=volstress1(km)
c
      sn(1,1)=strainold(km,1)
      sn(2,2)=strainold(km,2)
      sn(3,3)=strainold(km,3)
      sn(1,2)=strainold(km,4)
      sn(2,3)=strainold(km,5)
      sn(1,3)=strainold(km,6)
c
      sn(2,1)=strainold(km,4)
      sn(3,2)=strainold(km,5)
      sn(3,1)=strainold(km,6)
c
      dsn(1,1)=dstrain(km,1)
      dsn(2,2)=dstrain(km,2)
      dsn(3,3)=dstrain(km,3)
      dsn(1,2)=dstrain(km,4)
      dsn(2,3)=dstrain(km,5)
      dsn(1,3)=dstrain(km,6)
c
      dsn(2,1)=dstrain(km,4)
      dsn(3,2)=dstrain(km,5)
      dsn(3,1)=dstrain(km,6)
c
c Normal strain
      do 10 k=1,21
      nstrainold(k)=sn(1,1)*n(k,1)*n(k,1)+sn(2,2)*n(k,2)*n(k,2)+
     1sn(3,3)*n(k,3)*n(k,3)+sn(1,2)*n(k,1)*n(k,2)
c
      dnstrain(k)=dsn(1,1)*n(k,1)*n(k,1)+dsn(2,2)*n(k,2)*n(k,2)+
     1dsn(3,3)*n(k,3)*n(k,3)+dsn(1,2)*n(k,1)*n(k,2)
      nstrainnew(km,k)=nstrainold(k)+dnstrain(k)
c Deviatoric strain
      devstrainold(km,k)=nstrainold(k)-volstrainold(km)
      devstrainnew(km,k)=nstrainnew(km,k)-volstrainnew(km)
```

```fortran
      ddevstrain(km,k)=dnstrain(k)-dvolstrain(km)
      ed1=5*props(1)/((2+3*u)*(1+props(2)))
      if((devstressold(km,k)*devstrainold(km,k)).le.0.0)then
         eds=ed1
      else
         eds=amin1(ed1,(devstressold(km,k)/devstrainold(km,k)))
      endif
c checking for unloading
      if(devstressold(km,k).lt.00.and.devstrainold(km,k).lt.0.0.and.
     1ddevstrain(km,k).gt.0.0)then
       ed1=(1-c17)*ed1+c17*eds
      endif
      if(devstressold(km,k).gt.00.and.devstrainold(km,k).gt.0.0.and.
     1ddevstrain(km,k).lt.0.0)then
       ed1=(1-c17)*ed1+c17*eds
      endif
c using state variable no 9 to 29 for deviatoric stress
      devstressold(km,k)=stateold(km,8+k)
c new deviatoric stress
      devstress(km,k)=devstressold(km,k)+ed1*ddevstrain(km,k)
c Deviatoric bounderies
c +ve deviatoric boundery
      if((devstrainnew(km,k)-c5*c6*props(3)).ge.0.0)then
         mbd1=devstrainnew(km,k)-c5*c6*props(3)
      else
         mbd1=0.0
      endif

pbdevstress(km,k)=props(1)*props(3)*c5/(1+(mbd1/(props(3)*props(7)
     1*c7*c18))**2)
c -ve deviatoric boundery
      if((-devstrainnew(km,k)-c8*c9*props(3)).ge.0.0)then
         mbd2=-devstrainnew(km,k)-c8*c9*props(3)
      else
         mbd2=0.0
      endif
      nbdevstress(km,k)=-props(1)*props(3)*c8/(1+(mbd2/(props(3)*
     1props(7)*c7))**2)
c
      if(devstress(km,k).le.nbdevstress(km,k))then
         devstress1(km,k)=nbdevstress(km,k)
      else if(devstress(km,k).ge.pbdevstress(km,k))then
         devstress1(km,k)=pbdevstress(km,k)
      else
         devstress1(km,k)=devstress(km,k)
      endif
      devstressnew(km,k)=devstress1(km,k)
c Normal stress (Split)
      norstresss(km,k)=devstress1(km,k)+volstressn(km)
c Normal stress boundery
      if((nstrainnew(km,k)-c1*c2*props(3)*props(8)).ge.0.0)then
         mbn1=nstrainnew(km,k)-c1*c2*props(3)*props(8)
      else
         mbn1=0.0
      endif
```

```fortran
      if((-c4*volstressold(km)/ev1).ge.0.0)then
        mbn2=-c4*volstressold(km)/ev1
      else
        mbn2=0.0
      endif
      bnorstress(km,k)=props(1)*props(3)*props(8)*c1*
     1 exp(-(mbn1)/(props(3)*props(7)*props(8)*c3+mbn2))
      if(norstresss(km,k).ge.bnorstress(km,k))then
        norstressnews(km,k)=bnorstress(km,k)
      else
        norstressnews(km,k)=norstresss(km,k)
      endif
      norstressnew(km,k)=norstressnews(km,k)
      if(nstrainnew(km,k).gt.0.0.and.norstressnew(km,k).lt.0.0)then
      norstressnew(km,k)=0.0
      endif
c using state variable 30 to 50 for normal stress
      statenew(km,29+k)=norstressnew(km,k)
  10  continue
c new volumetric stress
      volstress2(km)=0.0
      do 30 k=1,21
      do 60 i=1,3
        f(k)=w(k)*norstressnew(km,k)*N(k,i)*N(k,i)
        volstress2(km)=f(k)+volstress2(km)
  60  continue
  30  continue
      volstressnew(km)=amin1(volstress2(km),volstressn(km))
      statenew(km,8)=volstressnew(km)
c new deviatoric stress
      do 40 k=1,21
      devstressnew(km,k)=norstressnew(km,k)-volstressnew(km)
      statenew(km,8+k)=devstressnew(km,k)
  40  continue
c tangential behaviour
      do 50 k=1,21
      mstrainold(k)=sn(1,1)*(m(k,1)*n(k,1)+m(k,1)*n(k,1))/2+
     1sn(2,2)*(m(k,2)*n(k,2)+m(k,2)*n(k,2))/2+sn(3,3)*(m(k,3)*
     2n(k,3)+m(k,3)*n(k,3))/2+sn(1,2)*(m(k,1)*n(k,2)+m(k,2)*
     3n(k,1))/2
c
      lstrainold(k)=sn(1,1)*(l(k,1)*n(k,1)+l(k,1)*n(k,1))/2+
     1sn(2,2)*(l(k,2)*n(k,2)+l(k,2)*n(k,2))/2+sn(3,3)*(l(k,3)*
     2n(k,3)+l(k,3)*n(k,3))/2+sn(1,2)*(l(k,1)*n(k,2)+l(k,2)*
     3n(k,1))/2
c
      dmstrain(k)=dsn(1,1)*(m(k,1)*n(k,1)+m(k,1)*n(k,1))/2+
     1dsn(2,2)*(m(k,2)*n(k,2)+m(k,2)*n(k,2))/2+dsn(3,3)*(m(k,3)*
     2n(k,3)+m(k,3)*n(k,3))/2+dsn(1,2)*(m(k,1)*n(k,2)+m(k,2)*
     3n(k,1))/2
c
      dlstrain(k)=dsn(1,1)*(l(k,1)*n(k,1)+l(k,1)*n(k,1))/2+
     1dsn(2,2)*(l(k,2)*n(k,2)+l(k,2)*n(k,2))/2+dsn(3,3)*(l(k,3)*
     2n(k,3)+l(k,3)*n(k,3))/2+dsn(1,2)*(l(k,1)*n(k,2)+l(k,2)*
     3n(k,1))/2
```

```fortran
      mstrainnew(km,k)=mstrainold(k)+dmstrain(k)
      lstrainnew(km,k)=lstrainold(k)+dlstrain(k)
      tstrainold(km,k)=(mstrainold(k))**2+(lstrainold(k))**2
      tstrainold(km,k)=sqrt(tstrainold(km,k))
      dtstrain(km,k)=(dmstrain(k))**2+(dlstrain(k))**2
      dtstrain(km,k)=sqrt(dtstrain(km,k))
      et1=ed1
c using state variable 51 to 71 for m-stress, and 72 to 92 for l-stress
      mstressold(km,k)=stateold(km,50+k)
      lstressold(km,k)=stateold(km,71+k)
      tstressold(km,k)=stateold(km,113+k)
c
      if((tstressold(km,k)*tstrainold(km,k)).le.0.0)then
         ets=et1
      else
         ets=amin1(et1,(tstressold(km,k)/tstrainold(km,k)))
      endif
c checking for unloading
      if(tstressold(km,k).lt.00.and.tstrainold(km,k).lt.0.0.and.
     1dtstrain(km,k).gt.0.0)then
        et1=(1-c17)*et1+c17*ets
      endif
      if(tstressold(km,k).gt.00.and.tstrainold(km,k).gt.0.0.and.
     1dtstrain(km,k).lt.0.0)then
        et1=(1-c17)*et1+c17*ets
      endif
      mstress1(km,k)=mstressold(km,k)+et1*dmstrain(k)
      lstress1(km,k)=lstressold(km,k)+et1*dlstrain(k)
c
      tstrainnew(km,k)=(mstrainnew(km,k))**2+(lstrainnew(km,k))**2
      tstrainnew(km,k)=sqrt(tstrainnew(km,k))
      tstress1(km,k)=(mstress1(km,k))**2+(lstress1(km,k))**2
      tstress1(km,k)=sqrt(tstress1(km,k))
      if(tstress1(km,k).eq.0.0)then
      rm(km,k)=0.0
      rm(km,k)=0.0
      else
      rm(km,k)=mstress1(km,k)/tstress1(km,k)
      rl(km,k)=lstress1(km,k)/tstress1(km,k)
      endif
c tangential boundery
      if(volstrainnew(km).ge.0.0)then
        mbt1=volstrainnew(km)
      else
        mbt1=0.0
      endif
      sigmano(km,k)=et1*props(3)*props(8)*c11/(1+c12*mbt1)
      if((-norstressnew(km,k)+sigmano(km,k)).ge.0.0)then
      mbt2=-norstressnew(km,k)+sigmano(km,k)
      else
      mbt2=0.0
      endif
      btstress(km,k)=et1*props(3)*props(4)*c10*mbt2/
     1 (et1*props(3)*props(4)+c10*mbt2)
      if(tstress1(km,k).gt.btstress(km,k))then
```

273

```fortran
         tstress2(km,k)=btstress(km,k)
        elseif(tstress1(km,k).lt.(-btstress(km,k)))then
           tstress2(km,k)=-btstress(km,k)
        else
           tstress2(km,k)=tstress1(km,k)
        endif
           tstressnew(km,k)=tstress2(km,k)
c
        mstressnew(km,k)=rm(km,k)*tstressnew(km,k)
        lstressnew(km,k)=rl(km,k)*tstressnew(km,k)
        statenew(km,50+k)=mstressnew(km,k)
        statenew(km,71+k)=lstressnew(km,k)
        statenew(km,113+k)=tstressnew(km,k)
   50 continue
c macro stress tensor
        delta(km,1)=1.0
        delta(km,2)=1.0
        delta(km,3)=1.0
        delta(km,4)=0.0
c
        sd1(km)=0.0
        do 70 k=1,21
           sd1(km)=(devstressnew(km,k)*(n(k,1)*n(k,1)-delta(km,1)/3)+
     1     lstressnew(km,k)*((l(k,1)*n(k,1)+l(k,1)*n(k,1))/2)+
     2
mstressnew(km,k)*((m(k,1)*n(k,1)+m(k,1)*n(k,1))/2))*w(k)+sd1(km)
   70 continue
        stressnew(km,1)=6*sd1(km)+volstressnew(km)*delta(km,1)
c
        sd2(km)=0.0
        do 80 k=1,21
           sd2(km)=(devstressnew(km,k)*(n(k,2)*n(k,2)-delta(km,2)/3)+
     1     lstressnew(km,k)*((l(k,2)*n(k,2)+l(k,2)*n(k,2))/2)+
     2
mstressnew(km,k)*((m(k,2)*n(k,2)+m(k,2)*n(k,2))/2))*w(k)+sd2(km)
   80 continue
        stressnew(km,2)=6*sd2(km)+volstressnew(km)*delta(km,2)
c
        sd3(km)=0.0
        do 90 k=1,21
           sd3(km)=(devstressnew(km,k)*(n(k,3)*n(k,3)-delta(km,3)/3)+
     1     lstressnew(km,k)*((l(k,3)*n(k,3)+l(k,3)*n(k,3))/2)+
     2
mstressnew(km,k)*((m(k,3)*n(k,3)+m(k,3)*n(k,3))/2))*w(k)+sd3(km)
   90 continue
        stressnew(km,3)=6*sd3(km)+volstressnew(km)*delta(km,3)
c
        sd4(km)=0.0
        do 110 k=1,21
           sd4(km)=(devstressnew(km,k)*(n(k,1)*n(k,2)-delta(km,4)/3)+
     1     lstressnew(km,k)*((l(k,1)*n(k,2)+l(k,2)*n(k,1))/2)+
     2
mstressnew(km,k)*((m(k,1)*n(k,2)+m(k,2)*n(k,1))/2))*w(k)+sd4(km)
  110 continue
        stressnew(km,4)=6*sd4(km)+volstressnew(km)*delta(km,4)
```

```
100  continue
      return
      end
```

C.4. DEEP BEAM SIMULATION
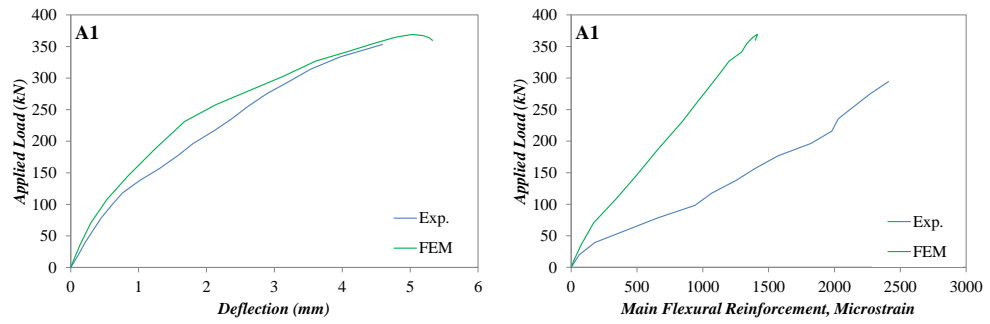
Figure C-4 Experimental and numerical load-deflection response and strain in the flexural reinforcing bars of beam A1
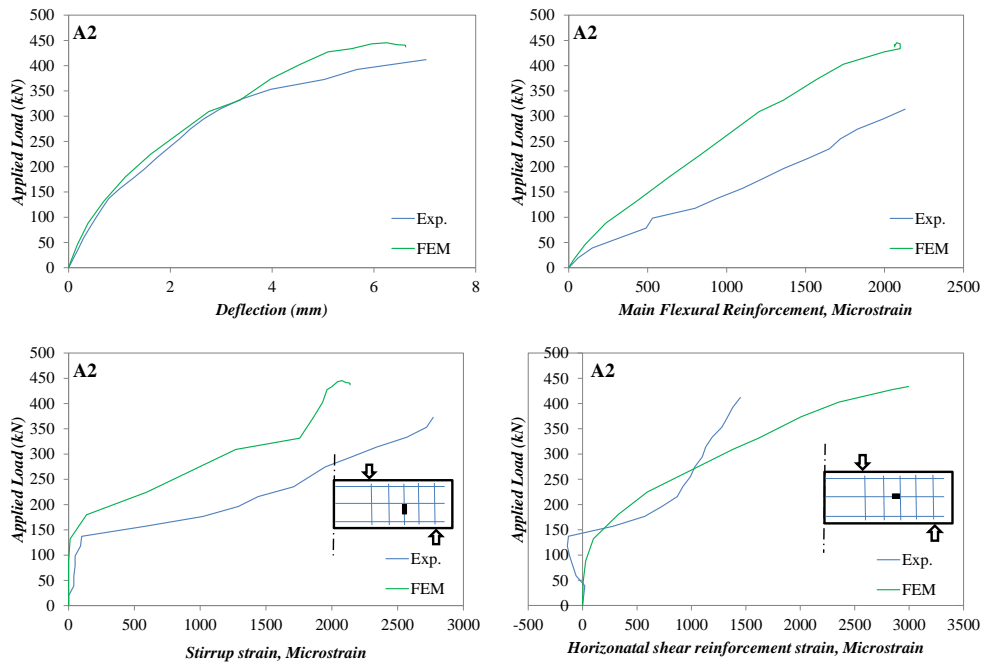
Figure C-5 Experimental and numerical load-deflection response and strain in the flexural and shear reinforcing bars of beam A2
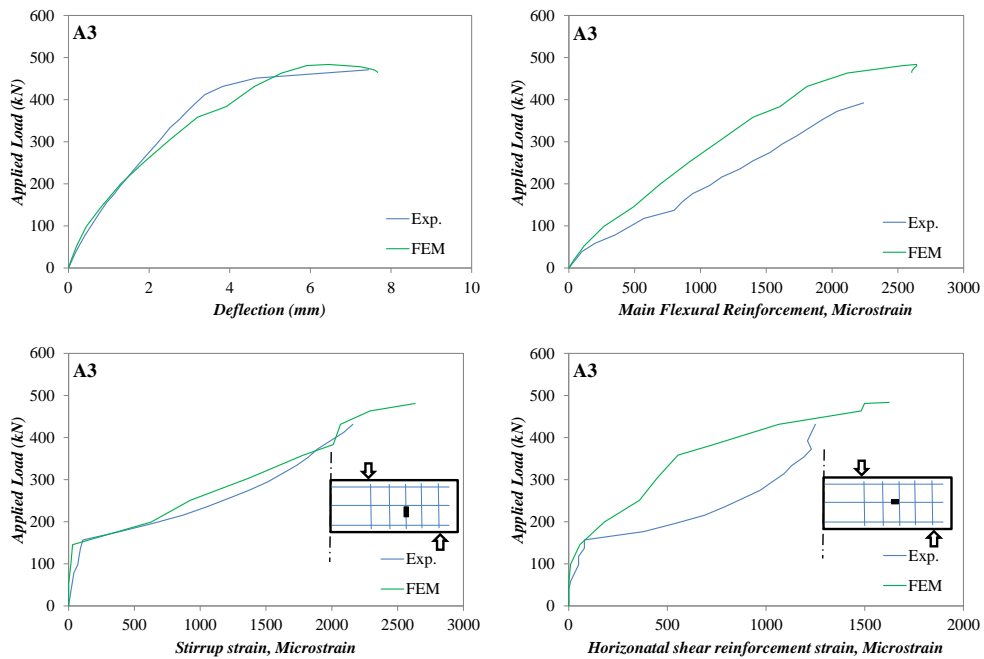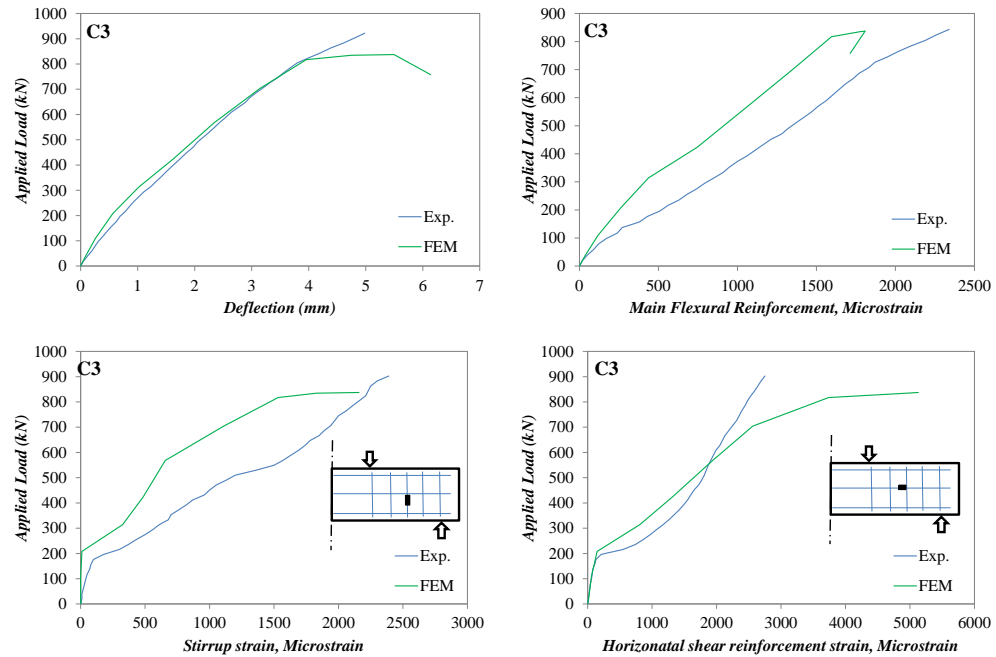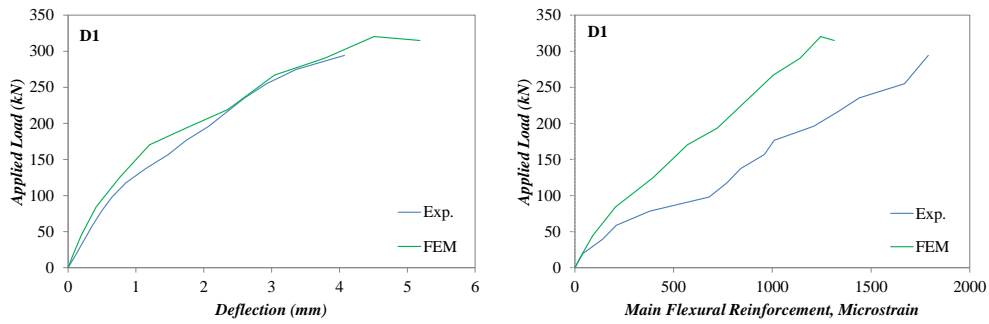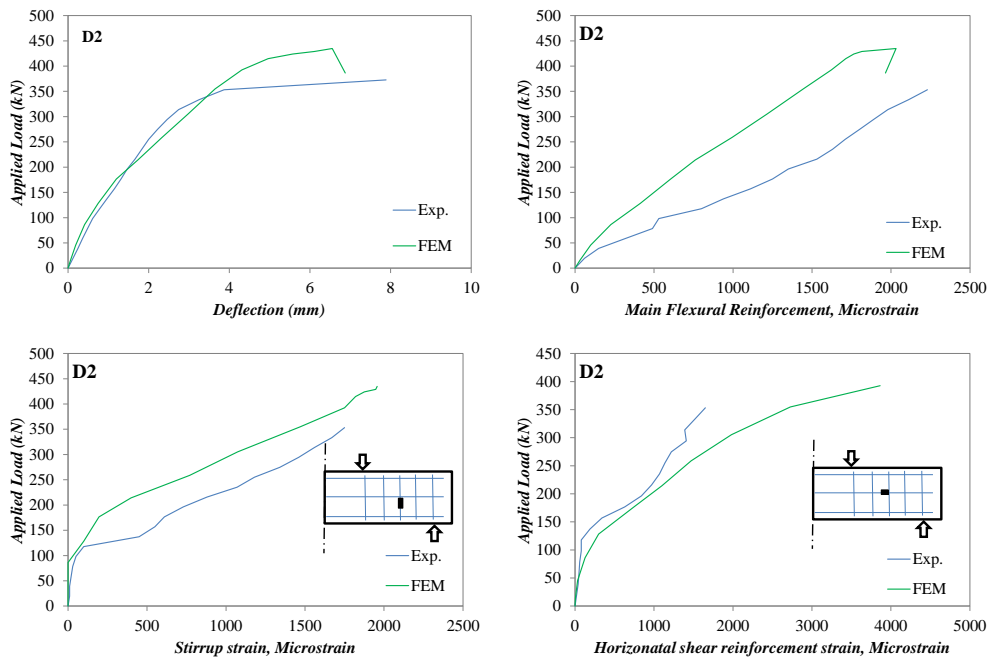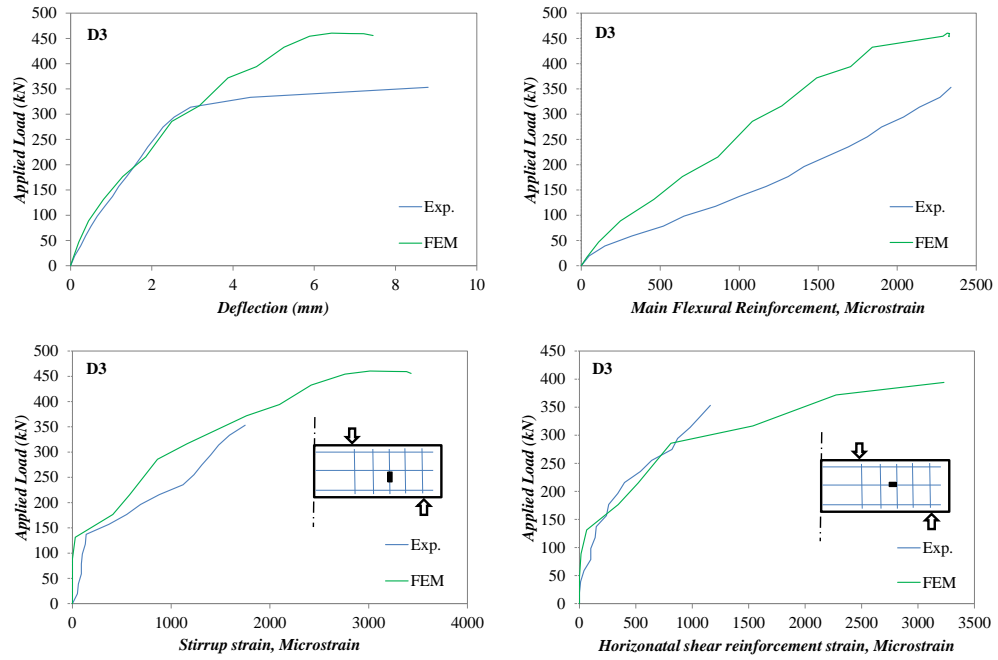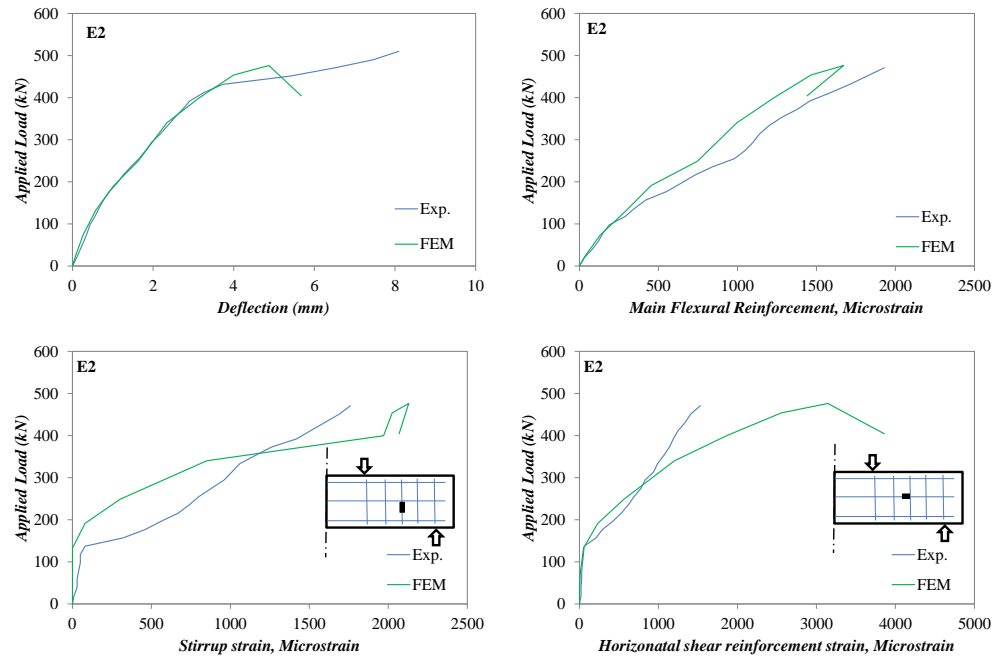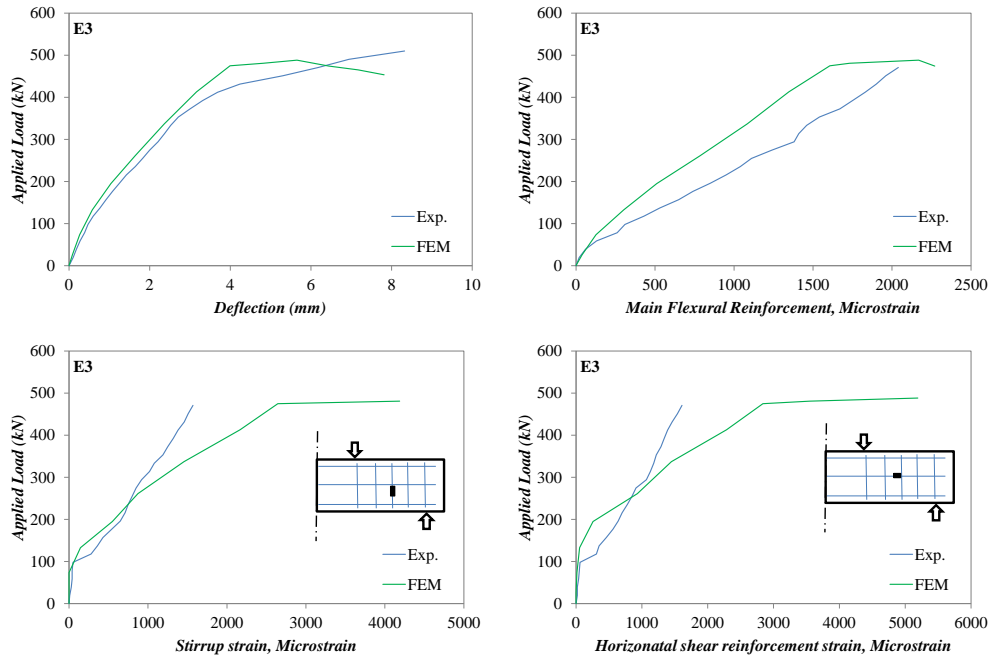

Figure C-6 Experimental and numerical load-deflection response and strain in the flexural and shear reinforcing bars of beam A3
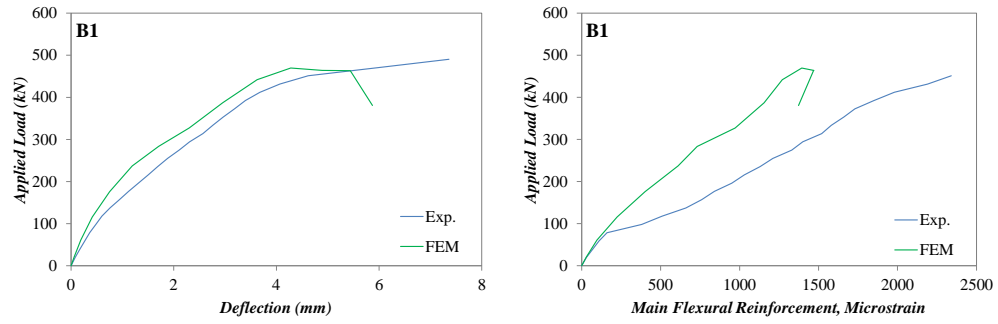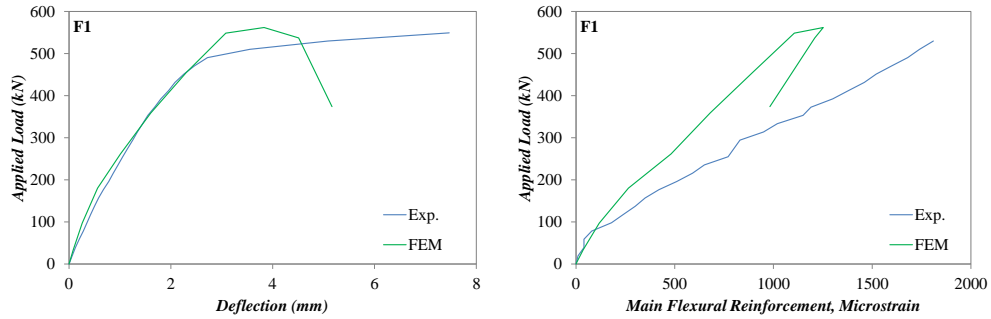
Figure C-7 Experimental and numerical load-deflection response and strain in the flexural reinforcing bars of beam B1
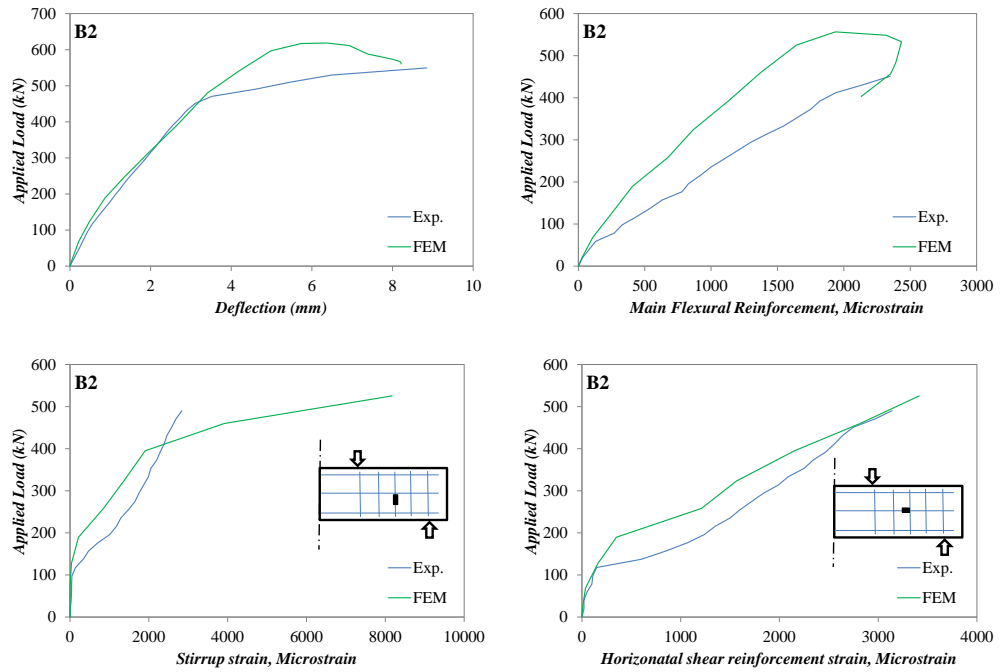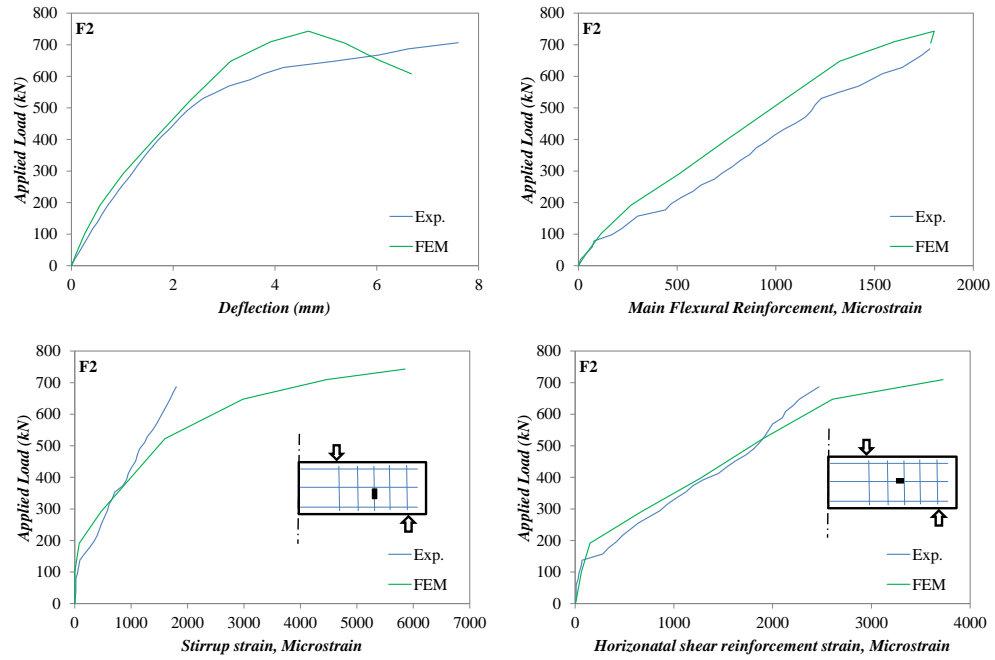

Figure C-8 Experimental and numerical load-deflection response and strain in the flexural and shear reinforcing bars of beam B2
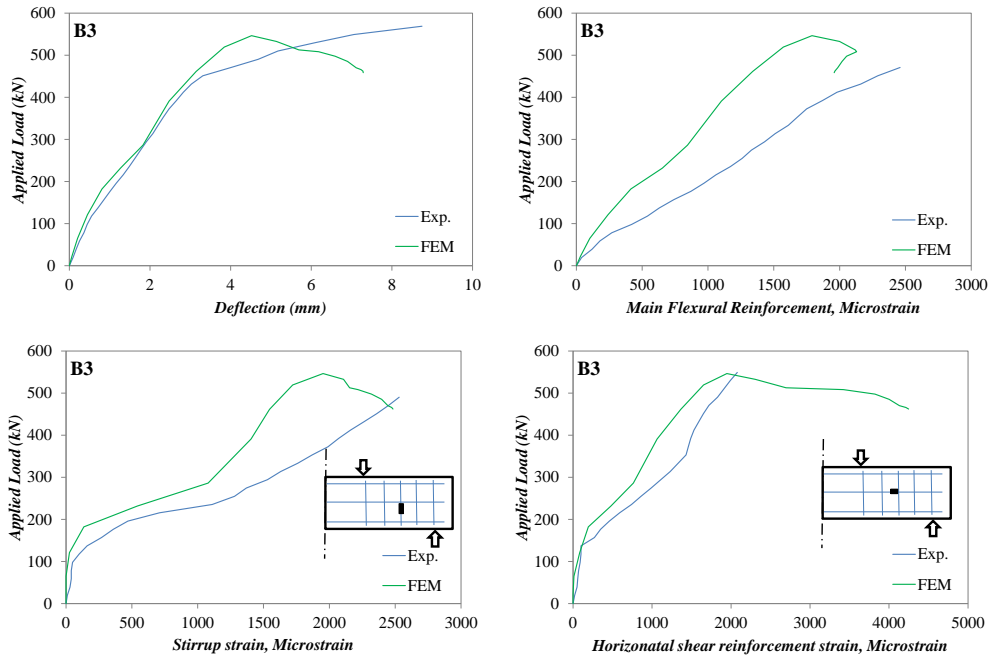
Figure C-9 Experimental and numerical load-deflection response and strain in the flexural and shear reinforcing bars of beam B3
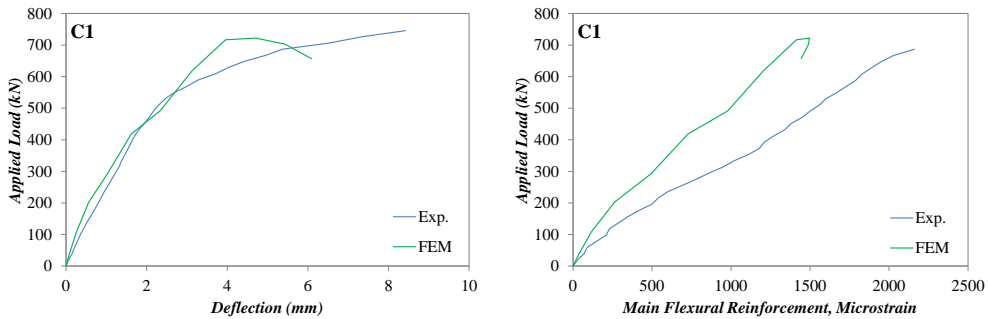
Figure C-10 Experimental and numerical load-deflection response and strain in the flexural reinforcing bars of beam C1
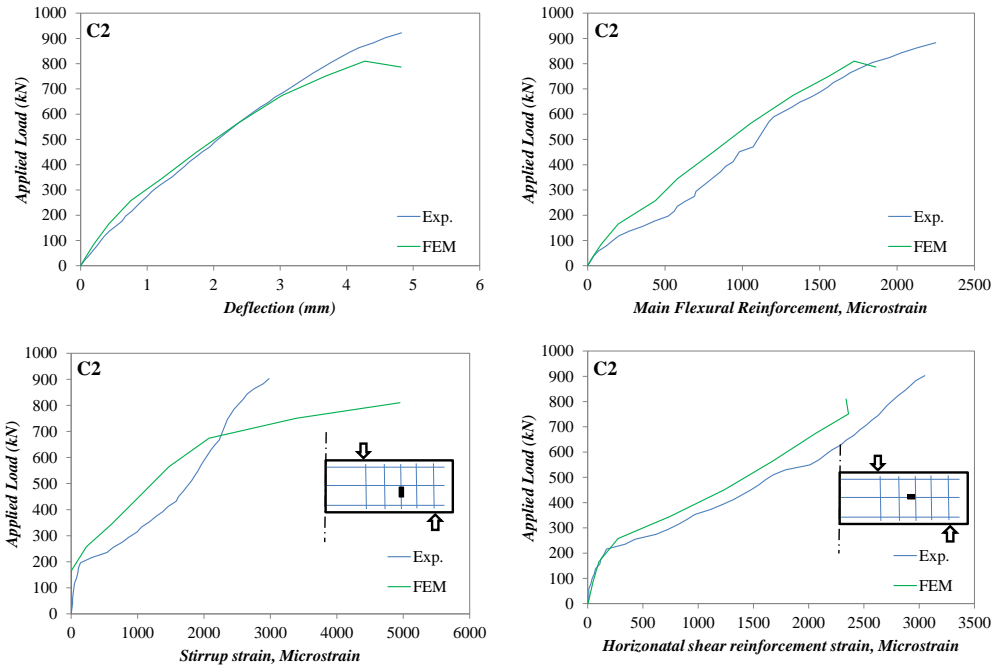
Figure C-11 Experimental and numerical load-deflection response and strain in the flexural and shear reinforcing bars of beam C2
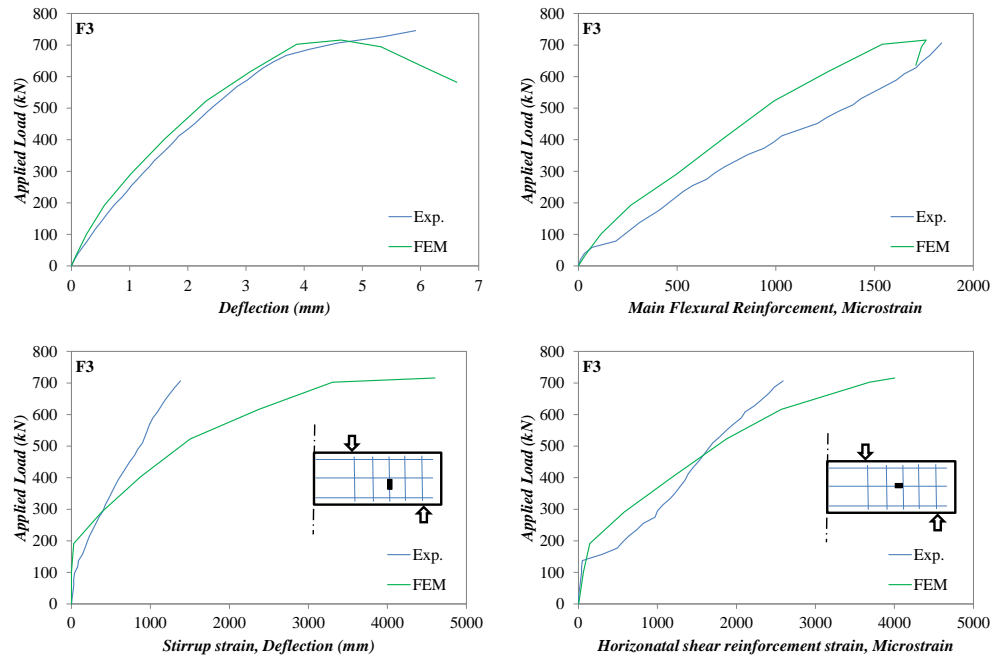

Figure C-12 Experimental and numerical load-deflection response and strain in the flexural and shear reinforcing bars of beam C3
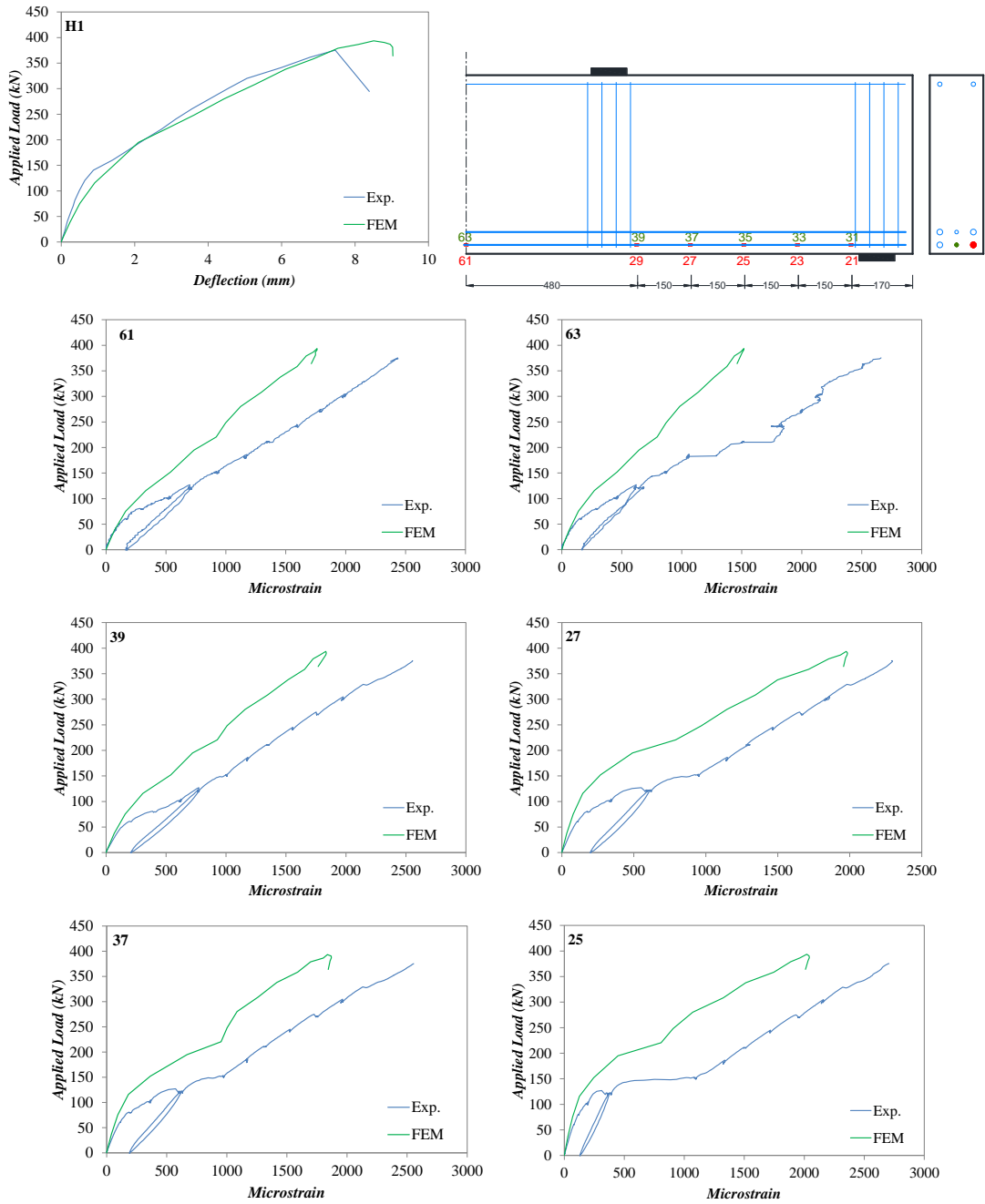
Figure C-13 Experimental and numerical load-deflection response and strain in the flexural reinforcing bars of beam D1
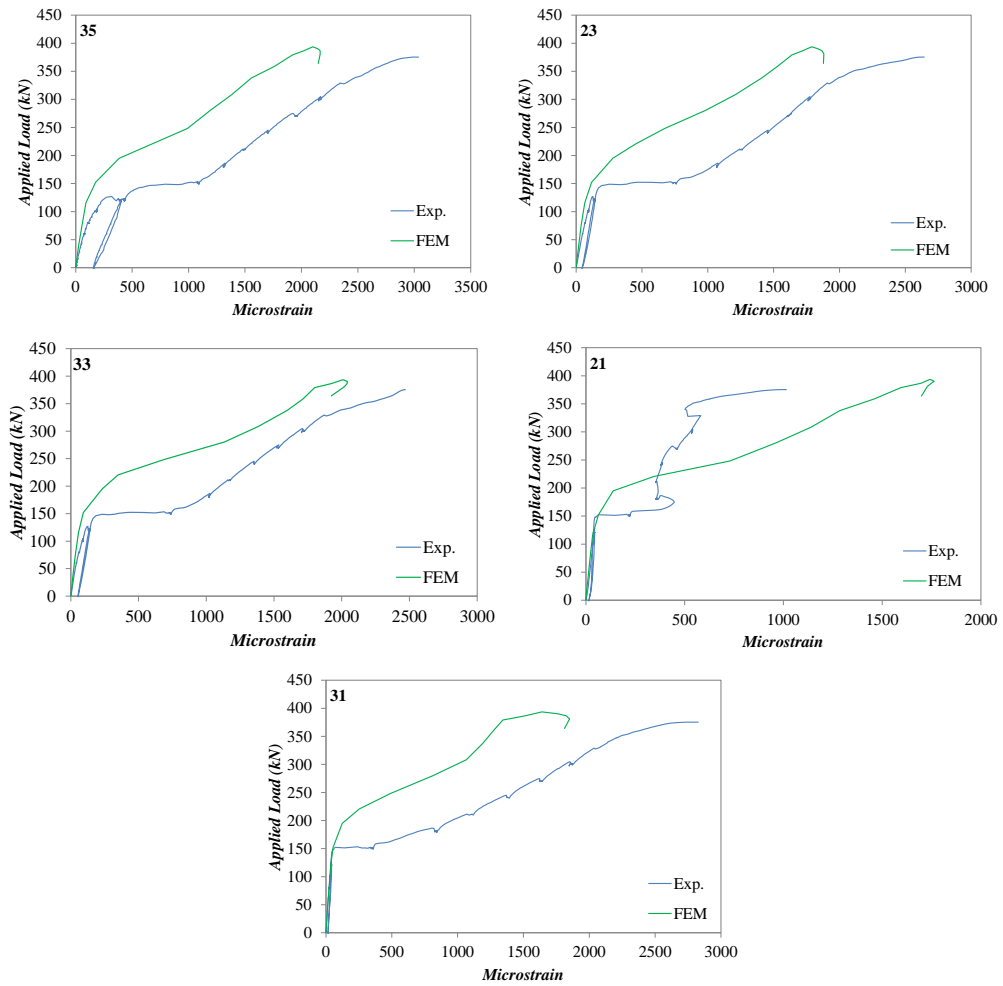

Figure C-14 Experimental and numerical load-deflection response and strain in the flexural and shear reinforcing bars of beam D2

Figure C-15 Experimental and numerical load-deflection response and strain in the flexural and shear reinforcing bars of beam D3

Figure C-16 Experimental and numerical load-deflection response and strain in the flexural and shear reinforcing bars of beam E2

281

Figure C-17 Experimental and numerical load-deflection response and strain in the flexural and shear reinforcing bars of beam E3
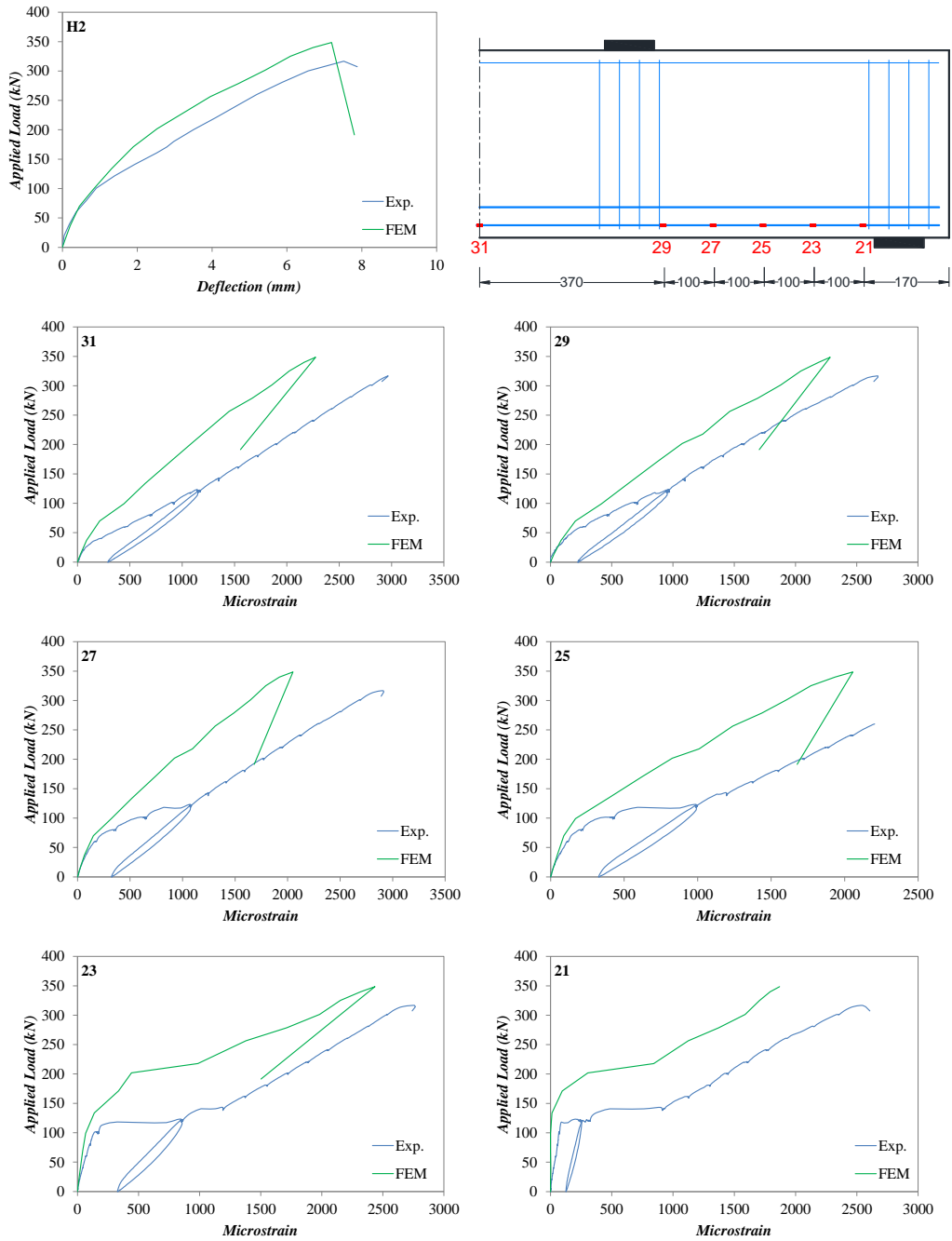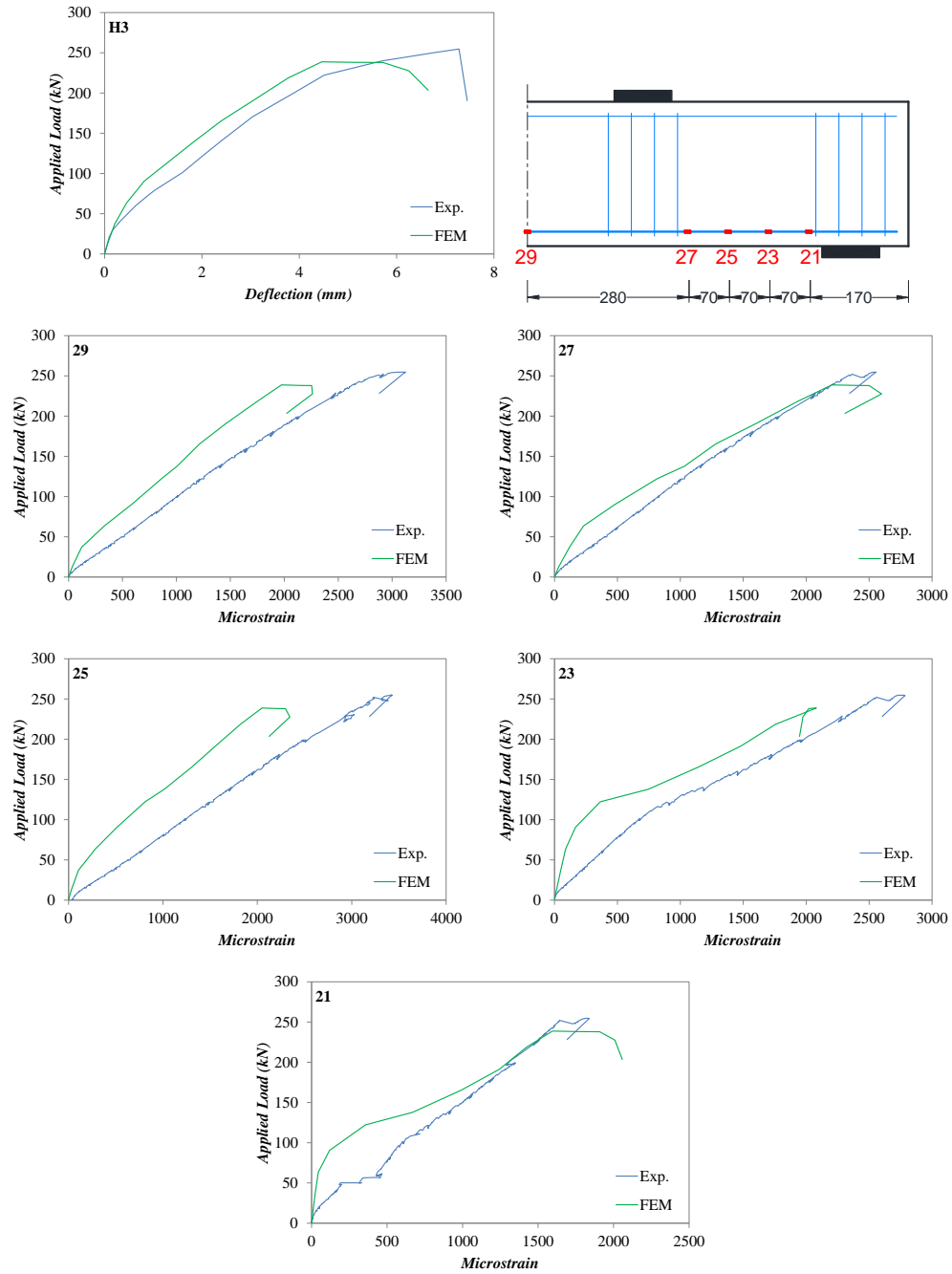

Figure C-18 Experimental and numerical load-deflection response and strain in the flexural reinforcing bars of beam F1

282

Figure C-19 Experimental and numerical load-deflection response and strain in the flexural and shear reinforcing bars of beam F2

Figure C-20 Experimental and numerical load-deflection response and strain in the flexural and shear reinforcing bars of beam F3

Figure C-21 Experimental and numerical load-deflection response and strain in the flexural reinforcing bars of beam H1
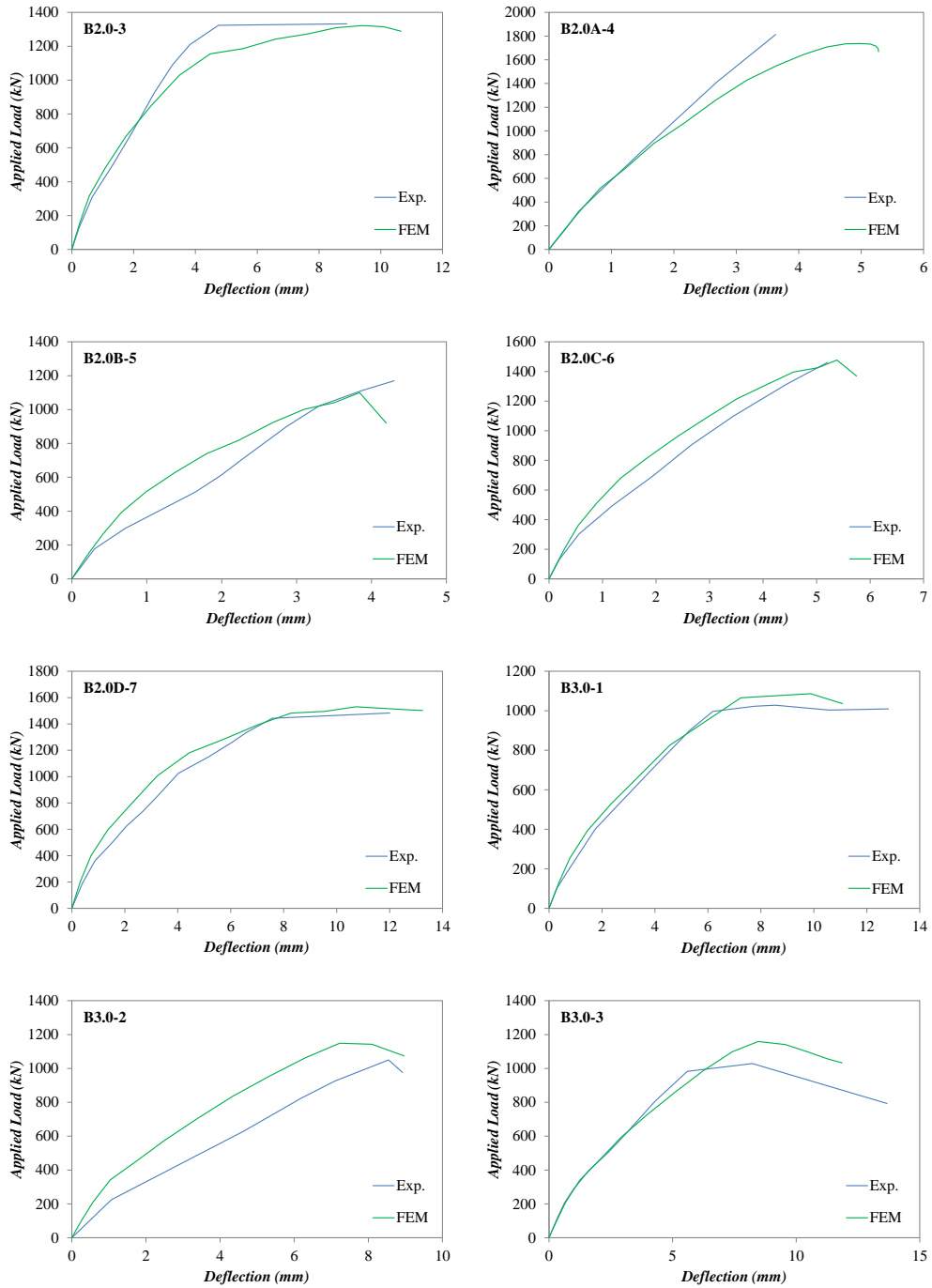
Figure C-21 Continued

285

Figure C-22 Experimental and numerical load-deflection response and strain in the flexural reinforcing bars of beam H2

Figure C-23 Experimental and numerical load-deflection response and strain in the flexural reinforcing bars of beam H3

Figure C-24 Experimental and numerical load-deflection response of the beams tested by Foster & Gilbert [68]
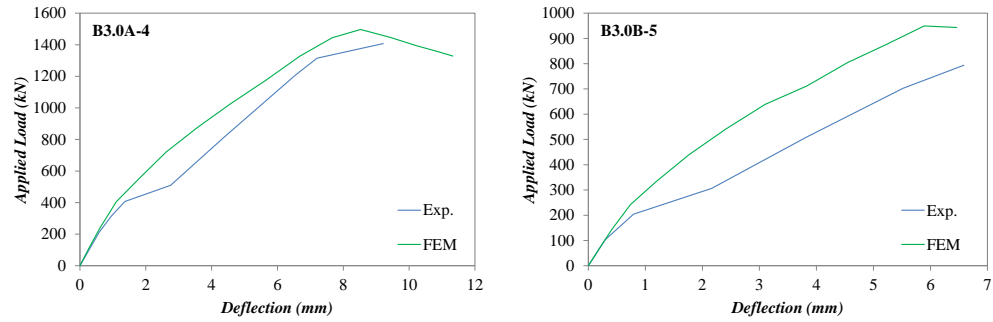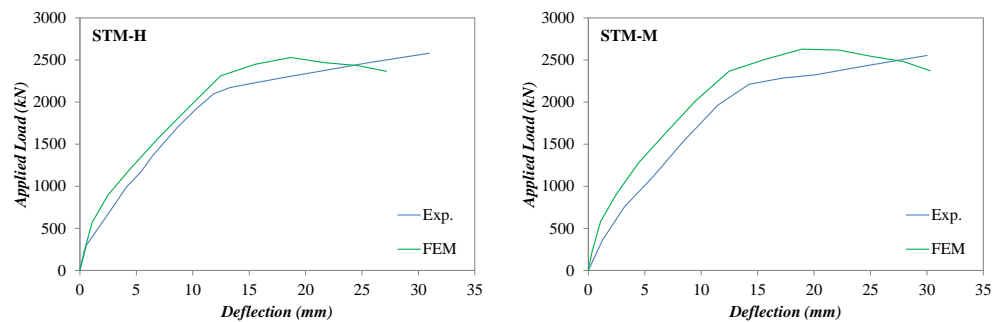
Figure C-24 Continued

Figure C-25 Experimental and numerical load-deflection response of the beams tested by Aguilar et al. [81]

C.5. SLENDER BEAM SIMULATION

Although the model discussed above was implemented to assess the behaviour of RC deep beams, which is the main aim of this work, it can also be used to simulate the behaviour of RC slender beams. The response of four slender beams from the literature was examined. The detail of the beams are summarized in Table C-1 and more details can be found in the original documents [82, 140]. The predicted load deflection responses for the analyzed beams along with the experimental responses are shown in Figure C-26. The numerical analysis yielded satisfactory results in terms of overall load-deflection response and capturing the shear capacity of the beams. However, in terms of strain developed in the shear reinforcement, no conclusions can be drawn as experimental data are not available. As fewer cracks are expected to develop in the shear span of slender beams than in deep beams, the conclusions drawn for the case of deep

289

beams on the ability of the model to correctly simulate the strain distribution in the shear span of slender beams requires further validation. However, this is beyond the scope of this research.

Table C-1 Summary of the slender beams simulated by the model

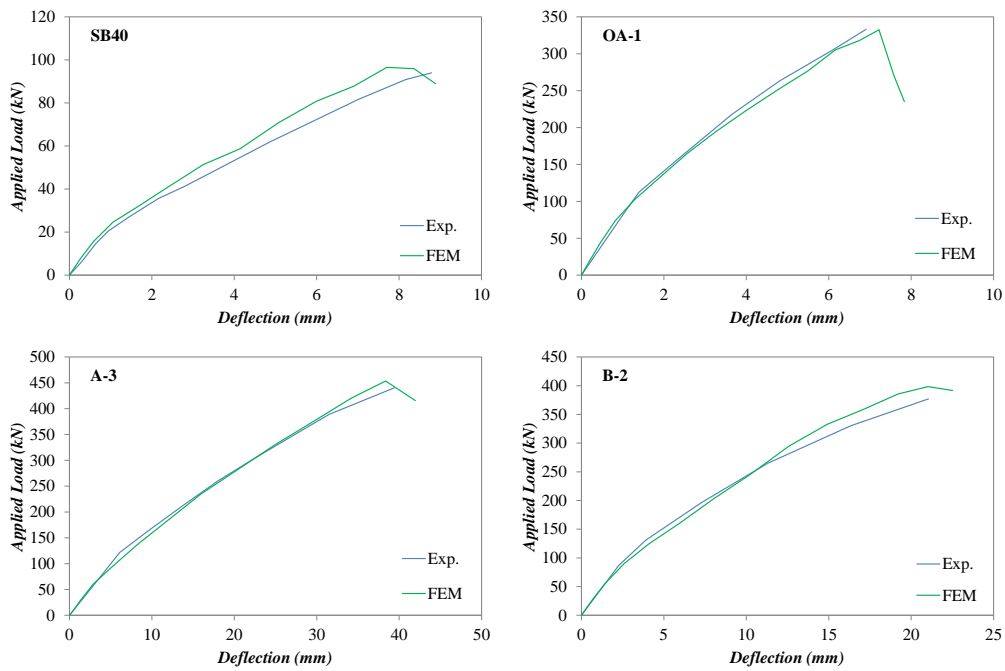|	Researcher	Specimen	L, mm	h, mm	b, mm	a, mm	f_c MPa	A_s mm^2	$\rho_{v\,\%}$	$\rho_{h\,\%}$	Failure Load kN
1	Guadagnini [82]	SB40	2500	250	150	750	43	452	0	0	90
4	Bresler and Scordelis [140]	OA-1	4060	560	305	1830	23	2464	0	0	334
2		A-3	6800	560	305	3200	35	3696	0.22	0	467
3		B-2	4970	560	230	2285	23	2464	0.29	0	400

Figure C-26 Experimental and predicted load–deflection curves of the slender beams

290